# Advanced Thermoplastic Nanocomposite Melt Processing Using an Improved Supercritical Carbon Dioxide Pretreatment for the Nanomaterial

By

John P. Quigley

Dissertation submitted to the faculty of the Virginia Polytechnic Institute and State University in partial fulfillment of the requirements for the degree of

DOCTOR OF PHILOSOPHY

In

Chemical Engineering

_____

Donald G. Baird, Chairman

Erdogan Kiran

Stephen Martin

Robert B. Moore

Michael J. Bortner

April 23, 2014

Blacksburg, VA

Keywords: nanocomposite, supercritical carbon dioxide, carbon nanotube, nanoclay

# Advanced Thermoplastic Nanocomposite Melt Processing Using an Improved Supercritical Carbon Dioxide Pretreatment for the Nanomaterial

John P. Quigley

## Abstract

Polymer nanocomposites have been proposed as lightweight replacements for traditional composite materials in various applications. Montmorillonite (MMT) and carbon nanotubes (CNTs) are two nanofillers which have accrued significant interest in the past 20 years due to their superior mechanical and electrical properties, respectively. However, efficient dispersion of the nanofiller and damage to CNTs prevent widespread utilization of these materials in polymer nanocomposites. Novel methods of nanocomposite generation combining the use of supercritical carbon dioxide ($scCO_2$) with melt compounding have been investigated to overcome these issues. The focus of this work is on developing the $scCO_2$ treatment of nanomaterial for thermoplastic nanocomposite generation. First, the supercritical carbon dioxide aided melt blending method was applied to nanoclay nanocomposites of Nylon 6/ and organoclay where the polymer may interact with the nanoclay surface. Second, the effect of $scCO_2$ processing of CNTs was investigated with special consideration to the processing variables. Finally, a study was carried out to analyze the electrical conductivity of polycarbonate nanocomposites generated using CNTs deagglomerated by $scCO_2$ processing.

The initial focus of this dissertation is the use of supercritical carbon dioxide ($scCO_2$) as a processing aid in the generation of nylon 6 nanocomposites in which the nylon 6 may interact with the nanoclay surface. Wide-angle X-ray diffraction, transmission electron microscopy, rheology, and tensile tests were carried out to investigate the effect of processing with $scCO_2$ on

the final composite morphology and properties. It was observed that mechanical properties of composites prepared with the $scCO_2$ aided melt blending method were similar to or higher than those reported in the literature for samples prepared with twin screw compounding. At 7.6 wt% nanoclay the modulus value reaches 4.75 ± 0.194 GPa which is one of the highest increases (1.7 GPa) reported for these materials processed at intermediate concentrations. Beyond 7.6 wt% the improvement due to $scCO_2$ processing matched that of direct blending.

The next objective of this work is to develop a method for the deagglomeration of commercially available multi-walled carbon nanotubes (MWCNTs) by manipulating processing variables and observing carbon nanotube aspect ratios after deagglomeration. High levels of deagglomeration of Baytubes® C 150 P and Nanocyl™ NC-7000 MWCNT agglomerates were observed, resulting in 30 fold and 50 fold decreases in bulk density, respectively, with median agglomerate sizes < 8 μm in diameter. These results were obtained while retaining the aspect ratio of the as-received nanomaterial, irrespective of the MWCNT agglomerate morphology. It was found that the supercritical temperature and pressure of 40°C and 7.86 MPa were the optimal temperature and pressure for maximum deagglomeration without damaging the MWCNTs.

The final goal of this work is to apply the $scCO_2$ aided melt blending process to generate polycarbonate/ carbon nanotube (CNT) nanocomposites with enhanced electrical conductivity and improved dispersion while maintaining the aspect ratio of the as-received CNTs. Different degrees of $scCO_2$ processed Baytubes® C 150 P CNT were benignly deagglomerated with $scCO_2$ resulting in 5 fold (5X), 10X, and 15X decreases in bulk density from the as-received CNTs. The CNT were melt compounded with polycarbonate using single screw melt extrusion and compression molded into plaques. A surface conductivity of $4.8 \times 10^{-8} \pm 2.0 \times 10^{-9}$ S was observed for samples prepared with the $scCO_2$ aided melt blending at 15X $scCO_2$ processing.

Electrical percolation thresholds as low as 0.83 wt% were observed for composites prepared with 15X CNTs using the $scCO_2$ aided melt blending method, while concentrations as high as 1.5% are required without $scCO_2$ processing. The percolation concentration in nanocomposites prepared with 15X $scCO_2$ processing and single screw extrusion is competitive with values reported for similar nanocomposites generated using twin screw melt compounding in the literature. Optical microscopy, transmission electron microscopy, and rheology were used to investigate the dispersion and mechanical network of CNTs in the nanocomposites. The dispersion of CNTs generally improved with $scCO_2$ processing compared to direct melt blending but was found to be significantly worse than that of twin screw melt compounded nanocomposites from the literature. Because the percolation thresholds are similar with substantially different extents of dispersion, the importance of maintaining longer CNTs during nanocomposite generation is emphasized.

**Original Contributions**

The following are considered to be significant original contributions of this research:

- The application of the supercritical carbon dioxide aided melt blending method to nylon 6/organically modified montmorillonite nanocomposites was studied. This work is the first to utilize the $scCO_2$ aided melt blending method to generate nanocomposites where the polymer matrix interacts favorably with the clay surface. The mechanical properties of the nanocomposites processed with $scCO_2$ and single screw melt compounding are competitive with twin screw melt compounded nanocomposites reported in the literature.

- The benign deagglomeration of MWCNT bundles using $scCO_2$ processing was investigated. This is the first attempt at quantitatively manipulating the variables during the $scCO_2$ processing of MWCNT agglomerates to obtain the most thorough deagglomeration possible while retaining the aspect ratio of MWCNTs. In addition, this is the first attempt to relate hydrodynamic models for the forces exerted on the MWCNTs during $scCO_2$ processing to the cohesive strength of the agglomerate, generating intuitive relationships between processing variables and the extent of deagglomeration of MWCNT bundles. This analysis enhances the understanding and extent of MWCNT bundle deagglomeration which led to significantly lower processing temperatures and pressures than utilized in previous work. Furthermore, this is the first attempt at correlating the deagglomeration of MWCNT bundles by $scCO_2$ processing to the aspect ratio of the nanomaterial. The MWCNT aspect ratio is maintained during $scCO_2$ deagglomeration, whereas other deagglomeration methods significantly reduce individual MWCNT lengths.

- CNT/polycarbonate nanocomposites were generated using the supercritical carbon dioxide aided melt blending method resulting in nanocomposites with enhanced surface conductivity. The efforts in this work are the first at generating melt compounded CNT nanocomposites while reporting retention of the aspect ratio of the CNTs. Furthermore, this is the first attempt at utilizing the $scCO_2$ aided melt blending method to achieve enhanced electrical properties in polymer nanocomposites. The $scCO_2$ processing of CNTs yields improved dispersion and electrical properties compared to direct blend melt processing. The measured percolation thresholds of samples implementing $scCO_2$ processing approach those of twin screw melt compounded nanocomposites from the literature. However, the dispersion in single screw melt compounded nanocomposites is worse than that of twin screw melt compounded nanocomposites. This phenomenon suggests the importance of retaining the aspect ratio of the CNTs during nanocomposite processing.

**Format of Dissertation**

This dissertation is written in manuscript format. Chapters 3, 4, and 5 are self-contained papers that have been submitted for journal publications, with Chapter 3 currently in print. The details concerning motivation, methodology, results, and conclusions are described in each chapter. The figures and tables referenced in a chapter are provided in the text of the manuscript.

**Acknowledgements**

The author would like to acknowledge his advisor Dr. Donald G. Baird for his support and guidance throughout the course of the author's PhD studies. The author would also like to thank Dr. Michael Bortner for his advice and encouragement, especially in preparation of the preliminary exam and in the editing process of Chapters 4 and 5. Furthermore, the author would like to acknowledge Dr. Erdogan Kiran for thoughtful conversations concerning the author's scientific approach to the dissertation work. The author would also like to thank his other committee members for their input as well: Dr. Stephen Martin and Dr. Robert Moore.

The author appreciates his family's support during his PhD studies. The author is grateful for his parents, and for their love and constant support which have been crucial to him throughout the years. He would also like to express gratitude to his sister and brother, Laura Quigley and James Quigley, whose guidance and friendship have been, and always will be, very important to him. The author would like to thank his extended family for their support.

The author would also like to acknowledge the current and former lab members who had an impact on his life and research:

- Kevin Herrington, Dr. Chen Chen, Chen Qian, Matt Hopkins, Prudvi Gaddam, Dr. Mike Heinzer, Dr. Syed Mazahir, Dr. Kevin Meyer, Dr. John Hofmann, Mark Cieslinski, Jianhua Huang

The author greatly appreciates the Chemical engineering department staff for their kindly assistance during his time at Virginia Tech:

- Tina Russell, Diane Cannaday, Nora Bentley Jane Price, Michael Vaught, Kevin Holshouser, and Riley Chan

Finally, he would like to thank his fiancée, Heather Grandelli. This work would not have been possible without her intelligent advice, understanding, unyielding friendship, and above all, her love. Thank you for everything.

**Table of Contents**

**List of Figures**

**List of Tables**

# Chapter 1. Introduction

The overall goal of this work is to improve the mechanical properties in nylon 6/montmorillonite nanocomposites and the electrical conductivity in polycarbonate/carbon nanotube nanocomposites by developing a supercritical carbon dioxide aided melt blending method. The introductory chapter will attempt to familiarize the reader with the materials, methods, and motivation for this study, followed by the formalized objectives.

## 1.1 Motivation

Polymers as molded materials, particularly thermoplastics, comprise a large portion of the polymer industry. They have been successfully reinforced using various filler materials, including glass fiber, carbon fiber, calcium carbonate, carbon black, and others. To obtain the composite properties desired, concentrations between 10-40 weight percent (wt%) are typical. The polymer/filler composites require such high concentrations due to low interaction potential and low interfacial areas, as well as limited filler properties compared to nanoscale materials. Nanoscale fillers possess fundamental properties, such as electrical and mechanical, greater than those of conventional fillers as reported in the literature. In addition, nanomaterials possess high surface area ratios which can lead to strong interactions between the nanofiller and the host polymer. Coupled with the nanofiller's aforementioned properties, composites with improved dispersion and enhanced properties may be generated at lower concentrations compared to conventional composites [1].

In recent decades nanomaterials have been verified as effective modifiers for thermoplastic materials. The resulting composites are known as nanocomposites, which are defined as a composite containing a material possessing a dimension on the nanometer ($10^{-9}$

meter) length scale. Montmorillonite (MMT) and carbon nanotubes (CNTs) are two particular nanofillers which have accrued a high level of interest in the past 20 years [2-5]. Thermoplastic nanocomposites of MMT and CNT have been shown to possess superior mechanical, conductive, thermal, and barrier properties compared to other materials, with potential for replacing current composites in industry [4, 6-9].

MMT is typically used to enhance mechanical properties in thermoplastics to replace traditional fillers such as glass fiber. An example of this is the mechanical reinforcement imparted by MMT in nylon 6, which is compared with that of glass fiber in Figure 1.1.

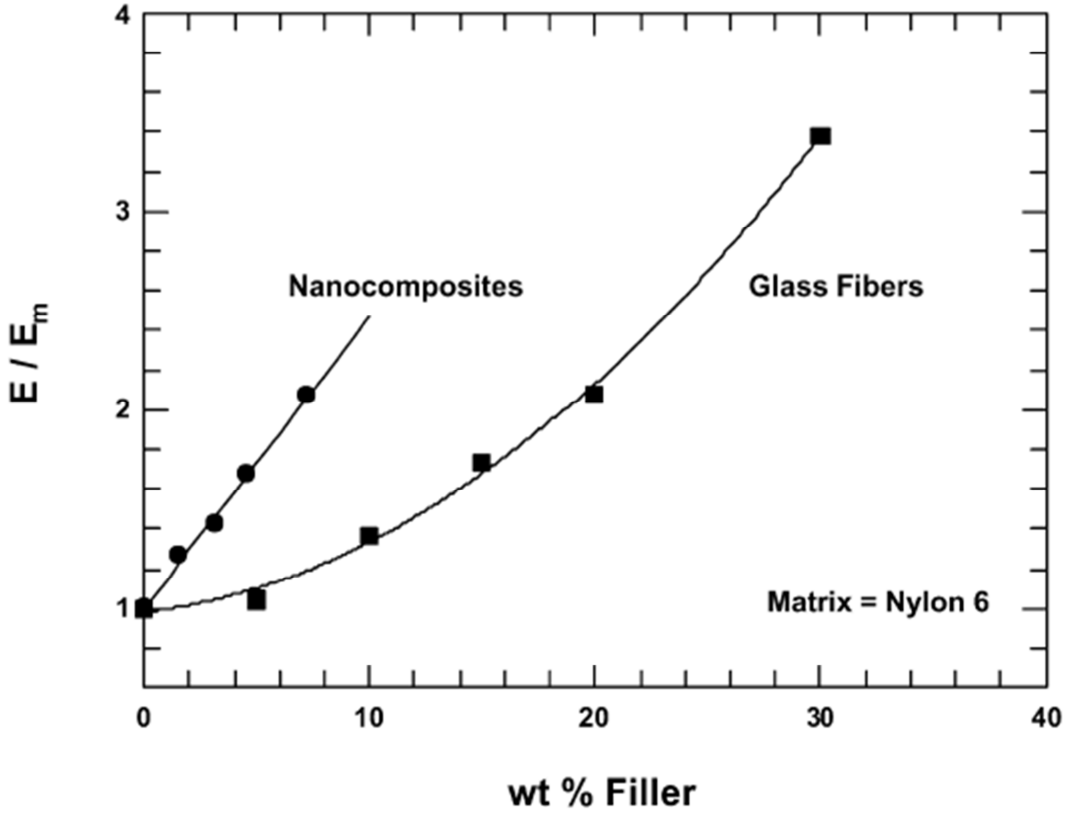


Figure 1.1. Comparison of Young's modulus improvements of nylon 6 with glass fiber and MMT for melt compounded composites, modified from [7]

The samples in Figure 1.1 when prepared using twin screw melt compounding, which will be discussed in more depth in Section 1.3. Figure 1.1 demonstrates that when an MMT/ polymer nanocomposite is processed effectively using a polymer (nylon 6) which can interact with the MMT surface, the Young's moduli of the nanocomposite may exceed those of current glass fiber composites. A twofold increase in modulus requires nearly three times the weight of glass fiber compared to OMMT for melt compounded nylon 6 composites which is illustrated in Figure 1.1. This is particularly attractive where light weight composites are desired in automotive applications to improve fuel economy or other high performance applications [5].

In the case of CNTs, the potential exists to replace carbon black as a conductive filler material [4, 5]. A schematic representation comparing the amount of CNTs or carbon black needed to reach electrical percolation in a thermoplastic composite is provided in Figure 1.2.

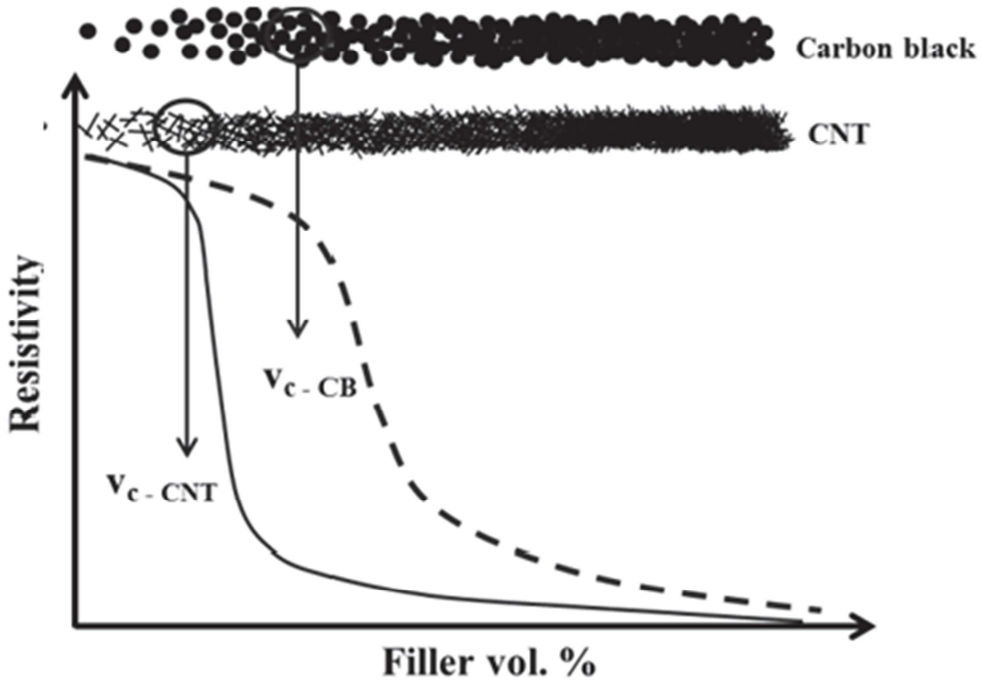


Figure 1.2. Schematic of electrical percolation thresholds for traditional filler (carbon black) compared to carbon nanotubes, modified from [10]

CNT nanocomposites possess the potential for significantly lower electrical percolation values due to CNTs' high aspect ratios and inherent conductivity compared to conventional conductive fillers. In a recent study, twin screw melt compounding was used to prepare composites of both CNTs and carbon black with polycarbonate. The authors observed that the carbon black composite required 4 times the amount of filler to reach electrical percolation (2wt% CNTs versus 8.75 wt% carbon black) [11]. These materials are of particular interest in high performance materials, where conductive properties associated with electrostatic dissipation may be accompanied by increased mechanical reinforcement from the CNTs [12].

## 1.2 Nanofillers

In this section, carbon nanotubes and montmorillonite will be introduced as the nanofillers used in this study. The structure and properties of each will be discussed, along with the challenges for efficiently dispersing the material in polymeric nanocomposites to obtain improved composite properties.

### 1.2.1 Nanoclay

Montmorillonite (MMT), or nanoclay as it will be referred to throughout this document, is a naturally occurring layered silicate with interesting properties for use in polymer nanocomposites. Due to its large surface area, high aspect ratio, and exceptional stiffness, MMT has received significant attention in the past 20 years [2, 5, 7, 9, 13]. Naturally occurring MMT presents as a stack of individual platelets, known as tactoids. The thickness of an individual platelet is approximately 1 nm, and the spaces between the clay platelets are known as galleries, possessing dimensions around 0.2 nm. A schematic of an MMT stack is presented in Figure 1.3

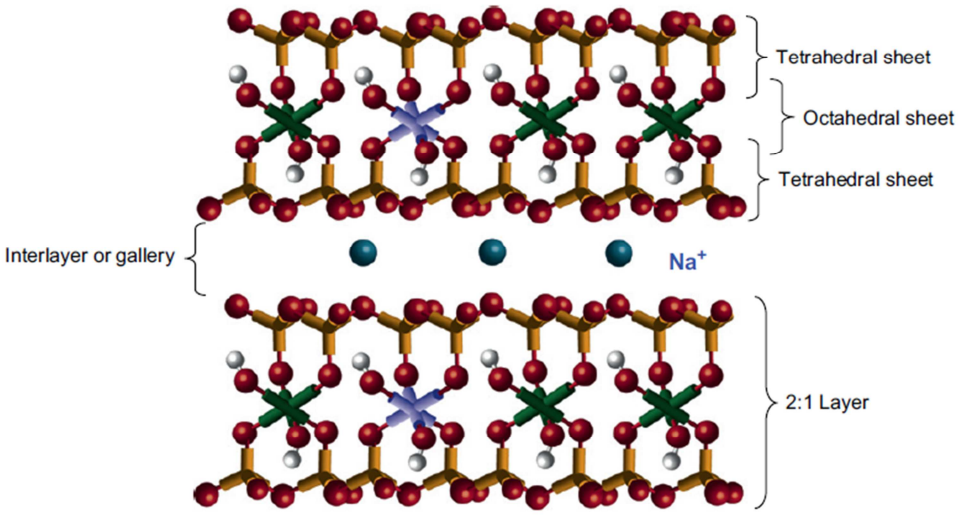


Figure 1.3. Schematic drawing of sodium montmorillonite modified from [5]

Montmorillonite platelets have lengths in the longest dimension between 100 nm and 200 nm, yielding average aspect ratios of roughly 150 [14, 15]. The high aspect ratio of montmorillonite promotes flow induced alignment which is important in providing mechanical reinforcement to thermoplastic nanocomposites. Montmorillonite is a very stiff material, with a theoretical modulus between 300 and 400 GPa from molecular simulations [16]. MMT also possesses a large surface area to volume ratio, promoting interactions of the polymer with the surface of the nanoclay. MMT may provide biaxial reinforcement in composites rather than uniaxial as is the case in fibers or rods due to its intrinsic platelet geometry.

The separation of MMT clay platelets from tactoids during nanocomposite processing may yield an immiscible, intercalated, or exfoliated morphology. Either exfoliated or partially exfoliated/intercalated nanocomposite morphologies are desired in the production of nanoclay composites to take advantage of the mechanical properties of individual platelets [2, 17, 18]. Intercalated clay morphology occurs when polymer chains diffuse into the gallery spacing of the layered structure, resulting in an increased gallery spacing on the order of a few nanometers [19].

The intercalated and exfoliated morphology both involve nano-scale reinforcement. If the clay layers are completely separated to create a disordered array, the composite is considered "exfoliated". However, the exfoliated morphology is difficult to obtain through traditional polymer nanocomposite generation processes due to the hydrophilic nature of MMT. In addition, the small gallery spacing (~1 nm) results in significant entropic barriers to polymer and solution transport which are crucial to separating the clay tactoids and improving nanocomposite properties.

In order to overcome the issues of immiscibility and polymer diffusion, organically modified montmorillonite (OMMT) has been developed. OMMT is naturally occurring MMT that has undergone a cation exchange reaction, replacing the hydrophilic cation on the surface of the phyllosilicate with an organic modification. This modification can vary depending on the application, but usually includes a long chain hydrocarbon to increase the gallery spacing between platelets. The average distance between clay layers increases by between 2 and 3 fold after surface modification, proving more space for the polymer to diffuse between the platelets [20, 21]. Therefore, the organic modification allows the nanoclay to interact with the polymer matrix while reducing the entropic barrier to polymer diffusion [17, 22]. Many nanoclay nanocomposites suffer from poor dispersion of the nanofiller even with organic modification due to the strong van der Waals interactions between clay platelets, leading to poor mechanical reinforcement. The exception is in nanocomposites of OMMT and polar polymers, such as nylon 6, where significant mechanical property enhancements have been reported [3, 23]. Following dispersion of the nanoclay, a processing method which promotes preferential orientation of the nanofiller in the field of flow must be accomplished to achieve the maximum mechanical reinforcement [7].

### 1.2.2 Carbon nanotubes

Following Iijima's publication on multi-wall carbon nanotubes (MWCNTs) in 1991, tremendous interest has focused on carbon nanotubes (CNTs) and their applications [24]. This is especially evident in the field of CNT reinforced composite materials due to their potential mechanical and conductive property enhancements [25, 26]. Carbon nanotubes are long cylinders of covalently bonded carbon atoms, essentially made up of rolled graphene. Idealized depictions of both single walled and multi walled carbon nanotubes are shown in Figure 1.4

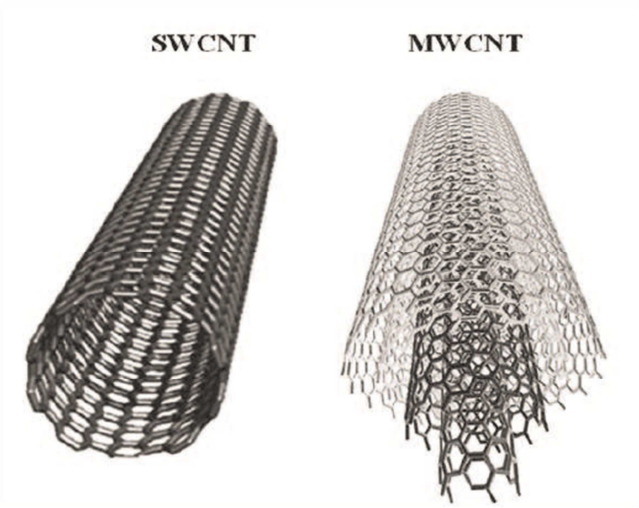


Figure 1.4. Depictions of SWCNT and MWCNT, respectively, modified from [27]

Single-walled carbon nanotubes (SWCNT) are comprised of a single sheet of rolled graphene resulting in a single nanotube, whereas multi-walled nanotubes (MWCNT) consist of concentrically rolled graphene sheets. Multi-walled nanotubes (MWCNT) typically possess diameters between 1 and 20 nm. The aspect ratio of CNT can reach values as high as several hundred thousand for long tubes. The intrinsic high aspect ratio of these materials has the potential to yield very low electrical percolation thresholds as well as significant mechanical reinforcement in thermoplastic nanocomposites [27, 28].

CNT are interesting candidates for nanocomposite reinforcement due to their intrinsic electrical and mechanical properties. The electrical conductivity of CNT have been reported to approach 2 x $10^7$ S m, which is similar to that of copper [29]. The mechanical properties of CNT are also impressive. The Young's Moduli and yield strength have been experimentally measured using atomic force microscopy. The moduli observed in these works range from 270 GPa to 1 TPa, and the measured strengths vary from 11 GPa to 200 GPa [30, 31]. CNT are synthesized by three methods: arc discharge, laser ablation, and chemical vapor deposition. Nanotubes produced by these methods typically contain surface defects which have been shown to decrease the electrical and mechanical properties. In addition, CNT obtained from industry typically exist in the form of large primary agglomerates which must be separated and dispersed in the polymer to take advantage of the individual CNT properties.

Commercially available CNT are typically provided in very large agglomerates with many entangled CNT. These bundles arise due to structural defects during the growth phase of synthesis, and van der Waals interactions between CNT. Examples of primary MWCNT agglomerates are shown in Figure 1.5.

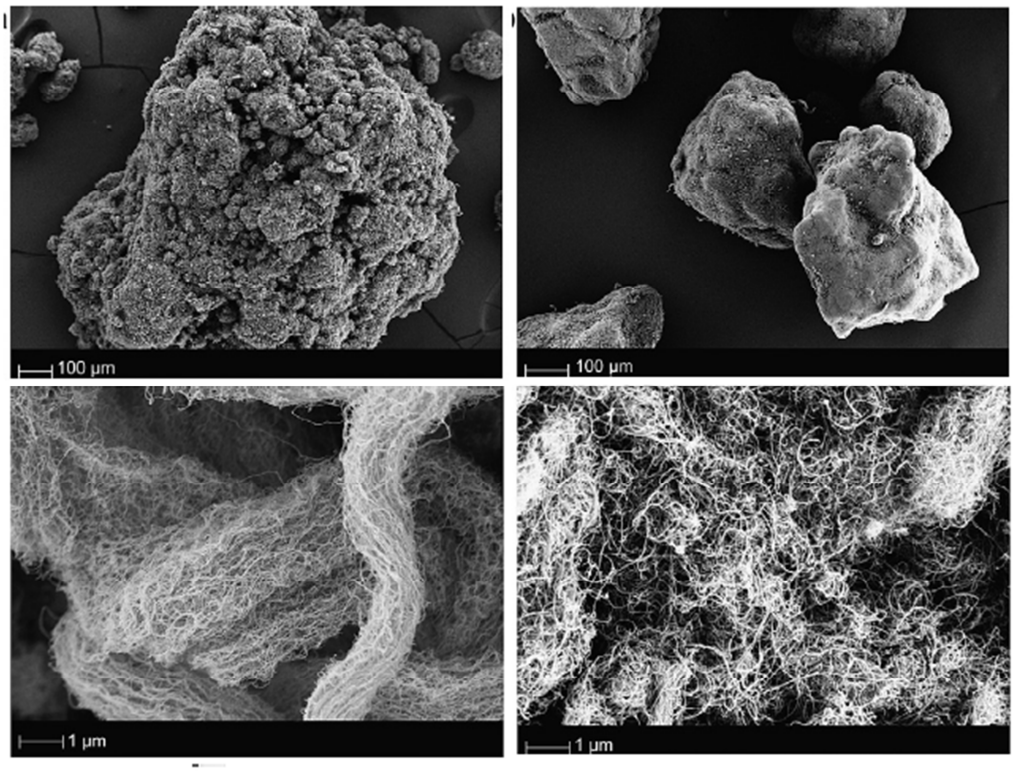


Figure 1.5. Example of primary agglomerates of CNT produced via chemical vapor deposition at low (top) and high (bottom) magnifications. Images on left are from- NC7000, CNT from Nanocyl, and images on right are from-Baytube C150P CNT from BayerMaterialscience. Modified from [6]

In the dispersion of large CNT agglomerates by fluid media, agglomerates are wetted by fluid, infiltrated by the fluid, and then broken apart by erosion and rupture mechanisms under applied stresses. Following erosion and rupture, nanotubes can be distributed homogenously within the polymer matrix [6, 32]. Efficient dispersion is an especially difficult task in nanocomposite generation, and generally requires intensive mixing through high shear melt compounding or sonication. However, both of these mixing methods can damage the CNT significantly when non-wetted agglomerate cores are ruptured. This may result in reduced mechanical and electrical properties for the nanocomposites [33, 34].

Both CNT and MMT possess interesting dimensions and material properties which make them interesting candidates for use in thermoplastic nanocomposites. In order to take advantage

of these material properties the nanofillers must be properly dispersed in the polymer matrix using an appropriate nanocomposite generation method. These methods will be discussed in the following section.

### 1.3 Nanocomposite generation methods

Current nanocomposites production methods include *In situ* polymerization, solution blending, and melt compounding. Individualization of the nanomaterial is desired during processing to obtain composites with improved properties. Nanocomposite generation must be accomplished while maintaining the integrity of the nanofiller, reducing processing costs, and with environmental consideration. The methods mentioned possess both advantages and drawbacks which will be briefly discussed in this section. Emphasis will be placed on the melt compounding of nylon6/OMMT and PC/CNT nanocomposites as they pertain to this study.

### 1.3.1 *In situ* polymerization

The *In situ* polymerization synthesis of thermoplastic nanocomposites begins with swelling of the nanomaterial with monomer or catalyst followed by polymerization. This is sometimes coupled with sonication which allows CNT or nanoclay to disperse effectively in the monomer. The polymerization step may force the nanomaterial apart, dispersing the filler during polymer synthesis [26, 35]. *In situ* polymerization was the method first used to synthesize nanoclay nanocomposites by the Toyota group in 1993 using nylon 6 and nanoclay [23]. The authors observed an increase in tensile modulus from 1.11 GPa to 1.87 GPa with the addition of 4.7 wt% clay. This method has successfully been applied to other systems of both CNT and MMT nanocomposites [36-43]. The drawbacks to *In situ* polymerization include long processing times, and the use of harmful solvents. In addition, this method is limited to certain types of polymers. More environmentally benign, flexible, and industrially scalable methods are desired to produce thermoplastic nanocomposites.

### 1.3.2 Solution blending

Solution blending is a common method for both nanoclay and CNT nanocomposite formation. In this technique the nanomaterial is suspended in a suitable solvent, which contains the polymer or a prepolymer, and dispersed with the aid of sonication. Following the dispersion step, the solvents can be removed either by drying in a vacuum oven for several days [44], or by using a co-solvent to “dry” the nanocomposite. Film casting methods and precipitation are also cited in the literature as viable approaches [4, 45]. Solution blending can lead to well dispersed nanocomposites, and is of interest where few raw materials are available. However, solution blending requires sonicative mixing which is expensive to scale, and can decrease the CNT aspect ratio [34]. Furthermore, the solvents required during processing may be environmentally

harmful, and are specific to a polymer-nanomaterial system making this method less flexible to other nanocomposites.

### 1.3.3 Melt compounding

Melt compounding is the preferable route to nanocomposite generation due to its scalability, low environmental impact, and flexibility [5, 6]. For most nanocomposites, sufficient dispersion of the nanofiller remains the largest obstacle in obtaining enhanced composite properties. If an affinity between the nanofiller and the polymer matrix does not exist, then dispersion is difficult to achieve. Intensive mixing with high shear [6, 32, 46-48], or the inclusion of compatibilizers are required to achieve sufficient dispersion for improved nanocomposite properties [49-57].

Melt processing of CNT nanocomposites can lead to nanocomposites with well dispersed nanomaterial and low electrical percolation thresholds, but may also damage the CNT during processing. Villmow et al. [48] studied the effects of screw configuration, residence time, and mixing elements on CNT morphology in polycaprolactone/CNT nanocomposites prepared with twin screw melt compounding. The authors observed significantly relatively low electrical percolation thresholds (~0.24 volume % CNT) when the CNT were well dispersed in the nanocomposite. In later work, CNT nanocomposites processed by the same method were analyzed to determine if twin screw melt compounding shortens the CNT. It was observed that the CNT were reduced by 70% of their initial length [33]. This occurs through rupture of the dry agglomerate core when high stresses are applied, breaking the agglomerate and entangled CNT in the process [32]. The reduction in aspect ratio may reduce the mechanical and electrical properties in the generated nanocomposite. Therefore, it is desired to overcome CNT damage during melt compounding of CNT nanocomposites.

Studies carried out by the Toyota research group in the early 90's have led to efforts in the field of melt compounded nanoclay-nylon 6 nanocomposites [3, 5, 46, 58, 59]. In work by Fornes et al. [11], a co-rotating twin screw extruder was used to melt compound nylon 6/ Cloisite 30B composites which were injection molded into tensile bars. They observed a 59% increase in modulus from the virgin matrix, from 2.75 GPa to 4.38 GPa for 6.1 wt % organoclay [59]. This study also investigated the effect of different organic modifiers on nylon 6 nanocomposite morphology and mechanical properties. They reported that increasing the OMMT organic modifier content beyond a critical value acts to shield nylon 6 from interacting with the clay surface. Improved dispersion of the nanofiller may be obtained by increasing the spacing between nanoclay platelets without increasing shielding effects from further organic modification, yielding nanocomposites with improved mechanical properties. This assertion may only apply to nanocomposite with favorable polymer-clay interactions, as increasing the amount of organic modifier in polyolefin nanocomposites has led to improved mechanical properties [9].

The main issue preventing widespread industrial melt processing of thermoplastic nanocomposites is efficient dispersion of the nanofiller. In systems where strong polymer-nanomaterial interactions do not exist, sufficient dispersion requires significant mixing energy through shear, sonication, or other methods. Furthermore, damage to CNTs occurs when processing with sonication and high shear mixing devices, resulting in diminished nanocomposite properties. The use of supercritical carbon dioxide ($scCO_2$) to process nanomaterial followed by melt compounding is of interest to overcome these issues.

### 1.4 Supercritical carbon dioxide aided melt blending

Carbon dioxide is non-toxic, non-flammable, abundant, recoverable, and possesses a low critical point compared to other fluids ($T_c$ = 31.1$^o$C, $P_c$ = 1073 psi). Supercritical carbon dioxide

($scCO_2$) possesses gas like viscosity and diffusivity, while retaining the swelling and solvent properties of typical organic solvents. $scCO_2$ has been investigated for several uses in polymer processing. These include foaming [60], plasticization of polymer melts [61-64], and to replace organic solvents during solution blending and *In situ* polymerization [65]. Supercritical carbon dioxide has also been reported as a processing aid during melt compounding of thermoplastic nanocomposites [47, 50, 66-75].

The use of supercritical carbon dioxide ($scCO_2$) in combination with single screw compounding has been considered as an alternative route for the preparation of polymer-clay nanocomposites in order to achieve improved dispersion leading to enhanced mechanical properties [47, 50, 66-75]. In this process, the nanoclay layers are delaminated by catastrophically depressurizing the $scCO_2$ from a pressurized vessel containing the nanomaterial. The $scCO_2$ treatment has been reported to increase the distance between nanoclay platelets, as is shown in Figure 1.6.

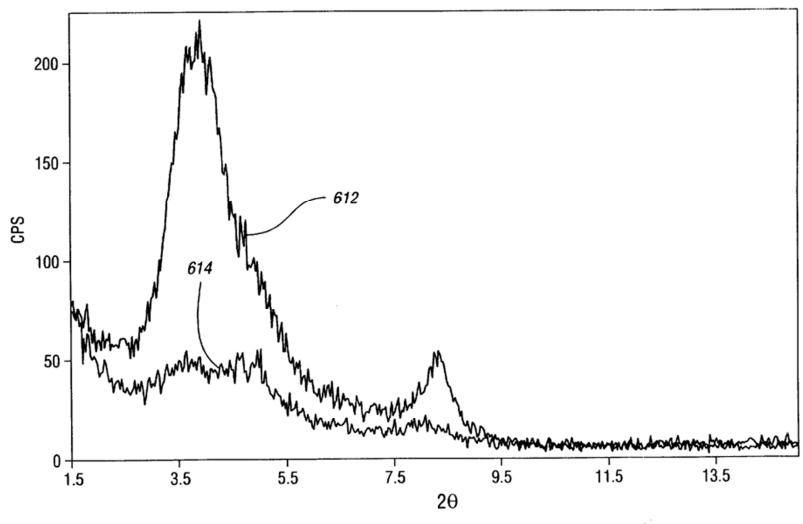


Figure 1.6. Wide angle X-ray diffraction (WAXD) pattern of nanoclay before (612) and after (614) $scCO_2$ treatment, modified from [71]

Following $scCO_2$ treatment, the nanoclay is melt compounded with the polymer to produce a nanocomposite. The increased interlayer spacing between nanoclay platelets promotes dispersion of the nanoclay in the polymer matrix, leading to enhanced mechanical properties. In a more recent study in our laboratory by Chen et al. [76], a semi-continuous method was developed that improved the nanoclay dispersion and mechanical properties in polypropylene nanocomposites with the aid of $scCO_2$. In this method, the $scCO_2$ and nanoclay is catastrophically depressurized over the polymer pellet bed of a modified hopper. The mixture is then melt compounded in a single screw extruder and pelletized. The initial efforts studying this method have focused on the use of nonpolar polymers such as polypropylene (PP), where an increase in modulus was observed with increasing clay concentration up to 10 wt% [76]. The most recent work in our laboratory investigated the effect of including a compatibilizer (maleated polypropylene (PP-*g*-Ma)) in this system [50]. A 41% increase in modulus was observed at 5 wt% organoclay for nanocomposites generating using the $scCO_2$ aided melt blending method. Alternatively, an increase in modulus of 61% was measured for nanocomposites processed with a 3:1 organoclay: PP-*g*-Ma ratio at 5 wt% organoclay. This suggested that polar clay/polymer interactions could be enhanced with the $scCO_2$ aided melt blending method. It was proposed in Section 1.3 that if the d-spacing of OMMT could be increased without increasing shielding effects then better interactions might be obtained in nanocomposites with preferential bonding between the nanofiller and polymer matrix. It follows that $scCO_2$ aided melt compounding could be used to improve the dispersion of OMMT in nylon 6 nanocomposites where significant interactions have been reported, therefore enhancing the mechanical properties.

The rapid expansion of a suspension consisting of supercritical carbon dioxide ($scCO_2$) and CNT has been cited in the literature as a benign way to deagglomerate CNT. Gulari et al.

[73] obtained a patent in 2008 suggesting this. In this patent, they provide a method of treating nanotubes with $scCO_2$ with the goal of coating the CNT with polymer before melt compounding. Previous work by Chen et. al. [75] in our lab investigated the $scCO_2$ expansion of CNT followed by melt compounding with a single screw extruder. The authors observed improved mechanical properties in polyphenylsulfone nanocomposites. In that effort, an initial optimization of the $scCO_2$ process was conducted, resulting in a ~6 fold decrease in the bulk density of the CNT (Nanocyl-NC7000). It was suspected that nanotubes were not damaged, but not verified by transmission electron microscopy (TEM). Other work has focused on using $scCO_2$ to separate nanotubes agglomerates without incorporation of the CNT into a composite. To et. al.[77] processed CNT bundles using a method known as the Rapid Expansion of Supercritical Suspensions (RESS). The authors in that work conducted limited SEM studies to investigate the final particle sizes, and did not mix the CNT with a polymer matrix. Furthermore, To et al. [77] did not attempt to improve, or understand this process. It is suspected that by studying the $scCO_2$ treatment of CNT bundles, more thorough deagglomeration may be achieved without damaging the nanomaterial. Coupling this with melt compounding by single or high shear mixing may yield nanocomposites with low electrical percolation thresholds.

The subjects reviewed in this introduction suggest three topics which may be investigated in order to advance the field of thermoplastic nanocomposite processing. Work by Chen et al. [50] on nanocomposites of slightly polar nanoclay and PP-*g*-Ma prepared by the $scCO_2$ aided melt blending method indicates that this method may be applied to highly polar polymer/ organoclay combinations, such as nylon 6/OMMT, to obtain superior mechanical properties compared to similar nanocomposites generated with conventional melt blending. Secondly, the $scCO_2$ processing of CNT must be studied in order to investigate the effect of processing

variables on the deagglomeration of CNT bundles, and the extent of damage to individual CNT following deagglomeration. Finally, the effect of improved deagglomeration of CNT bundles by $scCO_2$ processing on the $scCO_2$ aided melt blending method must be investigated. The benign deagglomeration of CNT may result in longer CNT than current melt compounding methods, yielding nanocomposites with low percolation thresholds and improved dispersion [75, 77, 78].

## 1.5 Statement of Objectives

This work is primarily focused on improving the properties of thermoplastic nanocomposites using a $scCO_2$ aided melt blending method. Three objectives have been proposed to accomplish this goal:

1. Investigate the ability of $scCO_2$ aided melt blending to enhance the dispersion of organically modified montmorillonite and improve the associated mechanical properties for highly interactive nanocomposites of organoclay and nylon 6.
2. Improve the supercritical carbon dioxide processing of carbon nanotube bundles to separate commercially available agglomerates as completely as possible while retaining the aspect ratio of the CNT.
3. Determine the effect of the improved $scCO_2$ aided melt blending on the surface conductivity of CNT/polycarbonate nanocomposites.

## References


[1] A. Okada and A. Usuki, "Twenty Years of Polymer-Clay Nanocomposites," *Macromolecular Materials and Engineering,* vol. 291, 2006.

[2] M. Alexandre and P. Dubois, "Polymer-layered silicate nanocomposites: preparation, properties and uses of a new class of materials," *Materials Science & Engineering R-Reports,* vol. 28, 2000.

[3] J.W. Cho and D.R. Paul, "Nylon 6 nanocomposites by melt compounding," *Polymer,* vol. 42, 2001.

[4] T. MacNally and P. Potschke, *Polymer Carbon Nanotube Composites: Preparation, Properties and Applications*. 2011: Woodhead Publishing Limited.

[5] D.R. Paul and L.M. Robeson, "Polymer nanotechnology: Nanocomposites," *Polymer,* vol. 49, 2008.

[6] I. Alig, P. Potschke, D. Lellinger, T. Skipa, S. Pegel, G.R. Kasaliwal, and T. Villmow, "Establishment, morphology and properties of carbon nanotube networks in polymer melts," *Polymer,* vol. 53, 2012.

[7] T.D. Fornes and D.R. Paul, "Modeling properties of nylon 6/clay nanocomposites using composite theories," *Polymer,* vol. 44, 2003.

[8] A.K.-T. Lau and D. Hui, "The revolutionary creation of new advanced materials—carbon nanotube composites," *Composites Part B: Engineering,* vol. 33, 2002.

[9] H.S. Lee, P.D. Fasulo, W.R. Rodgers, and D.R. Paul, "TPO based nanocomposites. Part 1. Morphology and mechanical properties," *Polymer,* vol. 46.

[10] H. Sang-ha, P. Young-Bin, H.Y. Kwan, and S.B. Dae, *Smart Materials and Structures Based on Carbon Nanotube Composites*. Carbon Nanotubes - Synthesis, Characterization, Applications. 2011.

[11] P. Potschke, M. Abdel-Goad, S. Pegel, D. Jehnichen, J.E. Mark, D.H. Zhou, and G. Heinrich, "Comparisons Among Electrical and Rheological Properties of Melt-Mixed Composites Containing Various Carbon Nanostructures," *Journal of Macromolecular Science Part a-Pure and Applied Chemistry,* vol. 47, 2010.

[12] M.D. Via, J.A. King, J.M. Keith, and G.R. Bogucki, "Electrical conductivity modeling of carbon black/polycarbonate, carbon nanotube/polycarbonate, and exfoliated graphite nanoplatelet/polycarbonate composites," *Journal of Applied Polymer Science,* vol. 124, 2012.

[13] P.C. LeBaron, Z. Wang, and T.J. Pinnavaia, "Polymer-layered silicate nanocomposites: an overview," *Applied Clay Science,* vol. 15, 1999.

[14] H.J. Ploehn and C.Y. Liu, "Quantitative analysis of montmorillonite platelet size by atomic force microscopy," *Industrial & Engineering Chemistry Research,* vol. 45, 2006.

[15] H. Van Olphen, "An introduction to clay colloid chemistry," *Journal of Pharmaceutical Sciences,* vol. 53, 1964.

[16] O.L. Manevitch and G.C. Rutledge, "Elastic properties of a single lamella of montmorillonite by molecular dynamics simulation," *Journal of Physical Chemistry B,* vol. 108, 2004.

[17] R.A. Vaia, K.D. Jandt, E.J. Kramer, and E.P. Giannelis, "Microstructural evolution of melt intercalated polymer-organically modified layered silicates nanocomposites," *Chemistry of Materials,* vol. 8, 1996.

[18] E.P. Giannelis, "Polymer layered silicate nanocomposites," *Advanced Materials,* vol. 8, 1996.
[19] S.S. Ray and M. Okamoto, "Polymer/layered silicate nanocomposites: a review from preparation to processing," *Progress in Polymer Science,* vol. 28, 2003.
[20] H. Heinz, R.A. Vaia, R. Krishnamoorti, and B.L. Farmer, "Self-Assembly of Alkylammonium Chains on Montmorillonite: Effect of Chain Length, Head Group Structure, and Cation Exchange Capacity," *Chemistry of Materials,* vol. 19, 2006.
[21] D.R. Paul, Q.H. Zeng, A.B. Yu, and G.Q. Lu, "The interlayer swelling and molecular packing in organoclays," *Journal of Colloid and Interface Science,* vol. 292, 2005.
[22] E. Giannelis, "A new strategy for synthesizing polymer-ceramic nanocomposites," *JOM,* vol. 44, 1992.
[23] A. Usuki, Y. Kojima, M. Kawasumi, A. Okada, Y. Fukushima, T. Kurauchi, and O. Kamigaito, "SYNTHESIS OF NYLON 6-CLAY HYBRID," *Journal of Materials Research,* vol. 8, 1993.
[24] S. Iijima, "Helical Microtubules of Graphitic Carbon," *Nature,* vol. 354, 1991.
[25] E.T. Thostenson, Z.F. Ren, and T.W. Chou, "Advances in the science and technology of carbon nanotubes and their composites: a review," *Composites Science and Technology,* vol. 61, 2001.
[26] J.N. Coleman, U. Khan, W.J. Blau, and Y.K. Gun'ko, "Small but strong: A review of the mechanical properties of carbon nanotube-polymer composites," *Carbon,* vol. 44, 2006.
[27] V. Choudhary and A. Gupta, *Polymer/Carbon Nanotube Nanocomposites*. Carbon Nanotubes - Polymer Nanocomposites. 2011.
[28] F. Hussain, M. Hojjati, M. Okamoto, and R.E. Gorga, "Review article: Polymer-matrix nanocomposites, processing, manufacturing, and application: An overview," *Journal of Composite Materials,* vol. 40, 2006.
[29] T.W. Ebbesen, H.J. Lezec, H. Hiura, J.W. Bennett, H.F. Ghaemi, and T. Thio, "Electrical conductivity of individual carbon nanotubes," *Nature,* vol. 382, 1996.
[30] J.P. Salvetat, A.J. Kulik, J.M. Bonard, G.A.D. Briggs, T. Stockli, K. Metenier, S. Bonnamy, F. Beguin, N.A. Burnham, and L. Forro, "Elastic modulus of ordered and disordered multiwalled carbon nanotubes," *Advanced Materials,* vol. 11, 1999.
[31] J.P. Salvetat, G.A.D. Briggs, J.M. Bonard, R.R. Bacsa, A.J. Kulik, T. Stockli, N.A. Burnham, and L. Forro, "Elastic and shear moduli of single-walled carbon nanotube ropes," *Physical Review Letters,* vol. 82, 1999.
[32] G.R. Kasaliwal, S. Pegel, A. Goldel, P. Potschke, and G. Heinrich, "Analysis of agglomerate dispersion mechanisms of multiwalled carbon nanotubes during melt mixing in polycarbonate," *Polymer,* vol. 51, 2010.
[33] B. Krause, R. Bolcit, and P. Potschke, "A method for determination of length distributions of multiwalled carbon nanotubes before and after melt processing," *Carbon,* vol. 49, 2011.
[34] K.L. Lu, R.M. Lago, Y.K. Chen, M.L.H. Green, P.J.F. Harris, and S.C. Tsang, "Mechanical damage of carbon nanotubes by ultrasound," *Carbon,* vol. 34, 1996.
[35] V. Mittal, *Characterization techniques for polymer nanocomposites*. Polymer nano-, micro- & macrocomposites,. 2012, Weinheim: Wiley-VCH. xvii, 360 p.
[36] A. Akelah and A. Moet, "Polymer-clay nanocomposites: Free-radical grafting of polystyrene on to organophilic montmorillonite interlayers," *Journal of Materials Science,* vol. 31, 1996.

[37] M. Alexandre, P. Dubois, T. Sun, J.M. Garces, and R. Jerome, "Polyethylene-layered silicate nanocomposites prepared by the polymerization-filling technique: synthesis and mechanical properties," *Polymer,* vol. 43, 2002.

[38] H.G.G. Dekking, "Propagation of vinyl polymers on clay surfaces. II. Polymerization of monomers initiated by free radicals attached to clay," *Journal of Applied Polymer Science,* vol. 11, 1967.

[39] P. Dubois, M. Alexandre, F. Hindryckx, and R. Jerome, "Polyolefin-based composites by polymerization-filling technique," *Journal of Macromolecular Science-Reviews in Macromolecular Chemistry and Physics,* vol. C38, 1998.

[40] P.M. Ajayan, O. Stephan, C. Colliex, and D. Trauth, "Aligned Carbon Nanotube Arrays Formed by Cutting a Polymer Resin-Nanotube Composite," *Science,* vol. 265, 1994.

[41] D. Baskaran, J.W. Mays, and M.S. Bratcher, "Polymer-grafted multiwalled carbon nanotubes through surface-initiated polymerization," *Angewandte Chemie-International Edition,* vol. 43, 2004.

[42] A. Funck and W. Kaminsky, "Polypropylene carbon nanotube composites by in situ polymerization," *Composites Science and Technology,* vol. 67, 2007.

[43] Z.J. Jia, Z.Y. Wang, C.L. Xu, J. Liang, B.Q. Wei, D.H. Wu, and S.W. Zhu, "Study on poly(methyl methacrylate)/carbon nanotube composites," *Materials Science and Engineering a-Structural Materials Properties Microstructure and Processing,* vol. 271, 1999.

[44] B.P. Grady, F. Pompeo, R.L. Shambaugh, and D.E. Resasco, "Nucleation of polypropylene crystallization by single-walled carbon nanotubes," *Journal of Physical Chemistry B,* vol. 106, 2002.

[45] Y. Xi, A. Yamanaka, Y.Z. Bin, and M. Matsuo, "Electrical properties of segreated ultrahigh molecular weight polyethylene/multiwalled carbon nanotube composites," *Journal of Applied Polymer Science,* vol. 105, 2007.

[46] L.M. Liu, Z.N. Qi, and X.G. Zhu, "Studies on nylon 6 clay nanocomposites by melt-intercalation process," *Journal of Applied Polymer Science,* vol. 71, 1999.

[47] C. Chen, J. Samaniuk, D.G. Baird, G. Devoux, M. Zhang, R.B. Moore, and J.P. Quigley, "The preparation of nano-clay/polypropylene composite materials with improved properties using supercritical carbon dioxide and a sequential mixing technique," *Polymer,* vol. 53, 2012.

[48] T. Villmow, B. Kretzschmar, and P. Potschke, "Influence of screw configuration, residence time, and specific mechanical energy in twin-screw extrusion of polycaprolactone/multi-walled carbon nanotube composites," *Composites Science and Technology,* vol. 70, 2010.

[49] N.N. Bhiwankar and R.A. Weiss, "Melt intercalation/exfoliation of polystyrene-sodium-montmorillonite nanocomposites using sulfonated polystyrene ionomer compatibilizers," *Polymer,* vol. 47, 2006.

[50] C. Chen and D.G. Baird, "Dispersion of nano-clay at higher levels into polypropylene with carbon dioxide in the presence of maleated polypropylene," *Polymer,* vol. 53, 2012.

[51] F.C. Chiu, S.M. Lai, J.W. Chen, and P.H. Chu, "Combined effects of clay modifications and compatibilizers on the formation and physical properties of melt-mixed polypropylene/clay nanocomposites," *Journal of Polymer Science Part B-Polymer Physics,* vol. 42, 2004.

[52] N. Hasegawa, M. Kawasumi, M. Kato, A. Usuki, and A. Okada, "Preparation and mechanical properties of polypropylene-clay hybrids using a maleic anhydride-modified polypropylene oligomer," *Journal of Applied Polymer Science,* vol. 67, 1998.

[53] Q.T. Nguyen and D.G. Baird, "Dispersion of nanoclay into polypropylene with carbon dioxide in the presence of maleated polypropylene," *Journal of Applied Polymer Science,* vol. 109, 2008.

[54] Y. Tang and M. Lewin, "Maleated polypropylene OMMT nanocomposite: Annealing, structural changes, exfoliated and migration," *Polymer Degradation and Stability,* vol. 92, 2007.

[55] K.H. Wang, M.H. Choi, C.M. Koo, Y.S. Choi, and I.J. Chung, "Synthesis and characterization of maleated polyethylene/clay nanocomposites," *Polymer,* vol. 42, 2001.

[56] Y. Wang, F.B. Chen, and K.C. Wu, "Twin-screw extrusion compounding of polypropylene/organoclay nanocomposites modified by maleated polypropylenes," *Journal of Applied Polymer Science,* vol. 93, 2004.

[57] Y. Wang, F.B. Chen, K.C. Wu, and J.C. Wang, "Shear rheology and melt compounding of compatibilized-polypropylene nanocomposites: Effect of compatibilizer molecular weight," *Polymer Engineering and Science,* vol. 46, 2006.

[58] T.D. Fornes and D.R. Paul, "Crystallization behavior of nylon 6 nanocomposites," *Polymer,* vol. 44, 2003.

[59] T.D. Fornes, P.J. Yoon, D.L. Hunter, H. Keskkula, and D.R. Paul, "Effect of organoclay structure on nylon 6 nanocomposite morphology and properties," *Polymer,* vol. 43, 2002.

[60] E. Kiran, "Foaming strategies for bioabsorbable polymers in supercritical fluid mixtures. Part I. Miscibility and foaming of poly(L-lactic acid) in carbon dioxide plus acetone binary fluid mixtures," *Journal of Supercritical Fluids,* vol. 54, 2010.

[61] J.S. Chiou, J.W. Barlow, and D.R. Paul, "Plasticization of glassy polymers by CO2," *Journal of Applied Polymer Science,* vol. 30, 1985.

[62] A. Garg, E. Gulari, and C.W. Manke, "Thermodynamics of Polymer Melts Swollen with Supercritical Gases," *Macromolecules,* vol. 27, 1994.

[63] M. Lee, C. Tzoganakis, and C.B. Park, "Effects of supercritical CO2 on the viscosity and morphology of polymer blends," *Advances in Polymer Technology,* vol. 19, 2000.

[64] M.D. Wilding and D.G. Baird, "Melt Processing and Rheology of an Acrylonitrile Copolymer With Absorbed Carbon Dioxide," *Polymer Engineering and Science,* vol. 49, 2009.

[65] Z.M. Liu, X.H. Dai, J. Xu, B.X. Han, J.L. Zhang, Y. Wang, Y. Huang, and G.Y. Yang, "Encapsulation of polystyrene within carbon nanotubes with the aid of supercritical CO2," *Carbon,* vol. 42, 2004.

[66] Q.T. Nguyen and D.G. Baird, "An improved technique for exfoliating and dispersing nanoclay particles into polymer matrices using supercritical carbon dioxide," *Polymer,* vol. 48, 2007.

[67] M. Garcia Leiner and A.J. Lesser, "CO2-assisted polymer processing: A new alternative for intractable polymers," *Journal of Applied Polymer Science,* vol. 93, 2004.

[68] L. Urbanczyk, C. Calberg, F. Stassin, M. Alexandre, R. Jerome, C. Jerome, and C. Detrembleur, "Synthesis of PCL/clay masterbatches in supercritical carbon dioxide," *Polymer,* vol. 49, 2008.

[69] J. Samaniuk, D. Litchfield, and D. Baird, "Improving the Exfoliation of Layered Silicate in a Poly(ethylene terephthalate) Matrix Using Supercritical Carbon Dioxide," *Polymer Engineering and Science*, vol. 49, 2009.

[70] M. Garcia-Leiner and A.J. Lesser, "Intercalation in polymer-clay nanocomposites promoted by supercritical carbon dioxide.," *Abstracts of Papers of the American Chemical Society*, vol. 226, 2003.

[71] C.W. Manke, E. Gulari, D.F. Mielewski, and E.C.-C. Lee, "System and method of delaminating a layered silicate material by supercritical fluid treatment," U.S. Patent, 2002.

[72] D.F. Mielewski, E.C.-c. Lee, C.W. Manke, and E. Gulari, "System and method of preparing a reinforced polymer by supercritical fluid treatment," U.S. Patent 6753360, 2004.

[73] E. Gulari, K. Rangaramanujam, and G.K. Serhatkulu, "Method of delaminating aggregated particles with a coating agent in a substantially supercritical fluid," US7387749, 2008.

[74] S. Horsch, G. Serhatkulu, E. Gulari, and R.M. Kannan, "Supercritical CO2 dispersion of nano-clays and clay/polymer nanocomposites," *Polymer*, vol. 47, 2006.

[75] C. Chen, M. Bortner, J.P. Quigley, and D.G. Baird, "Using supercritical carbon dioxide in preparing carbon nanotube nanocomposite: Improved dispersion and mechanical properties," *Polymer Composites*, vol. 33, 2012.

[76] C. Chen, J. Samaniuk, D.G. Baird, G. Devoux, M.Q. Zhang, R.B. Moore, and J.P. Quigley, "The preparation of nano-clay/polypropylene composite materials with improved properties using supercritical carbon dioxide and a sequential mixing technique," *Polymer*, vol. 53, 2012.

[77] D. To, S. Sundaresan, and R. Dave, "Nanoparticle mixing through rapid expansion of high pressure and supercritical suspensions," *Journal of Nanoparticle Research*, vol. 13, 2011.

[78] W.R. Jung, J.H. Choi, N. Lee, K. Shin, J.H. Moon, and Y.S. Seo, "Reduced damage to carbon nanotubes during ultrasound-assisted dispersion as a result of supercritical-fluid treatment," *Carbon*, vol. 50, 2012.

## Chapter 2. Literature Review

The review contained in Chapter 2 will be divided into four sections. Section 2.1 covers silicates as potential fillers for polymer nanocomposites with emphasis on montmorillonite (MMT) structure and properties. In Section 2.2, the morphology, generation methods, and composite properties of montmorillonite/ polymer nanocomposites are discussed. These topics are discussed with emphasis on the generation of nanocomposites using polymers that can interact with the clay surface, per Objective 1. Special attention is given to melt compounded nanocomposites of Nylon 6 and nanoclay. Section 2.3 introduces carbon nanotubes (CNTs) as potential nanofillers for polymer nanocomposites, presenting the structure, synthesis, and properties of CNTs. The discussion in Section 2.4 focuses on the morphology, generation methods, and properties of CNT polymer nanocomposites. The melt compounding of conductive polycarbonate/CNT nanocomposites is covered at length in accordance with Objective 3. Section 2.5 discusses supercritical carbon dioxide ($scCO_2$), its properties, current uses in polymer processing, and a brief discussion on the field of particle formation. The $scCO_2$ modification of nanomaterials for nanocomposites is discussed in accordance with Objective 1, 2 and 3.

## 2.1 Montmorillonite

This section introduces montmorillonite with attention to their structure and properties. The motivation for their use in mechanical reinforcement of thermoplastic nanocomposites is addressed.

### 2.1.1 Montmorillonite (nanoclay)

Naturally occurring layered silicates, particularly Montmorillonite (MMT), have the potential to improve the properties in polymer nanocomposites. MMT's high modulus, abundance, light weight nature, large surface area and relatively high aspect ratio (length/thickness) lead to interesting composite properties when they are combined with polymer matrices [1-5]. In its pristine form, MMT is found as a stack of individual platelets, known as tactoids. The characteristic distance between individual MMT platelets, known as the *d*- spacing or basal spacing, is 0.96 nm. The thickness of an individual platelet is reported at 0.94 nm thick [6]. The space between individual clay platelets, known as the clay gallery, is about 0.2 nm. The montmorillonite platelets have lengths in the longest dimension between 100 nm and 150 nm, yielding aspect ratios of around 150 [7]. The high aspect ratio of montmorillonite allows it to align in the field of flow, which is important in providing mechanical support, gas barrier properties, and in fire retardant applications [8]. Furthermore, the platelet geometry of MMT allows it to provide biaxial reinforcement, unlike fibers or rods that largely provide uniaxial reinforcement. In addition, montmorillonite is a very stiff clay material. Molecular simulations suggest that MMT possesses a modulus between 300 and 400 GPa [8].

The properties and geometry of MMT make it a desirable choice as a nanofiller for polymer nanocomposites. However, MMT is kept from more widespread application because of its strong van der Waals interactions between individual platelets which prevent ideal

reinforcement, coupled with lack of miscibility in many polymers. Organically modified montmorillonite has been investigated as a means to overcome these issues.

### 2.1.2 Organically modified montmorillonite (OMMT)

The use of organically modified montmorillonite (OMMT) improves miscibility with the polymer matrix and increases the d-spacing between nanoclay platelets to reduce the entropic barrier to polymer diffusion. Poor dispersion in polymer nanocomposites may arise due to immiscible blends of inorganic clay with organic polymer. In addition, the small gallery spacing (~1 nm) results in significant entropic barriers to polymer motions which are crucial in separating the clay tactoids [5]. The exception to the rule is hydrophilic polymers such as poly(ethylene oxide) [9] and poly(vinyl alcohol) [10] that interact readily with the surface of MMT. In order to make MMT interact more favorably with other polymer matrices, a "compatibilizer" is required which improves interactions of the clay and polymer enthalpically, while decreasing the entropic barrier to polymer diffusion between clay galleries [11, 12].

OMMT is generated via a cation exchange reaction on pristine MMT. The hydrophilic cation on the surface of the nanoclay is replaced with a compatibilizer which varies depending on the matrix of interest. The cations which occupy the surface of MMT may be hydrated sodium ($Na^+$) or potassium ($K^+$) cations. A schematic drawing of MMT with a sodium cation is shown in Figure 1.3 [5]. To generate OMMT, an ion-exchange reaction is carried out to replace the cation on the surface with a surfactant, which may vary depending on the desired use. A table of commercially available (Southern Clay Products) OMMT with different surfactants is summarized in Table 2.1.

Table 2.1. Comparison of different counter ions used for MMT with the commercial product names (Southern Clay Products) and modifier concentrations. Adapted from [13].

| Product Name | Counter Ion | Modifier Concentration (meq/100g clay) |
|---|---|---|
| Cloisite 10A | 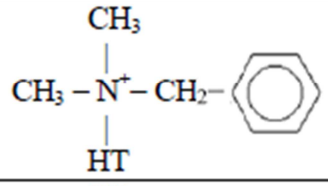 | 125 |
| Cloisite 15A | 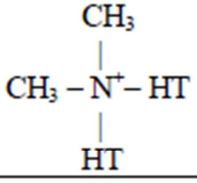 | 125 |
| Cloisite 20A | 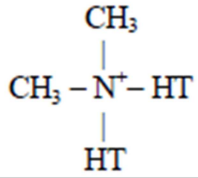 | 95 |
| Cloisite 25A | 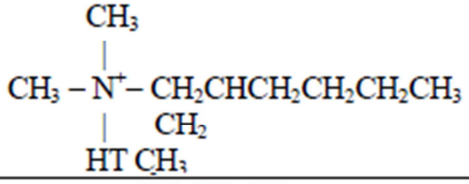 | 95 |
| Cloisite 30B | 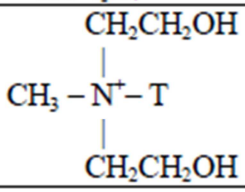 | 90 |

Types of surfactants include primary, secondary, tertiary, and quaternary alkylammonium or alkylphosphonium cations. The average distance between clay layers increases by between 2 and 3 fold following the cation exchange reaction [14, 15].The increase of gallery spacing helps to improve the transport of polymer chains between clay platelets. The organic cations can also be augmented to contain functionalities that might interact with the polymer of interest. An example is Cloisite 30B (Table 2.1) with which hydroxyl functionality is included using a hydroxy-ethyl functional gorup. This compatibilizes the interface for interactions with polymer matrices such as nylon 6. Many combinations of these surfactant functionalities have been analyzed in the literature [16, 17].

OMMT is a preferable PLS nanocomposite filler in polymer nanocomposites. In its pristine state, MMT exists in stacks with strong van der Waals forces that must be overcome to take advantage of the individual platelet's aspect ratio, modulus, and other favorable properties. Although OMMT helps by increasing the initial gallery spacing, completely separating and dispersing the nanomaterial is a difficult task.

## 2.2 Nanoclay nanocomposites

In this section, the subject of polymer nanoclay nanocomposites is addressed. First, the morphology of nanoclay nanocomposites is discussed, followed by the processing routes used to obtain these composites. Nanoclay nanocomposite properties are discussed with relevant references to literature as well. To satisfy Objective 1, the melt compounding of nylon 6 organoclay nanocomposites is reviewed thoroughly.

### 2.2.1 Nanoclay nanocomposite morphologies

One of the most difficult tasks in obtaining nanoclay nanocomposites with improved properties is efficient separation of the nanoclay platelets. Commercial OMMT is available in powder form, with aggregates on the order of 8 μm consisting of multiple tactoids per agglomerate [5]. Different degrees of separation are realized on the nanoscale and result in different apparent morphologies. Polymer/ clay nanocomposite morphologies are typically characterized through transmission electron microscopy (TEM) and wide-angle X-ray diffraction (WAXD). In this section, the techniques used to observe morphological changes in clay/polymer nanocomposites are addressed. This is followed by a discussion of the immiscible, intercalated, and exfoliated morphologies which arise during clay nanocomposite generation.

#### 2.2.1.1 Characterization of OMMT Composite Morphology

WAXD and TEM are the two most commonly used methods to identify and describe nanoclay/polymer nanocomposite morphology. Both techniques offer quantitative analysis of dispersion in OMMT/ polymer nanocomposites, although TEM is more commonly used as a qualitative method of morphological characterization.

Wide angle X-ray diffraction (WAXD) is a characterization method in which crystalline structures may be identified. In this process, an X-ray beam is directed at an incident angle to the sample. Typical angles surveyed for WAXD measurements are between $2\theta = 1^{o} - 10^{o}$ for investigating nanoclay morphology. When the incident beam comes in contact with a crystalline lattice in the material being tested, the beam is diffracted onto a detector at varying intensities. A characteristic peak is generated in the WAXD pattern at a relative intensity. In order to interpret the WAXD pattern, Bragg's law is utilized (Eq. 2.1). In Bragg's law, $\lambda$ represents wavelength of the X-ray used in the experiment, d is the spacing between the diffraction lattice planes (in this case, the clay platelets) and $\theta$ is the measured diffraction angle.

$$\lambda = 2d \sin\theta \qquad (2.1)$$

By controlling $\lambda$ and $\theta$ during testing, the distance between clay platelets, or d, can be calculated as an average value over the composite. A typical WAXD pattern of virgin organoclay is presented in Figure 2.1.

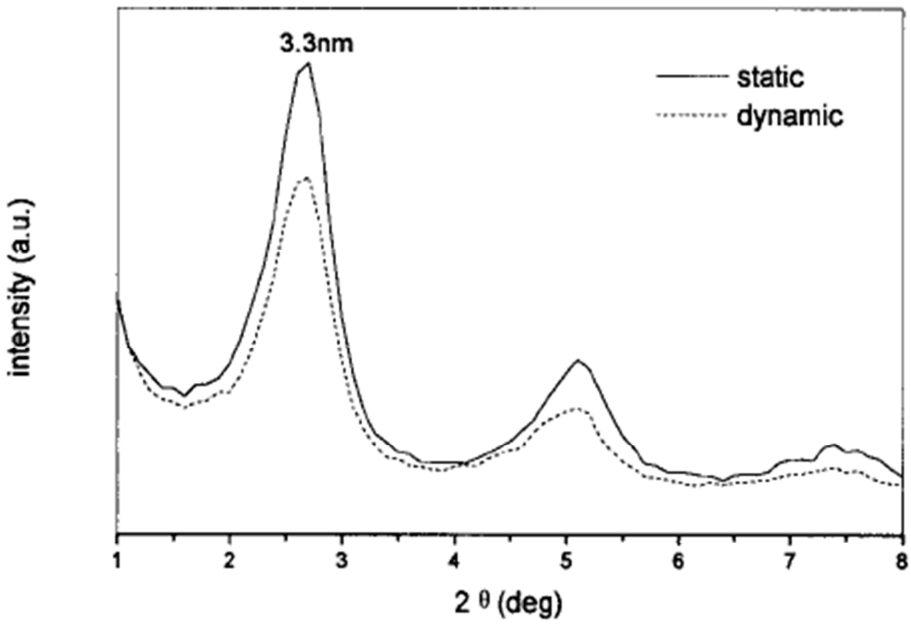


Figure 2.1. Example of typical WAXD pattern of nanoclay, modified from [18]

The peak observed at around $2\theta = 2.5^{o}$ in Figure 2.1 is the characteristic peak for the particular clay utilized in Zhang et al. [18]. If a shift or broadening in this peak is observed from the XRD pattern of the nanocomposite, then the basal spacing of the nanoclay has changed, indicating an alteration in morphology [5]. The extent of shift or broadening can be used to calculate the average distance between clay platelets quantitatively by calculating d, or qualitatively by observing a disappearance in the peak.

Transmission electron microscopy (TEM) is commonly used to observe morphological differences in polymer nanocomposites by observing structures on the micro and nanoscale. In this technique an electron beam is shot through an ultra-thin specimen and detected by a camera on the other side. Electron density gradients in the sample yield the contrast for the observed image with darker areas representing areas of higher electron density. This can also be indicative of a thicker section of polymer when non-uniform slices are cut during microtoming. In the case

of polymer nanocomposites, the MMT manifests as dark regions while the polymer rich areas are displayed as lighter regions. A representative TEM image of a polymer nanocomposite is shown in Figure 2.2.

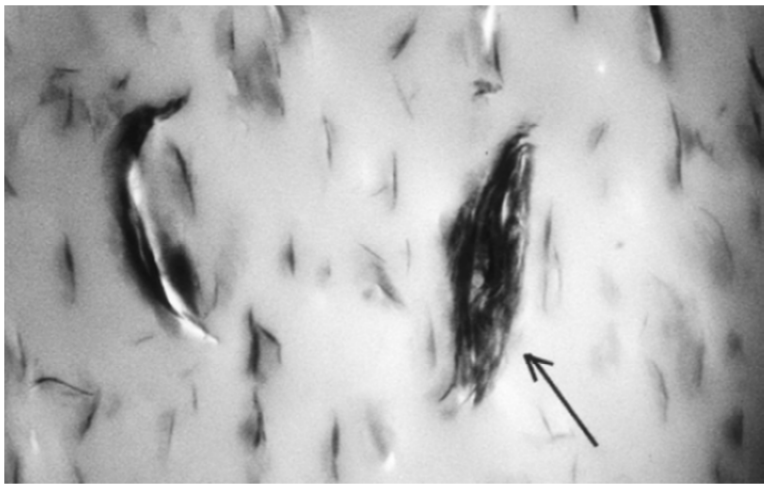

Figure 2.2. TEM image of polycarbonate nanoclay PLS with the arrow accenting the region of nanoclay aggregation, modified from [19]

A quantitative representation of the dispersion may be obtained by counting the number of individual nanoclay particles in a unit area of the image. This must be repaeated over a variety of magnifications and different regions to obtain an adequate representation. A full description of using this methodology to quantify TEM images for polymer nanocomposites is provided in [5]

Utilizing TEM and WAXD, sufficient characterization of nanoclay nanocomposite morphology is possible. These are powerful tools which can yield important information about the polymer-nanoclay interactions. However they must be carefully utilized to generate a circumspect and cohesive understanding of the nanocomposite morphology.

In the following section the various types of morphologies observed in nanoclay-polymer nanocomposites are discussed. Immiscible, intercalated, and exfoliated morphologies are analyzed with representative TEM images, WAXD patterns, and pictorial diagrams.

#### 2.2.1.2 Immiscible

A phase separated (immiscible) morphology is the least desired composite morphology, where separation of the tactoids is not observed. A visual representation of a clay/polymer composite with immiscible morphology, a representative TEM image, and example of a WAXD pattern are provided in Figure 2.3.

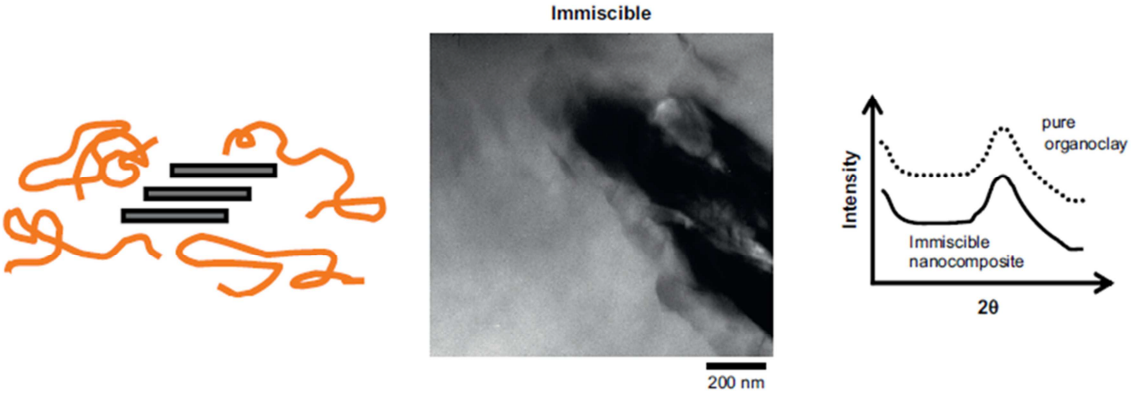


Figure 2.3. Visual representation (left) of immiscible morphology. Supported by wide-angle X-ray Diffraction (WAXD) (right) and transmission electron microscopy TEM (middle). These images are modified from [5]

As can be seen from the WAXD pattern of an immiscible composite, the characteristic peak of the clay associated with Bragg's law *d*-spacing is neither shifted nor broadened due to little or no separation of the platelets from the initial tactoid. It should possess the same structure as the powder form, and therefore present the same characteristic peaks. The TEM provides visual evidence of the morphology in Figure 2.3, where the dark region is comprised of hundreds of clay platelets forming a large tactoid. Composites with this morphology possess similar properties to traditional micro composites as the dimensions of the filler do not exceed the micro scale ($10^{-6}$ meter). In order to achieve improved composite properties on the nanoscale, either exfoliated or partially exfoliated/intercalated nanocomposite morphology is desired [1, 11, 20].

#### 2.2.1.3 Intercalated

Intercalated clay morphology occurs when polymer chains diffuse into the gallery spacing of the layered structure, resulting in a gallery spacing on the order of a few nanometers [7]. A visual representation of a clay/polymer composite with intercalated morphology, a representative TEM image, and example of a WAXD pattern are provided in Figure 2.4.

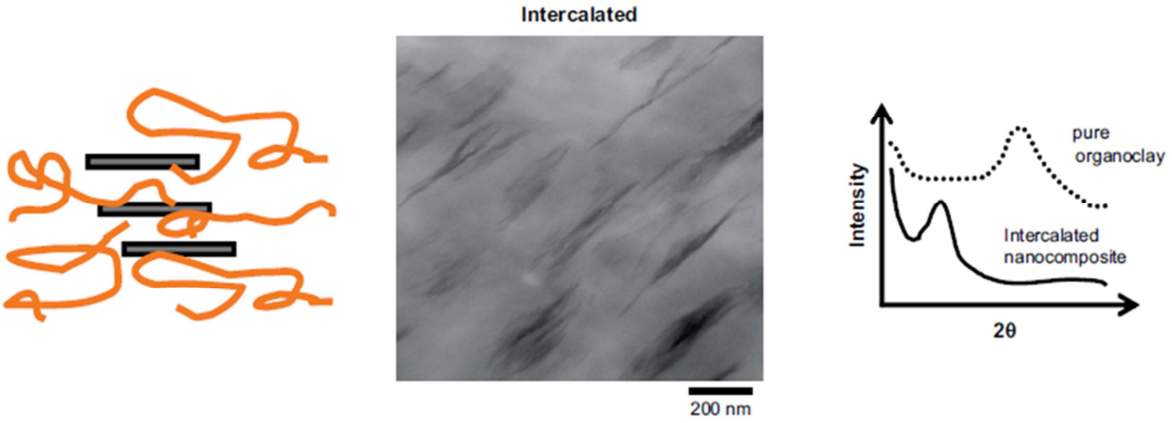


Figure 2.4 Visual representation (left) of intercalated morphology. Supported by wide-angle X-ray Diffraction (WAXD) (right) and transmission electron microscopy TEM (middle). These images are modified from [5]

Typically one or a few layers of polymer lie between clay tactoids in this morphology which is observed as a shift of the WAXD peak to lower angles of 2θ (see Figure 2.4, right). The average gallery spacing between the clay tactoids has increased, but not to the degree of platelet individualization (exfoliation) The TEM provides visual evidence of the morphology in Figure 2.4, where the dark regions indicate tactoids on the order of several clay platelets in thickness. Composites exhibiting these morphologies may possess similar properties to ceramics and other conventional composites [7, 21].

#### 2.2.1.4 Exfoliated

A disordered array of individual platelets indicates that the composite is “exfoliated”, and that the tactoids have been completely dispersed in the polymer matrix. An exfoliated morphology permits the nanoclay to provide reinforcement on the scale of an individual platelet. A visual representation of a nanoclay/polymer composite with exfoliated morphology, a representative TEM image, and example of a WAXD pattern are provided in Figure 2.5.

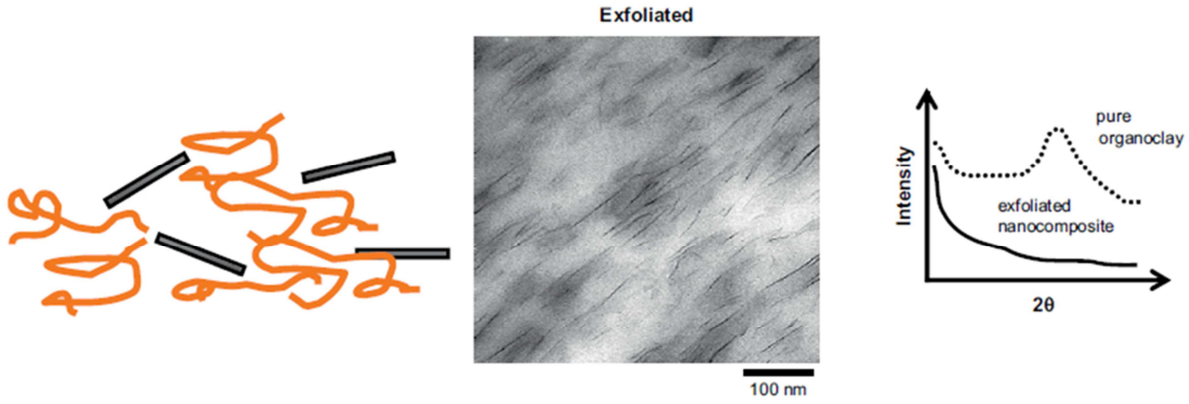


Figure 2.5. Visual representation (left) of exfoliated morphology. Supported by wide-angle X-ray Diffraction (WAXD) (right) and transmission electron microscopy TEM (middle). Modified from [5]

Because there is no regular spacing of the platelets, the characteristic peak in the WAXD pattern is no long present, as is evident in Figure 2.5 [5]. The TEM in Figure 2.5 provides visual evidence of the the individualized platelets as well.

In order for the polymer chains to diffuse between the clay tactoids and occupy an entropically unfavorable confined space, significant amounts of energy must be present between the polymer and clay, and/or large external forces must be applied [22-24]. Therefore, the intercalated and exfoliated morphologies are be difficult to achieve through traditional polymer nanocomposite generation techniques. Even in the case of enthalpically favorable polymer/clay

interactions, preparation methods which apply shear stresses, sonication, or other means of dispersion are required to individualize the nanoclay platelets [25, 26].

### 2.2.2 Processing methods for producing nanoclay/nanocomposites

Preparation methods have been developed to generate polymer/nanoclay nanocomposites with favorable morphologies. These include *In situ* polymerization, solution blending, and melt intercalation [25-27]. Each of these methods has advantages and disadvantages which are described in this section.

#### 2.2.2.1 *In situ* Polymerization

Commercially successful nanoclay nanocomposites were first generated via *in situ* polymerization by the Toyota group in 1993 using the Nylon 6/nanoclay system [26]. *In situ* polymerization synthesis begins with swelling of the nanomaterial with monomer or catalyst followed by polymerization. During polymerization, the clay platelets are forced apart by the polymer chains as the matrix polymerizes. This acts to disperse the filler while synthesizing the polymer matrix [28].

The Toyota group carried out further research on nylon 6/layered silicate nanocomposites prepared via *In situ* polymerization [29-39]. One of the processes they investigated is schematically represented in Figure 2.6, where caprolactam monomer was used to swell the filler material.

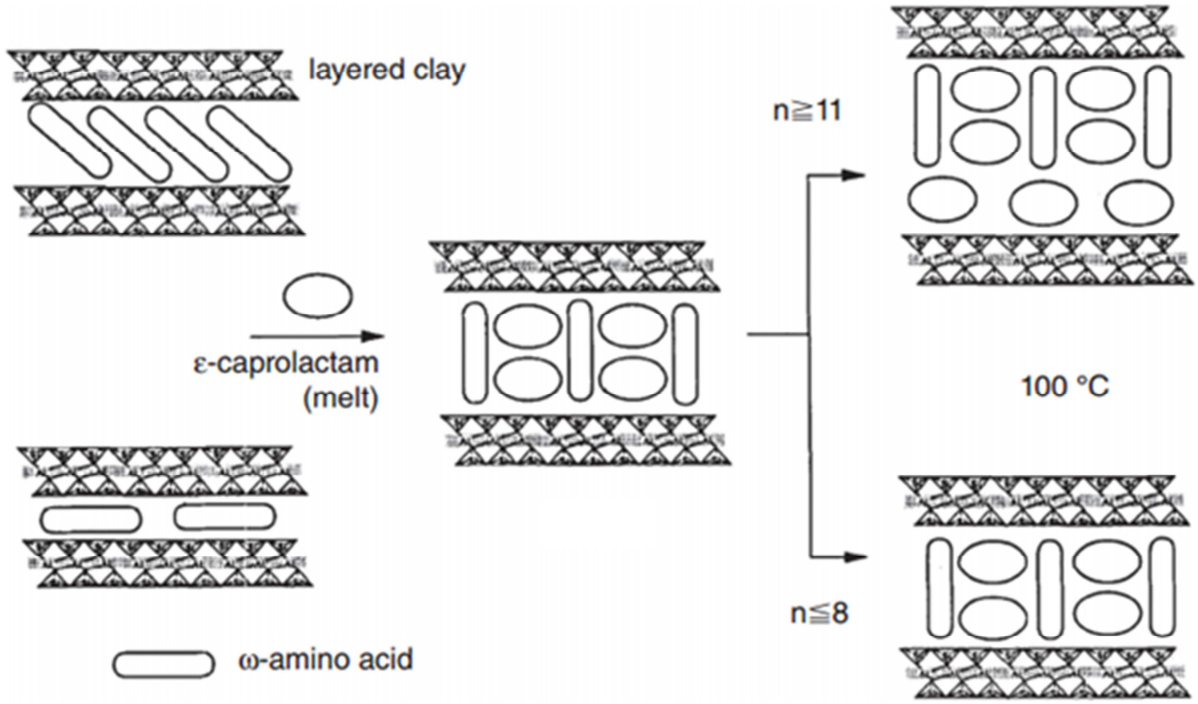


Figure 2.6. Illustration of *In situ* polymerization synthesis of polyamide/MMT nanocomposite modified from [34]

The nanoclay was swelled step with caprolactam monomer followed by a ring opening polymerization which was initiated by heating the mixture in an autoclave to 250$^{o}$C for 48 hours. The resulting nylon 6 nanocomposite possessed an exfoliated morphology below 15 wt% filler, and an intercalated morphology above this concentration. The composites were injection molded into car parts to test their viability as replacements for conventional glass fiber composites used as timing belt housings. The nylon 6 nanocomposites were found to be a superior replacement in terms of mechanical performance [34].

Poly(ethylene teraphtalate)/MMT composites have been synthesized using *in situ* polymerization. Lee et al. [40] generated nanocomposites with a mixture of intercalated/exfoliated morphology using this method. The process used is illustrated in Figure 2.7.

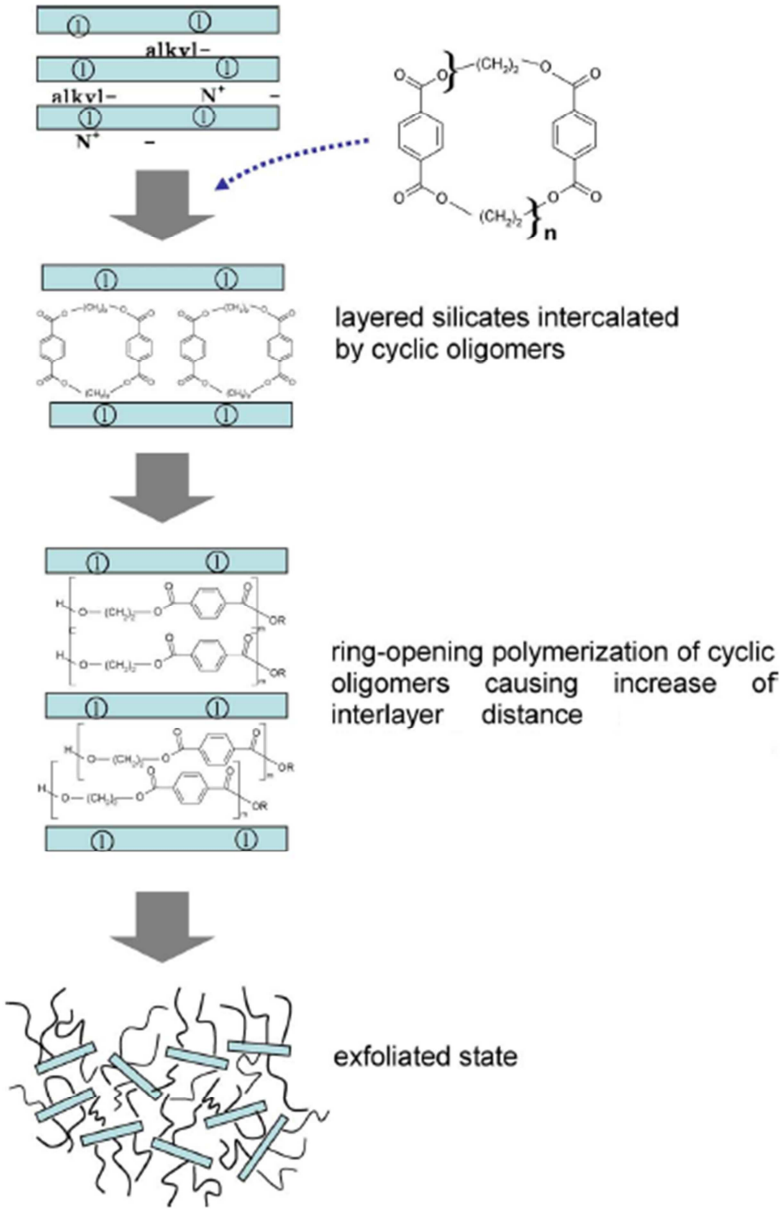


Figure 2.7. PET nanocomposite synthesis via *In situ* polymerization modified from [40]

In this method, the authors swelled the silicate layers with ethylene terephthalate oligomers, followed by ring-opening polymerization of the cyclic oligomers. This resulted in an increase in the interlayer spacing of the clay, and a more intercalated state. The generation of PET nanocomposites can be difficult due to a large entropic hindrance to polymer diffusion between nanoclay galleries. Lee et al. [40] were able to avoid this issue by introducing low viscosity

oligomers which can diffuse between the galleries more readily. This was followed by polymerization to generate the PET nanocomposites.

Polyethylene has been prepared in the presence of MMT using ethylene monomers to obtain polymer/nanoclay nanocomposites. Alexandre and Dubois [41, 42] accomplished this by utilizing a method they refer to as polymerization-filling. In this technique, the nanomaterial is pretreated with a metallocene complex catalyst (in this case, Ziegler-Natta) that is anchored to the surface of the platelets. Polymerization is then induced using ethylene monomer. The authors observed an exfoliated morphology by TEM and XRD studies. Furthermore, they observed an increase in stress at break of 7 MPa coupled with a decrease in the strain at break for nanocomposites prepared at 4.1 wt% MMT.

Exfoliated and intercalated morphologies are commonly observed in nanoclay/polymer nanocomposites prepared with *in situ* polymerization. However, this method requires long processing times, sonicative mixing, and solvents in order to obtain the desired product. This limits *in situ* polymerization as a widespread nanocomposite generation method. In addition, *in situ* polymerization nanocomposite generation methods are limited to certain types of polymers. More environmentally benign and industrially scalable methods are desired to produce polymer/nanoclay nanocomposites in most applications.

#### 2.2.2.2 Solution blending

Solution blending is a common method for polymer/nanoclay nanocomposite generation. In this method, the nanoclay is exfoliated in a suitable solvent which either contains the dissolved polymer, or in the case of insoluble polymers, a prepolymer. This may be

accomplished with the aid of sonication or other mixing methods. This process is illustrated in Figure 2.8.

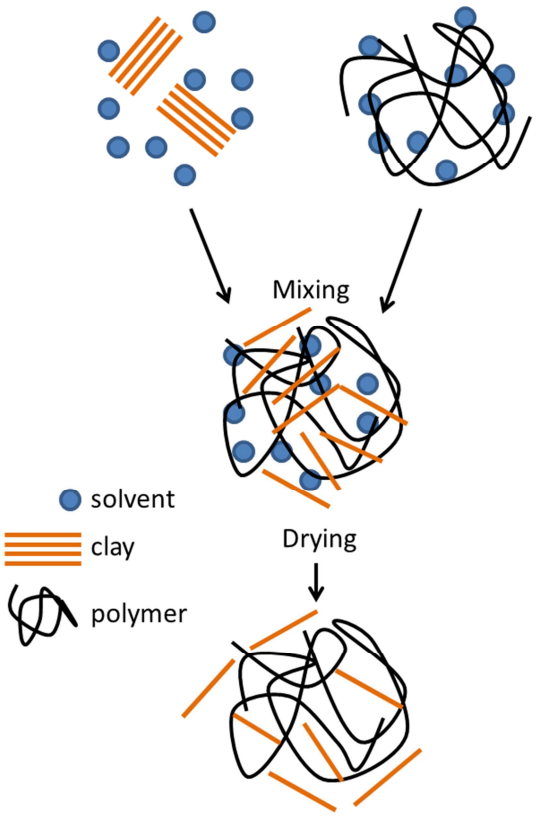


Figure 2.8. Representative illustration of solution blend processing of a polymer/nanoclay nanocomposite

During the mixing step, the polymer may diffuse between individual clay stacks, yielding an exfoliated or intercalated morphology after the solvent has been removed. However, during the drying step reaggregation of the nanoclay presents significant problems [1].

Polyethylene/nanoclay nanocomposites have been generated using solution blend methods with organic solvents. Jeon et al. [43] generated low density polyethylene nanocomposites by utilizing acetonitrile as a solvent for the polymer. The nanoclay utilized in this study was a sodium montmorillonite modified with a protonated dodecylamine. The authors observed a partially exfoliated morphology through TEM and XRD measurements. In addition,

Jeon et al. [43] attempted to dissolve a high density polyethylene polymer in a mix of xylene and benzonitrile, as the high density matrix was insoluble in the acetonitrile used to dissolve the low density polyethylene. The authors observed only mild intercalation based on their XRD and TEM results. This indicates that the xylene/benzonitrile solvent was unsuitable, emphasizing the issues in finding suitable solvents to produce exfoliated polymer/clay nanocomposites generated by solution blending.

Avella et al. [44] generated isotactic polypropylene (*i*-PP)/OMMT nanocomposites via a solution blending method, and studied the degree of exfoliation and composite properties of the nanocomposites. The authors dissolved the OMMT and polymer in dichlorobenzene using an ultrasonic bath before filtering and collecting the product. They formed an exfoliated nanocomposite at 1 wt% loading as observed using WAXD. At the addition of 3 wt% organoclay, they observed a return of the characteristic nanoclay peak, indicative of a mixed exfoliated/intercalated nanocomposite. Above 3 wt%, they failed to observe nanoscale dispersion of the OMMT. The Young's Modulus of the composites was found to increase by 220 MPa compared to the virgin *i*-PP at 3 wt% OMMT. At higher filler content, the stiffness was observed to decrease due to the aggregation of the filler material resulting in a micro-composite.

The solution blending method of polymer/nanoclay nanocomposite generation may be successful at producing intercalated and exfoliated composites, but presents several limitations. A favorable solvent for both the nanomaterial as well as the polymer must be chosen. These solvents may be costly to handle or remove, and can be harmful to the environment. The mixing of the precursors is achieved through sonication or ultrasonication, which can be costly and difficult to scale to industrial processes. Additionally this process is most commonly considered a batch operation, which further limits industrial scalability. Composite generation methods

lacking the use of solvent, which are inherently more scalable and may be applied to a wide range of thermoplastics are more preferable.

#### 2.2.2.3 Melt blending

Melt intercalation, or melt blending, is the preferable method of nanoclay nanocomposite generation due to its low cost, lack of harmful solvents, flexibility, and general scalability to industry, although efficient dispersion of the nanoclay can be difficult to obtain[5]. The mixing of nanomaterial and polymer in melt blending or compounding occurs when stresses are imposed to the mixture of melted thermoplastic polymer and nanomaterial in a melt mixing device, such as an extruder, injection molding device, or a batch melt mixer. The stresses act to break up the aggregates of clay tactoids, shearing the stacks into smaller ones, and dispersing them throughout the polymer matrix. While the nanoclay platelets are peeled apart, the melted polymer may diffuse between the clay platelets, increasing the extent of nanoclay dispersion. This process is represented pictorially in Figure 2.9.

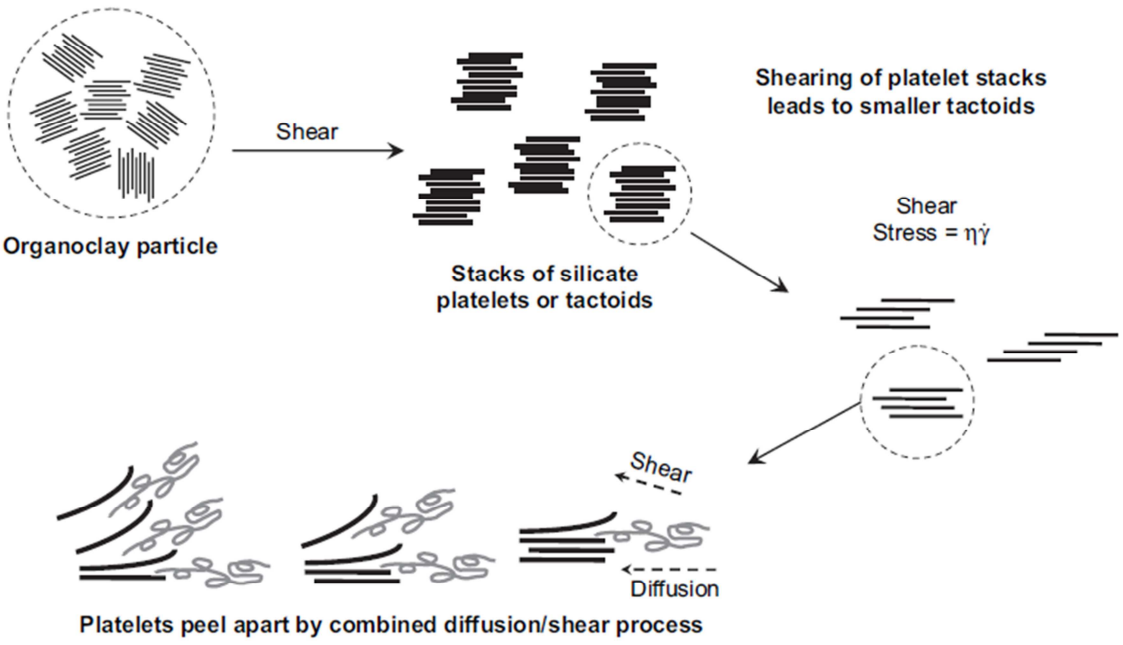

Figure 2.9. Diagram of idealized melt compounding generation of nanoclay nancomposites, modified from [45]

The shear stresses help separate the clay layer by layer until sufficient stresses are obtained or residence time has passed to separate the nanoclay tactoids. Once the polymer diffuses into the clay galleries, it must then be distributed throughout the bulk polymer phase to create a well-dispersed nanocomposite [25, 45-53]. Even when applying higher shear stresses to the melt, the degree of particle breakup and distribution may not be sufficient as dispersion may be limited by poor nanoclay/polymer interactions. However, if there is an affinity for the polymer and the nanofiller, enthalpic interactions may assist in fully exfoliating the nanofiller [54]. Because of this, nanocomposites melt compounded with polymers that possess potential for favorable interactions with the nanoclay may exhibit the most potential for industrial application. If there is not an affinity, then effective dispersion is more difficult to achieve. Either intensive mixing with high shear rates [50, 55] or the inclusion of compatibilizers that have favorable interactions with both the polymer and nanofiller are required to achieve sufficient dispersion [56-64]. The first part of this subsection discusses composites of nanoclay and polymer which may interact with the clay surface that are generated by melt compounding. Following this, nanocomposites produced with polyolefins where the bonding between the polymer are discussed.

Some of the first studies of the melt blend generation of polymer/nanoclay nanocomposites were carried out by Liu et al. [50] in 1999. In one of these studies, the authors investigated nylon 6/ OMMT nanocomposites prepared by twin screw extrusion. Similar to the work by the Toyota group, they were able to take advantage of the favorable interactions between nylon 6 and OMMT to produce exfoliated nanocomposites. The authors thoroughly investigated the properties of the resulting nanocomposites with WAXD, TEM, heat distortion measurements, and tensile measurements. Liu et al. [50] observed a decrease in tensile strength

beyond the addition of 4.2 wt% organoclay, but continuing increase in Young's Modulus up to 20 wt%. WAXD measurements suggested an exfoliated morphology below 5 wt%, but partially intercalated morphologies at concentrations above this. At 4.2 wt%, the authors observed an increase in the tensile modulus from 3.0 to 4.1 GPa, and an increase in the yield strength from 68.2 to 91.3 MPa.

Dr. Don R. Paul's group at the University of Texas has conducted extensive experiments on nylon 6/ OMMT nanocomposites prepared with both single screw and twin screw melt compounding. Much of this work has been carried out in collaboration with Dr. Fornes and others at Southern Clay Products (now Byk Additives). These authors have investigated various aspects of nylon/6 OMMT nanocomposites including matrix molecular weight, screw configuration, processing time, multiscale composites, organic modifier of the nanomaterial, crystallization behavior, and have made comparison of models to melt compounded nanocomposite properties [2, 5, 45-47, 52, 65-77]. Due to the nature of these works and the large contributions they have lent to the field of melt compounding of nanocomposites, the next few paragraphs will be utilized to summarize and highlight the key findings of this group in the past 15 years as they pertain to nylon 6 nanocomposites.

Cho et al. [25] studied the differences in melt compounding nanocomposites using twin screw and single screw extrusion for nylon 6/OMMT nanocomposites. The OMMT used in this study was montmorillonite exchanged with bis(hydroxyethyl) (methyl) rapeseed alkyl ammonium chloride. It was found that the twin screw extruder, with significantly higher shear rates and residence times, produced more exfoliated nanocomposites than single screw melt compounding. The nanocomposites extruded with single screw melt compounding were exposed to a second pass in the extruder to mimic longer residence times, however this was still

insufficient to produce a completely exfoliated nanocomposites. The WAXD measurements of the resulting composites are compared in Figure 2.10.

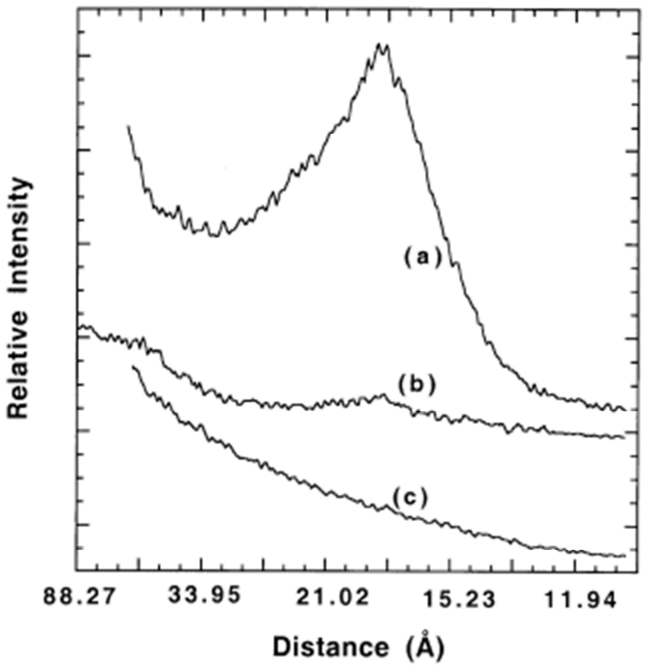


Figure 2.10. WAXD measurements of (a) pure organoclay, (b) nanocomposite formed by single screw compounding, and (c) twin screw compounding

These results were further validated with TEM. In addition to this comparison, the authors compared their findings to nylon 6 filled glass fiber composite and observed a 1 GPa increase in modulus for 3.16 wt% mineral filler (not including the organic content) compared to the virgin matrix, accompanied by a 17 MPa increase in yield strength. The authors compared the 3.16 wt% nanocomposite to a 5 wt% glass fiber/nylon 6 composite prepared in the same way and observed a 0.6 GPa increase in modulus, and an 8 MPa increase in strength for the nanocomposite. These findings illustrate the benefits of utilizing OMMT to replace traditional glass fiber in nylon 6 polymer composites Furthermore, the authors reported negligible increases in viscosity using nanoclay filler, suggesting improved processability for these nanocomposites.

In following work, Fornes et al. [45] investigated the effect of matrix molecular weight on the delamination of nanoclay in nylon 6 nanocomposites prepared by melt compounding. The authors processed nanocomposites using the OMMT mentioned in the previous paragraph with low ($M_N$ = 16,400), medium ($M_N$ = 22,000) and high ($M_N$ = 29,300) molecular weight nylon 6 using a Haake intermeshing co-rotating twin screw extruder. Following extrusion, the nanocomposites were injection molded to analyze the effect of nylon 6 molecular weight on the composite properties. Through TEM and WAXD, the authors found that higher viscosity polymers transfer more stress to the nanomaterial, achieving the full separation of platelets during melt processing. Exfoliated morphologies were observed for both the medium and high molecular weight composites, while a mixture of intercalated and exfoliated was observed for the low molecular weight sample. In addition, the high molecular weight nanocomposites possessed higher moduli, impact strengths, and yield strength.

The effect of different organic modifiers on the nanocomposite properties of polymer nanoclay nanocomposites was investigated by Don Paul's group as well. The focus of a study by Fornes et al. [47] was to investigate polymer/clay interactions and nanoclay exfoliation in nanocomposites prepared by melt compounding in a twin screw extruder. To accomplish this, Fornes et al. [47] compared various organic modifiers in order to determine their effect on the nanocomposite properties. The authors compared alkyl chain lengths, the effect of hydroxyl modification versus methyl modification, milliequivalent ratio (MER), degree of saturation, quaternary and tertiary substitutions, and number of alkyl tails on the modification. The types of modification and the nomenclature used in the study are summarized in Table 2.2, along with the comparisons that were made.

Table 2.2. Summary of nomenclature for different organic modifers of MMT (a), with the comparisons made to determine organic modifier effects (b) conducted in a study by Fornes et al. [47], modified from [47]

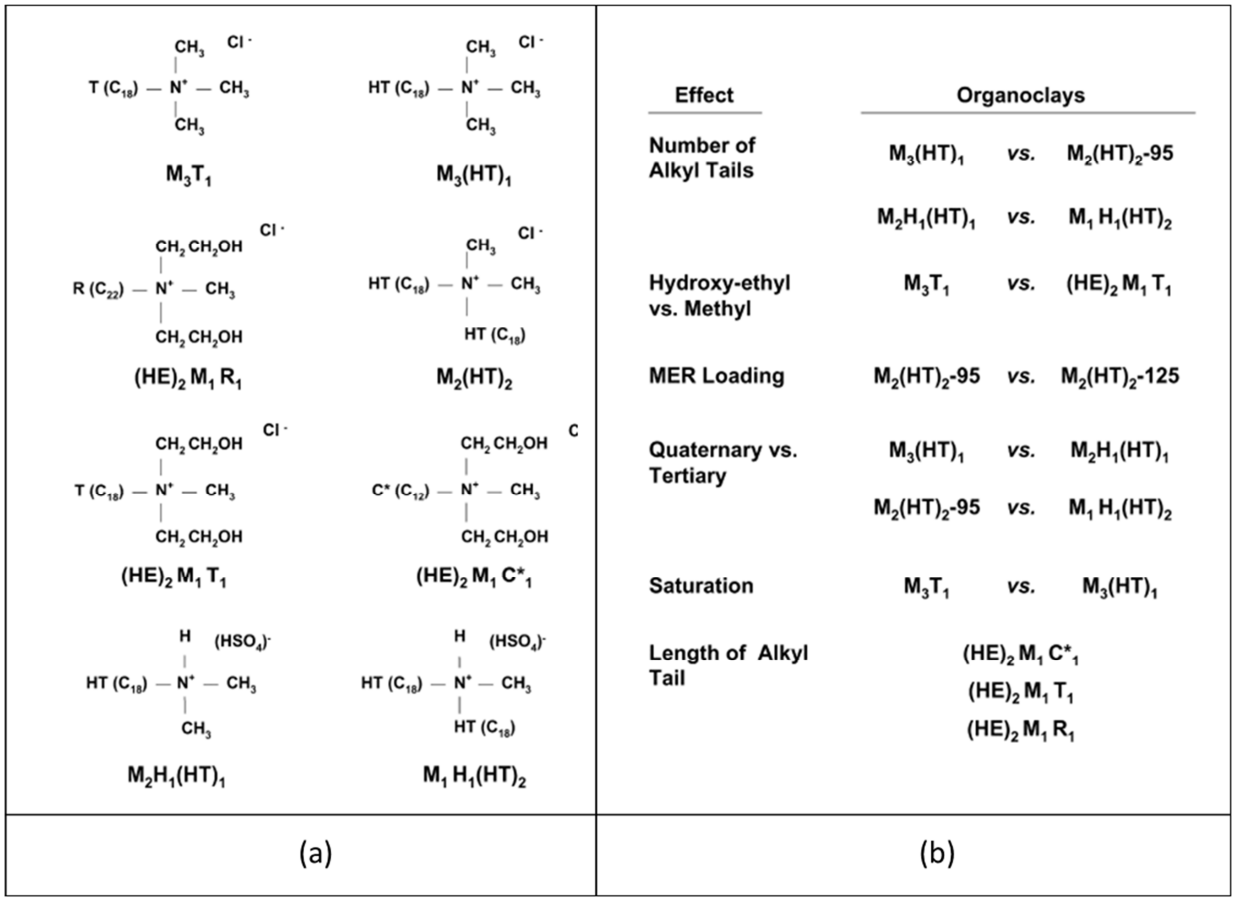


The authors observed that the greater the distance between platelets in the organoclay (the more surfactant added to the virgin clay) the lower the mechanical properties of the resulting composite. This may be counterintuitive, as it was suggested earlier that increasing the d-spacing between nanoclay platelets may reduce the entropic barrier to polymer diffusion during nanocomposite generation. Therefore, this effect was attributed to the surfactant shielding potential interactions between the polymer and nanoclay surface, as nylon 6 interacts favorably with the surface of montmorillonite. If the d-spacing could be increased while mitigating shielding effects, then better interaction might be obtained. Fornes et al. [47] also observed that one long alkyl chain on the organic modification led to improved mechanical properties and

exfoliation compared to nanocomposites prepared with nanoclay possessing an organic modification with two long alkyl chains. The authors suggest that this may also be linked to shielding effect. Another interesting finding in this study was that methyl groups on the substituted amine produced more exfoliated nanocomposites with enhanced properties compared to 2-hydroxy-ethyl groups. It has been suggested that nanocomposites of nylon and Cloisite 30B may interact with one another due to hydrogen bonding of the hydroxyl groups in the organic modification of Cloisite 30B with carbonyl groups of nylon 6 [53]. The findings by Fornes et al. [47] in this study suggest that interaction of the polar groups of nylon 6 with the surface of the clay are important to exfoliation and reinforcement of nanocomposites of nanoclay and nylon 6, rather than the substituents of the organic modification [38]. As such, the hydroxyl functionality may act to shield the nylon 6 from the nanoclay surface due to the hydroxide functionalities being more bulky than methyl substituents. This study suggests that using an intermediate amount of organic modification to helps overcome cohesive forces between the neighboring clay platelets without inducing shielding effects is desirable. This study is limited to the understanding of the nylon 6/OMMT system, but the principles discussed may be applied to many systems with the potential for favorable clay/polymer interactions.

In an attempt to improve the nanoclay dispersion in nylon 6/nanoclay nanocomposites prepared via single screw melt extrusion, the effective residence time has been investigated by means of reprocessing the nanocomposites [25, 48, 78]. In a study by Cho et al. [25] no difference was observed by extruding nylon 6/clay nanocomposites multiple times. Similar results were obtained from Russo et al. [78], where further reaggregation was observed by the authors when the extrudate from the first melt compounding step was reprocessed. In work by Gawad et al. [48], however, the authors observed improved dispersion and exfoliation of the

nanocomposite subjected to multiple passes in the extruder using Cloisite 30B and nylon 6. The authors suggest that reprocessing at higher temperatures results in better dispersion, although this is counterintuitive to other results where lower temperatures and higher viscosities result in improved exfoliation [45].

Polycarbonate (PC) has been considered for use in OMMT nanocomposites as well. Yoon et al. [19, 79] conducted an in-depth study on PC/OMMT nanocomposites, similar to previous work on nylon 6 nanocomposites in Don R. Paul's group. Utilizing the same twin screw melt compounding process described earlier, the authors investigated the effects of different ypes of organoclay and the matrix molecular weight on the nanocomposite mechanical properties and morphology. Regarding the organic modification, the authors observed the most exfoliated morphologies in nanocomposites generated with organic filler that was miscible with the polymer (polyoxyethylene and octadecylalkyl tails). This suggests the use of organic modification which increases the gallery spacing while remaining partially miscible with the polymer remains the preferred route to polymer intercalation with the nanoclay in nanocomposites where interactions between the polymer and nanoclay surface are absent. In this study, limited exfoliation was observed, with mostly intercalated and immiscible morphologies detected with TEM and WAXD.

The generation of polyolefin/nanoclay nanocomposites by melt compounding methods has been investigated in the literature, though few reports have produced exfoliated nanocomposites without the use of compatibilizers. Hotta et al. [80] melt compounded linear low density polyethylene (LLDPE) with organoclay using twin screw melt compounding with the aid of a compatibilizer (maleic anhydride grafted polyethylene). This strategy for compatibilization is well documented as an effective way to produce intercalated polyolefin/OMMT

nanocomposites. In this process, a small amount of maleic anhydride grafted polyolefin which is miscible with the host polymer is melt compounded with the organoclay and host polymer. The anhydride groups of the compatibilizer enhance the affinity of the polymer for the clay through polar interactions, improving the dispersion and separation of the nanoclay during melt processing. In this study, the authors varied the amount of maleic anhydride grafted LLDPE (LLDPE-g-MA) and investigated the effect on the nanocomposite morphology. WAXD patterns gathered from the resulting melt compounded composites are illustrated in Figure 2.11.

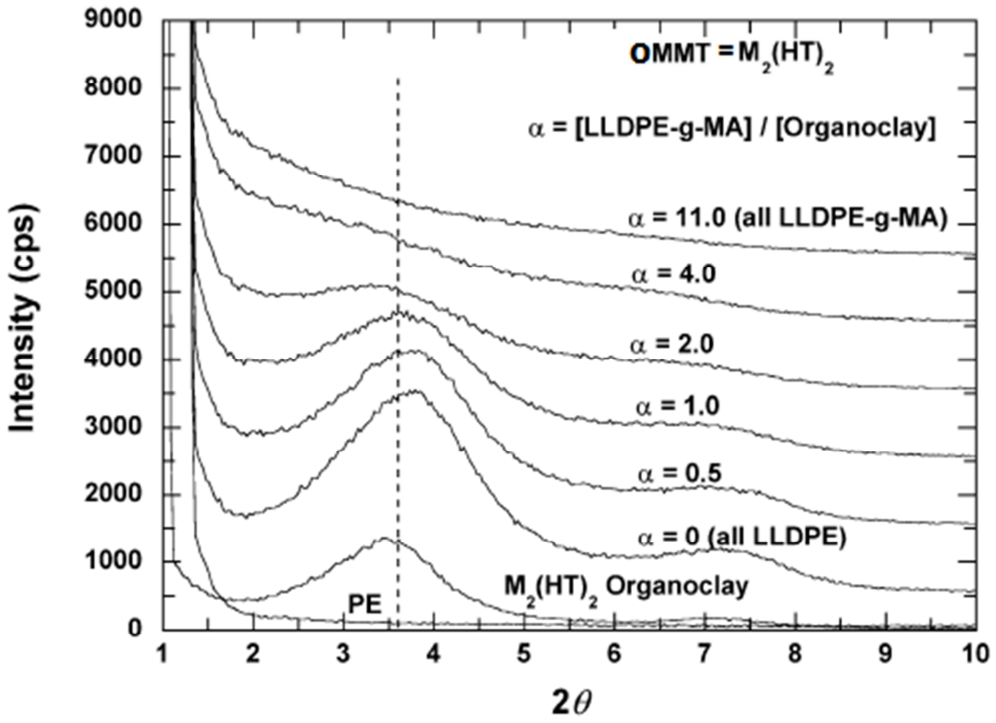


Figure 2.11. WAXD patters of LLDPE, OMMT, and LLDPE/OMMT nanocomposites with different amounts of LLDPE-g-MA. Modified from [80]

This WAXD pattern illustrates the effect of LLDPE-g-MA on nanocomposite morphology. Larger amounts of compatibilizer yield improvements in the extent of exfoliation in the melt compounded nanocomposites. However, the improved interactions did not translate into mechanical improvements due to the low modulus of the compatibilizer in this study. This

suggests an optimal amount of compatibilizer must be added to improve the dispersion of nanofiller while limiting the effect of decreasing structural reinforcement introduced by maleic anhydride modification.

Polypropylene has been investigated as a host polyolefin for nanoclay in melt compounded nanocomposites with maleic anhydride grafted compatibilizer. Wang et al. [63] melt compounded polypropylene (PP)/OMMT nanocomposites with maleic anhydride grafted PP (PP-g-MA) by twin screw melt compounding. The authors observed similar results as Hotta et al. [80] where a nanocomposites prepared with intermediate amounts of PP-g-MA showed improved mechanical properties compared to the virgin matrix. Furthermore, Wang et al. [63] observed that medium and high viscosity polypropylene led to improved mechanical properties and nanoclay dispersion. The largest increase in tensile modulus observed by the authors was 0.8 GPa compared to the virgin matrix with a high molecular weight compatibilizer using 0.5 MA content and 5 wt% organoclay. These results were supported by TEM and WAXD.

Of the polymer nanocomposite processing and synthesis methods discussed in this section, melt compounding is the most scalable to industry but still retains some drawbacks such as efficient dispersion of the nanomaterial during nanocomposite generation. In many cases novel mixing methods which might improve the dispersion of the nanofiller are preferable to obtain the best composite properties while maintaining the flexibility and scalability of melt compounding. These methods are discussed in later sections.

### 2.2.3 Nanoclay/Polymer composite properties

Nanoclay/polymer nanocomposites generated using OMMT may possess enhanced material properties compared to those of the virgin matrix. The property improvements observed

in polymer/OMMT nanocomposites arise from the intrinsic nanofiller properties as discussed in Section 2.1.1. With the addition of low amounts (<5 wt%) of nanofiller, nanocomposites may exhibit properties significantly greater than those of the pure matrix. These properties include mechanical reinforcement, heat distortion temperature, flame retardency, coefficient of thermal expansion and barrier properties. The rheological properties of polymer nanocomposites are also affected by the inclusion of nanomaterial. The rheological response of the material may give an idea of the micro and meso structures of the nanocomposites, as well as help understand the processability of the material in the melt state, or in the case of amorphous polymers, the liquid-like regime. The nanocomposite properties vary depending on the degree of dispersion of the OMMT, the orientation of the filler particles, the polymer-clay interactions, and other factors. The following section is dedicated to the properties of thermoplastic/OMMT nanocomposite properties.

#### 2.2.3.1 Mechanical properties

The improved mechanical reinforcement observed in nanocomposites of polymer and OMMT is interesting due to the potential for these nanocomposites to replace macro scale composites of polymer and glass fiber or talc. The Young's modulus, tensile strength, and brittleness of the nanocomposite are three important mechanical properties of interest and are discussed in further detail below.

Young's modulus improvements have been reported by Dr. Don R. Paul's group in nylon 6 nanocomposites prepared with surface modified MMT/ polymer nanocomposites processed via twin screw melt compounding. The nanoclay modification in this work was a hydroxyl functionalized Cloisite 30 B from Southern Clay Products, and the nanocomposites were generated using a co-rotating twin screw extruder to melt compound the material followed by

injection molding tensile bars to orient the nanoclays. The largest improvement in Young's modulus from this system was reported by Fornes et al. [47]. The authors observed a well exfoliated morphology which resulted in a 1.63 GPa increase in modulus from the virgin matrix, from 2.75 GPa to 4.38 GPa for 6.1 wt% clay in a high molecular weight nylon. Furthermore, the authors compared the mechanical properties of nylon 6/OMMT nanocomposites to glass fiber filled nylon composites. This comparison is illustrated in Figure 1.1 [2]. In order to generate a composite with a Young's modulus twice as large as the virgin matrix, about three times more glass fiber is required to obtain the same properties as the OMMT nanocomposite. This is a significant advantage where light weight parts are desired with biaxial reinforcement, as opposed to heavier, uniaxial reinforced glass fiber composites [81]. An additional practical advantage is that the surface of nylon 6 nanocomposites possess a smoother finish than those of glass fiber composites. Although the improvements in Young's modulus are promising, when considering the overall mechanical properties of an engineered material, other factors such as the yield strength must also be addressed. The yield strength for OMMT nanocomposites of nylon 6 increases by ~20 MPa up to 10 wt% organoclay, but levels off after this. Alternatively, glass filled composites of Nylon 6 increase in tensile strength beyond 30 wt% filler, where a tensile strength increase of ~65 MPa compared to the virgin matrix is observed. Therefore, when using nanocomposites at concentrations greater than 10 wt % OMMT, other routes such as multiscale composites of glass fiber, OMMT, and Nylon 6 might be considered [2, 25, 52]. The mechanical properties of thermoplastics may be enhanced significantly with the addition of small amounts of OMMT in nylon 6 and other polymers which interact favorably with the clay surface, but less success has been observed with polyolefin nanocomposites.

Thermoplastic polyolefin (TPO) nanocomposites generated via melt compounding are of interest for replacing current composites in industry due to their potential to provide enhanced mechanical properties, but poor exfoliation is often observed in these materials. This is due to the poor interactions between the polymer matrix and nanofiller. Lee et al. [4] produced TPO nanocomposites of polypropylene and OMMT using twin screw melt compounding and observed increases in composite stiffness of 0.8 GPa compared to the virgin PP matrix using 7 wt% organoclay. Although they did not observe significant exfoliation from TEM and XRD results, they were able to obtain interesting composite properties. In this study, the authors suggest that TPO nanocomposites may be able to replace current talc filled polyolefin composites. A comparison of relative moduli of the TPO/OMMT composites with TPO and talc is illustrated in Figure 2.12.

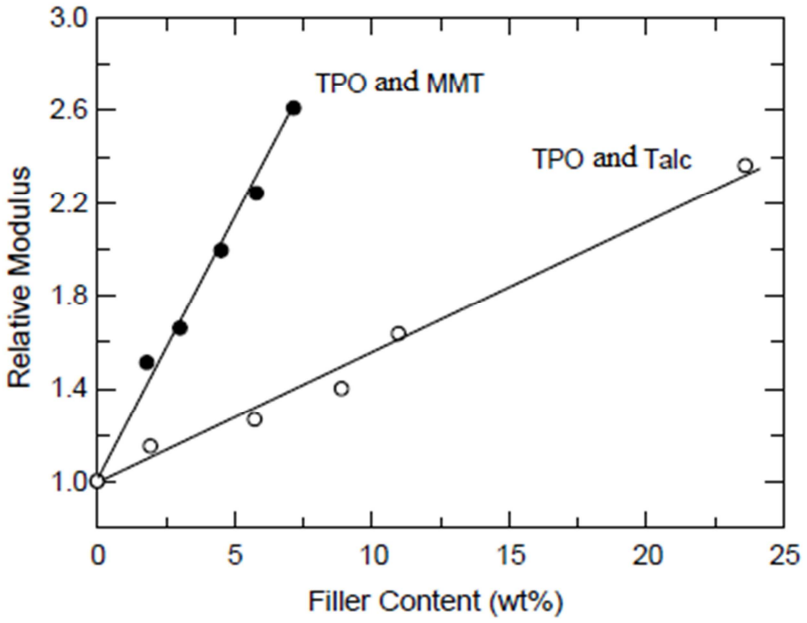


Figure 2.12. Comparison of realative Young's modulii of TPO/OMMT composites with TPO/Talc composites modified from [4]

As can be seen from Figure 2.12, nearly four times the weight of talc is required to produce a doubling in Young's modulus compared to TPO/OMMT nanocomposites. Especially in automobile applications where fuel savings are important, the lightweight materials might be obtained by using OMMT rather than talc.

It is often desired to maintain or improve the tensile strength of a nanocomposite while improving the Young's modulus. Fornes et al. [45] observed increases in the strength and Young's modulii of nylon 6 nanocomposites with increasing organoclay content, to about 20 wt% OMMT. In this study, the authors compared matrix molecular weights and their effect on nanocomposite properties for twin screw melt compounded Nylon 6/OMMT nanocomposites. The yield strength values are compared with nanoclay content and matrix molecular weight in Figure 2.13.

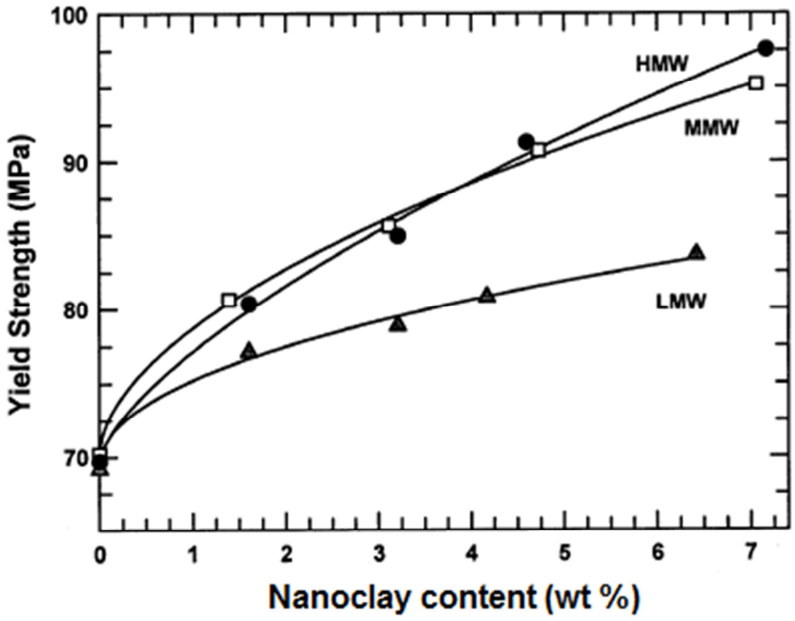


Figure 2.13. Yeild strength as a function of nanoclay content and matrix molecular weight for nylon 6/organoclay nanocomposites, modified from Fornes et al. [45]

The authors observed that molecular weight influences the yield strength of the composites, as illustrated in Figure 2.13. It was reported that the higher viscosities from the high molecular weight composites produce higher shear rates during melt compounding leading to more exfoliated nanocomposites, and therefore improved yield strength.

Improvements in yield strength are difficult to obtain in polyolefin nanocomposites and other thermoplastic composites which do not contain functionalities that interact with the clay surface [5]. Due to the lack of effective stress transfer from polyolefin nanocomposites to the clay, the strength in these composites suffers, or does not improve. This is illustrated in Figure 2.14, where polypropylene/OMMT composites prepared via twin screw melt compounding were analyzed by Manias et al. [82].

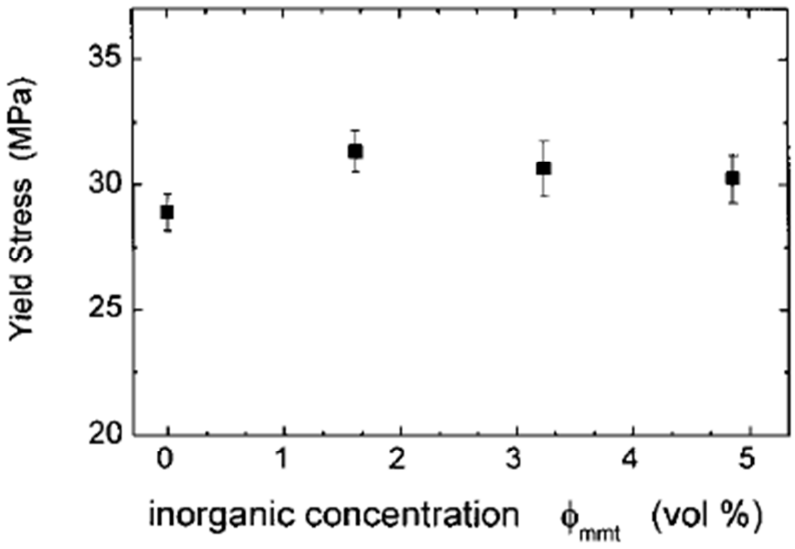


Figure 2.14. Comparison of yield stress at different concentrationos of nanoclay in nanocomposite modified from [82]

Figure 2.14 indicates that no improvement in yield strength is observed in TPO/OMMT nanocomposites. However when including a small amount of compatibilizer, an improvement may be observed. Work by Reichert et al. [83] indicated that after suitable PP-g-MA

compatibilizers were melt compounded with the host matrix, considerable tensile property enhancements realized in both tensile modulus and yield strength. It is suspected that if the stress transfer between the matrix is even partially transferred to the nanofiller, the yield strength may benefit.

The ductility of polymer-clay nanocomposites, which is determined by the elongation at break value, is also an important material property. Generally, the addition of fillers decreases the ductility of polymers. With conventional composites such as glass fiber and talc, this is generally evident at all concentrations, and especially at high concentrations (10- 20 wt%). This phenomena has also been observed for nanocomposites. In early work, it was suggested that elongation at break of the nanocomposites might be enhanced or maintained when using MMT [84]. Later work has determined that ductility of polymer nanocomposites may only be enhanced in limited cases. At very low concentrations (< 1 wt% organoclay) some authors have reported increases in ductility. Ibanes et al. [85] observed increased ductility in nylon 6/OMMT drawn composites at 1 wt% OMMT. The authors claim that the nanoclays act to disrupt the intercrystalline tie chains which would otherwise induce a physically cross-linked network. Much of the effect on ductility of the nanocomposites has to do with the degree of cyrstallinity, or crystallization kinetics in semi-crystalline polymers. These effects have been thoroughly investigated by Fornes et al. [47] with nylon 6 and OMMT nanocomposites prepared via twin screw melt compounding. The authors of this work observed increasing crystallization kinetics at low concentrations, as the clay acts as nucleating agents for heterogeneous nucleation. At higher concentrations (>3 wt%), the clay disrupts the crystallization kinetics, creating physical barriers which hinder the polymer chains to diffuse and form spherulites. Although the amorphous content of these composites was found to be higher than for low concentration composites, at

such large nanofiller concentrations the brittle nature of the nanoclay dominates the composite properties and the elongation to break decreases.

#### 2.2.3.2 Heat distortion temperature

The heat distortion temperature (HDT) of polymers may be significantly altered with the addition of OMMT. Heat distortion temperature refers to the temperature at which a sample deforms a predetermined amount under an applied load, otherwise known as softening. Fornes et al. [2] investigated the HDT of nylon 6/OMMT nanocomposites prepared with twin screw melt compounding. The authors observed increases in the HDT by as much as $100^{o}$ C for about 7 wt% OMMT in the nanocomposite. Similar effects are reported for glass fiber composites, albeit at much higher concentrations of filler. These observations are important as similar increases in the HDT of chemically modified materials are difficult to obtain.

#### 2.2.3.3 Flame retardency

The flame resistance of polymer nanocomposites has been reported as an important property of polymer/OMMT materials. Theories suggest that the nanoclay/polymer interface is important to good char formation [86]. The char that is formed protects the bulk material by preventing continual surface regeneration of available fuel. The most significant flame retardency effect attributed to OMMT nanocomposites is the ability to reduce the maximum heat release rate compared to the pure polymer [86]. This effect is represented in a theoretical graph in Figure 2.15.

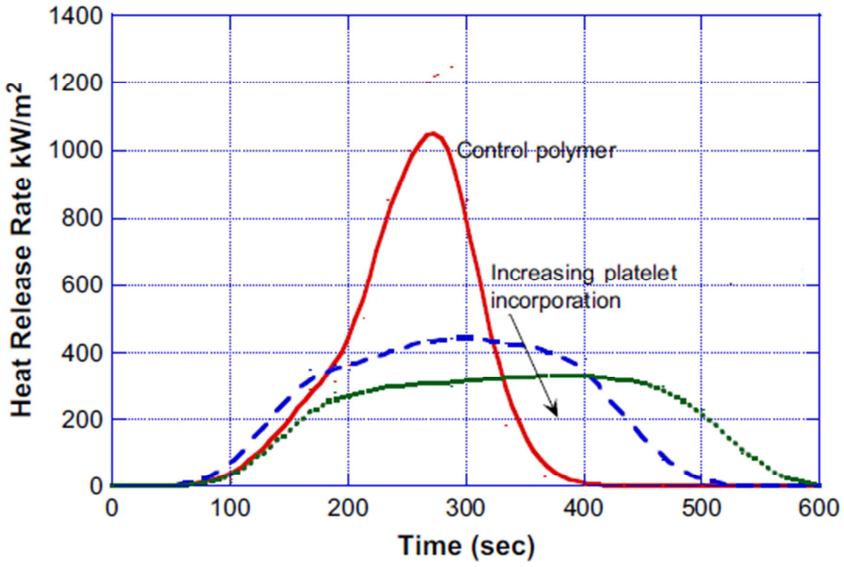


Figure 2.15. Generalized behavior of MMT nanocomposites in cone calorimetry testing modified from [5]

Although the maximum heat release rate is decreased for OMMT nanocomposites, the total amount of heat release is maintained, meaning a flame will burn cooler for longer. The practical application of this is in minimizing flame propagation from the nanocomposite material to its nearest neighbor. In terms of traditional flammability, polymer/OMMT nanocomposites tend to fail the general pass/fail test for ASTM standard. The most marked improvement involves reducing the total amount of flame retardant additive required to pass the flammability test [87]. Although these findings have been observed for TPOs [88] as well as nylon 6 [89], the advances are not attributed to certain polymeric systems. The degree of exfoliation and dispersion of the nanofiller is the most important variable. If clay is well dispersed, then the char surface may form evenly to decrease flammability of the composite, whereas a less dispersed system will not form an even char, providing more fuel for combustion [87-89].

#### 2.2.3.4 Coefficient of thermal expansion

Thermoplastic materials may possess high coefficients of thermal expansion (CTE) which can result in dimensional changes during the molding of parts, as well as changes in temperature in the ambient air. In automotive applications, this is a particularly undesirable trait where the molded thermoplastic parts must be used in combination with metal parts that possess low CTE. Glass fibers and other traditional fillers do not significantly affect the CTE in thermoplastic composites, but when high surface area/high aspect ratio nanofillers are included such as OMMT, the CTE may be significantly affected [76].

Thermoplastic/MMT nanocomposites possess higher CTE's due to the high CTE of MMT. As the polymer tries to expand, the platelets resist this change which induces opposing stresses in the material, reducing the CTE of the nanocomposite. Yoon et al. [76] observed this effect in nylon 6/OMMT nanocomposites prepared with twin screw melt compounding. The results are illustrated in Figure 2.16.

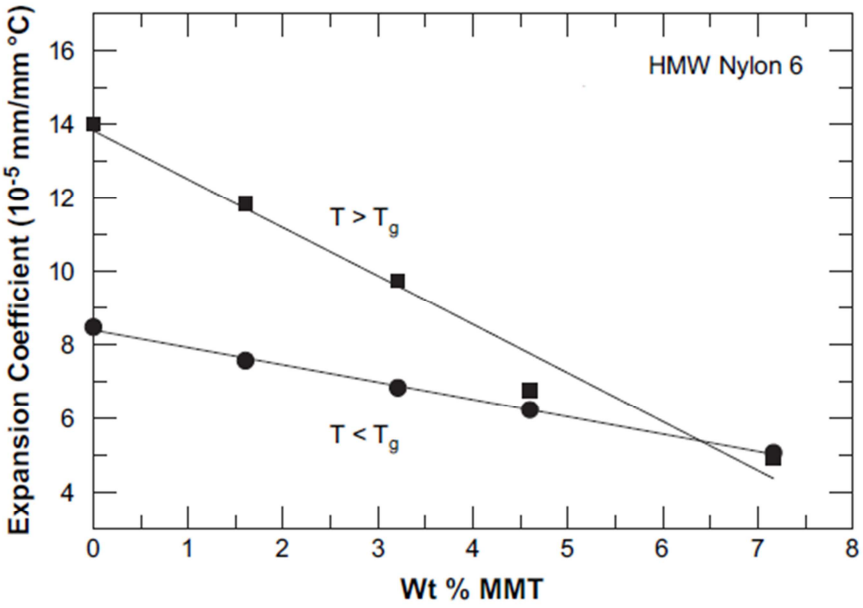


Figure 2.16. Coefficient of thermal expansion of nylon 6/OMMT nanocomposites at different concentrations. Comparisons of studies conducted above the Tg and below the Tg are included, modified from [5]

In fiber-like materials, the effect is not as pronounced as for platelets where the restraining effect is possible in two dimensions rather than one. However, the dispersion and alignment of the nanoparticles has a significant effect on the dimensional stability and stresses which must be taken into account during processing. These results are similar for TPO polymers as well [90].

#### 2.2.3.5 Barrier Properties

The barrier properties of thermoplastics can be significantly improved with the addition of inorganic montmorillonite, but the improvement in barrier depends strongly on the extent of dispersion and on the loading level of nanofiller. When the nanofiller is sufficiently exfoliated in the polymer matrix, penetrant molecules must diffuse a more tortuous path than in the virgin matrix. A schematic of this effect is illustrated in Figure 2.17.

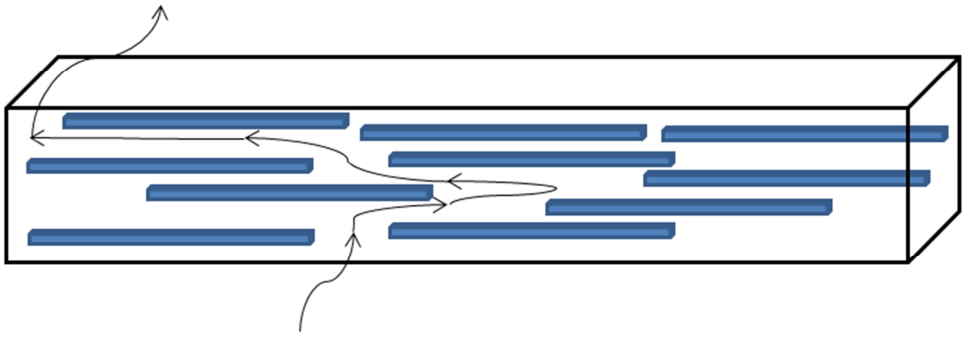

Figure 2.17. Schematic drawing of barrier properties improved with MMT. Line drawing potential path of penetrant gas molecule

When nanocomposites containing fillers with high aspect ratios, such as OMMT, possess significantly exfoliated morphologies, enhanced barrier properties are obtained.

The barrier properties from various epoxy composites were analyzed and compared to the d-spacing of the nanoclay in these composites by Osman et al. [91]. The results are summarized in Figure 2.18.

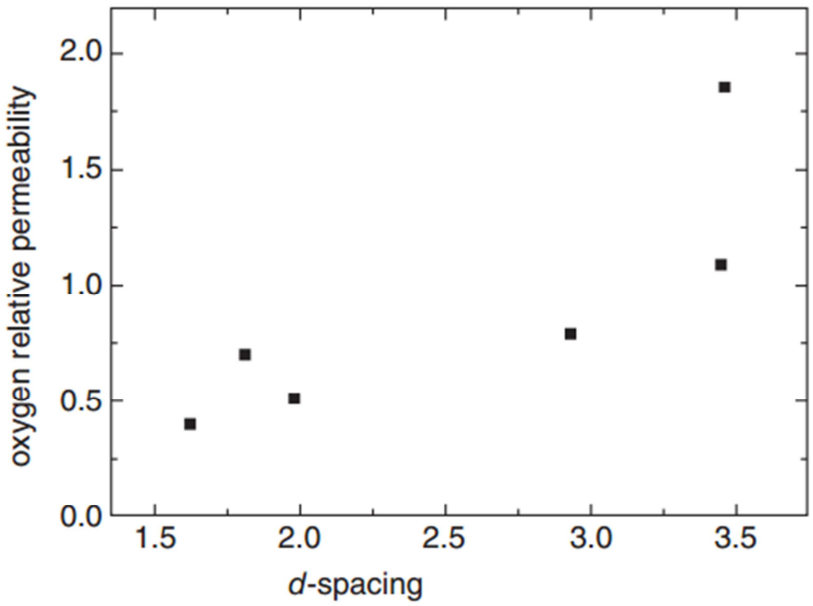


Figure 2.18. Barrier properties of composites based on the basal spacing, modified from [91]

In this study, the authors found that the degree of intercalation had no effect on the gas permeation properties, and therefore only exfoliated nanocomposites could significantly improve the gas barrier properties. In the case of the exfoliated nanocomposites, significant oxygen barrier properties were observed compared to the virgin matrix [91].

PET nanocomposites have been investigated for barrier properties in both academia and industry due to their application in improving plastic bottles for carbonated beverages. The ability to improve the barrier properties in PET with minimal addition of MMT was investigated by Kim et al. [92] where the authors observed a doubling in the reduction of gas permeability with as little as 1 wt % MMT in nanocomposites produced with *in situ* polymerization. Similar studies by Choi et al. [93] were conducted where the authors prepared PET nanocomposites using nanoclay with a supported catalyst to polymerize the matrix. The authors report between 10-15 fold decreases in the permeability of $O_2$ with the addition of 1-5 wt% clay. The inclusion

of low amounts of exfoliated MMT is desired in these applications in order to retain the clarity of the PET bottles that might be manufactured.

#### 2.2.3.6 Rheological properties

Rheological properties are important to understanding the micro and meso structure of polymer nanocomposites, as well as the processability of melt compounded nanocomposites. Where WAXD and TEM are more direct measures of nanoclay dispersion, rheology is an indirect tool. Due to the scope of this literature review, it is assumed that the reader has a base knowledge of rheology, and only concepts required to understand rheology as it applies to nanocomposites are explained. Additionally, the scope of this section focuses on the analysis of dynamic oscillatory shear experiments as they are related to the current work.

The storage modulus (G') behavior as a function of frequency for nanocomposite melts is often analyzed to determine the state of dispersion or exfoliation in polymer nanocomposites from dynamic oscillatory shear experiments. Rheological properties of polymer/nanoclay nanocomposites were first studied by Krishnamoorti et al. [94] where the authors investigated end-tethered PCL and nylon 6 nanocomposites produced with *In situ* polymerization. The authors utilized time temperature superposition (TTS) and shifted G' values at different concentrations to a reference temperature of 55$^{o}$C. This allowed the authors to comment on the rheological response of the material. The storage modulus versus frequency TTS plots are illustrated in Figure 2.19.

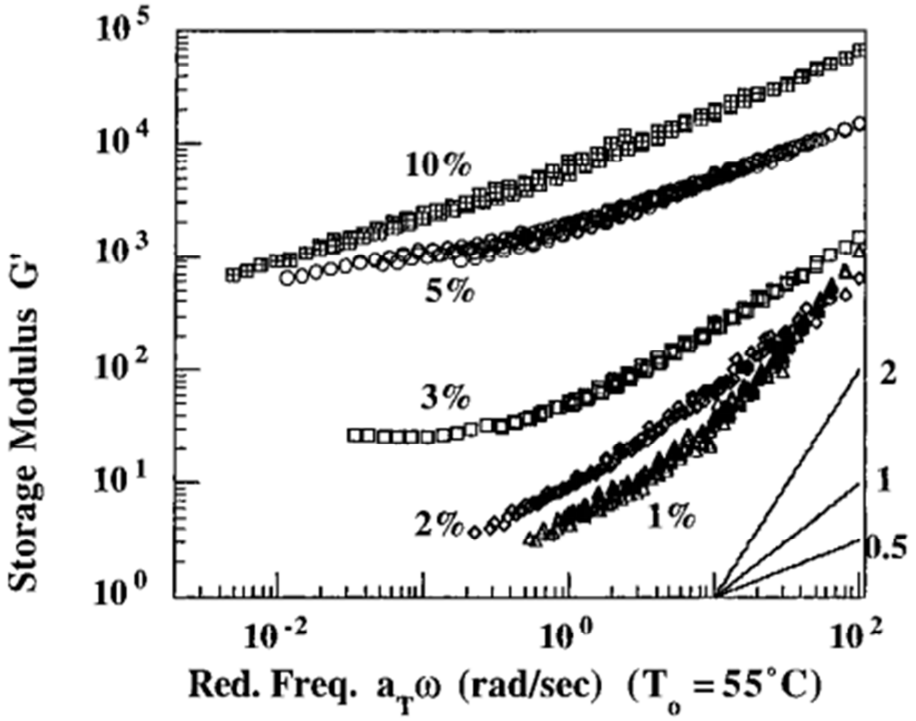


Figure 2.19. Storage modulus versus shifted frequency for PLC based silicate nanocomposites, modified from [94]

From the storage Modulus data, Krishnamoorti et al. [94] were able to interpret some general trends. Normally, a slope ($G'/a_Tw$) of 1 or 2 is expected for non-cross-linked polymers in plots of G' versus frequency. However, with small additions of clay the authors observed significant reductions in these slopes. The authors suggest this may be due to the formation of a network in the molten state known as percolation. Theoretically, this percolation indicates that a continuous physical network of polymer and nanomaterial, or nanomaterial and nanomaterial, has been established in the sample. A reduction in the slope of the plots in Figure 2.19, or a plateau in the G' values is often used to suggest a rheologically percolated network resulting from exfoliated nanocomposites. However, this can be misleading as similar behavior has been seen for composites known to possess intercalated morphologies, or to be phase separated from the polymer matrix [57, 60]. In these cases, the meso-structure, or percolated network, is formed of

agglomerated nanoclays at high concentrations. For this reason, rheology must be used carefully when being applied to morphological considerations.

Plots of complex viscosity (η*) versus frequency may also yield characteristic behavior which indicate a rheologically percolated network in polymer nanocomposites. Furthermore, this is a more direct way of measuring the processability of a nanocomposite following application to the Cox-Merz rule. Although direct use of the Cox-Merz rule may not be valid due to nano effects, it can still be helpful in determining the melt viscosities of the nanocomposites. Fornes et al. [45] studied the dynamic mechanical responses of different molecular weight nylon 6 nanocomposites which are illustrated in Figure 2.20.

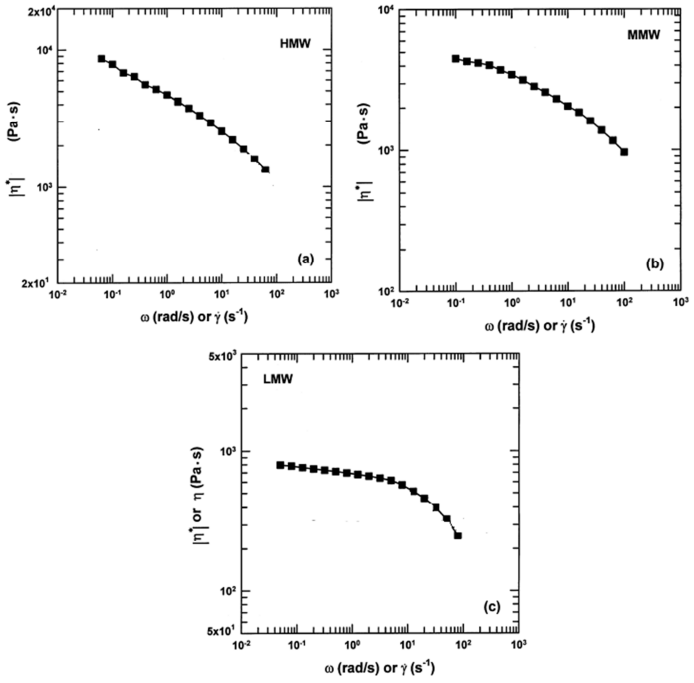


Figure 2.20. Complex viscosity versus frequency of nylon 6 /OMMT nanocomposites prepared with different matrix molecular weights modified from Fornes et al. [45]

The authors observed similar terminal behavior (high frequency) for each of the composites for the complex viscosity, but at lower frequencies the complex viscosity of each was notably

different. At higher molecular weights, non-Newtonian behavior was observed at low frequencies, but at lower molecular weights more Newtonian behavior was observed. Fornes et al. [45] attributed this to different degrees of exfoliation in the polymer nanocomposites. It has been suggested that a tail in η* at low frequencies is indicative of a percolated network, as is seen in the top left graph of Figure 2.20. Indeed, the degree of exfoliation was shown to be higher for the HMW nanocomposites in this study through WAXD and TEM as well. However, these same tendencies have arisen in immiscible nanocomposites at high concentrations [13, 57, 95]. Poslinski [96] studied rheological properties of filled polymer systems and observed that at a higher volume fraction of filler, the viscosity curve will translate to higher values. Since as dispersion increases, the volume fraction of filler increases (stacks versus individual platelets), observations of this nature can be used to make correlations about morphology. This is evident in Figure 2.20 where the magnitude of the viscosity curves increases with greater degrees of dispersion (HMW>MMW>LMW). Poslinski [96] also observed that the onset of shear thinning will shift to lower frequencies with increasing filler content, or with more dispersed material. The correlations from a complex viscosity curve may provide information regarding the extent of dispersion for nanomaterial in a nanocomposite system, but rheologically percolated networks may be observed where large agglomerates still exist. Therefore, η* versus frequency plots should only be used to indirectly analyze the morphology of thermoplastic nanocomposites.

Polymer/nanoclay nanocomposites may possess interesting mechanical, flame retardant, barrier, thermal expansion, or heat distortion properties compared to the virgin matrix, and have the potential for replacing conventional thermoplastic composites in industry. However, a suitable nanocomposite generation method which disperses and distributes the nanoclay in the polymer matrix must be chosen. Melt compounding is a favorable choice for nanocomposite

generation, especially when the polymer of choice interacts favorably with the nanoclay surface. However, twin screw or high shear melt compounding is often required which can be costly and energy intensive. In lieu of costly twin screw melt compounding, novel single screw melt compounding nanocomposite generation methods must be explored.

## 2.3 Carbon nanotubes

Following Iijima's publication on multi-wall carbon nanotubes (MWNTs) in 1991 [97], tremendous interest has focused on carbon nanotubes (CNTs) in the area of CNT reinforced composite materials due to their mechanical and conductive properties [98, 99]. Although the first observation of CNT by TEM was reported by Radushkevich et al. [100], and they were already being utilized industrially by Hyperion Catalysis Inc.(Cambridge, OH, USA) following a patent in 1987 [101], it wasn't until Iijima's paper that widespread attention was brought to the field. In this section, CNT structure, synthesis via chemical vapor deposition, properties, and potential applications are introduced and discussed. Special attention is paid to multi-walled carbon nanotubes for potential application as fillers for polymers with improved conductivity and mechanical properties.

### 2.3.1 CNT structure

Carbon nanotubes are long cylinders of covalently bonded carbon atoms, made up of rolled graphite or graphene sheets. There are two major types of CNTs, single-walled and multi-walled CNTs. Single-walled CNTs (SWCNTs) are comprised of rolled graphene resulting in a single nanotube, whereas multi-walled nanotubes (MWCNTs) consist of rolled graphite which results in concentrically rolled graphene sheets. Figure 1.4 shows pictorial representations of types of CNTs [102]. The diameter of the nanotubes can be as small as ~1 nm, or as large as tens of nanometers for both SWCNTs and MWCNTs. For MWCNTs, the distance between coaxial

graphene cylinders is approximately 0.34 nm, which is the interlayer distance of typical graphene sheets. The lengths of MWCNTs can be between a few hundred nanometers, and several microns long. SWCNTs are usually capped in the ends with a fullerene molecule, and in some cases can be centimeters long. The aspect ratio of CNTs can be as low as ten for very short tubes, or as high as several hundred thousand for long tubes [102, 103].

An important morphological characteristic of CNTs is their chirality, and each nanotube's properties differ drastically depending on this attribute. The chirality of the CNTs can vary, with three main morphologies: arm-chair, chiral, and zigzag, as illustrated in Figure 2.21 .

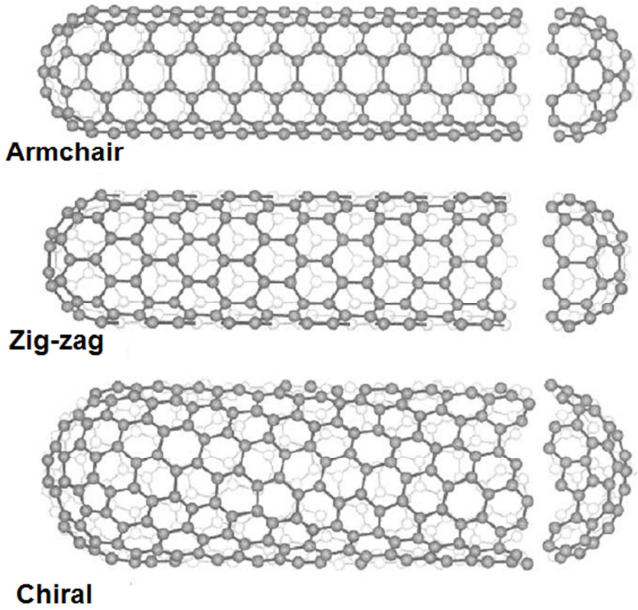


Figure 2.21. Different potential morphologies of CNTs, adapted from [103]

The configuration of the hexagonal carbon lattice packing defines a chiral vector (m,n) and an associated angle. Lau et al. [104] described that when the value calculated by m - n/3 is an integer, the SWCNT is metallic and so acts as one conductively. If not, then the CNT acts as a semi-conductor. This vector can also be used to determine the diameter of the CNT once the chirality is deduced. These morphologies exist for individual SWCNT, but MWCNTs can exhibit

several chiralities at once, making their properties difficult to predict, with both metallic and semi-conductor properties [103].

### 2.3.2 CNT Synthesis: Chemical vapor deposition

The chemical vapor deposition (CVD) method of CNT synthesis was first utilized to produce MWCNTs by Endo et al. [105] in 1993. This process was later adapted by Dal et al. [106] to produce SWCNTs using a cobalt catalyst. In CVD, hydrocarbon, metal catalyst, and inert gas are introduced into a reactor. The components are then reacted between 700$^{o}$C – 900$^{o}$C and the nanotubes form on a substrate from decomposition of the hydrocarbon. In this case, the diameter of the CNTs is determined by the size of the catalyst particles in the reactor. The mechanism of CNT growth can either be "base growth" ((a) Figure 2.22), where the catalyst remains at the nanotube base and the nanotube grows out, or "tip growth" where the catalyst stays at the tip of the growing nanotube ((b) Figure 2.22). The CVD process and these growth mechanisms are illustrated in Figure 2.22.

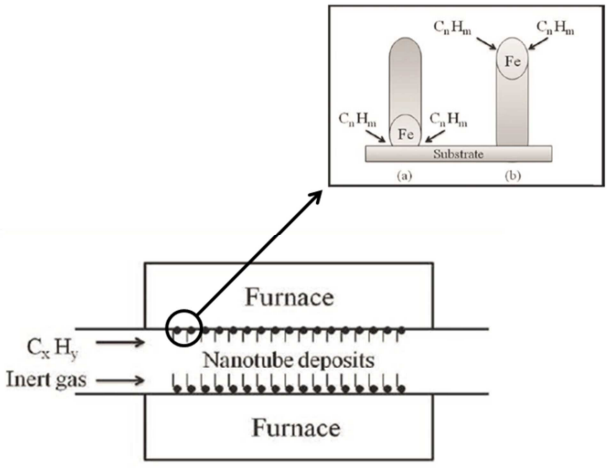


Figure 2.22. Illustration of CVD CNT synthesis, inset represents (a) base growth and (b) tip growth modes, modified from [102]

This synthesis method provides more control over the length and structure of the CNTs than the other common processes. In addition, the chemical vapor deposition method has the potential to provide the most bulk material as an industrial process. However, CNTs produced with CVD are structurally inferior to those produced with laser ablation and arc discharge, with more defects resulting in decreased mechanical properties and conductive potential. In addition, due to the growth mechanisms involved with CVD, different CNT structures such as bamboo-like CNTs can be formed. This occurs when the CNT growth phase closes around the catalyst as it proceeds along the CNT, causing the internal structure of the CNT to be essentially compartmentalized [105].

### 2.3.3 CNT properties

The highly ordered structure of CNTs leads to outstanding mechanical, thermal, and conductive properties of the nanomaterial. Due to the size of the particles, however, it is difficult to obtain experimental values for their stiffness, strength, and electrical conductivity. Both theoretical and direct experiments have been carried out to calculate the values in the literature, which are reviewed in this subsection.

#### 2.3.3.1 CNT Mechanical properties

The direct determination of mechanical properties of CNTs has been carried out by Treacy et al. [107] in 1996. In this work, the authors calculated the amplitude of thermal vibrations by using TEM and temperatures of 800$^{o}$C. An average stiffness of 1.8 TPa was reported by the authors. In more recent work by Yu et al. [108, 109] in 2000, stress-strain experiments were conducted using a “nanostressing stage” inside a scanning electron microscope (SEM). The authors observed the strength of the outer wall of MWCNTs to be between 11 – 63 GPa at fracture strains of 12 wt%. The reported modulus values ranged between 270 to 950 GPa,

which are lower than those previously predicted. These values were found to be related to the number of defects on the CNTs, as well as bends and twists in the conformation of the tube [110]. Other methods have been utilized to determine the mechanical properties of CNTs, including micro-Raman spectroscopy [111], and AFM on individually suspended nanotubes [112, 113]. The moduli reported in these works range from 270 GPa to 1 TPa, and the strengths vary from 11 GPa to 200 Gpa. In general, the experimental values observed for CNT suggest that the potential for structural reinforcement of MWCNTs is significant, although they vary significantly.

#### 2.3.3.2 CNT Electrical conductivity

The electrical conductivity of CNTs was first theoretically modeled in work by Mintmire et al. in 1992 [114]. In this work, the authors investigated different parameters on the electrical properties of CNTs, and observed that the chirality and the diameter of the CNTs strongly influence the electrical properties [115]. The electrical conductivity of CNTs can be described as metallic or semi-conducting depending on the chirality. This arises from the nature of the $\pi$ bonding and anti-bonding bonds perpendicular to the CNT surface. Arm-chair nanotubes are expected to be metallic, while 1/3 of zigzag and 1/3 of the chiral tubes are expected to be metallic, with the remaining configurations presenting as semi-conductors. This applies to MWCNTs as well, since they contain a mixture of these chiralities in their structure [116, 117].

Experimental investigations of the electrical conductivity of CNTs were performed by Ebbesen et al. [118]. In this work, the authors conducted four point probe testing of eight individual MWCNTs and reported a wide range of conductivities, with the lowest being ~20 S m, and the highest approaching $2 \times 10^7$ S m. For SWCNTs, the conductivity has been reported to between $10^5$ and $10^6$ S/m for metallic tubes, and 10 S/m for semi-conducting tubes.

Imperfections in the CNTs greatly affect the electrical conductivity [118]. Therefore, bulk and commercially grown CNT consistently possess inferior properties to both theoretical and idealized experimental values.

The unique structure of CNTs has resulted in investigations of the mechanical, thermal, and conductive properties. The intrinsic qualities of CNTs compared to current filler materials such as carbon black suggest significant potential for nanotubes as thermoplastic fillers. For the scope of this work, the focus will shift from covering both SWCNTs and MWCNTs to only MWCNTs. The reference to CNTs beyond this section refers to MWCNTs only.

## 2.4 Nanotube nanocomposites

Polymer/CNT nanocomposites have been developed in the past two decades in order to take advantage of the properties of CNTs. Combined with their low density and high aspect ratio, the mechanical, electrical, and thermal properties of CNT make them prime candidates for polymer nanocomposite filler material. However, most nanotubes produced using industrial synthesis methods, such as chemical vapor deposition, result in a powder product with severely aggregated nanotubes that must undergo significant downstream processing in order to take advantage of the individual CNT properties. In this section, the morphologies of polymer/CNT nanocomposites are discussed, followed by the typical processing methods utilized to produce the nanocomposites. Finally, the properties of these nanocomposites are discussed in depth. The production of CNT nanocomposites by melt blending for electrically conductive materials are emphasized with special attention to the nanotube aspect ratios of CNTs in polycarbonate nanotube nanocomposites.

### 2.4.1 CNT nanocomposite morphologies

In order for thermoplastic composites to benefit from the properties of the nano-filler, CNT must be sufficiently separated from primary agglomerates and distributed throughout the polymer matrix during nanocomposite generation. Due to the unique nature of CNT agglomeration and the immense difficulty associated with individualizing the filler in polymer composites, few systems have realized the full potential of CNT property enhancements [119-121].

The first step in CNT dispersion requires that initial agglomerates (primary agglomerates, (a) Figure 2.23) be debundled during CNT composite processing. This is referred to as primary deagglomeration. Primary deagglomeration must be followed by distribution of the individual nanotubes in the polymer matrix to produce an evenly dispersed nanocomposite ((b) Figure 2.23). This is a difficult task, however, due to the van der Waals forces which attract CNTs to one another. Furthermore, long range motions between carbon nanotubes in the polymer matrix lead to reaggregation, or flocculation, of the nanofiller (secondary agglomeration, (c) Figure 2.23) [122]. However, this phenomenon leads to improved electrical conductivity so is usually induced during processing [122]. Each of these morphological instances are illustrated as TEM images in Figure 2.23

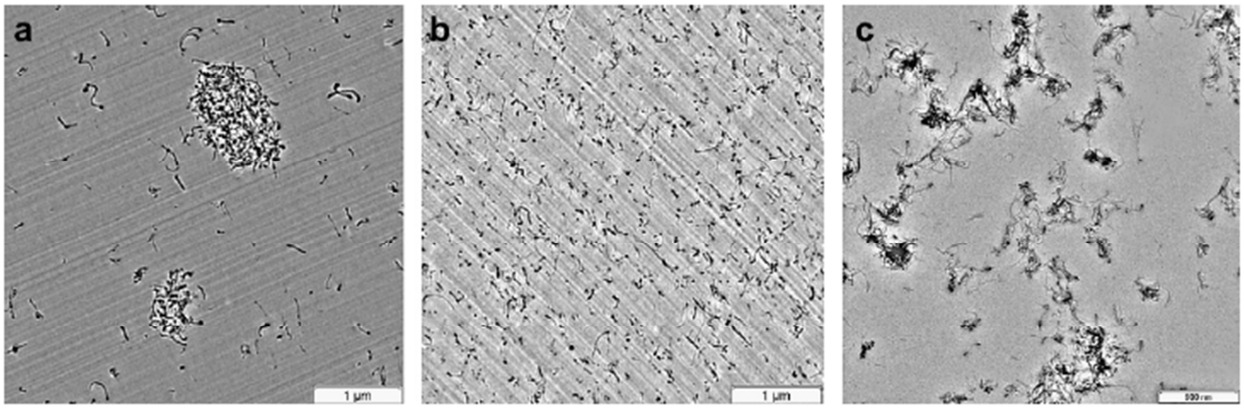

Figure 2.23. Examples of (a) primary agglomerates, (b) well dispersed nanotubes, and (c) secondary agglomerates

This subsection addresses the techniques used to analyze dispersion of CNTs in polymer nanocomposites, and the mechanisms for dispersion and distribution.

#### 2.4.1.1 Optical microscopy and TEM

Optical microscopy (OM), or light microscopy, is a technique that is used to quantify micron scale morphology in CNT nanocomposites. Sample preparation for OM involves microtoming relatively thick samples (500 nm – 5 microns thick) of a CNT nanocomposite, followed by capturing an image of these slices with a light microscope at moderate magnification. The thick sections used in OM allow larger volume fractions of the nanocomposite to be represented for morphological analysis, which permit a more representative sample size of the bulk material than with TEM. The image is then modified with a band pass filter or other contrast enhancer, and the particle sizes are identified using software such as ImageJ. One disadvantage to this technique is that you must compare samples prepared at the same weight percent nanofiller in order to make meaningful conclusions about the degree of dispersion. An example of a set of comparative OM images of CNT nanocomposites is shown in Figure 2.24.

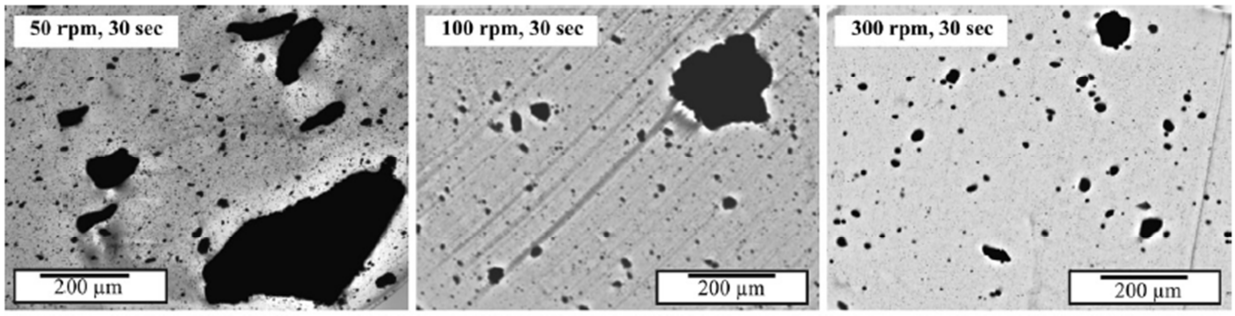


Figure 2.24. Comparison of PC/CNT nanocomposite OM images processed with twin screw extrusion at different RPMs modified from [123]

Villmow et al. [124] compared extrusion parameters in PC/CNT composites, including extruder speed. Figure 2.24 illustrates that the degree of dispersion was observed to increase significantly with rotational speed at the same concentration, where dark regions in the optical micrographs indicate nanotube aggregates and lighter regions are polymer rich regions (which may include disperse CNTs). These results can be quantified in many ways, but one of the more common methods is illustrated by the percent area of aggregates, shown below in Equation (2.2).

$$A_A = \frac{A_{CNT}}{A_O} * 100\% \tag{2.2}$$

$A_A$ represents the area fraction of undispersed primary CNT agglomerates which can be used to compare the effectiveness of a processing method at CNT dispersion. $A_{CNT}$ is the area occupied by the remaining CNT agglomerates (dark regions in Figure 2.24) and $A_O$ is the total area of the image. A detailed instruction on how to use this method with more quantitative analyses is given in McNally and Potschke [125]. Although this is a very effective technique to determine the bulk dispersion of CNTs in a nanocomposite, only particles on the micron scale may be identified. This indicates that particles not observed as agglomerates are assumed as “disperse”. This may not be the case, however, as they may exist as sub-micron scale agglomerates. Therefore, TEM must be utilized to observe interactions on sub-micron scales in combination with OM.

TEM is generally accepted as the primary means of nanoscale morphological characterization in CNT polymer nanocomposites. The specifics of TEM will not be discussed here, as they were briefly presented in Section 2.2.1.1. As with nanoclay composite characterization, TEM images of CNT nanocomposites represent small sections of the larger nanocomposite, and may be misleading because of this. However if enough images are taken at

different magnifications, a sufficient representative image set may be generated. In this manner, either quantitative or qualitative information about the nanoscale dispersion of the CNT nanocomposite may be divulged. As a qualitative tool, regions of larger aggregates can be identified and homogenous distribution of the filler may be recognizable. An example of a comparison such as this is shown in Figure 2.25.

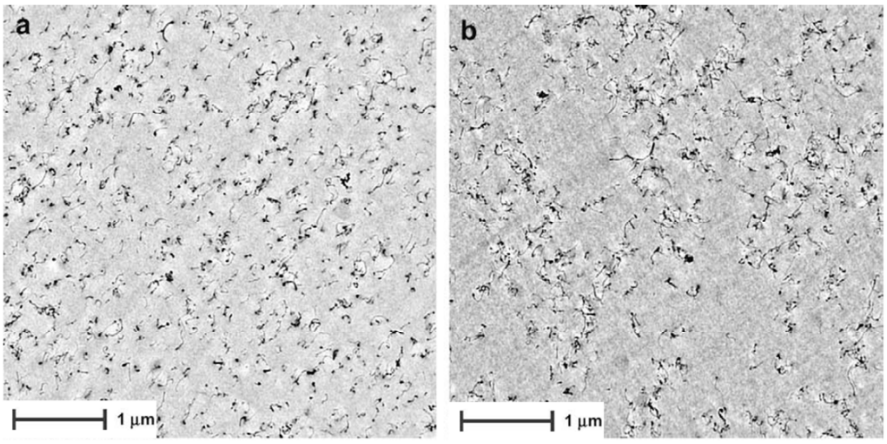


Figure 2.25. CNT/Polycarbonate nanocomposites injection molded at fast (a) and slow (b) injection speeds at a concentration of 0.875 wt % CNTs

Figure 2.25 illustrates different morphologies for images (a) and (b), where (b) contains less disperse nanomaterial than (a). Alternatively, quantitative spatial distribution of the CNTs can be estimated. Pegel et al. [126] describe a distribution coefficient ($Q_P$) which can be calculated from TEM images, and describes the divergence from a random Poisson distribution of particles in the filler matrix. Therefore, a $Q_P$ = 1 represents fully disperse nanotubes. Increasing values correspond to higher degrees of aggregation [122]. Further quantitative analyses of TEM images for CNT nanocomposites are beyond the scope of the current work, but may be procured from McNally and Potschke [125].

Neither OM nor TEM are sufficient for characterizing the overall morphology of CNT/polymer nanocomposites as standalone methods. For this reason, it is recommended that OM and TEM be used as complimentary techniques to one another when investigating the morphology of CNT/polymer nanocomposites. By observing both the primary agglomerate morphology and nanoscale dispersion in the nanocomposite, a more circumspect understanding may be obtained.

#### 2.4.1.2 Dispersion of CNT

A significant barrier to incorporating CNTs in polymers is to individualize, or debundle, the CNTs from large initial agglomerates and thereafter disperse them in the polymer matrix or solution. For this reason, the method of nanocomposite generation is especially difficult with CNT nanocomposites [122, 123]. Although mixing methods may be different for dispersing CNTs in solution blending, *In situ* polymerization, and melt blending, the dispersion mechanisms may be related. The initial agglomerates are wetted by polymer, infiltrated by polymer, and broken up by erosion and rupture mechanisms. Following this, the nanotubes tubes can be distributed throughout the polymer matrix. These topics will be discussed in the following paragraphs with theoretical models included where appropriate. It should be noted that each of these mechanisms may occur simultaneously during CNT dispersion [122]. For a more thorough treatment on this topic, the author would suggest reading Chapter 4 of the tome edited by MacNally and Potschke [125].

In order to understand how CNTs may be successfully dispersed, the structure and formation of primary agglomerates must first be identified. Carbon nanotubes received from industrial methods typically possess a bundled structure, known as “primary agglomerates”, presenting as entangled entities. These arrangements arise due to structural defects during the

growth phase of synthesis, and van der Waals interactions between CNTs. This is especially true for CNTs made in large scale fluidized bed reactors. An example of primary MWCNT agglomerates are shown in Figure 1.5, from Section 1.2.2 [122]. Both sets of MWCNT presented in this image possess individual CNT diameters around 10 nm, and are supplied in large agglomerates in the form of powder [127]. These nanotubes can be entangled and intertwined with one another in a tightly packed state. It is interesting to note that the type and extent of entanglement depends on the specific variety of CNTs. In Figure 1.5 from Section 1.2.2, the Baytubes (Baytube C150P) aggregate in smaller, tighter bundles, referred to as a "bird's nest" by Alig et al. [122], resulting in a high bulk density between 120-170 kg/m$^3$. The Nanocyl tubes (Nanocyl NC7000) are bundled in a "combed yarn" like structure, which is more loosely packed than the Baytube structure, resulting in a bulk density of ~60 kg/ m$^3$. This bulk density is related to the dispersability of CNT bundles by the strength of the agglomerate. CNT agglomerate strength has been estimated in the literature, and is important to understanding the forces required to destroy primary agglomerates. The Rumpf equation [128] may be applied to the strength of agglomerates, but must be modified for CNTs due to the existence of interlocking between individual tubes in the primary agglomerate. Therefore, a modified Rumpf equation (Equation (2.3)) which incorporates a stereological approach for isotropic fiber systems may be utilized for primary CNT agglomerates, as discussed in Stoyan et al. [122, 129].

$$\sigma_M = \frac{f * F_N}{2 * A_o} \qquad (2.3)$$

The strength of the agglomerates ($\sigma_M$ ) is calculated from the mean force for fiber pull out of agglomerate ($F_N$), the packing density ($f$), and the particle surface area ($A_o$). Certain concepts are useful to draw from Eqn. 3 when discussing the dispersability of primary CNT agglomerates.

Higher packing densities lead to larger cohesive forces in the agglomerates, as do larger values of $F_N$ which arise from more entangled agglomerates. As an example, the Baytubes discussed earlier would possess larger values of both packing density and $F_N$ compared to the Nanocyl tubes, due to the morphology of the agglomerates. Theoretically, when an applied stress for deagglomeration matches or exceeds this value, deagglomeration may occur via rupture mechanisms, which are discussed in further detail in following paragraphs. This model may be oversimplified, as it shows strong deviations due to the inhomogeneity of CNT agglomerates, but is still useful for discussion purposes [122].

The wetting of initial agglomerates is a crucial step in efficient dispersion of CNTs in a polymer matrix. This is highly dependent on the interactions between the fluid and the CNT agglomerates. Fluids with similar interfacial energies as CNTs may wet the surface of CNTs more readily. The greater the affinity of the wetting fluid for the CNTs, the better the ability of the fluid to wet the agglomerate. This can be improved by including functional groups on the CNT that may interact more readily with the wetting fluid. Generally, polar solvents and polymers possess greater wetting capability for CNT agglomerates, due to the polar nature of CNTs. Conversely, polyolefin polymer matrices and nonpolar solvents are less effective at wetting the CNT agglomerates [130, 131].

Polymer infiltration into the CNT bundles is essential to the dispersion of the initial agglomerates. Once polymer infiltrates the CNT agglomerates, the agglomerate cohesive strength may be significantly reduced, permitting easier dispersion. This mechanism can be estimated by infiltration of a fluid into porous media, as described by the Lucas-Washburn equation below (Equation (2.4)) [132].

$$h(t)^2 = \frac{r * \gamma * \cos\theta * t}{2\eta_1} \quad (2.4)$$

In this relation, the time dependent infiltration length is $h(t)^2$, $\eta_1$ is the dynamic viscosity of the fluid, $\gamma$ is the interfacial tension between the media and the fluid, $\theta$ is the contact angle, and $r$ is the pore radius. If $r$ can be increased, or $\eta_1$ decreased, infiltration length can be increased, and infiltration of the fluid into the agglomerate improved. Therefore, if we start with CNT possessing low bulk density, or utilize a low viscosity fluid, infiltration into the primary agglomerate is improved, and the barrier to dispersion is decreased. This model agrees well with experimental data, where solvents infiltrate CNT agglomerates more readily than viscous polymers. It follows that low viscosity thermosets are also more effective than thermoplastic elastomers at CNT infiltration. Another consequence of this relation is that smaller agglomerates which require shorter distances for fluid transport will experience infiltration more readily than larger agglomerates. Although useful, the Lucas-Washburn equation does not take into account some important factors, such as potential exclusions arising from small pore diameters and a large polymer radius of gyration, and external pressures arising during processing. Fluid infiltration of the primary aggregates is an essential step during CNT dispersion by decreasing the overall CNT agglomerate strength, and decreasing the stresses required to deagglomerate primary CNT bundles [122, 132].

Primary CNT agglomerate disintegration occurs through two mechanisms known as rupture and erosion. Rupture is a bulk phenomenon where larger agglomerates are broken into smaller ones on short timescales. Erosion is a surface phenomenon where individual nanotubes are peeled away from the surface of the agglomerate through attrition, which occurs over longer timescales. These mechanisms are depicted pictorially in Figure 2.26.

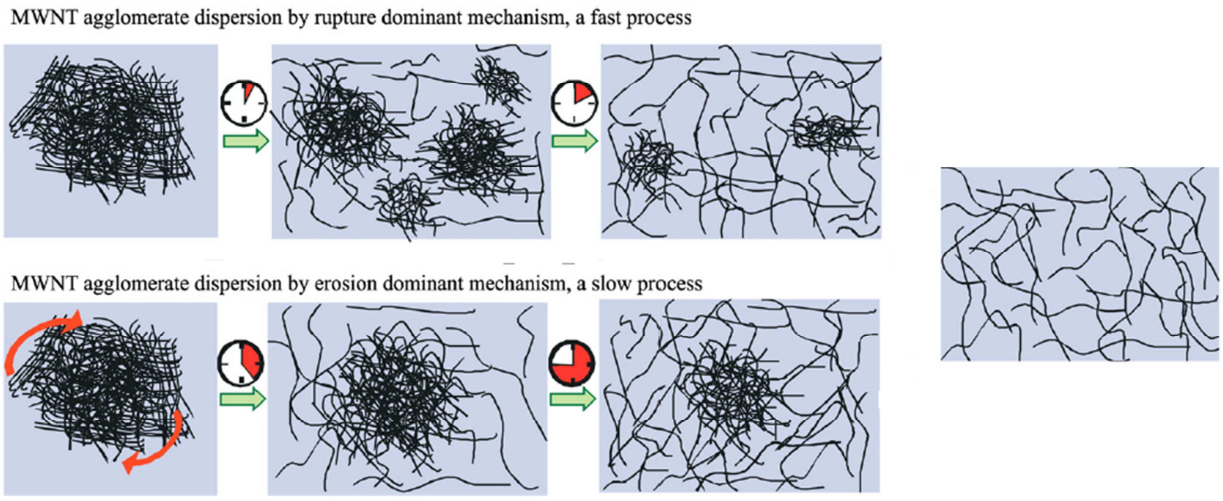


Figure 2.26. Pictoral representaion of erosion and rupture dispersion mechanisms with appropraite timescales attached for reference, modified from [123]

These mechanisms may occur simultaneously during dispersion in a polymer melt or solution, but each is distinctly different. The rupture mechanism (top Figure 2.26) requires higher stresses to break the initial agglomerates, but occurs on faster time scales than erosion. It follows that rupture deagglomeration is a more violent process than that of erosion [133]. This phenomenon can be observed in TEM of CNT nanocomposites as presented in Figure 2.27.

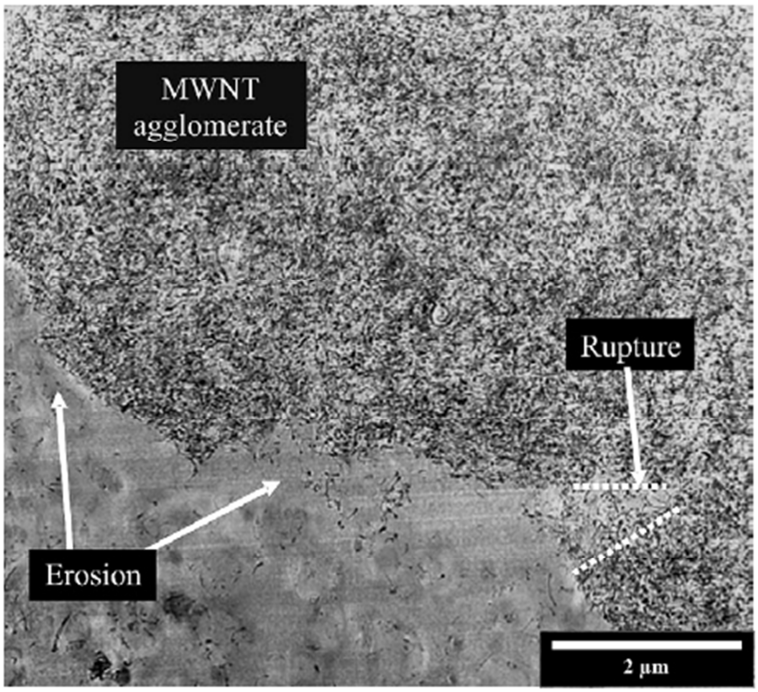


Figure 2.27. TEM of CNT nanocomposite with agglomerate and individual nanotubes. Regions of erosion and rupture dispersion mechanisms are highlighted, modified from [123]

During rupture, the crack shown in Figure 2.27 will propagate, leading to smaller agglomerates of different sizes. Rupture occurs nearly instantaneously when a sufficient shear stress is applied to the bundle. The timescales of rupture based dispersion of initial agglomerates is attractive for industrial process. However, rupture typically results in damage to the CNTs, decreasing the potential improved properties associated with the nanofiller [122]. Rupture causes breakage of the dry agglomerate core along the "crack" highlighted in Figure 2.27, leading to pull out of individual CNTs which are likely entangled with the main agglomerate. Inevitably, this will break individual CNTs, especially near surface defects. If these surfaces could be wetted before rupture, disentanglement may be more readily accomplished with less damage. During erosion, surface nanotube and small surface agglomerates are removed from the primary agglomerates in a mechanism similar to peeling, which is illustrated in the lower portion of Figure 2.26. This

requires significantly lower stresses, but may require very long timescales. Furthermore, the damage of the CNT is significantly less with this type of dispersion mechanism [123].

The dominating dispersion mechanisms, whether rupture or erosion, may be estimated in certain conditions by a dimensionless number called the fragmentation number (*Fa*). This concept was developed by Hansen et al. [134] and represents the ratio of vicious stresses to cohesive agglomerate stresses. The relation for *Fa* is given below in Equation (5).

$$Fa = \frac{\eta * \gamma}{\sigma_M} \tag{2.5}$$

The viscosity is given by $\eta$ and the shear rate applied to the surface of the CNTs is $\gamma$. In order to modify this model to apply to other mixing methods, the value of $\eta * \gamma$ must be replaced by the relevant stresses induced by mixing. The agglomerate strength, $\sigma_M$, was provided earlier in Equation (2.3). When the value of *Fa* exceeds one, rupture mechanisms dominate during mixing. In a process dominated entirely by rupture (*Fa*>>1, short timescales) the primary CNT agglomerates will be broken down into smaller and smaller agglomerates until individual tubes remain. Significant shortening of the CNTs is likely to occur in this scenario, without sufficient infiltration and wetting of the internal agglomerate. When erosion dominates the dispersion of the initial agglomerates (*Fa*<<*1,* very long timescales), CNTs will be peeled off the edge of the agglomerate, leading to minimal damage [122]. In order to reduce processing times and maintain CNT integrity, a compromise of rupture and erosion dispersion is usually desired.

Well dispersed CNTs tend to reform loose agglomerates in both solutions and liquid like polymer states. This is due to the long-range interactions between nanotubes, and is strongly dependent on the viscosity of the suspending media. This phenomenon is known as “secondary

agglomeration". These loose agglomerates are important in the formation of both rheological and electrical percolation in CNT/polymer nanocomposites. Secondary agglomerates are significantly more loosely packed than initial agglomerates, and can be easily broken up and reformed depending on experimental conditions [135]. Pegel et al. [136] studied PC/CNT nanocomposites and observed that secondary agglomeration leads to better electrical and thermal conductivity than aligned nanotubes. This phenomenon is discussed in more depth in Section 2.4.3 which discusses CNT nanocomposite properties as they pertain to rheological and electrical percolation thresholds.

The dispersion of CNT agglomerates involves wetting of the CNT primary agglomerates with the dispersing fluid, infiltration of the fluid into the agglomerate, and dispersion of the nanomaterial through rupture and erosion mechanisms. The individual CNTs or small bundles dispersed from initial agglomerates may be evenly distributed in the fluid and undergo secondary agglomeration or flocculation. Several models exist to describe these mechanisms, and are helpful in understanding the dispersion process during polymer/CNT nanocomposite generation. The next section is dedicated to these generation methods, which require intensive mixing to disperse and distribute the CNTs in polymer.

### 2.4.2 Processing methods for producing polymer/CNT nanocomposites

The three most common techniques for preparing polymer/CNT nanocomposites are *in situ* polymerization, solution blending, and melt compounding. Each of these methods must sufficiently deagglomerate the nanotubes in the polymer matrix, as well as disperse them on the nanoscale. To accomplish this, adequate stresses and mixing must be applied, which often leads to damage of the CNTs. This section addresses each of these nanocomposite generation methods

as they pertain to polymer/CNT nanocomposites with discussions on the drawbacks and positive attributes of each.

#### 2.4.2.1 *In situ* polymerization

Generation of polymer/CNT nanocomposites via *In situ* polymerization has been studied extensively in recent years. The concepts and implementation of this method is similar to that introduced in Section 2.2.2.1 for nanoclay nanocomposites, excepting that the nanomaterial utilized here are CNTs. *In situ* polymerization involves mixing the CNTs in a suitable monomer or resin, followed by polymerization of the monomer. During this process, the dispersion of CNTs may be accomplished by ultrasonic mixing. Sonicative mixing is a slightly complicated process, and may damage the CNTs. Therefore this topic is addressed briefly in this section. Following this, a brief discussion of literature in the field of *In situ* polymerization generation of polymer/CNT nanocomposites is reviewed.

Sonication is the most common form of dispersing CNTs from primary agglomerates for both *in situ* polymerization and solution blend nanocomposite generation. Sonication is the use of sound waves, formed either by bath or a probe, to force acoustic cavitation. Acoustic cavitation occurs as a result of sound waves forming bubbles, followed by runaway implosion of these bubbles which releases immense local force [137]. These sound waves can either be sonic, with frequencies <20 kHz, or ultrasonic, with frequencies >20 kHz. The cavitation process may result in the deagglomeration of CNT bundles but can also damage the CNTs. Lu et al. [138] first observed damage to CNTs dispersed with sonicative mixing by investigating TEM images of the nanotubes. The authors report buckling, bending, and dislocations to the CNT surface. Later work by Bradaire et al. [139] observed a drop in the electrical conductivity in CNT nanocomposites generated using intensive ultrasonic mixing by two orders of magnitude. The

authors suggest that shortening of the nanotubes resulted in a decrease in the CNT lengths, decreasing the electrical conductivity in the generated nanocomposites. This damage may be due to the rupture of dry agglomerates (Section 2.4.1.2) which can be mitigated by using a fluid which can sufficiently infiltrate and wet the CNT bundles. In some cases, short sonication times are required to fully disperse the CNTs due to strong solvent-CNT interactions, leading to improved wetting and infiltration. One such solvent is chloroform, which can disperse most commercially available CNT readily. In cases such as this, minimal damage to the CNTs is observed after sonication. Although solvents such as chloroform have been shown to successfully disperse CNTs without damaging them, little or no literature is available on nanocomposites generated with their aid [140].

Polymer tethered CNTs are some of the most interesting materials for CNT nanocomposite applications as they utilize covalent bonding of the polymer matrix with the CNTs to improve interactions with the bulk material [99]. This technique is especially useful when generating nanocomposites using unstable or insoluble polymers that may not be processed by solution or melt blending [102]. Some of the first work done in this field of tethered CNT polymer nanocomposites was by Jia et al. [141] where poly (methyl methacrylate) (PMMA) was polymerized with CNTs. AIBN was utilized as the initiator after the CNTs were distributed in monomer MMA using sonication. It was observed that some of the PMMA grafted to the surface, due to the initiator opening Pi-Pi bonds on the CNT surface. The authors reported improved mechanical and heat deflection temperatures in their nanocomposites up to nearly 10 wt% nanofiller. In one variation of this method, known as the “grafting to” method, functionalized groups are covalently attached to nanotube surfaces. Following this, the functional surface reacts with monomer during polymerization [142]. In another method, known as

"grafting from", an initiator may be covalently anchored to the CNT surface. This is followed by inclusion of the monomer, and finally polymerization from the surface of the nanotube. The methodology of this technique is summarized in Figure 2.28.

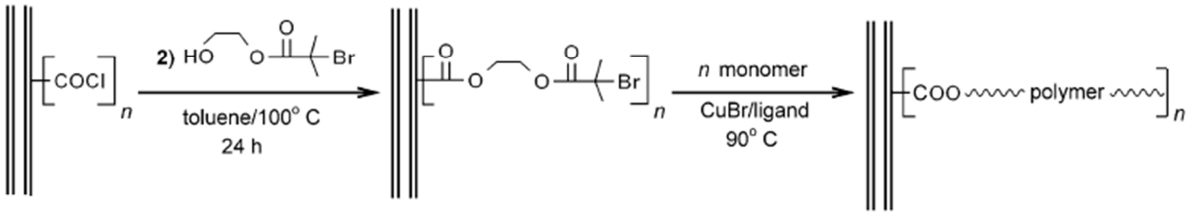


Figure 2.28. "Grafting from" *In situ* polymerization of a polymer from original COCl functionalized surface, modified from [143]

This method yields high concentration nanocomposites with relatively good interactions between the polymer and nanotubes.

Another form of grafting is used for the synthesis of polyolefin CNT nanocomposites which utilizes a heterogeneous catalyst rather than initiators or grafted functional groups. In this method, metallocene catalysts such as methylaluminoxane (MAO) may be covalently anchored to the CNT surface in a tethering technique with a heterogeneous catalyst. Following polymerization, the nanocomposite concentrations may be as high as 25 wt% CNTs depending on the processing conditions utilized [125].

*In situ* polymerization can be applied to many nanotube/polymer variations, but it is still limited in practice to specific polymer/CNT systems. Furthermore, the necessity of sonication, harmful solvents and lengthy processing times make *in situ* polymerization difficult to scale for large scale nanocomposite generation. Therefore, other methods are desired to generate polymer/CNT nanocomposites.

#### 2.4.2.2 Solution blending

Solution blend processing is the most common form of composite generation for CNT/polymer nanocomposites. In this method, CNTs are sufficiently dispersed in a suitable solvent, mixed with a polymer or prepolymer, and precipitated to form the nanocomposite product. Dispersion of the CNTs in the initial solvent is often carried out through sonication of the solvent/CNT mixture. Following the mixing step, the solvent can be removed either by drying in a vacuum oven for several days [144], or by removing the solvent via adding an anti-solvent to "dry" the nanocomposite [125, 145]. This sub section will briefly overview existing literature on CNT nanocomposites generated by these methods.

Polypropylene/SWCNT nanocomposites have been prepared by Grady et al. [144] using Decalin (Decahydronaphthalene) as a solvent for the polymer. Due to the poor interactions with the polymer, the solution was kept between 70 and 140$^{o}$C to ensure solvation. The resulting solution and SWCNT mixture was sonicated to obtain conductive nanocomposites with dispersed morphology, however no comments were made as to the length of the CNTs after sonicaiton [146]. Toluene has also been suggested as an effective solvent for PP by Assouline et al. [147] PP/MWCNT nanocomposites were prepared with this solvent using sonicative mixing yielding nanocomposites with good dispersion as evidenced by TEM. Ultra high molecular weight poly ethylene nanocomposites of MWCNT have also been synthesized using Decalin and Parrafin as solvents by Bin et al. [146]. In this study, the authors observed improved dispersion for the Decalin solvent compared to the Paraffin which was supported by conductivity and SEM measurements.

Polymer/CNT nanocomposites may be formed via solution blending with relative success. Solution blending requires few raw materials and limited thermal processing equipment,

but also requires extended processing time and environmentally harmful solvents. Furthermore, recovery of the nanocomposite can lead to reaggregation of the CNTs and residual solvent in the composite material. [43, 148]. Finally, solution blending requires sonication to adequately mix the materials, which has been shown to shorten the carbon nanotubes [125, 138]. Therefore, more environmentally friendly and benign processing methods are desired.

#### 2.4.2.3 Melt Compounding

Melt compounding methods of polymer/CNT nanocomposite generation are desired due to the lack of harmful solvents involved, reduced processing times, and ease of processing. Large initial CNT bundles are deagglomerated via shear stresses applied to the agglomerate during melt compounding, and subsequently distributed throughout the matrix. As with the other nanocomposite generation methods, deagglomeration of CNTs and subsequent dispersion are the main issues facing widespread implementation. In addition, damage to the nanofiller is commonly observed when applying high shear rates to rupture primary CNT agglomerates in twin screw melt compounding and high shear melt mixing devices. The issue of CNT damage during melt compounding is addressed followed by a review of polymer/CNT nanocomposites prepared by melt compounding, with special attention to the effect of processing conditions on the dispersion and distribution of CNT agglomerates.

The shortening of CNTs in polymer/CNT nanocomposites prepared via melt compounding has been reported in the literature. Krause et al. [140] recently developed a technique for determining nanotube length distributions in polycarbonate (PC) nanotube nanocomposites. In this study, the authors presented a method for investigating the damage to Nanocyl NC7000 and Baytube C150 HP CNTs. The nanotubes were first dispersed in chloroform under sonication for three minutes to investigate the aspect ratios before melt

compounding. The nanotubes and dispersant were then dropped onto a TEM carbon grid, and over 300 nanotube lengths and diameters were measured using TEM. The resulting length distributions are shown as histograms in Figure 2.29.

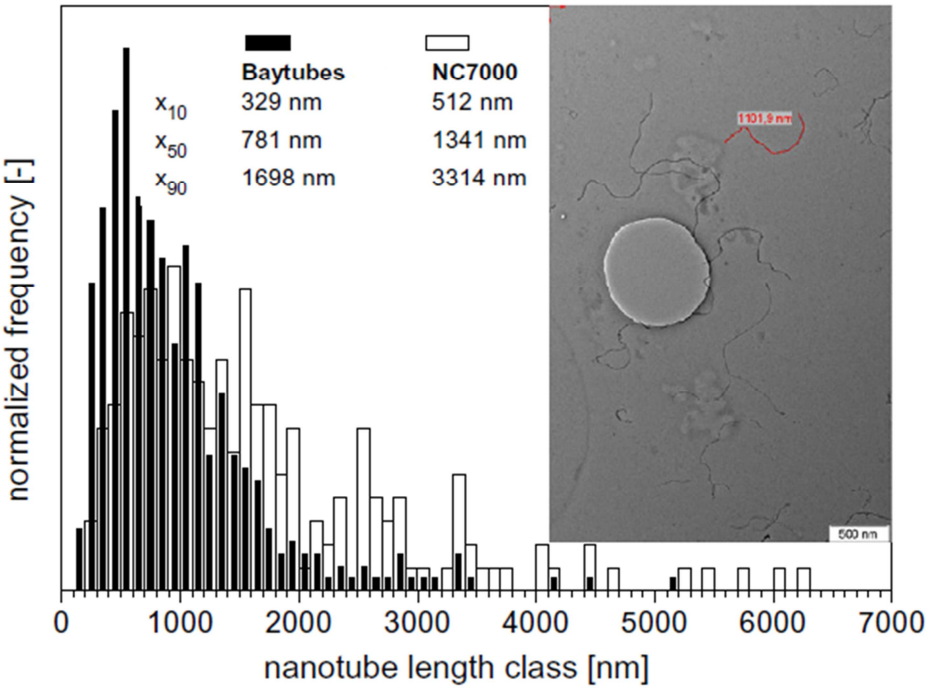


Figure 2.29. Normalized frequency of CNT lengths as observed from TEM measurements for Baytube C150HP and Nanocyl NC700 nanotubes, with sample CNT length measurement, modified from Kkrause et al. [140]

The authors investigated the effect of melt compounding these CNTs in polycarbonate using high shear melt compounding. Nanocyl NC7000 nanotube/polycarbonate composites were prepared from a master batch of 7.5 wt% CNTs, diluted to 2 wt% with a co-rotating twin-screw melt extruder. Polycarbonate/ Baytube C150HP nanocomposites were generated at 1 wt% using a DACA micro compounder with two conical co-rotating screws. The resulting nanocomposite pellets were then dissolved in chloroform and sonicated for 3 minutes. The resulting suspension was dropped on TEM grids, and over 300 CNT lengths were measured from the images. The

results for both nanocomposites and the as-received CNTs are illustrated in histograms in Figure 2.30.

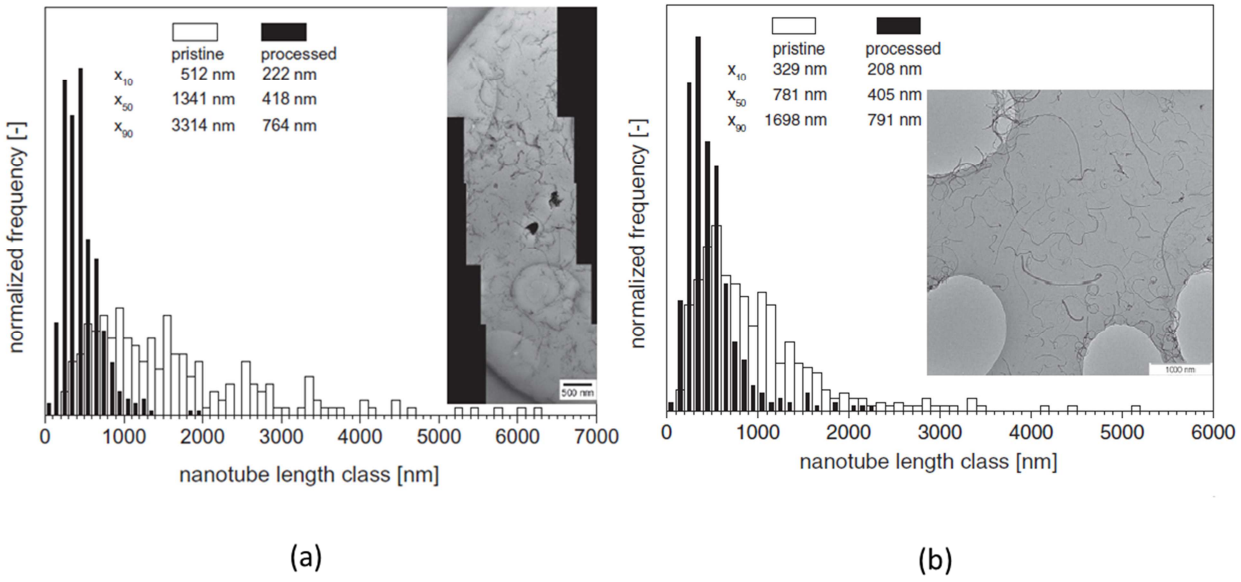


Figure 2.30. Length distributions of CNTs after high shear melt compounding. (a) Nanocyl nanotubes after twin screw melt compounding and (b) Baytube nanotubes after twin screw helical melt compounding, modified from [140]

It was observed that the Nanocyl CNTs had shortened by 70% of their initial length from twin screw melt compounding, from ~1300 nm to ~400 nm median length. The Baytube CNTs were reduced to 50% of their initial length, from ~800 nm to ~400 nm by high shear melt processing in a microcompounding device. The melt compounding conditions utilized in this study were at moderate shear rates and over normal residence times. The authors suggest that rupture of dry CNT agglomerate core during melt compounding leads to the shortening of the CNTs. These findings indicate that more benign methods of debundling primary CNT agglomerates must be investigated.

Kasaliwal et al. [123] investigated the dispersion mechanisms involved in melt compounding CNT nanocomposites with polycarbonate. Their primary goal was to discover

when rupture and erosion mechanisms would dominate primary agglomerate dispersion during melt compounding. The authors processed MWCNT/PC nanocomposites at 1 wt% using a micro-compounding device. They varied the mixing times from 30 seconds to 30 minutes, and the mixing speeds from 50 RPM to 300 RPM to analyze the effect of shear rate and residence time on the deagglomeration mechanism and degree of dispersion in the nanocomposites. Some of the pertinent results are illustrated in Figure 2.31.

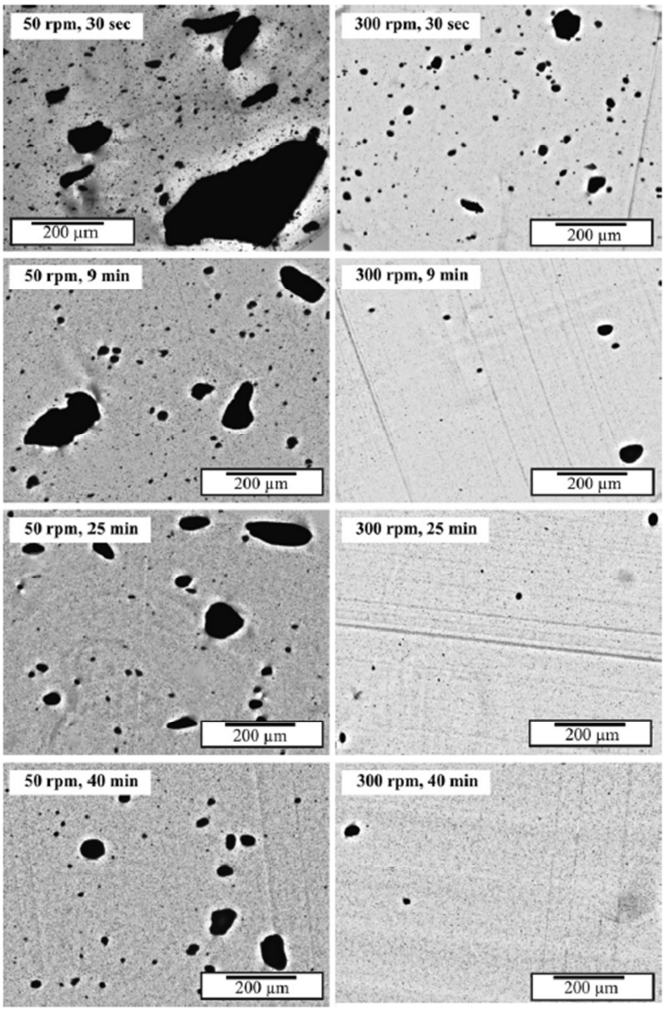


Figure 2.31. Optical micrograph of PC/CNT nanocomposites at 1 wt% CNT. The effect of residence time and mixing speed were analyzed, modified from Kasaliwal et al. [123]

The authors were able to quantify the degree of dispersion by using optical micrographs of the nanocomposites. Equation (2.2) was utilized along with statistical analyses of agglomerate size, shear rate, and other parameters. At low mixing speeds, the authors observed that dispersion was dependent on both rupture and erosion of the primary agglomerates. Higher shear rates shifted the dominating mechanism to rupture, as verified by TEM. Using this study and previous theories, they were able to develop models which might predict when rupture and erosion mechanisms will dominate during melt compounding of polymer/CNT nanocomposites.

Lin et al. [149] compared the mixing efficiencies of three different micro compounding devices with MWCNT in a polymer matrix. MWCNT/polycarbonate nanocomposites were melt compounded using a masterbatch provided by Hyperion catalysts. A DACA micro-compounder and two homemade devices were utilized to obtain the polycarbonate nanocomposites. Each of these devices consisted of two conical co-rotating screws with a bypass channel. This allowed the material to circulate for varying residence times. The authors conducted rheological, electrical, TEM, and AFM analysis on the composites. The least aggregated nanocomposites were obtained from the DACA micro-compounder, although extensive shortening to the CNTs was also observed. This suggests that although improved dispersion in CNT nanocomposites may be obtained, more intensive shear rates applied during melt mixing may lead to more damaged CNTs.

Work by Villmow et al. [124] investigated the effects of throughput, residence time, and screw configuration on CNT morphology in polycarpolatcone/CNT nanocomposites prepared with twin screw melt compounding. Different screw elements considered during this analysis are illustrated in Figure 2.32.

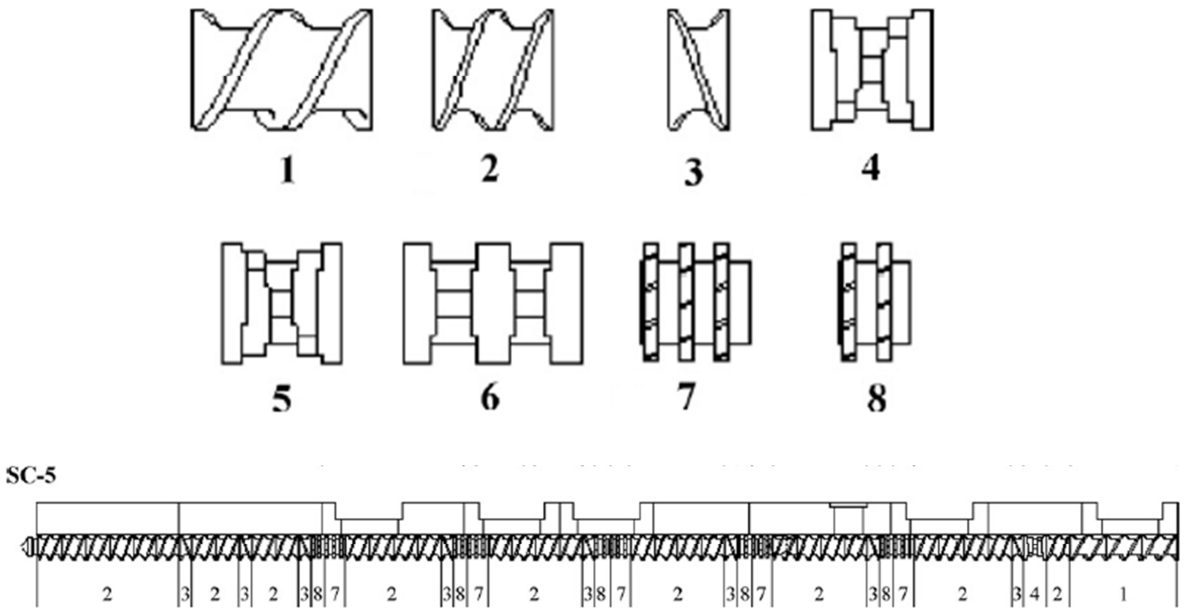


Figure 2.32. Screw elements considered in optimization of twin screw melt compounding (top) and the optimal screw design in the study (bottom). Conveying elements (1,2), back-conveying elements (3), kneading elements (4-6), and mixing elements (7,8) are illustrated. Modified from Villmow et al. [124]

The rotation speed, throughput, and screw configuration were correlated with the residence time and specific mixing energy input during mixing. The specific mixing energy is calculated by Equation (2.6).

$$SME = \frac{\tau * N}{\dot{m}} \text{ (kJ/kg)} \qquad (2.6)$$

In the above equation, $\tau$ is the drive torque of the extruder (kJ), $N$ is the rotation speed ($min^{-1}$), and $\dot{m}$ is the throughput (kg/min). The values of residence time and specific mechanical energy were compared to the area fraction of aggregates. The screw configurations labeled as dispersive (containing mostly mixing elements) led to better CNT dispersion in the melt compounded nanocomposites. The authors observed that higher mixing speeds (500 RPM) also led to improved dispersion so long as a minimum residence time was reached. Furthermore, these

designs led to lower SME which may result in less damage to the CNTs and lower operating costs.

Melt compounding may be an effective method of polymer/CNT nanocomposite generation, but requires intensive mixing to disperse primary CNT agglomerates and efficiently distribute the nanofiller. These methods can damage the nanotubes due to rupture mechanisms dominating at high shear rates. In some cases, this effect can shorten the CNT by up to 70% of their initial length [140]. Damaging the CNTs results in lower aspect ratios, requiring higher concentrations of nanofiller to reach electrical percolation. In addition, lowering the aspect ratio of CNTs decreases the potential for CNTs to provide mechanical strengthening to the nanocomposite. More benign melt compounding methods that disperse the CNTs while retaining CNT aspect ratios are desired.

### 2.4.3 CNT/Polymer composite properties

This subsection is concerned with the properties of MWCNT thermoplastic nanocomposites prepared by melt compounding methods. Mechanical, electrical, and thermal properties are addressed with specific focus on the electrical conductivity of polycarbonate/CNT nanocomposites. The rheological properties of CNT nanocomposites are also be considered in order to divulge the structure and dynamics of CNT networks in polymer/CNT nanocomposites.

#### 2.4.3.1 Mechanical properties

Carbon nanotubes possess high stiffness (~1 TPa) and strength (100 MPa) which are desirable attributes for nanofillers used in the application of thermoplastic nanocomposites. Dispersion is especially important to improve mechanical reinforcement of CNT nanocomposites as agglomerates above a certain size may act as stress concentrators inducing cracks and fracture

in the composite [125]. In addition, orientation can contribute to enhanced mechanical reinforcement. For this reason, melt compounded CNT nanocomposites are frequently injection molded to orient the CNTs. This section will deal with examples of CNT nanocomposite mechanical properties discussed in the literature.

Melt spinning is an effective way to align the CNT in the field of flow which may lead to increased mechanical properties, such as ultimate strength, young's modulus, and elongation at break. Potschke et al. [150] prepared polycarbonate/MWCNT nanocomposites at 2 wt% CNT by a masterbatch dilution process using twin screw melt blending. Following this, the composites were melt spun at various take-up velocities ranging from 50 m/min to 800 m/min. The resulting nanocomposites were analyzed for orientation using TEM, which can be seen below in Figure 2.33.

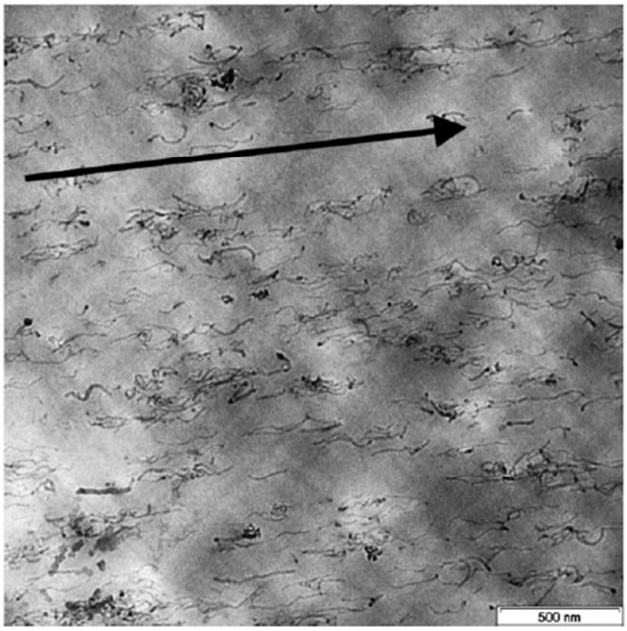


Figure 2.33. Orientation of MWCNT nanocomposites processed by melt spinning at a take-up velocity of 400 mm/min, modified from [150]

The CNTs were observed to orient in the field of flow, as highlighted by the arrow in Figure 2.33. However, even with preferential orientation and adequate dispersion, the mechanical properties did not significantly improve in the PC/CNT nanocomposites. A comparison of the virgin matrix modulus and that of the melt spun fibers is illustrated in Figure 2.34.

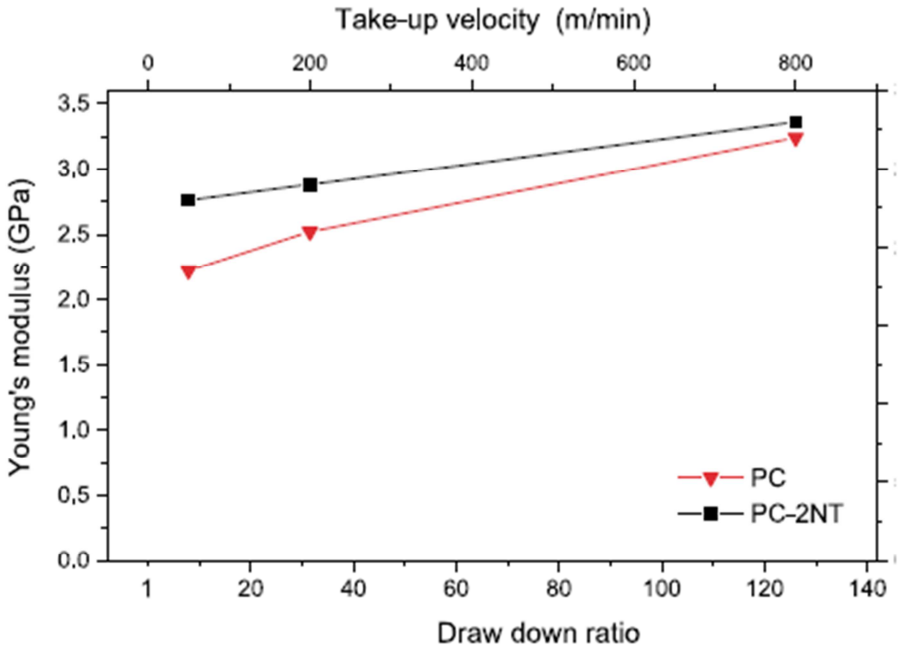


Figure 2.34. Mechanical properties of MWCNT polycarbonate nanocomposites processed by melt spinning at different take-up velocities, modified from [150]

Only slight enhancement in the modulus was observed in the composite fibers compared to the virgin matrix. The disparity is more pronounced at lower take-up velocities which would correspond to less oriented CNTs, which is counter-intuitive. The authors also reported a decrease in the true stress at break and elongation values compared to pure PC. The lack of improvement could be due to damage to the CNTs resulting in decreased mechanical reinforcement. In addition, poor CNT-polymer interactions would significantly reduce the potential for improved mechanical properties [150].

The mechanical properties of polyethylene (PE) nanocomposites of MWCNT prepared with twin screw melt compounding have been reported. McNally et al. [151] prepared MWCNT/PE nanocomposites up to 10 wt% CNTs and conducted mechanical testing. The results of this study are illustrated in Figure 2.35.

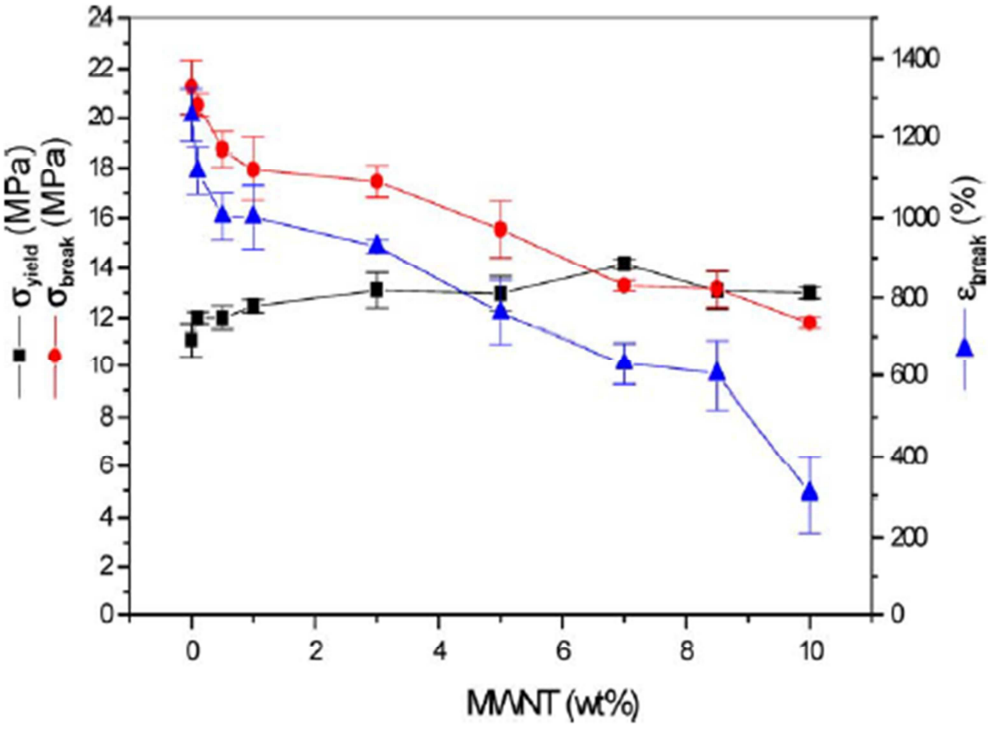


Figure 2.35. Mechanical properties of polyethylene MWCNT nanocompsoites prepared with twin screw melt compounding at different concentrations, modified from [151]

The authors observed a decrease in ultimate tensile strength and elongation at break of the nanocomposites with increasing MWCNT content. The CNTs were well dispersed in the polymer matrix, as observed from OM and TEM results. It could be that damage to the carbon nanotubes during melt compounding coupled with poor CNT/polymer interactions led to decreased mechanical properties.

Few examples from the literature report significantly improved mechanical properties in MWCNT/polymer nanocomposites processed by melt compounding. Limited mechanical reinforcement is observed in CNT/polymer nanocomposites, even in the case of highly oriented CNTs. This may be due to shortening of the CNTs during processing, insufficient polymer/nanotube interactions, and lack of complete dispersion of CNT agglomerates.

#### 2.4.3.2 Electrical conductivity

Electrically insulating thermoplastics may become conductive with the addition of small amounts of CNTs, whereas conventional fillers such as carbon black typically require higher concentrations [5, 125, 152]. Polymer/CNT nanocomposites are of particular interest in the field of high performance electrostatic dissipation and electromagnetic interference shielding. By adding a sufficient amount of nanofiller, an electrically conductive network (in the conductivity range of the CNTs utilized) may be obtained. This phenomenon is known as electrical percolation, and the concentration where this occurs is known as the electrical percolation threshold. The degree of dispersion, CNT length, purity, and other factors may affect the electrical percolation point in a polymer/CNT nanocomposite. In order for electrical percolation to occur, nanotube contacts are not necessary. The distance between CNTs must be such that electron ‘hopping’ and ‘tunneling’ may occur from one CNT to the next [151]. Electrical percolation is illustrated in the conductivity curve of Figure 1.2, where the resistivity decreases by a significant amount over a small change in concentration. If more CNTs are added to the composite, a plateau in the electrical conductivity will be observed [125]. The following section is dedicated to discussing the effect of processing conditions on the electrical properties of polymer/CNT nanocomposites prepared via melt compounding, with special consideration to PC/CNT nanocomposites.

Potschke et al. [153] investigated the volume conductivity of various polycarbonate composites using graphite, carbon black, and CNTs as the filler material. The authors utilized an optimized screw configuration and processing method previously developed by Villmow et al. [124] using twin screw melt compounding. The melt compounded nanocomposites were compression molded to induce secondary agglomeration of the well dispersed CNTs. Secondary agglomeration of dispersed CNTs has been reported to improve the electrical conductivity in polymer/CNT nanocomposites [154]. For this reason, polymer/CNT nanocomposites are often compression molded to promote partial reagglomeration of the CNTs. The authors investigated CNTs, expanded graphite, and carbon black and compared the electrical percolation thresholds. The authors observed percolation points of 8.75 wt% for the carbon black composite, 2 wt% CNT for the CNT nanocomposite, and 4 wt% graphite for the graphite nanocomposite. These results indicate that CNT/polymer nanocomposites possess the potential for significantly lower electrical percolation values compared to carbon black/polymer and graphite/polymer composites, leading to lighter weight composites and reduced impact on the optical clarity of the composite.

Polycarbonate nanotube nanocomposites were prepared at 1 wt % CNT by Kasaliwal et al. [123] in a masterbatch dilution process using Baytube C150HP as the nanomaterial. The preparation of these nanocomposites is discussed in Section 2.4.2.3, where specific mixing energy and dispersion was correlated to shear rate, residence time, and mixing speed. The samples were compression molded and analyzed for volume electrical conductivity. The results are plotted against the specific mixing energy in Figure 2.36.

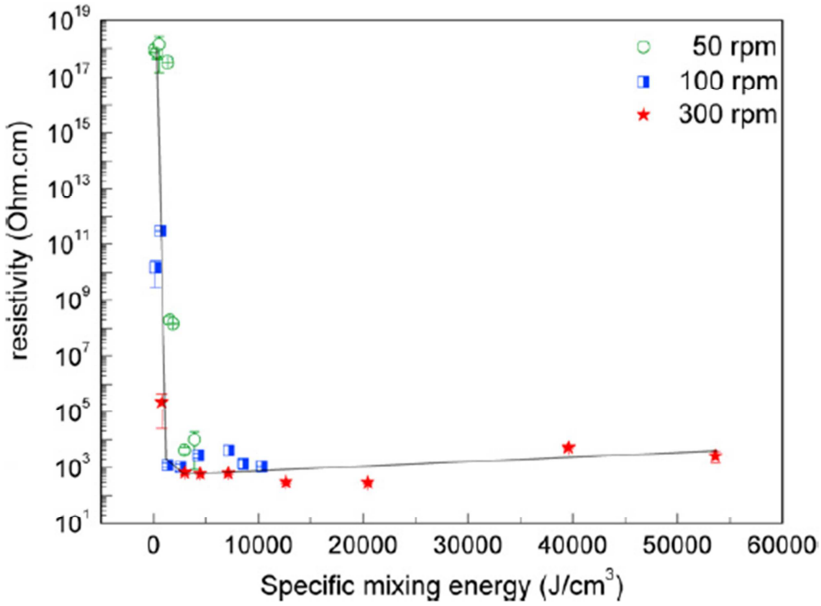


Figure 2.36 Resistivity of 1 wt% polycarbonate nanconocomposites prepared at diffferent rotation speeds, modified from Kasaliwal et al. [123]

This work demonstrates the importance of processing conditions during melt compounding on the electrical percolation threshold in polymer/CNT nanocomposites. By applying more intensive mixing at similar nanofiller concentrations, the authors were able to produce more electrically conductive nanocomposites. However at high SME values a slight increase in the resistivity is observed. This suggests that the CNT may be damaged during nanocomposite preparation, reducing the volume conductivity of the melt compounded nanocomposites. From Figure 2.36, an SME value of ~20,000 is optimal.

Polymer/CNT nanocomposites were prepared using high shear microcompounding devices to analyze the effect of different processing machinery on the composite electrical properties in work by Lin et al. [149]. The morphological results of this study were discussed in Section 2.4.2.3 in greater detail. The nanocomposites prepared by these methods resulted in electrical percolation thresholds of 0.50 wt% CNTs and 0.75 wt % CNTs for the home-made

devices, and 1.00 wt % CNTs for the DACA microcompounder. These results are contrary to the morphological observations reported earlier (Section 2.4.2.3) where the greatest degree of dispersion was observed for nanocomposites prepared with the DACA microcompounding device. The authors investigated the melt compounded CNTs for damage to determine this discrepancy. The authors observed that the CNTs from nanocomposites processed using the DACA microcompounder were more damaged than those processed with the home made devices, resulting in higher percolation thresholds [155]. This study exemplifies the need to retain CNT aspect ratios during processing of nanocomposites.

The volume conductivity of melt compounded Nylon 6/CNT nanocomposites were investigated in recent work by by Krause et al. [156]. The nanocomposites were generated using a DACA micro compounder at different mixing speeds, and compared to Nylon 6/6 nanocomposites. Although the microscale dispersion increased with higher mixing speeds, the conductivity suffered as illustrated in Figure 2.37.

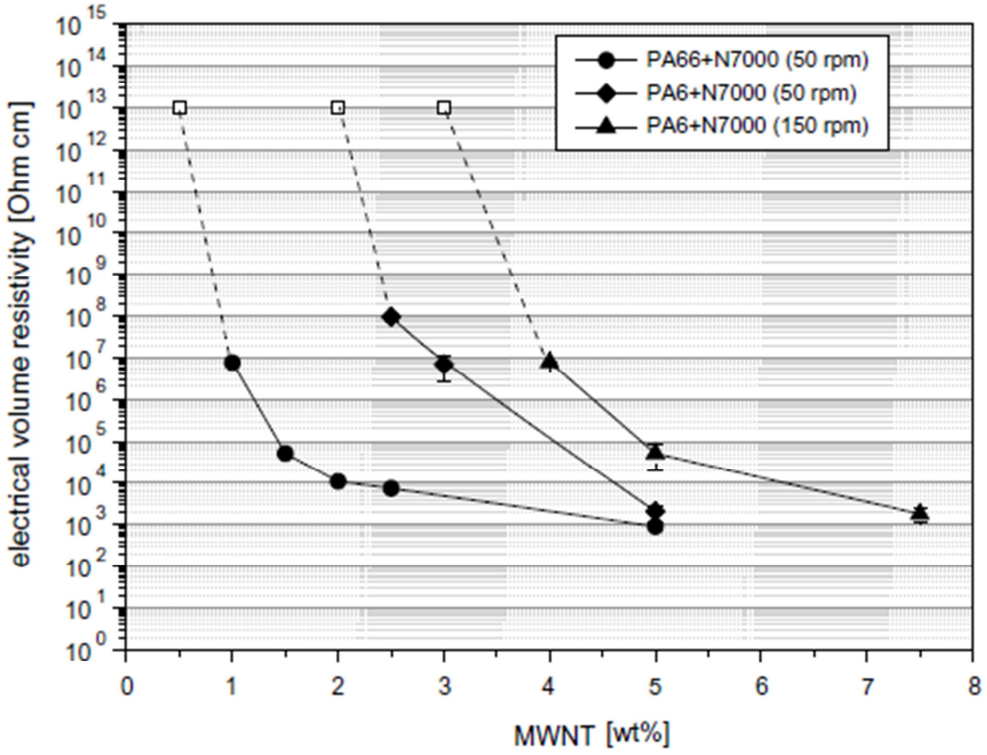


Figure 2.37. Electrical percolation curves of Nylon 6 and Nylon 66 with different mixing speeds, modified from Kruase et al. [156]

The percolation threshold of Nylon 6/CNT nanocomposites is greater than ~5 wt%, which increases for the nanocomposites prepared at greater mixing speeds. The authors suggest that significant breakage to the CNTs may occur at the higher mixing speeds (150 RPM), resulting in increased percolation concentrations. This work indicates that breakage of the CNT must be mitigated while striving for the most dispersed nanocomposites [156]. Furthermore, Figure 2.37 shows that nylon 6,6/CNT nanocomposites possess lower percolation thresholds than nylon 6/CNT nanocomposites. The authors indicate that similar interfacial energies between the nylon 6,6 and CNTs may lead to improved dispersion of the nanomaterial through the infiltration and wetting of the primary agglomerates.

The electrical conductivity of thermoplastic/CNT nanocomposites prepared by melt compounding depends on the type of polymer, the length and purity of the CNTs, and the

processing conditions. The potential exists for CNTs to replace carbon black for composites in applications where electrostatic dissipation or electromagnetic interference shielding is desired. However, damage to the CNTs during melt compounding can decrease the electrical conductivity of polymer nanocomposites, and therefore must be taken into consideration during nanocomposite generation.

#### 2.4.3.3 Rheological properties

Rheological measurements of polymer/CNT nanocomposites are useful to obtain information about the physical network of CNTs in the polymer (rheological percolation), as well as the extent of dispersion of CNT agglomerates in the polymer. The relation of the degree of dispersion, or deagglomeration to the rheology is not as direct as optical microscopy or TEM. However, when coupled with these methods rheology is a powerful tool for polymer/CNT nanocomposite characterization. The scope of this section focuses on small amplitude dynamic oscillatory shear experiments. Small amplitude dynamic oscillatory shear experiments prevent the breakup of secondary CNT agglomerates. This allows more accurate measurements of the CNT network structure in the polymer. Steady shear measurements may prevent the formation of secondary agglomerates, which may reduce the accuracy of an observed percolated network [122, 157]. The effects of CNT dispersion and rheologically percolated networks on the dynamic response of polymer/CNT nanocomposites are discussed, with emphasis on trends observed in the storage modulus (G') and complex viscosity ($\eta^*$). The differences between electrical and rheological percolation are also addressed.

Storage modulus (G') versus frequency data may be analyzed to make comments on the degree of dispersion, or rheological percolation, in CNT nanocomposites. However, there can be several manifestations of this network and so rheology alone is insufficient to determine the type

of network formed in the polymer nanocomposite melt. An example of such a variation is shown in Figure 2.38

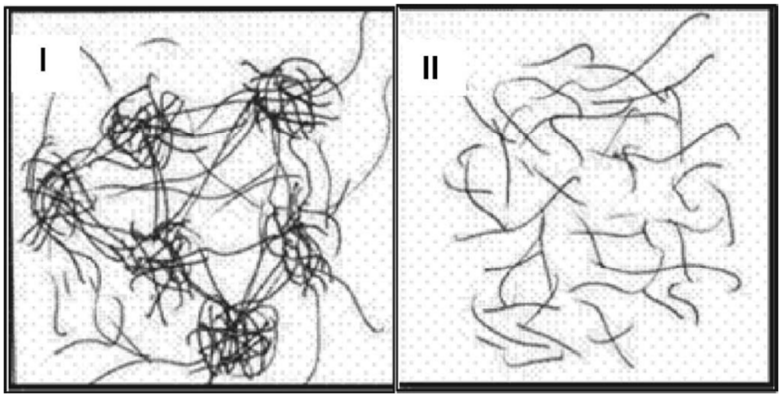


Figure 2.38. Two types of rheologically percolated networks observed in nanocomposites, only CNTs are pictured. A percoalted network of agglomerates (I) connected by individual CNT, and a percolated network of individual CNT (II), modified from [157]

For this reason, characterization of polymer/CNT nanocomposites must be carried out with discretion. In order to fully characterize the rheologically percolated network, OM, TEM and rheology should be utilized to verify the type of network present. Abdel-goad et al. [135] investigated the effect of CNT inclusion on the rheological response of polycarbonate. The authors prepared polycarbonate/MWCNT nanocomposites over a narrow region of concentrations (0.25 wt % to 3 wt%) in order to investigate the onset of rheological percolation. The authors observed increasing values of G' with increasing nanofiller content, as illustrated in Figure 2.39 [158].

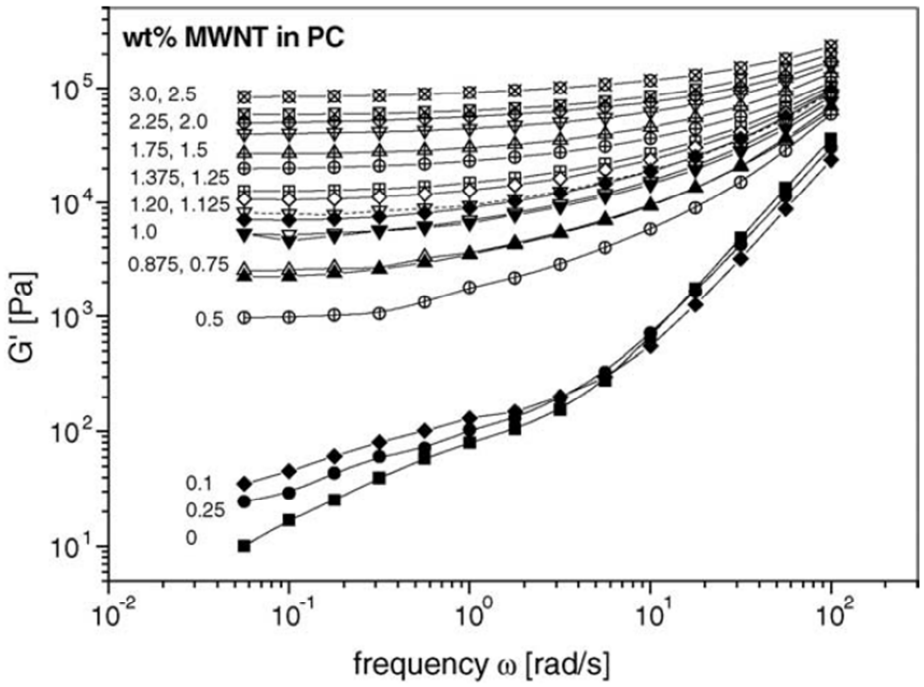


Figure 2.39. Storage modulus (G') versus frequency for CNT nanocomposites of polycarbonate and MWCNT at different concentrations, modified from Abdel-goad et al. [135]

Above 0.25 wt%, a transition from terminal liquid-like to solid-like behavior was observed with a "plateau" developing in the G' curve at low frequencies. In addition, the authors indicate that the relaxation exponent ($G' \sim \omega^n$) decreases as the CNT content increases. Beyond the onset of rheological percolation, the dependence of G' on frequency approaches zero. These trends have been correlated to the formation of rheological percolation thresholds in the literature [135].

Observations of the complex viscosity ($\eta^*$) as a function of frequency can yield indirect information about the dispersion and mechanical CNT network in polymer nanocomposite melts. The complex viscosities of PC/CNT nanocomposites prepared by Abdel-goad et al. [135] were investigated in order to further analyze the onset of the rheological percolation threshold. The findings are illustrated in Figure 2.40.

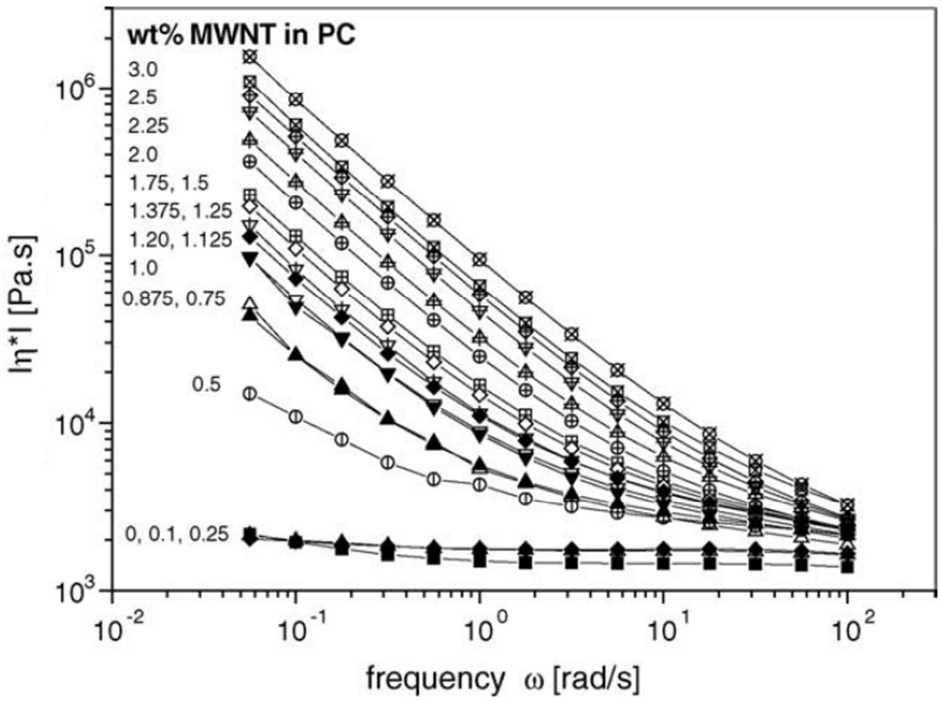


Figure 2.40. Complex viscosity (η*) versus for CNT nanocomposites of polycarbonate and MWCNT at different concentrations, modified from [135]

Below the "percolation threshold" of 0.5 wt%, nearly Newtonian behavior is observed for the nanocomposites. Above this concentration, the frequency dependence of complex viscosity drastically changes, especially at low frequencies. This "tail" is recognized as a shift from liquid like to solid like behavior, indicating rheological percolation. As with analyses involving the storage modulus, these observations may be misleading if taken as stand-alone evidence of a well-dispersed polymer/CNT nanocomposite. Therefore, it is suggested to supplement rheological measurements with both OM and TEM to capture the nano, micro, and bulk morphology of a nanocomposite.

An understanding of the physical network of CNTs in polymer nanocomposites may be gained from rheological measurements, although a direct correlation from this phenomenon to an electrically percolated network is not valid. Fundamentally, the mechanisms of percolation are

different. These methods differ in that polymer chain immobility (below the polymer $T_g$) and the distance between neighboring nanotubes determine the rheological and electrical percolation threshold, respectively [151]. The formation of entanglements between polymer chains and nanotubes may lead to a physical (rheological) network before the CNTs are close enough to be electrically percolated [135]. An in depth analysis of the fundamental differences between these concepts is covered in Alig et al. [122] and in a book edited by McNally and Potschke [125].

Rheology is an important supplemental tool used to understand the state of CNT dispersion and the mechanically percolated network of CNTs in polymer nanocomposites. In order to observe these networks, dynamic oscillatory shear experiments carried out at low strain rates are preferred in order to prevent disruption of the physically entangled network. The presence of rheological networks may be identified in both the storage modulus and complex viscosity as a function of frequency. The networks that form in CNT nanocomposites may arise from interconnected agglomerates rather than individual CNTs and, therefore, rheological analyses of these should be coupled with direct dispersion characterization methods such as OM and TEM.

Electrically conductive polymer/CNT nanocomposites prepared via melt compounding are of interest to replace conventional carbon black composites. However damage to the CNTs due to high shear melt compounding and insufficient dispersion of the nanofiller are significant issues which must be overcome. Furthermore, the cost of operating twin screw extruders compared to single screw melt compounding devices can be large. Therefore single screw melt compounding is often desired, which results in more benign mixing. However, dispersion of CNTs suffers in single screw melt compounding due to low shear stresses. Therefore, novel

single screw melt compounding methods which disperse primary CNT agglomerates in polymer matrices while retaining CNT aspect ratios are of interest.

## 2.5 Supercritical carbon dioxide

This section is concerned with supercritical carbon dioxide ($scCO_2$) and its applications in polymer nanocomposite formation. First, an introduction to supercritical fluids and supercritical carbon dioxide is presented, followed by a brief overview of the field of particle formation, with special attention to the $scCO_2$ treatment of CNT. Finally, the formation of nanocomposites using $scCO_2$ is addressed. These topics are discussed with consideration to the benign treatment of OMMT and CNTs with $scCO_2$ for the application of melt compounded nanocomposites.

### 2.5.1 Properties of supercritical carbon dioxide

A supercritical fluid (SCF) is a fluid that exists above the critical temperature ($T_c$) and pressure ($P_c$), possessing physiochemical properties intermediate of the material's gas and liquid states. SCFs exhibit liquid-like densities coupled with gas-like viscosities and diffusivities. The properties of these materials are easily tunable depending on pressure and temperature. They are capable of replacing conventional solvents with the added benefit of rapid mass transfer rates, making them ideal candidates in extraction processes and in particle formation [159-161]. In addition, the low viscosity and high diffusivities of SCFs allows them to be considered as plasticizers for many polymers and for use in polymer foaming applications [160, 162-165].

Carbon dioxide is a practical SCF choice because it is non-toxic, non-flammable, abundant, recoverable, and possesses a low critical point compared to other materials ($T_c$ =

31.1°C, $P_c$ = 1073 psi). The advantages to using supercritical carbon dioxide ($scCO_2$) rather than other fluids for SCF applications are summarized in Table 2.3.

Table 2.3. Critical properties and remarks on select fluids, modified from [161]

| Fluid | $T_c$ (°C) | $P_c$ (MPa) | Remarks |
|---|---|---|---|
| Carbon dioxide | 31.2 | 7.38 | – |
| Ammonia | 132.4 | 11.29 | Toxic |
| Water | 374.1 | 22.1 | High $T_c$, corrosive |
| Ethane | 32.5 | 4.91 | Flammable |
| Propane | 96.8 | 4.26 | Flammable |
| Cyclohexane | 279.9 | 4.03 | High $T_c$ |
| Methanol | 240.0 | 7.95 | High $T_c$ |
| Ethanol | 243.1 | 6.39 | High $T_c$ |
| Isopropanol | 235.6 | 5.37 | High $T_c$ |
| Acetone | 235.0 | 4.76 | High $T_c$ |

Another interesting characteristic of $scCO_2$ includes the lack of residue in treated materials, which negates the need for solvent removal downstream of anything processed with $scCO_2$ [161, 166].

Due to these interesting properties, $scCO_2$ has been investigated in the fields of solvent extraction, particle formation, polymer processing, and many others. For the scope of this review, the applications of $scCO_2$ for the generation of nanoparticles, and as a processing aid to the formation of polymer nanocomposites are considered.

### 2.5.2 Nanoparticle generation using scCO2

The density, diffusivity, permeability, and mass transfer properties of $scCO_2$ mark it as an ideal candidate for the processing of nanomaterials. By controlling the properties of $scCO_2$ and experimental configurations, nanoparticles with specific size distributions, morphologies, and compositions may be obtained. $scCO_2$ may be utilized to generate nanoparticles via chemical

transformations, or physical transformations. The chemical transformations may utilize $scCO_2$ as a reaction media. The physical transformations incorporate $scCO_2$ as a solvent, solute, anti-solvent, and suspension media [167]. This section focuses on the physical transformations in particle formation, as chemical transformations are beyond the scope of the current work [161]. The rapid expansion of supercritical solutions (RESS), rapid expansion of supercritical solutions into a liquid solvent (RESOLV), and supercritical anti-solvent precipitation (SAS) are introduced briefly. The rapid expansion of high pressure and supercritical suspensions (REHPS) are discussed with examples from literature [161, 167, 168].

#### 2.5.2.1 Rapid expansion of supercritical solutions

The rapid expansion of supercritical solutions (RESS) is a method of nanoparticle formation in which a solute having sufficient solubility in $scCO_2$ may be generated into nanomaterial without the use of organic solvents. The RESS process involves saturating the solute of choice with adequate amounts of supercritical fluid solvent. This is followed by depressurizing the solution through an insulated nozzle (or heated, to prevent icing due to Joule-Thompson effect) into a secondary low pressure chamber. A schematic drawing of this process is shown in Figure 2.41.

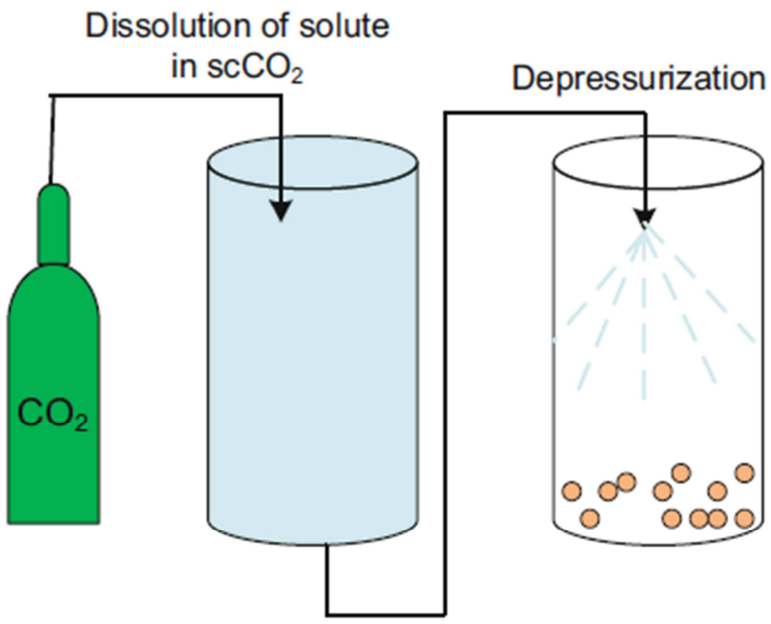


Figure 2.41. Schematic of RESS process, modified from [161]

The particle size distribution and morphology of the product depends on the temperature, pressure drop, residence time, solubility of solute in the SCF, impact distance of the jet against the secondary vessel surface, nozzle geometry, and other parameters [169]. The rapid release of the solution causes disintegration of the initial solute, forming significantly smaller particles. This occurs due to the rapid phase transition experienced by the $CO_2$ from the supercritical to the gaseous state. During this transformation, the solvent power of $CO_2$ drops immensely, forcing precipitation of the solute. The precipitation occurs as a result of nucleation, coagulation and condensation of the particles. Because of the rapid phase change, predominantly homogenous nucleation occurs, permitting smaller particle sizes, and narrower particle size distributions compared to heterogeneous nucleation. Another mechanism involves supersonic free jet rates occurring between the nozzle and vessel. In the transfer from the high pressure vessel to the low pressure one very high shear rates can either break-up or nucleate particles. A thorough

description of this phenomena is provided in Sanli et al. [161] with appropriate models and energetic considerations.

The RESS is an interesting method used for the formation of nanoparticles, but has drawbacks. The supersonic jet that is formed during rapid depressurization of the high pressure vessel may lead to coalescence, forming needle-like particles. Electrostatic charges can also be induced during the transfer from the high pressure to low pressure vessel, arising from fast relative motions between the nanoparticles, resulting in reaggregation [170]. Other methods may form nanoparticles using the same principles as RESS while avoiding the issues of reaggregation which will be discussed in the following section.

#### 2.5.2.2 Rapid expansion of supercritical solutions into a liquid solvent

The aggregation issues mentioned in the previous section may be overcome by modifying RESS in a process known as the rapid expansion of supercritical solutions into liquid solvents (RESOLV). This method is similar to RESS, except rather than releasing the supercritical solution into an empty pressure vessel (or vacuum) it is sprayed into a liquid solvent. It has been suggested that reaggregation of the particles may occur in the supersonic jet during RESS. By including a solvent, particle formation may be “quenched”, narrowing the size distribution and reducing aggregation [161, 167, 168]. RESOLV is an advantageous modification to RESS in that it allows for smaller and more discrete particle size distributions to be obtained. However, this introduces a solvent which must be removed in downstream processing. Therefore, in order to remove the nanoparticles, a recovery step must be introduced [167].

#### 2.5.2.3 Rapid expansion of high pressure and supercritical suspensions

The formation of nanoparticles from materials which are insoluble in $scCO_2$ are often desired. The process known as rapid expansion of high pressure and supercritical suspensions (REHPS) is a modification of RESS where the material to be disintegrated is not soluble in $scCO_2$, rather it may only be suspended in the supercritical fluid [171, 172]. The apparatuses are similar for the REHPS process, where the depressurization of the suspension into a low pressure vessel allows the substrate to be broken up into nanoparticles from larger primary agglomerates. However, the primary particle formation mechanism results from the high shear experienced by the particles when the fluid flows through the capillary and the nozzle, and in the supersonic jet which breaks up agglomerates into micro and nano-sized particulate. The rapid expansion of $scCO_2$ bubbles to "push apart" the particulate has also been cited as a contributing mechanism in this process [171, 173]. The capillary length, nozzle geometry, temperature, pressure differential, and other variables affect the particle sizes obtained with this method.

Extensive work on this method has been conducted by Rajesh Dave's group at New Jersey Institute of Technology. In 2008, some of the first work using the REHPS method was reported by Narh et al. [171]. The authors used REHPS on CNT bundles to deagglomerate them and dry-coat polyethylene oxide. The authors observed significantly better dispersion in the mixture prepared with sonication compared to the sample prepared with the REHPS processing. In later work, To et al.[174] examined the effect of REHPS on nanotube bundles and in mixing with other nanoparticles. The authors conducted limited particle size analysis to investigate the effect of treatment with $scCO_2$, and did not mix the CNTs with a polymer matrix. The study by To et al. [174] was aimed mainly at nanoparticle mixing and focused on silica and titania nanoparticles. In both of these works, TEM analysis was not conducted to investigate CNT aspect ratios after supercritical fluid treatment, and the effect of $scCO_2$ processing on

nanocomposite properties was ignored Furthermore, no optimization was conducted to maximize the deagglomeration of the CNTs.

More recently, a report by Jung et. al.[175] suggested utilizing $scCO_2$ as a processing aid to reduce the damage to CNTs before sonication. In this study, the authors treated the CNTs with both $scCO_2$ and supercritical ethane, but the supercritical suspension was not transferred to a secondary vessel. This suggests that the authors effectively ignored the primary mechanisms of particle breakup in the REHPS process. After $scCO_2$ treatment, the CNTs were sonicated for different time periods in sodium-dodecyl-sulfate (SDS). The authors utilized light absorbance to quantify the dispersability of the CNTs. The findings are illustrated in Figure 2.42.

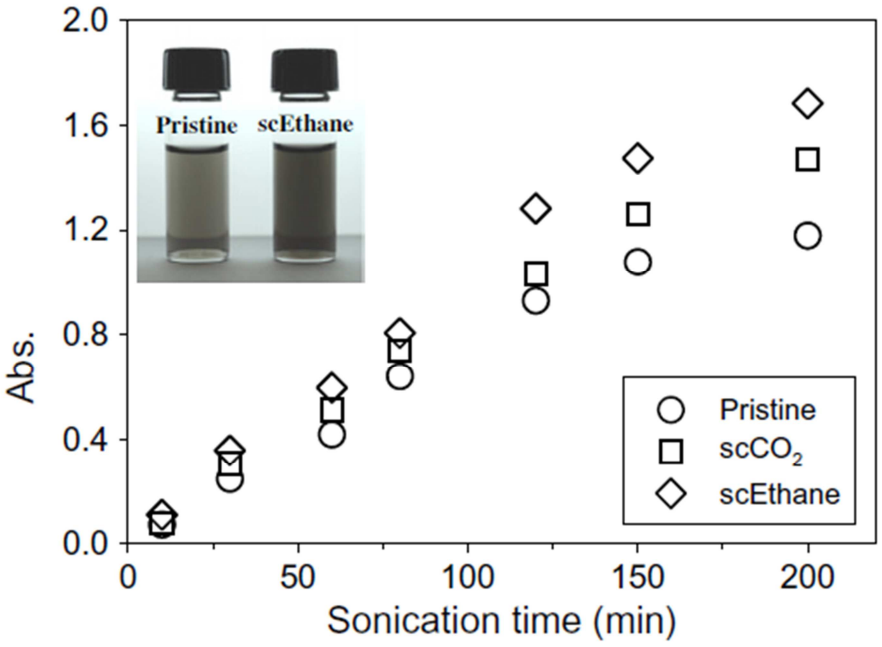


Figure 2.42. Absorbance versus sonication time for CNTs with varying pretreatments. Inset includes images of CNT suspensions of SDS and SCF treated CNT for visual reference, modified from Jung et al. [175]

The authors utilized Raman spectroscopy to determine that damage to the CNTs occurred in nanotubes which did not receive supercritical fluid treatment. Similar to other work, no attempt

was made to optimize the deagglomeration or understand the mechanism with regard to the $scCO_2$ processing.

Although the REHPS was only recently introduced in the literature, Manke et al. [176] have been using a method nearly identical to this technique to produce polymer/nanoclay nanocomposites since 2002. The REHPS process utilized by Dave's group[171] was developed independently but in a parallel to Manke's method. Manke's method has been utilized for PLS nanocomposites in the literature, and was extended to include CNT recently by Gulari et al. [177] in a blanket patent. However, this method has only recently been applied to CNT/polymer nanocomposites in the literature by Chen et al. [173].

The REHPS process applied to supercritical mixtures is a relatively simple technique, but can be immensely effective in the deagglomeration of large agglomerates to form nanoscale particles. Coupled with melt compounding, REHPS may provide more benign treatment of CNTs and lead to better dispersion in both CNT and nanoclay nanocomposites to generate materials with enhanced electrical and mechanical properties.

#### 2.5.2.4 Supercritical anti-solvent precipitation

The formation of nanoparticles from a solute which is entrained in an organic or other solvent requires application of the supercritical anti-solvent precipitation (SAS) method. In SAS, the solvent in which the solute is initially contained must be soluble in the SCF (the anti-solvent, $scCO_2$ for these examples), whereas the solvent is not. When the $scCO_2$ comes in contact with the initial solution, it forms a new supersaturated solution forcing precipitation of the solute and formation of the particulate. Because of the enhanced mass transfer rates of supercritical fluids, the solution of SCF and solvent occurs rapidly, forcing precipitation to occur. This induces

homogenous nucleation, and as a result, small particles and narrow size distributions. The SAS process essentially combines two methods, extraction of a solvent and generation of the nano-particulate [167, 178]. This process is especially useful when a continuous operation may be engineered with proper nozzle-jet designs in mind. The limits to implementing this process arise from adequate modeling of ternary thermodynamics to successfully design the process.

The field of particle formation from SCFs utilizes the properties of supercritical fluids to produce nano-sized particulate. Although this field was only briefly dealt with in this review, more thorough coverage can be found in recent reviews by Yeo et al., Reverchon et al. and Sanli et al. [161, 167-169].

### 2.5.3 $scCO_2$ aided nanocomposite formation

Due to its solvent properties, high mass transfer rates, and other interesting properties, $scCO_2$ has been utilized in the formation of polymer nanocomposites in the literature [179, 180]. Particularly, $scCO_2$ may be utilized to replace solvents in *in situ* polymerization and solution blending nanocomposite generation methods. In addition, the supercritical fluid may be utilized to augment the nanomaterials during, or before the melt compounding processes. This section focuses on $scCO_2$ aided melt compounding methods to produce nanocomposites of polymer/CNT and polymer/OMMT.

#### 2.5.3.1 Melt compounding

It has been asserted during this review that melt compounding is the most scalable, environmentally friendly, and versatile method to produce polymer nanocomposites. However, effective dispersion of the nanofiller and damage to the CNTs during processing remain large obstacles to widespread implementation of this process. Supercritical carbon dioxide processing

of nanomaterial as an aid to melt blending has been cited in the literature as an environmentally benign route to obtain increased dispersion in polymer nanocomposites of OMMT and CNTs [13, 57, 60, 95, 173, 176, 177, 181-194]. In addition, it has been suggested that significantly less damage occurs to the CNT during primary deagglomeration if pretreated with $scCO_2$, although this has not been verified with TEM [173, 175]. Therefore, nanocomposite generation methods which utilize $scCO_2$ to process the nanomaterial in combination with melt compounding are of interest.

The initial patent for the delamination of nanoclay for incorporation in polymer nanocomposites was filed by a group from General Motors with Charles W. Manke as the primary author [176]. This method describes soaking the nanoclay in $scCO_2$, and rapidly depressurizing the mixture into a secondary vessel to delaminate the nanoclay platelets. This is schematically represented along with an XRD of the nanoclay before and after $scCO_2$ treatment in Figure 2.43.

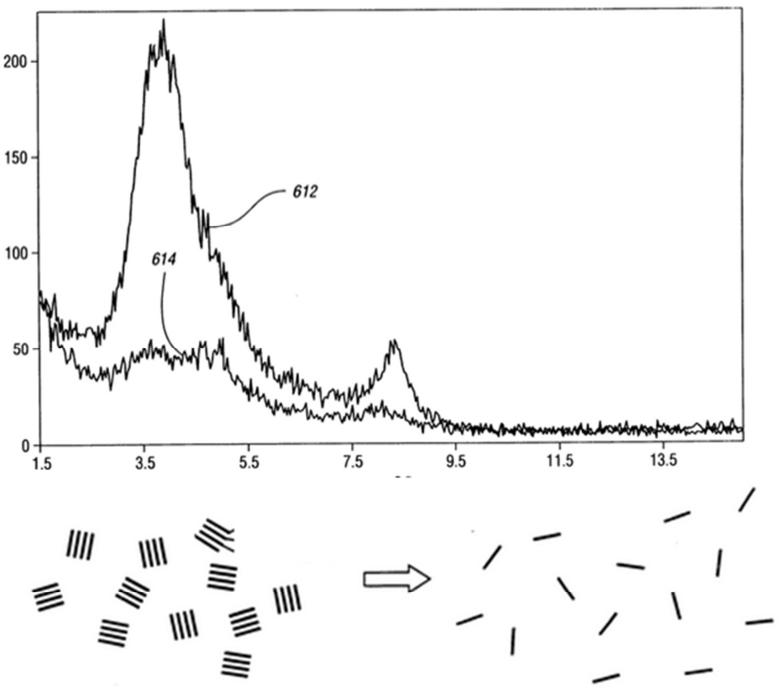


Figure 2.43. XRD pattern of nanoclay before (612) and after (614) $scCO_2$ treatment (top), schematically represented (bottom), modified from [176]

This patent also suggests mixing the nanoparticles with a polymer matrix to provide improved mechanical properties, although it doesn't provide a technical description of the process. It wasn't until a follow-up patent in 2004 by Mielewski et al. [191] that the authors provided procedures for mixing the $scCO_2$ treated nanoclays with polymers to form nanocomposites. The authors suggest several methods, one of which is providing the nanoclay and polymer through separate hoppers, and directly injecting the nanoclay and $scCO_2$ into the extruder to mix with the polymer. Although the use of extruders in combination with $scCO_2$ treatment of nanoclay is suggested in this patent, further literature describing the success of this method is absent.

Gulari and co-workers [177, 181, 189, 195, 196] have contributed multiple works pertaining to nanocomposites of nanoclay and polymer prepared with supercritical fluid processing and melt compounding. In this method, the authors mix nanomaterial, $scCO_2$, and

polymer in an autoclave above the supercritical point of $CO_2$. The authors suggest that the method of nanoclay delamination is dominated by the transport of polymer chains into the clay galleries via the $scCO_2$, coupled with a rapid depressurization of the mixture partially exfoliating the clays. This is contrary to the work in particle formation using the REHPS, where mixing with a polymer might act to hinder the ability of the nanoclay to fully delaminate into individual platelets.

The use of supercritical carbon dioxide ($scCO_2$) to exfoliate the nanoclay, followed by melt blending in a single screw extruder has been studied in the literature [55, 57, 95, 184-186, 197-199]. Lesser et al. [184-186] studied the effect of $scCO_2$ treatment of nanoclay before melt compounding, and observed an 85% increase in the gas barrier properties of polystyrene nanocomposites.

Nguyen et al. [95] conducted similar studies as Lesser and coworkers with polypropylene/OMMT nanocomposites. This process relied on the rapid expansion of nanoclay directly injected into a multi-stage extruder. Polypropylene (PP) OMMT nanocomposites were produced using this method and compared to composites prepared with traditional melt compounding. A schematic of this apparatus is illustrated in Figure 2.44.

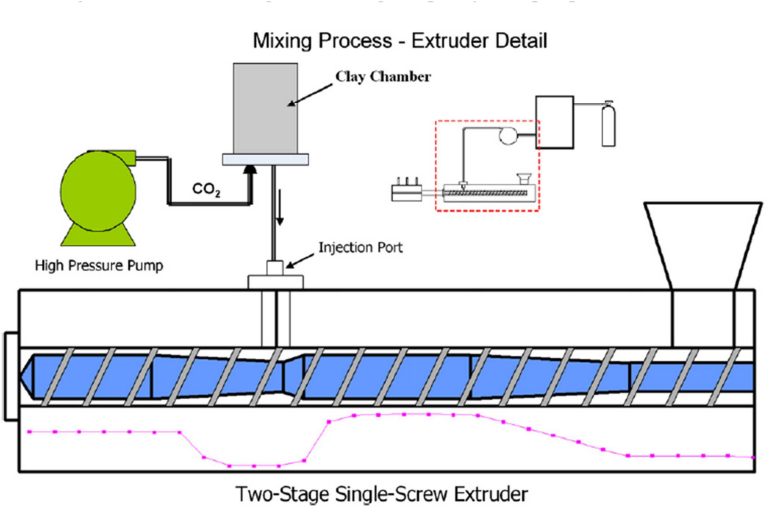


Figure 2.44. Apparatus for Ngyuens method of scCO2 aided melt blending, modified from [95]

The authors observed a 54% increase in modulus with this method at 6.6 wt% organoclay. The drawbacks of this method were that it operated as a batch process, and required additional equipment.

In a previous study, Chen et al. [55] developed a semi-continuous process that improved the nanoclay dispersion in polypropylene nanocomposites with the aid of $scCO_2$. This process was modified from Ngyuen's method. In this process, the nanoclay layers were delaminated by catastrophically depressurizing the $scCO_2$ treated clay over the polymer pellet bed in a modified hopper. The mixture was then melt compounded in a single screw extruder and pelletized. This method also provided a sequential mixing technique where high concentration nanocomposites of PP and OMMT may be obtained by reducing the compounding steps, and therefore the collapse of clay. The authors observed a 63% increase in Young's modulus compared to the virgin matrix with the sequential mixing technique at 10 wt% OMMT, compared to a 31% increase in modulus for direct melt compounding [182].

The dispersion of nanoclay in nanocomposites where the polymer may possess enthalpically favorable interactions with the nanoclay surface may be enhanced by the $scCO_2$ aided melt blending method. As the entropic barrier to intercalation is decreased by nanoclay delamination from $scCO_2$ processing, the groups with potential for interactions will be exposed, increasing the enthalpic couplings in the nanocomposite. The potential for this was first realized by Ngyuen et al. [60] and later improved by Chen et al. [57] by including a PP-*g*-Ma compatibilizer to increase the enthalpic interactions in PP/OMMT composites produced with the $scCO_2$ aided melt blending method. In Chen's work on PP-*g*-Ma modified PP nanocomposites, the authors observed an increase in modulus from the pure matrix of 41% for 5 wt% organoclay with PP when processing the composite with the $scCO_2$ aided melt blending method. Alternatively, the composite processed with a 3:1 ratio of nanoclay to PP-*g*-Ma and 5 wt% organoclay using the same method showed an increase in modulus of 61% compared to the pure matrix. This suggested that polar clay/polymer interactions could be enhanced with the $scCO_2$ aided melt blending method. The TEM of nanocomposites prepared at 10 wt% with and without compatibilizer with and without $scCO_2$ treatment are shown in Figure 2.45

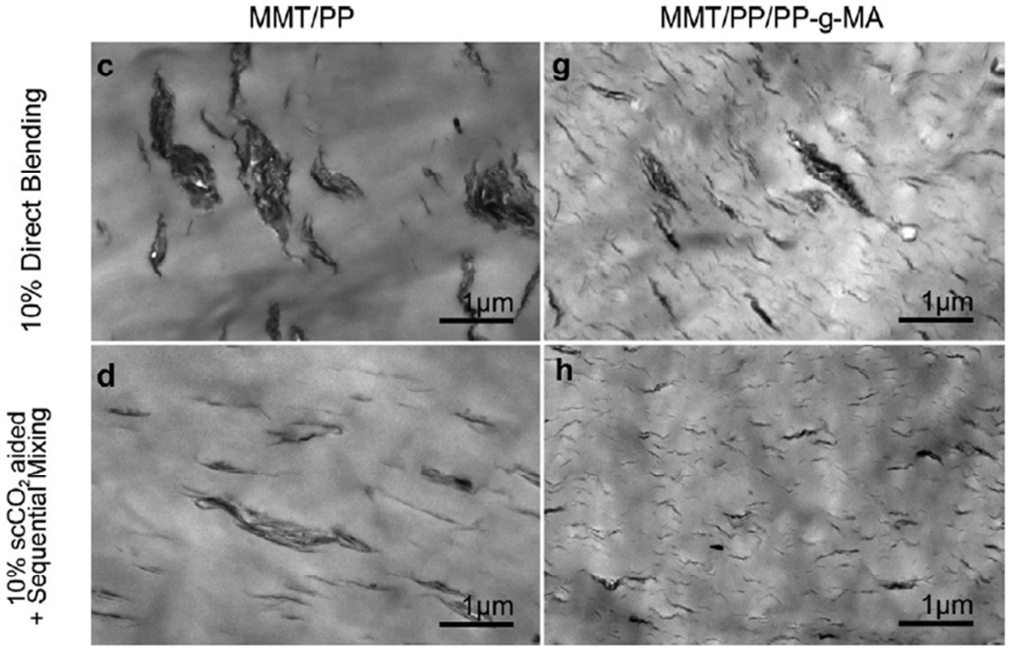


Figure 2.45. TEM of MMT/PP nanocomposites prepared at 10 wt% with and without compatibilizer with and without $scCO_2$treatment, modified from [57]

This work suggests that the application of this method to a nanocomposite with the potential for strong polymer/nanoclay interactions, such as nylon 6 and OMMT, may yield even further enhanced dispersion and mechanical properties.

The production of CNT nanocomposites by using supercritical fluid treatment with melt blending has been briefly reported in the literature. Gulari et al. [177] patented a method for treating the CNTs, similar to the patent by Manke et al. [176]. However, CNTs were only mentioned in a list of nanomaterials that have “potential” for nanocomposite formation using this method. Ma et al. [200] prepared MWCNT/PP nanocomposites by melting PP and CNT in an autoclave and mixing in the presence of $scCO_2$. The $scCO_2$ was vented after composite formation, in a method similar to Gulari’s procedure. However, this negates any of the effects that the rapid expansion might provide since the CNT/$scCO_2$ mixture does not experience the shear rates induced during rapid flow from the high pressure to low pressure vessel. The authors

provided mechanical properties and suggested that $scCO_2$ treatment provided improved properties even though they are within experimental error of traditionally melt compounded composites. Other work has focused on using $scCO_2$ to separate nanotubes without incorporation of the CNTs into a composite, as was reported in Section 2.5.2.3 for the REHPS method of particle formation. Although Jung et al. [175] reported on the formation of nanocomposite films, the characterization through surface conductivity was limited and vague.

A recent report by Chen et al. [173] focused on using $scCO_2$ processing in combination with melt blending of CNT polymer nanocomposites. In this work, Chen et al. [173] reported improved mechanical properties in Radel/CNT nanocomposites by using $scCO_2$ processing of CNTs followed by single screw melt compounding. An initial optimization of the $scCO_2$ process was conducted, resulting in a ~6 fold decrease in the bulk density of the CNTs (Nanocyl-NC7000). A picture of the CNTs before and after $scCO_2$ treatment is shown in Figure 2.46


Figure 2.46. Nanocyl NC700 before and after $scCO_2$ treatment, showing a ~6 fold decrease in bulk density, modified fromChen et al. [173]

During the optimization, the authors suggested that higher pressures and longer soak times resulted in the best deagglomeration of the primary CNT agglomerates. However, soak time was not minimized, and temperature was not considered. SEM images were also investigated for

signs of any damage due to $scCO_2$ processing. It was suggested that nanotubes were not damaged by this observation, but not verified by transmission electron microscopy (TEM). Chen et al. [173] observed a 38% improvement in the Young's modulus at 7 wt% CNTs with $scCO_2$ treatment compared to a 7% improvement in nanocomposites prepared without $scCO_2$ processing. Neither optical microscopy nor TEM were obtained to determine the morphology of the nanocomposite, although SEM studies suggested that the CNTs were relatively well dispersed and participated in the reinforcement of the composite.

The use of $scCO_2$ in combination with melt blending to prepare thermoplastic nanocomposites has been reviewed. The potential for increasing the dispersion of the nanomaterial in the melt by preprocessing it with $scCO_2$ can lead to improved properties of the nanocomposites. The potential for advances to this process exist for both nanoclay nanocomposites and carbon nanotube nanocomposites.

From this literature review, several assertions may be made concerning the field of polymer nanocomposites of nanoclay and CNTs prepared with melt compounding. Nanomaterials (particularly CNTs and OMMT) possess interesting properties that make them ideal candidates for use in thermoplastic nanocomposites. The most preferable method of generating these nanocomposites is melt compounding. However, insufficient dispersion of nanofiller during melt compounding and damage to the CNTs are issues which must be overcome. The $scCO_2$ treatment of nanomaterial for use in melt compounding may be effective at increasing the dispersion in thermoplastic nanocomposites of CNTs and nanoclay, and has been suggested as a more benign method of CNT treatment. It is suspected that improved dispersion in these systems would yield enhanced mechanical reinforcement from nanoclays and improved electrical conductivity from CNTs.

## References


[1] M. Alexandre and P. Dubois, "Polymer-layered silicate nanocomposites: preparation, properties and uses of a new class of materials," *Materials Science & Engineering R-Reports,* vol. 28, 2000.

[2] T.D. Fornes and D.R. Paul, "Modeling properties of nylon 6/clay nanocomposites using composite theories," *Polymer,* vol. 44, 2003.

[3] P.C. LeBaron, Z. Wang, and T.J. Pinnavaia, "Polymer-layered silicate nanocomposites: an overview," *Applied Clay Science,* vol. 15, 1999.

[4] H.S. Lee, P.D. Fasulo, W.R. Rodgers, and D.R. Paul, "TPO based nanocomposites. Part 1. Morphology and mechanical properties," *Polymer,* vol. 46.

[5] D.R. Paul and L.M. Robeson, "Polymer nanotechnology: Nanocomposites," *Polymer,* vol. 49, 2008.

[6] H. Van Olphen, "An introduction to clay colloid chemistry," *Journal of Pharmaceutical Sciences,* vol. 53, 1964.

[7] S.S. Ray and M. Okamoto, "Polymer/layered silicate nanocomposites: a review from preparation to processing," *Progress in Polymer Science,* vol. 28, 2003.

[8] O.L. Manevitch and G.C. Rutledge, "Elastic properties of a single lamella of montmorillonite by molecular dynamics simulation," *Journal of Physical Chemistry B,* vol. 108, 2004.

[9] P. Aranda and E. Ruizhitzky, "Poly(Ethylene Oxide)-Silicate Intercalation Materials," *Chemistry of Materials,* vol. 4, 1992.

[10] K.A. Carrado, P. Thiyagarajan, and D.L. Elder, "Polyvinyl alcohol clay complexes formed by direct synthesis," *Clays and Clay Minerals,* vol. 44, 1996.

[11] R.A. Vaia, K.D. Jandt, E.J. Kramer, and E.P. Giannelis, "Microstructural evolution of melt intercalated polymer-organically modified layered silicates nanocomposites," *Chemistry of Materials,* vol. 8, 1996.

[12] E. Giannelis, "A new strategy for synthesizing polymer-ceramic nanocomposites," *JOM,* vol. 44, 1992.

[13] C. Chen, "The Manufacture of Polymer Nanocomposite Materials Using Supercritical Carbon Dioxide," 2011.

[14] H. Heinz, R.A. Vaia, R. Krishnamoorti, and B.L. Farmer, "Self-Assembly of Alkylammonium Chains on Montmorillonite: Effect of Chain Length, Head Group Structure, and Cation Exchange Capacity," *Chemistry of Materials,* vol. 19, 2006.

[15] D.R. Paul, Q.H. Zeng, A.B. Yu, and G.Q. Lu, "The interlayer swelling and molecular packing in organoclays," *Journal of Colloid and Interface Science,* vol. 292, 2005.

[16] A. Blumstein, "Polymerization of adsorbed monolayers. II. Thermal degradation of the inserted polymer," *Journal of Polymer Science Part A: General Papers,* vol. 3, 1965.

[17] R. Krishnamoorti, R.A. Vaia, and E.P. Giannelis, "Structure and dynamics of polymer-layered silicate nanocomposites," *Chemistry of Materials,* vol. 8, 1996.

[18] Q. Zhang, Y. Wang, and Q. Fu, "Shear-induced change of exfoliation and orientation in polypropylene/montmorillonite nanocomposites," *Journal of Polymer Science Part B-Polymer Physics,* vol. 41, 2003.

[19] P.J. Yoon, D.L. Hunter, and D.R. Paul, "Polycarbonate nanocomposites. Part 1. Effect of organoclay structure on morphology and properties," *Polymer,* vol. 44, 2003.

[20] E.P. Giannelis, "Polymer layered silicate nanocomposites," *Advanced Materials,* vol. 8, 1996.
[21] A. Okada and A. Usuki, "Twenty Years of Polymer-Clay Nanocomposites," *Macromolecular Materials and Engineering,* vol. 291, 2006.
[22] E. Manias, H. Chen, R. Krishnamoorti, J. Genzer, E.J. Kramer, and E.P. Giannelis, "Intercalation Kinetics of Long Polymers in 2 nm Confinements," *Macromolecules,* vol. 33, 2000.
[23] R.A. Vaia and E.P. Giannelis, "Lattice model of polymer melt intercalation in organically-modified layered silicates," *Macromolecules,* vol. 30, 1997.
[24] R.A. Vaia and E.P. Giannelis, "Polymer Melt Intercalation in Organically-Modified Layered Silicates: Model Predictions and Experiment," *Macromolecules,* vol. 30, 1997.
[25] J.W. Cho and D.R. Paul, "Nylon 6 nanocomposites by melt compounding," *Polymer,* vol. 42, 2001.
[26] A. Usuki, Y. Kojima, M. Kawasumi, A. Okada, Y. Fukushima, T. Kurauchi, and O. Kamigaito, "SYNTHESIS OF NYLON 6-CLAY HYBRID," *Journal of Materials Research,* vol. 8, 1993.
[27] C. Oriakhi, "Nano sandwiches," *Chemistry in Britain,* vol. 34, 1998.
[28] V. Mittal, *Characterization techniques for polymer nanocomposites*. Polymer nano-, micro- & macrocomposites,. 2012, Weinheim: Wiley-VCH. xvii, 360 p.
[29] Y. Kojima, A. Usuki, M. Kawasumi, A. Okada, T. Kurauchi, and O. Kamigaito, "Sorption of Water in Nylon-6 Clay Hybrid," *Journal of Applied Polymer Science,* vol. 49, 1993.
[30] Y. Kojima, A. Usuki, M. Kawasumi, A. Okada, T. Kurauchi, and O. Kamigaito, "One-Pot Synthesis of Nylon-6 Clay Hybrid," *Journal of Polymer Science Part a-Polymer Chemistry,* vol. 31, 1993.
[31] Y. Kojima, A. Usuki, M. Kawasumi, A. Okada, T. Kurauchi, and O. Kamigaito, "Synthesis of Nylon-6-Clay Hybrid by Montmorillonite Intercalated with Epsilon-Caprolactam," *Journal of Polymer Science Part a-Polymer Chemistry,* vol. 31, 1993.
[32] Y. Kojima, A. Usuki, M. Kawasumi, A. Okada, T. Kurauchi, O. Kamigaito, and K. Kaji, "Fine-Structure of Nylon-6-Clay Hybrid," *Journal of Polymer Science Part B-Polymer Physics,* vol. 32, 1994.
[33] Y. Kojima, A. Usuki, M. Kawasumi, A. Okada, T. Kurauchi, O. Kamigaito, and K. Kaji, "Novel Preferred Orientation in Injection-Molded Nylon 6-Clay Hybrid," *Journal of Polymer Science Part B-Polymer Physics,* vol. 33, 1995.
[34] A. Okada and A. Usuki, "The chemistry of polymer-clay hybrids," *Materials Science & Engineering C-Biomimetic Materials Sensors and Systems,* vol. 3, 1995.
[35] A. Okada, A. Usuki, T. Kurauchi, and O. Kamigaito, "Polymer-Clay Hybrids," *Hybrid Organic-Inorganic Composites,* vol. 585, 1995.
[36] A. Usuki, M. Kawasumi, Y. Kojima, A. Okada, and T. Kurauchi, "Synthesis and Properties of Diamine-Modified Nylon 6-Clay Hybrid," *Kobunshi Ronbunshu,* vol. 52, 1995.
[37] A. Usuki, M. Kawasumi, Y. Kojima, A. Okada, T. Kurauchi, and O. Kamigaito, "Swelling Behavior of Montmorillonite Cation Exchanged for Omega-Amino Acids by Epsilon-Caprolactam," *Journal of Materials Research,* vol. 8, 1993.

[38] A. Usuki, A. Koiwai, Y. Kojima, M. Kawasumi, A. Okada, T. Kurauchi, and O. Kamigaito, "Interaction of Nylon-6 Clay Surface and Mechanical-Properties of Nylon-6 Clay Hybrid," *Journal of Applied Polymer Science,* vol. 55, 1995.
[39] A. Usuki, K. Okamoto, A. Okada, and T. Kurauchi, "Synthesis and Properties of Acrylic Resin Clay Hybrid," *Kobunshi Ronbunshu,* vol. 52, 1995.
[40] S.S. Lee, Y.T. Ma, H.W. Rhee, and J. Kim, "Exfoliation of layered silicate facilitated by ring-opening reaction of cyclic oligomers in PET-clay nanocomposites," *Polymer,* vol. 46, 2005.
[41] M. Alexandre, P. Dubois, T. Sun, J.M. Garces, and R. Jerome, "Polyethylene-layered silicate nanocomposites prepared by the polymerization-filling technique: synthesis and mechanical properties," *Polymer,* vol. 43, 2002.
[42] P. Dubois, M. Alexandre, F. Hindryckx, and R. Jerome, "Polyolefin-based composites by polymerization-filling technique," *Journal of Macromolecular Science-Reviews in Macromolecular Chemistry and Physics,* vol. C38, 1998.
[43] H.G. Jeon, H.T. Jung, S.W. Lee, and S.D. Hudson, "Morphology of polymer/silicate nanocomposites - High density polyethylene and a nitrile copolymer," *Polymer Bulletin,* vol. 41, 1998.
[44] M. Avella, S. Cosco, G.D. Volpe, and M.E. Errico, "Crystallization behavior and properties of exfoliated isotactic polypropylene/organoclay nanocomposites," *Advances in Polymer Technology,* vol. 24, 2005.
[45] T.D. Fornes, P.J. Yoon, H. Keskkula, and D.R. Paul, "Nylon 6 nanocomposites: the effect of matrix molecular weight," *Polymer,* vol. 42, 2001.
[46] T.D. Fornes and D.R. Paul, "Crystallization behavior of nylon 6 nanocomposites," *Polymer,* vol. 44, 2003.
[47] T.D. Fornes, P.J. Yoon, D.L. Hunter, H. Keskkula, and D.R. Paul, "Effect of organoclay structure on nylon 6 nanocomposite morphology and properties," *Polymer,* vol. 43, 2002.
[48] A.A. Gawad, A.M.K. Esawi, and A.R. Ramadan, "Structure and properties of nylon 6-clay nanocomposites: effect of temperature and reprocessing," *Journal of Materials Science,* vol. 45, 2010.
[49] S. Granick and K. Binder, *Polymers in confined environments*. Advances in polymer science,. 1999, Berlin ; New York: Springer. vi, 292 p.
[50] L.M. Liu, Z.N. Qi, and X.G. Zhu, "Studies on nylon 6 clay nanocomposites by melt-intercalation process," *Journal of Applied Polymer Science,* vol. 71, 1999.
[51] K. Masenelli-Varlot, E. Reynaud, G. Vigier, and J. Varlet, "Mechanical properties of clay-reinforced polyamide," *Journal of Polymer Science Part B-Polymer Physics,* vol. 40, 2002.
[52] Y. Yoo, M.W. Spencer, and D.R. Paul, "Morphology and mechanical properties of glass fiber reinforced Nylon 6 nanocomposites," *Polymer,* vol. 52, 2011.
[53] X.G. Zhang and L.S. Loo, "Morphology and Mechanical Properties of a Novel Amorphous Polyamide/Nanoclay Nanocomposite," *Journal of Polymer Science Part B-Polymer Physics,* vol. 46, 2008.
[54] R.A. Vaia, H. Ishii, and E.P. Giannelis, "Synthesis and Properties of 2-Dimensional Nanostructures by Direct Intercalation of Polymer Melts in Layered Silicates," *Chemistry of Materials,* vol. 5, 1993.
[55] C. Chen, J. Samaniuk, D.G. Baird, G. Devoux, M. Zhang, R.B. Moore, and J.P. Quigley, "The preparation of nano-clay/polypropylene composite materials with improved

properties using supercritical carbon dioxide and a sequential mixing technique," *Polymer,* vol. 53, 2012.
[56] N.N. Bhiwankar and R.A. Weiss, "Melt intercalation/exfoliation of polystyrene-sodium-montmorillonite nanocomposites using sulfonated polystyrene ionomer compatibilizers," *Polymer,* vol. 47, 2006.
[57] C. Chen and D.G. Baird, "Dispersion of nano-clay at higher levels into polypropylene with carbon dioxide in the presence of maleated polypropylene," *Polymer,* vol. 53, 2012.
[58] F.C. Chiu, S.M. Lai, J.W. Chen, and P.H. Chu, "Combined effects of clay modifications and compatibilizers on the formation and physical properties of melt-mixed polypropylene/clay nanocomposites," *Journal of Polymer Science Part B-Polymer Physics,* vol. 42, 2004.
[59] N. Hasegawa, M. Kawasumi, M. Kato, A. Usuki, and A. Okada, "Preparation and mechanical properties of polypropylene-clay hybrids using a maleic anhydride-modified polypropylene oligomer," *Journal of Applied Polymer Science,* vol. 67, 1998.
[60] Q.T. Nguyen and D.G. Baird, "Dispersion of nanoclay into polypropylene with carbon dioxide in the presence of maleated polypropylene," *Journal of Applied Polymer Science,* vol. 109, 2008.
[61] Y. Tang and M. Lewin, "Maleated polypropylene OMMT nanocomposite: Annealing, structural changes, exfoliated and migration," *Polymer Degradation and Stability,* vol. 92, 2007.
[62] K.H. Wang, M.H. Choi, C.M. Koo, Y.S. Choi, and I.J. Chung, "Synthesis and characterization of maleated polyethylene/clay nanocomposites," *Polymer,* vol. 42, 2001.
[63] Y. Wang, F.B. Chen, and K.C. Wu, "Twin-screw extrusion compounding of polypropylene/organoclay nanocomposites modified by maleated polypropylenes," *Journal of Applied Polymer Science,* vol. 93, 2004.
[64] Y. Wang, F.B. Chen, K.C. Wu, and J.C. Wang, "Shear rheology and melt compounding of compatibilized-polypropylene nanocomposites: Effect of compatibilizer molecular weight," *Polymer Engineering and Science,* vol. 46, 2006.
[65] Y.C. Ahn and D.R. Paul, "Rubber toughening of nylon 6 nanocomposites," *Polymer,* vol. 47, 2006.
[66] F. Chavarria and D.R. Paul, "Comparison of nanocomposites based on nylon 6 and nylon 66," *Polymer,* vol. 45, 2004.
[67] F. Chavarria, R.K. Shah, D.L. Hunter, and D.R. Paul, "Effect of melt processing conditions on the morphology and properties of nylon 6 nanocomposites," *Polymer Engineering and Science,* vol. 47, 2007.
[68] T.D. Fornes, D.L. Hunter, and D.R. Paul, "Effect of sodium montmorillonite source on nylon 6/clay nanocomposites," *Polymer,* vol. 45, 2004.
[69] T.D. Fornes, D.L. Hunter, and D.R. Paul, "Nylon-6 nanocomposites from alkylammonium-modified clay: The role of alkyl tails on exfoliation," *Macromolecules,* vol. 37, 2004.
[70] T.D. Fornes and D.R. Paul, "Structure and properties of nanocomposites based on nylon-11 and-12 compared with those based on nylon-6," *Macromolecules,* vol. 37, 2004.
[71] T.D. Fornes, P.J. Yoon, and D.R. Paul, "Polymer matrix degradation and color formation in melt processed nylon 6/clay nanocomposites," *Polymer,* vol. 44, 2003.

[72] J. Huang and D.R. Paul, "Comparison of fracture behavior of nylon 6 versus an amorphous polyamide toughened with maleated poly(ethylene-1-octene) elastomers," *Polymer,* vol. 47, 2006.
[73] J.J. Huang, H. Keskkula, and D.R. Paul, "Comparison of the toughening behavior of nylon 6 versus an amorphous polyamide using various maleated elastomers," *Polymer,* vol. 47, 2006.
[74] D.M. Laura, H. Keskkula, J.W. Barlow, and D.R. Paul, "Effect of rubber particle size and rubber type on the mechanical properties of glass fiber reinforced, rubber-toughened nylon 6," *Polymer,* vol. 44, 2003.
[75] R.K. Shah and D.R. Paul, "Nylon 6 nanocomposites prepared by a melt mixing masterbatch process," *Polymer,* vol. 45, 2004.
[76] P.J. Yoon, T.D. Fornes, and D.R. Paul, "Thermal expansion behavior of nylon 6 nanocomposites," *Polymer,* vol. 43, 2002.
[77] H.R. Dennis, D.L. Hunter, D. Chang, S. Kim, J.L. White, J.W. Cho, and D.R. Paul, "Effect of melt processing conditions on the extent of exfoliation in organoclay-based nanocomposites," *Polymer,* vol. 42, 2001.
[78] G.M. Russo, V. Nicolais, L. Di Maio, S. Montesano, and L. Incarnato, "Rheological and mechanical properties of nylon 6 nanocomposites submitted to reprocessing with single and twin screw extruders," *Polymer Degradation and Stability,* vol. 92, 2007.
[79] P.J. Yoon, D.L. Hunter, and D.R. Paul, "Polycarbonate nanocomposites: Part 2. Degradation and color formation," *Polymer,* vol. 44, 2003.
[80] S. Hotta and D.R. Paul, "Nanocomposites formed from linear low density polyethylene and organoclays," *Polymer,* vol. 45, 2004.
[81] K.Y. Lee and D.R. Paul, "A model for composites containing three-dimensional ellipsoidal inclusions," *Polymer,* vol. 46, 2005.
[82] E. Manias, A. Touny, L. Wu, K. Strawhecker, B. Lu, and T.C. Chung, "Polypropylene/Montmorillonite nanocomposites. Review of the synthetic routes and materials properties," *Chemistry of Materials,* vol. 13, 2001.
[83] P. Reichert, H. Nitz, S. Klinke, R. Brandsch, R. Thomann, and R. Mulhaupt, "Poly(propylene)/organoclay nanocomposite formation: Influence of compatibilizer functionality and organoclay modification," *Macromolecular Materials and Engineering,* vol. 275, 2000.
[84] F.L. Beyer, N.C.B. Tan, A. Dasgupta, and M.E. Galvin, "Polymer-layered silicate nanocomposites from model surfactants," *Chemistry of Materials,* vol. 14, 2002.
[85] C. Ibanes, L. David, M. De Boissieu, R. Seguela, T. Epicier, and G. Robert, "Structure and mechanical behavior of nylon-6 fibers filled with organic and mineral nanoparticles. I. Microstructure of spun and drawn fibers," *Journal of Polymer Science Part B-Polymer Physics,* vol. 42, 2004.
[86] S. Bourbigot, S. Duquesne, and C. Jama, "Polymer nanocomposites: How to reach low flammability?," *Macromolecular Symposia,* vol. 233, 2006.
[87] B. Schartel, M. Bartholmai, and U. Knoll, "Some comments on the main fire retardancy mechanisms in polymer nanocomposites," *Polymers for Advanced Technologies,* vol. 17, 2006.
[88] H. Qin, S. Zhang, C. Zhao, G. Hu, and M. Yang, "Flame retardant mechanism of polymer/clay nanocomposites based on polypropylene," *Polymer,* vol. 46, 2005.

[89] T. Kashiwagi, R.H. Harris Jr, X. Zhang, R.M. Briber, B.H. Cipriano, S.R. Raghavan, W.H. Awad, and J.R. Shields, "Flame retardant mechanism of polyamide 6–clay nanocomposites," *Polymer,* vol. 45, 2004.
[90] H. Lee, P.D. Fasulo, W.R. Rodgers, and D.R. Paul, "TPO based nanocomposites. Part 2. Thermal expansion behavior," *Polymer,* vol. 47, 2006.
[91] M.A. Osman, V. Mittal, M. Morbidelli, and U.W. Suter, "Epoxy-layered silicate nanocomposites and their gas permeation properties," *Macromolecules,* vol. 37, 2004.
[92] S.H. Kim and S.C. Kim, "Synthesis and properties of poly(ethylene terephthalate)/clay nanocomposites by in situ polymerization," *Journal of Applied Polymer Science,* vol. 103, 2007.
[93] W.J. Choi, H.J. Kim, K.H. Yoon, O.H. Kwon, and C.I. Hwang, "Preparation and barrier property of poly(ethylene terephthalate)/clay nanocomposite using clay-supported catalyst," *Journal of Applied Polymer Science,* vol. 100, 2006.
[94] R. Krishnamoorti and E.P. Giannelis, "Rheology of end-tethered polymer layered silicate nanocomposites," *Macromolecules,* vol. 30, 1997.
[95] Q.T. Nguyen and D.G. Baird, "An improved technique for exfoliating and dispersing nanoclay particles into polymer matrices using supercritical carbon dioxide," *Polymer,* vol. 48, 2007.
[96] A.J. Poslinski, M.E. Ryan, R.K. Gupta, S.G. Seshadri, and F.J. Frechette, "Rheological Behavior of Filled Polymeric Systems .1. Yield Stress and Shear-Thinning Effects," *Journal of Rheology,* vol. 32, 1988.
[97] S. Iijima, "Helical Microtubules of Graphitic Carbon," *Nature,* vol. 354, 1991.
[98] E.T. Thostenson, Z.F. Ren, and T.W. Chou, "Advances in the science and technology of carbon nanotubes and their composites: a review," *Composites Science and Technology,* vol. 61, 2001.
[99] J.N. Coleman, U. Khan, W.J. Blau, and Y.K. Gun'ko, "Small but strong: A review of the mechanical properties of carbon nanotube-polymer composites," *Carbon,* vol. 44, 2006.
[100] L.V. Radushkevich, Luk'yanovich, V.M., *Zhurnal Fizicheskoi Khimii,* vol. 26, 1952.
[101] H.G. Tennent, "Carbon fibrils, method for producing same and compositions containing same," 4,663,230, 1987.
[102] V. Choudhary and A. Gupta, *Polymer/Carbon Nanotube Nanocomposites*. Carbon Nanotubes - Polymer Nanocomposites. 2011.
[103] F. Hussain, M. Hojjati, M. Okamoto, and R.E. Gorga, "Review article: Polymer-matrix nanocomposites, processing, manufacturing, and application: An overview," *Journal of Composite Materials,* vol. 40, 2006.
[104] A.K.-T. Lau and D. Hui, "The revolutionary creation of new advanced materials—carbon nanotube composites," *Composites Part B: Engineering,* vol. 33, 2002.
[105] M. Endo, K. Takeuchi, S. Igarashi, K. Kobori, M. Shiraishi, and H.W. Kroto, "The Production and Structure of Pyrolytic Carbon Nanotubes (Pcnts)," *Journal of Physics and Chemistry of Solids,* vol. 54, 1993.
[106] H.J. Dal, A.G. Rinzler, P. Nikolaev, A. Thess, D.T. Colbert, and R.E. Smalley, "Single-wall nanotubes produced by metal-catalyzed disproportionation of carbon monoxide," *Chemical Physics Letters,* vol. 260, 1996.
[107] M.M.J. Treacy, T.W. Ebbesen, and J.M. Gibson, "Exceptionally high Young's modulus observed for individual carbon nanotubes," *Nature,* vol. 381, 1996.

[108] M.F. Yu, O. Lourie, M.J. Dyer, K. Moloni, T.F. Kelly, and R.S. Ruoff, "Strength and breaking mechanism of multiwalled carbon nanotubes under tensile load," *Science,* vol. 287, 2000.
[109] M.F. Yu, B.S. Files, S. Arepalli, and R.S. Ruoff, "Tensile loading of ropes of single wall carbon nanotubes and their mechanical properties," *Physical Review Letters,* vol. 84, 2000.
[110] C.L. Kane and E.J. Mele, "Size, shape, and low energy electronic structure of carbon nanotubes," *Physical Review Letters,* vol. 78, 1997.
[111] O. Lourie, D.M. Cox, and H.D. Wagner, "Buckling and collapse of embedded carbon nanotubes," *Physical Review Letters,* vol. 81, 1998.
[112] J.P. Salvetat, A.J. Kulik, J.M. Bonard, G.A.D. Briggs, T. Stockli, K. Metenier, S. Bonnamy, F. Beguin, N.A. Burnham, and L. Forro, "Elastic modulus of ordered and disordered multiwalled carbon nanotubes," *Advanced Materials,* vol. 11, 1999.
[113] J.P. Salvetat, G.A.D. Briggs, J.M. Bonard, R.R. Bacsa, A.J. Kulik, T. Stockli, N.A. Burnham, and L. Forro, "Elastic and shear moduli of single-walled carbon nanotube ropes," *Physical Review Letters,* vol. 82, 1999.
[114] J.W. Mintmire, D.H. Robertson, B.I. Dunlap, R.C. Mowrey, D.W. Brenner, and C.T. White, "Electronic-Structure of Fullerene Tubules," *Electrical, Optical, and Magnetic Properties of Organic Solid State Materials,* vol. 247, 1992.
[115] J.W. Mintmire and C.T. White, "Electronic and Structural-Properties of Carbon Nanotubes," *Carbon,* vol. 33, 1995.
[116] M.S. Dresselhaus, G. Dresselhaus, and P.C. Eklund, "Raman scattering in fullerenes," *Journal of Raman Spectroscopy,* vol. 27, 1996.
[117] M.S. Dresselhaus, G. Dresselhaus, and R. Saito, "Physics of Carbon Nanotubes," *Carbon,* vol. 33, 1995.
[118] T.W. Ebbesen, H.J. Lezec, H. Hiura, J.W. Bennett, H.F. Ghaemi, and T. Thio, "Electrical conductivity of individual carbon nanotubes," *Nature,* vol. 382, 1996.
[119] J. Baets, A. Godara, J. Devaux, and I. Verpoest, "Toughening of polymerized cyclic butylene terephthalate with carbon nanotubes for use in composites," *Composites Part A: Applied Science and Manufacturing,* vol. 39, 2008.
[120] M. Micusik, M. Omastova, I. Krupa, J. Prokes, P. Pissis, E. Logakis, C. Pandis, P. Potschke, and J. Pionteck, "A Comparative Study on the Electrical and Mechanical Behaviour of Multi-Walled Carbon Nanotube Composites Prepared by Diluting a Masterbatch With Various Types of Polypropylenes," *Journal of Applied Polymer Science,* vol. 113, 2009.
[121] K. Prashantha, J. Soulestin, M.F. Lacrampe, P. Krawczak, G. Dupin, and M. Claes, "Masterbatch-based multi-walled carbon nanotube filled polypropylene nanocomposites: Assessment of rheological and mechanical properties," *Composites Science and Technology,* vol. 69, 2009.
[122] I. Alig, P. Potschke, D. Lellinger, T. Skipa, S. Pegel, G.R. Kasaliwal, and T. Villmow, "Establishment, morphology and properties of carbon nanotube networks in polymer melts," *Polymer,* vol. 53, 2012.
[123] G.R. Kasaliwal, S. Pegel, A. Goldel, P. Potschke, and G. Heinrich, "Analysis of agglomerate dispersion mechanisms of multiwalled carbon nanotubes during melt mixing in polycarbonate," *Polymer,* vol. 51, 2010.

[124] T. Villmow, B. Kretzschmar, and P. Potschke, "Influence of screw configuration, residence time, and specific mechanical energy in twin-screw extrusion of polycaprolactone/multi-walled carbon nanotube composites," *Composites Science and Technology,* vol. 70, 2010.
[125] T. MacNally and P. Potschke, *Polymer Carbon Nanotube Composites: Preparation, Properties and Applications*. 2011: Woodhead Publishing Limited.
[126] S. Pegel, T. Villmow, and P. Potschke, "Quantification of dispersion and distribution of carbon nanotubes in polymer composites using microscopy techniques," *Polymer-Carbon Nanotube Composites: Preparation, Properties and Applications*, 2011.
[127] F.Y. Castillo, R. Socher, B. Krause, R. Headrick, B.R. Grady, R. Prada-Silvy, and P. Potschke, "Electrical, mechanical, and glass transition behavior of polycarbonate-based nanocomposites with different multi-walled carbon nanotubes," *Polymer,* vol. 52, 2011.
[128] H. Rumpf, "Zur Theorie der Zugfestigkeit von Agglomeraten bei Kraftübertragung an Kontaktpunkten," *Chem. Ing. Tech.,* vol. Volume 42, 1970.
[129] D. Stoyan, W.S. Kendall, and J. Mecke, *Stochastic geometry and its applications*. 2nd ed. Wiley series in probability and statistics Applied probability and statistics. 1995, Chichester ; New York: Wiley. xix, 436 p.
[130] A.H. Barber, S.R. Cohen, S. Kenig, and H.D. Wagner, "Interfacial fracture energy measurements for multi-walled carbon nanotubes pulled from a polymer matrix," *Composites Science and Technology,* vol. 64, 2004.
[131] A.H. Barber, S.R. Cohen, and H.D. Wagner, "Static and dynamic wetting measurements of single carbon nanotubes," *Physical Review Letters,* vol. 92, 2004.
[132] E.W. Washburn, "The Dynamics of Capillary Flow," *Physical Review,* vol. 17, 1921.
[133] I. Manas-Zloczower, A. Nir, and Z. Tadmor, "Dispersive Mixing in Internal Mixers—A Theoretical Model Based on Agglomerate Rupture," *Rubber Chemistry and Technology,* vol. 55, 1982.
[134] S. Hansen, D.V. Khakhar, and J.M. Ottino, "Dispersion of solids in nonhomogeneous viscous flows," *Chemical Engineering Science,* vol. 53, 1998.
[135] M. Abdel-Goad and P. Potschke, "Rheological characterization of melt processed polycarbonate-multiwalled carbon nanotube composites," *Journal of Non-Newtonian Fluid Mechanics,* vol. 128, 2005.
[136] S. Pegel, P. Potschke, T. Villmow, D. Stoyan, and G. Heinrich, "Spatial statistics of carbon nanotube polymer composites," *Polymer,* vol. 50, 2009.
[137] K.S. Suslick and D.J. Flannigan, "Inside a collapsing bubble: Sonoluminescence and the conditions during cavitation," *Annual Review of Physical Chemistry,* vol. 59, 2008.
[138] K.L. Lu, R.M. Lago, Y.K. Chen, M.L.H. Green, P.J.F. Harris, and S.C. Tsang, "Mechanical damage of carbon nanotubes by ultrasound," *Carbon,* vol. 34, 1996.
[139] S. Badaire, P. Poulin, M. Maugey, and C. Zakri, "In situ measurements of nanotube dimensions in suspensions by depolarized dynamic light scattering," *Langmuir,* vol. 20, 2004.
[140] B. Krause, R. Bolcit, and P. Potschke, "A method for determination of length distributions of multiwalled carbon nanotubes before and after melt processing," *Carbon,* vol. 49, 2011.
[141] Z.J. Jia, Z.Y. Wang, C.L. Xu, J. Liang, B.Q. Wei, D.H. Wu, and S.W. Zhu, "Study on poly(methyl methacrylate)/carbon nanotube composites," *Materials Science and*

*Engineering a-Structural Materials Properties Microstructure and Processing*, vol. 271, 1999.
[142] K.F. Fu, W.J. Huang, Y. Lin, L.A. Riddle, D.L. Carroll, and Y.P. Sun, "Defunctionalization of functionalized carbon nanotubes," *Nano Letters*, vol. 1, 2001.
[143] D. Baskaran, J.W. Mays, and M.S. Bratcher, "Polymer-grafted multiwalled carbon nanotubes through surface-initiated polymerization," *Angewandte Chemie-International Edition*, vol. 43, 2004.
[144] B.P. Grady, F. Pompeo, R.L. Shambaugh, and D.E. Resasco, "Nucleation of polypropylene crystallization by single-walled carbon nanotubes," *Journal of Physical Chemistry B*, vol. 106, 2002.
[145] Y. Xi, A. Yamanaka, Y.Z. Bin, and M. Matsuo, "Electrical properties of segreated ultrahigh molecular weight polyethylene/multiwalled carbon nanotube composites," *Journal of Applied Polymer Science*, vol. 105, 2007.
[146] Y. Bin, A. Yamanaka, Q.Y. Chen, Y. Xi, X.W. Jiang, and M. Matsuo, "Morphological, electrical and mechanical properties of ultrahigh molecular weight polyethylene and multi-wall carbon nanotube composites prepared in decalin and paraffin," *Polymer Journal*, vol. 39, 2007.
[147] E. Assouline, A. Lustiger, A.H. Barber, C.A. Cooper, E. Klein, E. Wachtel, and H.D. Wagner, "Nucleation ability of multiwall carbon nanotubes in polypropylene composites," *Journal of Polymer Science Part B-Polymer Physics*, vol. 41, 2003.
[148] M. Lebron-Colon, M.A. Meador, J.R. Gaier, F. Sola, D.A. Scheiman, and L.S. McCorkle, "Reinforced Thermoplastic Polyimide with Dispersed Functionalized Single Wall Carbon Nanotubes," *Acs Applied Materials & Interfaces*, vol. 2, 2010.
[149] B. Lin, U. Sundararaj, and P. Potschke, "Melt mixing of polycarbonate with multi-walled carbon nanotubes in miniature mixers," *Macromolecular Materials and Engineering*, vol. 291, 2006.
[150] P. Potschke, H. Brunig, A. Janke, D. Fischer, and D. Jehnichen, "Orientation of multiwalled carbon nanotubes in composites with polycarbonate by melt spinning," *Polymer*, vol. 46, 2005.
[151] T. McNally, P. Potschke, P. Halley, M. Murphy, D. Martin, S.E.J. Bell, G.P. Brennan, D. Bein, P. Lemoine, and J.P. Quinn, "Polyethylene multiwalled carbon nanotube composites," *Polymer*, vol. 46, 2005.
[152] I. Szleifer and R. Yerushalmi-Rozen, "Polymers and carbon nanotubes—dimensionality, interactions and nanotechnology," *Polymer*, vol. 46, 2005.
[153] P. Potschke, M. Abdel-Goad, S. Pegel, D. Jehnichen, J.E. Mark, D.H. Zhou, and G. Heinrich, "Comparisons Among Electrical and Rheological Properties of Melt-Mixed Composites Containing Various Carbon Nanostructures," *Journal of Macromolecular Science Part a-Pure and Applied Chemistry*, vol. 47, 2010.
[154] I. Alig, D. Lellinger, S.M. Dudkin, and P. Potschke, "Conductivity spectroscopy on melt processed polypropylene-multiwalled carbon nanotube composites: Recovery after shear and crystallization," *Polymer*, vol. 48, 2007.
[155] R. Andrews, D. Jacques, M. Minot, and T. Rantell, "Fabrication of carbon multiwall nanotube/polymer composites by shear mixing," *Macromolecular Materials and Engineering*, vol. 287, 2002.

[156] B. Krause, P. Potschke, and L. Haussler, "Influence of small scale melt mixing conditions on electrical resistivity of carbon nanotube-polyamide composites," *Composites Science and Technology,* vol. 69, 2009.
[157] Z.H. Fan and S.G. Advani, "Rheology of multiwall carbon nanotube suspensions," *Journal of Rheology,* vol. 51, 2007.
[158] P. Potschke, T.D. Fornes, and D.R. Paul, "Rheological behavior of multiwalled carbon nanotube/polycarbonate composites," *Polymer,* vol. 43, 2002.
[159] L.A. Blanchard and J.F. Brennecke, "Recovery of organic products from ionic liquids using supercritical carbon dioxide," *Industrial & Engineering Chemistry Research,* vol. 40, 2001.
[160] A.I. Cooper, "Polymer synthesis and processing using supercritical carbon dioxide," *Journal of Materials Chemistry,* vol. 10, 2000.
[161] D. Sanli, S.E. Bozbag, and C. Erkey, "Synthesis of nanostructured materials using supercritical CO(2): Part I. Physical transformations," *Journal of Materials Science,* vol. 47, 2012.
[162] S.K. Goel and E.J. Beckman, "Generation of Microcellular Polymeric Foams Using Supercritical Carbon-Dioxide," *Abstracts of Papers of the American Chemical Society,* vol. 204, 1992.
[163] S.K. Goel and E.J. Beckman, "Generation of Microcellular Polymeric Foams Using Supercritical Carbon-Dioxide .2. Cell-Growth and Skin Formation," *Polymer Engineering and Science,* vol. 34, 1994.
[164] S.K. Goel and E.J. Beckman, "Generation of Microcellular Polymeric Foams Using Supercritical Carbon-Dioxide .1. Effect of Pressure and Temperature on Nucleation," *Polymer Engineering and Science,* vol. 34, 1994.
[165] E. Kiran, "Foaming strategies for bioabsorbable polymers in supercritical fluid mixtures. Part I. Miscibility and foaming of poly(L-lactic acid) in carbon dioxide plus acetone binary fluid mixtures," *Journal of Supercritical Fluids,* vol. 54, 2010.
[166] J.L. Kendall, D.A. Canelas, J.L. Young, and J.M. DeSimone, "Polymerizations in supercritical carbon dioxide," *Chemical Reviews,* vol. 99, 1999.
[167] E. Reverchon and R. Adami, "Nanomaterials and supercritical fluids," *Journal of Supercritical Fluids,* vol. 37, 2006.
[168] S.D. Yeo and E. Kiran, "Formation of polymer particles with supercritical fluids: A review," *Journal of Supercritical Fluids,* vol. 34, 2005.
[169] J. Jung and M. Perrut, "Particle design using supercritical fluids: Literature and patent survey," *The Journal of Supercritical Fluids,* vol. 20, 2001.
[170] E. Reverchon, G. Dellaporta, R. Taddeo, P. Pallado, and A. Stassi, "Solubility and Micronization of Griseofulvin in Supercritical Chf3," *Industrial & Engineering Chemistry Research,* vol. 34, 1995.
[171] K.A. Narh, A.T. Agwedicham, and L. Jallo, "Dry coating polymer powder particles with deagglomerated carbon nanotubes to improve their dispersion in nanocomposites," *Powder Technology,* vol. 186, 2008.
[172] D. To, R. Dave, X. Yin, and S. Sundaresan, "Deagglomeration of nanoparticle aggregates via rapid expansion of supercritical or high-pressure suspensions," *Aiche Journal,* vol. 55, 2009.

[173] C. Chen, M. Bortner, J.P. Quigley, and D.G. Baird, "Using supercritical carbon dioxide in preparing carbon nanotube nanocomposite: Improved dispersion and mechanical properties," *Polymer Composites,* vol. 33, 2012.
[174] D. To, S. Sundaresan, and R. Dave, "Nanoparticle mixing through rapid expansion of high pressure and supercritical suspensions," *Journal of Nanoparticle Research,* vol. 13, 2011.
[175] W.R. Jung, J.H. Choi, N. Lee, K. Shin, J.H. Moon, and Y.S. Seo, "Reduced damage to carbon nanotubes during ultrasound-assisted dispersion as a result of supercritical-fluid treatment," *Carbon,* vol. 50, 2012.
[176] C.W. Manke, E. Gulari, D.F. Mielewski, and E.C.-C. Lee, "System and method of delaminating a layered silicate material by supercritical fluid treatment," U.S. Patent, 2002.
[177] E. Gulari, K. Rangaramanujam, and G.K. Serhatkulu, "Method of delaminating aggregated particles with a coating agent in a substantially supercritical fluid," US7387749, 2008.
[178] E. Reverchon, "Supercritical antisolvent precipitation of micro- and nano-particles," *Journal of Supercritical Fluids,* vol. 15, 1999.
[179] M. Bahrami and S. Ranjbarian, "Production of micro- and nano-composite particles by supercritical carbon dioxide," *Journal of Supercritical Fluids,* vol. 40, 2007.
[180] D.L. Tomasko, X.M. Han, D.H. Liu, and W.H. Gao, "Supercritical fluid applications in polymer nanocomposites," *Current Opinion in Solid State & Materials Science,* vol. 7, 2003.
[181] R.J. Bellair, M. Manitiu, E. Gulari, and R.M. Kannan, "Investigation of Clay Modifier Effects on the Structure and Rheology of Supercritical Carbon Dioxide-Processed Polymer Nanocomposites," *Journal of Polymer Science Part B-Polymer Physics,* vol. 48, 2010.
[182] C. Chen, J. Samaniuk, D.G. Baird, G. Devoux, M.Q. Zhang, R.B. Moore, and J.P. Quigley, "The preparation of nano-clay/polypropylene composite materials with improved properties using supercritical carbon dioxide and a sequential mixing technique," *Polymer,* vol. 53, 2012.
[183] P.D. Fasulo, D.A. Okonski, R.A. Ottaviani, and W.R. Rodgers, "Method for making nanocomposite materials," 2008.
[184] M. Garcia-Leiner and A.J. Lesser, "Intercalation in polymer-clay nanocomposites promoted by supercritical carbon dioxide.," *Abstracts of Papers of the American Chemical Society,* vol. 226, 2003.
[185] M. Garcia-Leiner and A.J. Lesser, "Polymer nanocomposites prepared by supercritical carbon dioxide-assisted polymer processing," *Abstracts of Papers of the American Chemical Society,* vol. 227, 2004.
[186] M. Garcia-Leiner and A.J. Lesser, "Intercalated polymer nanocomposites prepared in supercritical carbon dioxide.," *Mechanical Properties of Nanostructured Materials and Nanocomposites,* vol. 791, 2004.
[187] K. Goren, L.M. Chen, L.S. Schadler, and R. Ozisik, "Influence of nanoparticle surface chemistry and size on supercritical carbon dioxide processed nanocomposite foam morphology," *Journal of Supercritical Fluids,* vol. 51, 2010.

[188] K. Goren, O.B. Okan, L.M. Chen, L.S. Schadler, and R. Ozisik, "Supercritical carbon dioxide assisted dispersion and distribution of silica nanoparticles in polymers," *Journal of Supercritical Fluids,* vol. 67, 2012.
[189] S. Horsch, G. Serhatkulu, E. Gulari, and R.M. Kannan, "Supercritical CO2 dispersion of nano-clays and clay/polymer nanocomposites," *Polymer,* vol. 47, 2006.
[190] D.W. Litchfield, D.G. Baird, P.B. Rim, and C. Chen, "Improved mechanical properties of poly(ethylene terephthalate) nanocomposite fibers," *Polymer Engineering & Science,* vol. 50, 2010.
[191] D.F. Mielewski, E.C.-c. Lee, C.W. Manke, and E. Gulari, "System and method of preparing a reinforced polymer by supercritical fluid treatment," U.S. Patent 6753360, 2004.
[192] J. Samaniuk, D. Litchfield, and D. Baird, "Improving the Exfoliation of Layered Silicate in a Poly(ethylene terephthalate) Matrix Using Supercritical Carbon Dioxide," *Polymer Engineering and Science,* vol. 49, 2009.
[193] K. Yang and R. Ozisik, "Effects of processing parameters on the preparation of nylon 6 nanocomposites," *Polymer,* vol. 47, 2006.
[194] Q. Zhao and E.T. Samulski, "Supercritical CO2-mediated intercalation of PEO in clay," *Macromolecules,* vol. 36, 2003.
[195] M. Manitiu, R.J. Bellair, S. Horsch, E. Gulari, and R.M. Kannan, "Supercritical Carbon Dioxide-Processed Dispersed Polystyrene-Clay Nanocomposites," *Macromolecules,* vol. 41, 2008.
[196] M. Manitiu, S. Horsch, E. Gulari, and R.M. Kannan, "Role of polymer-clay interactions and nano-clay dispersion on the viscoelastic response of supercritical CO2 dispersed polyvinylmethylether (PVME)-Clay nanocomposites," *Polymer,* vol. 50, 2009.
[197] G.M. A.J. Lesser, "Polymer-Clay Nanocomposites Prepared in Supercritical Carbon Dioxide," *ANTEC 2004*,2004.
[198] L.E. Mielewski DF, Manke CW, Gulari E., 2004.
[199] E.G. C.W Manke, D.F Mielewski, E.C Lee, "System and method of delaminating a layered silicate material by supercritical fluid treatment," 2002.
[200] J. Ma, H. Deng, and T. Peijs, "Processing of Poly(propylene)/Carbon Nanotube Composites using scCO(2)-Assisted Mixing," *Macromolecular Materials and Engineering,* vol. 295, 2010.

# Chapter 3. Improved Mechanical Properties of Melt Compounded Organoclay/Nylon 6 Nanocomposites Using a Supercritical Carbon Dioxide Pretreatment for the Nanomaterial

John P. Quigley[1], Donald G. Baird[1,2]

1. Department of Chemical Engineering, Virginia Tech, Blacksburg, Virginia 24061, USA,
2. Macromolecules and Interfaces Institute, Virginia Tech, Blacksburg, Virginia 24061, USA

## 3.1 Abstract

The use of supercritical carbon dioxide ($scCO_2$) as a processing aid to help exfoliate nanoclays and improve their dispersion after melt blending in polymer matrices has been reported in the literature by our laboratory and others. Previous work has focused on nonpolar polymers such as polypropylene. In this work, the supercritical aided melt blending method with single screw compounding was applied to an organoclay/ nylon 6 composite system with favorable interactions. Wide-angle X-ray diffraction, transmission electron microscopy, dynamic mechanical testing, and tensile tests are provided to investigate the effect of processing with $scCO_2$ on the final composite morphology and properties. It was found that properties of composites prepared with the $scCO_2$ aided method were similar to or higher than those reported in the literature for samples prepared with twin screw compounding. At 7.6 wt% the modulus value reached 4.75 GPa which is one of the highest increases (1.7 GPa) reported for these materials processed at intermediate concentrations. Beyond 7.6 wt% the improvement due to $scCO_2$ processing matches that of direct blending. It is possible that with the use of a twin screw extruder, the modulus would continue to increase. The use of nylon illustrates the importance of having functionalities which can interact with the clay during $scCO_2$ aided melt compounding.

## 3.2 Background and Motivation

In 1993 the Toyota research group revealed a major breakthrough by successfully preparing nylon 6-nanoclay composites with enhanced properties. Specifically, they saw an increase from 1.11 GPa to 1.87 GPa in tensile modulus with the addition of 4.7 wt% clay by preparing composites with *In situ* polymerization [1, 2]. Since this breakthrough, researchers have thoroughly investigated the potential for clay nanocomposites with superior barrier, thermal, flame retardant, ablative, and mechanical properties [2-6].

In order to achieve improved composite properties, either exfoliated or partially exfoliated/intercalated nanocomposite morphology is desired [7-9]. Intercalated clay morphology occurs when polymer chains diffuse into the gallery spacing of the layered structure, resulting in a gallery spacing on the order of a few nanometers [10]. The intercalated and exfoliated morphology both involve nano-scale reinforcement. If the clay layers are completely pushed apart to create a disordered array, the composite is considered to be "exfoliated".

Different preparation methods are used to achieve these morphologies, including *In situ* polymerization, solution blending, and melt intercalation [1, 11, 12]. Melt intercalation, or melt compounding, is the preferable method of nanocomposite generation due to its low cost, lack of harmful solvents, flexibility, and general scalability to industry [13]. In the melt compounding of polymer-clay nanocomposites, homogenous dispersion of the filler and exfoliation of the clay tactoids are particularly difficult tasks, and are typically achieved only in systems with favorable clay-polymer interactions [14, 15].

In order to enhance the polymer-clay interactions, organically treated montmorillonite (organoclay) is often used during melt intercalation. The organoclay is obtained by chemically

modifying the surface of the pristine montmorillonite through cation exchange reactions [16, 17]. This surface modification helps to compatibilize the interface for interactions with the polar or nonpolar matrices, depending on the end use desired. In addition, cation exchange carried out with long chain surfactant molecules increase the gallery spacing between the silicate layers. The increase of gallery spacing helps to separate the stacked nanoclay layers allowing for easier transport of polymer chains between the clay platelets, improving the degree of exfoliation for the final composite.

The promising studies on the mechanical properties of nanoclay composites carried out by the Toyota research group in the early 90's has led to massive efforts on the nanoclay-nylon 6 system, especially in the field of twin screw melt compounding [12-14, 18-22]. The first melt compounding studies on this system were carried out by Liu et al., [14] where they found a 37% increase in tensile modulus at 4.7 wt% nanoclay in nylon 6 using a twin screw for dispersing the nanofiller. Some of the most comprehensive work on this system has been carried out by D.R. Paul's group at the University of Texas, Austin, by twin screw compounding surface treated nanoclays and nylon 6 [12, 18-22]. In a paper by Fornes et al. [11], this group used a co-rotating twin screw extruder to melt compound nylon 6/ Cloisite 30B composites and then injection molded tensile bars. They found a 59 % increase in modulus from the virgin matrix, from 2.75 GPa to 4.38 GPa for 6.1 wt% organoclay [19]. They were able to produce some of the best improvements in mechanical properties for nylon 6 composites prepared by melt intercalation [19, 23]. Although twin screw compounding is capable of providing nanocomposites with higher degrees of dispersion than single screw compounding [12], twin screw compounding requires more capital, energy, and material costs to operate. Consequently, novel methods which utilize single screw compounding in combination with novel dispersing steps are desired.

The use of supercritical carbon dioxide ($scCO_2$) in combination with single screw compounding has been considered as an alternative route for the preparation of polymer-clay nanocomposites in order to achieve similar dispersions as twin screw compounding [24-35]. Nguyen et al. [24] developed a method to combine the benefits of melt compounding with the exfoliating capability of $scCO_2$. The process relied on rapid expansion of the clay followed by direct injection into the extruder. In a more recent study in our laboratory by Chen et al. [15], a semi-continuous method was developed that improved the nanoclay dispersion with the aid of $scCO_2$ based on Nguyen's method. In this process, the nanoclay layers are delaminated by catastrophically depressurizing the $scCO_2$ treated clay into the polymer pellet bed of a modified hopper. The mixture is then melt compounded in a single screw extruder and pelletized. The initial efforts based on this method have focused on the use of nonpolar polymers such as polypropylene (PP), where it has been observed that the modulus continued to increase with increasing clay concentration up to 10 wt% [15]. In the most recent work in our laboratory, the effect of maleated polypropylene (PP-*g*-Ma) on organoclay/polypropylene nanocomposites with the $scCO_2$ aided melt blending was investigated [26]. The increase in modulus from the pure matrix was 41% for 5 wt% organoclay with PP when processing the composite with the $scCO_2$ aided melt blending method. Alternatively, the composite processed with a 3:1 ratio of nanoclay to PP-*g*-Ma and 5 wt% organoclay using the same method showed an increase in modulus of 61% compared to the pure matrix. This suggested that polar clay/polymer interactions could be enhanced with the $scCO_2$ aided melt blending method.

In the current work, the process developed by Chen et al. [25] was applied to the well documented Cloisite 30B/ nylon 6 (organoclay/nylon 6) nanocomposite system. Building on organoclay/PP-*g*-Ma/PP work from Chen et al. [26] we applied $scCO_2$ aided melt blending

method to an organoclay/thermoplastic system with highly polar groups with potential for favorable clay/polymer interactions. A pressurized chamber was utilized to soak the organoclay in $scCO_2$, expand the suspension and blow it over the polymer pellet bed, followed by melt compounding using a single-screw extruder. A series of organoclay/nylon 6 composites was prepared at 1 weight percent (wt%), 3 wt%, 5 wt%, 7 wt%, and 10 wt% by the $scCO_2$ aided method and conventional direct blending (DB). Wide-angle X-ray diffraction (WAXD), transmission electron microscopy (TEM), and dynamic mechanical properties from rheology were carried out to determine the effect of processing method on composite morphologies. The mechanical properties were also analyzed to determine the effectiveness of the $scCO_2$ aided melt blending method compared to that of twin screw compounding

## 3.3 Experimental Methods and Materials

### 3.3.1 Materials

The polymer matrix used in this study was nylon 6 (Aegis H50LN) which was obtained from Honeywell (Richmond, VA) and used as received. The number average molecular weight is 16,000 g/mol, with a polydispersity of 2. The melt index of the polymer is 9.8 g/10min at 220$^{o}$C and a load of 1 kg. The organoclay (Cloisite30B) was obtained from Southern Clay Products, Inc. (Gonzalez, TX) and was used as-received. Cloisite 30B is a surface modified montmorillonite obtained through a cation exchange reaction, where the sodium cation is replaced by bis(2-hydroxy-ethyl) methyl tallow quaternary ammonium cations.

### 3.3.2 Preparation of Nanocomposites

The processing method used is referred to as $scCO_2$ aided melt blending method ($scCO_2$). The $scCO_2$ aided melt blending method is a procedure developed by Chen et al. [24] in our laboratory and involves blowing the expanded nanoclay directly into the hopper filled with polymer pellets, followed by processing the composite immediately. Nylon pellets and organic modified nanoclay were dried separately at 80°C overnight. The organooclay was put in a pressurized chamber and allowed to be in direct contact with $scCO_2$ at 3000 psi (20.6 MPa), at 80°C for 12hrs. These conditions were utilized in the current study as they have been previously developed in our laboratory. The effect of these and other processing variables on the deagglomeration of nanofiller aggregates is addressed in other work [36]. The dried nylon 6 pellets were placed inside a 18.92 liter (5 gallon) pressure vessel. The organoclay and nylon 6 pellets were mixed as clay was released rapidly with the $CO_2$ into the 18.92 liter (5 gallon) pressure vessel. The organoclay and polymer mixture was collected and fed into the extruder hopper to simulate a modified hopper as described in Chen et al. [15]. The organoclay/nylon 6

mixture was then extruded at an average melt temperature of 220$^{o}$C and a screw speed of 25 rpm using a single screw Killion KL-100 extruder with a 25.4 mm (1 in) diameter and a L/D of 30:1. A capillary die was used with a 1.59 mm diameter and 20:1 L/D. The nanocomposite strands were chopped into 3-5 mm long cylindrical pellets and dried at 80°C in a vacuum oven overnight. The dried composite pellets were injection molded with an Arburg Allrounder (model 221-55-250) injection molding machine. Nitrogen was flowed over the pellet bed to prevent moisture uptake during the injection molding process. The Arburg Allrounder consisted of a 22-mm diameter barrel, L/D of 24, and a screw with a variable root diameter from approximately 14.25 mm at the feed to 19.3 mm at the exit. A check ring non-return valve and an insulated nozzle that was 2 mm in diameter were part of the apparatus. The composites were injection molded with a melt temperature of 220°C, a mold temperature of 80°C, a holding pressure of 500 KPa, a screw speed of 200 rpm, and a type V dog bone mold compliant with ASTM standard D638-10.

The conventional direct blending method (DB) was used to prepare nanocomposites for comparison purposes. In this approach, the organically modified nanoclay was used as received. The clay and nylon 6 were mechanically mixed in a Kitchen Aid type mixer and dried together at 80 °C overnight in a vacuum oven. The mixture was then fed to an extruder as specified above.

The actual organoclay content of the composites was determined using a burn-off technique. The samples were heated in an ashing oven for 2 hours at 500$^{o}$C. The reported concentrations are an average of three samples. The nanocomposite concentrations reported here include the organic modifier.

### 3.3.3 Wide-angle X-ray Diffraction

Wide-angle X-ray diffraction (WAXD) characterization was carried out with a Philips Xpert Pro diffractometer with a Cu Kα source (wavelength of 0.154 nm). Injection molded samples were ground into a fine powder for the WAXD scans. Particle size was controlled by using an ultrafine metal mesh. The system was operated at a tension of 45 kV and a current of 40 mA. The tests were performed at a scan rate of $0.1^{o}$/min and a step size of $0.05^{o}$ from $2\theta = 1.5^{o}$ to $10^{o}$.

### 3.3.4 Transmission Electron Microscopy

Transmission electron microscopy (TEM) was used as a comprehensive characterization technique for morphology. TEM measurements were generated with a Philips EM420T with an accelerating voltage of 100 kv. The TEM samples, around 70 nm thick, were cut with a cryomicrotome equipped with a diamond knife at -60°C. Injection molded samples were used for the TEM measurements.

### 3.3.5 Dynamic Mechanical Properties

Dynamic mechanical measurements on the nanocomposites were performed using a Rheometrics Mechanical Spectrometer model 800 (RMS-800). The extruded pellets were compression molded into 25 mm diameter disks at $230^{o}$C under 1 metric ton for 3 minutes before the mold was cooled. Compression molded samples were dried overnight in a vacuum oven at $80^{o}$C before rheological testing. Dynamic frequency sweep experiments were performed under a continuous nitrogen atmosphere using a 25 mm cone and plate fixture with 0.1 radian angle and a gap of 0.05 mm at $240^{o}$C in the linear viscoelastic region of the materials. The linear viscoelastic limit was determined using strain sweeps at a frequency of 10 rad/s at the same temperature ($240^{o}$C). It was found that dynamic frequency sweep experiments could be

conducted at a strain of 5%. The storage moduli (G') of the materials as functions of angular frequency (ω) (ranging from 0.1 rad/s to 100 rad/s) were obtained at a temperature of 240$^{o}$C.

### 3.3.6 Tensile Properties

Tensile tests on the dog bones were performed at room temperature with an Instron model 4204 testing machine (Instron, Grove City, PA). An extensometer was used to accurately measure Young's modulus. The load was measured with a 5-kN load cell, while the crosshead speed was kept at 1.27 mm/min during all tensile tests. For all tests, the average and the standard deviation were calculated from at least five samples, and data points greater than two standard deviations from the mean were omitted. Elongation at break values reported are normalized to the virgin matrix due to limitations of the apparatus.

## 3.4 Results and Discussion

### 3.4.1 Wide-angle X-ray Diffraction

WAXD was conducted to investigate the degree of exfoliation of the organoclay/ nylon 6 composites. The highest concentrations prepared, virgin organoclay, and virgin matrix's WAXD patterns are compared in Figure 1.

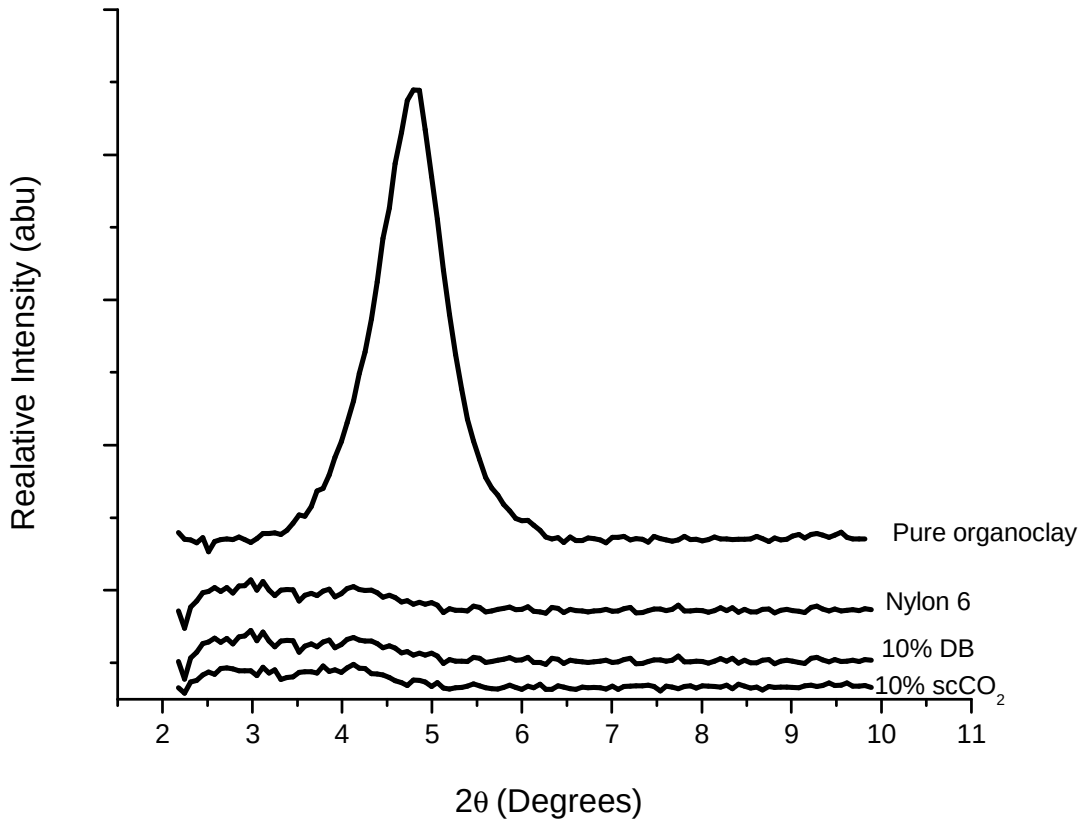


Figure 3.1. Wide-angle X-ray diffraction results for concentrations of interest

The characteristic peak of Cloisite 30B is found at $2\theta = 4.8^{o}$. The decrease or disappearance of this peak in a diffraction pattern is often attributed to an exfoliated nanocomposite [19, 37]. Even at the highest concentrations prepared in this work, no peak is present as is evident from the patterns for the 10 wt% samples in Figure 3.1. In work by Cho et al. [12], the authors saw a characteristic peak with single screw compounding at 5 wt% in an organoclay/nylon 6 system, but only used one pass in the extruder. Previous work done with single screw compounding and two passes by Gawad et al. [38] with nylon 6 and Cloisite 30B mimics the processing history and materials investigated here. In the WAXD patterns for this system, they saw disappearance of the 5 wt% peaks, but did not investigate higher concentrations. Zhang et al. [37] investigated concentrations as high as 10 wt% with an amorphous polyamide and Cloisite 30B without the appearance of a WAXD peak, but used a Haake Polydrive melt mixer rather than extruder. The WAXD results in Figure 3.1 suggest that an exfoliated morphology exists at all concentrations, which is supported by findings in the literature [12, 14, 37, 38] . Additional analysis of dispersion and exfoliation will be conducted in following sections using TEM and rheology.

### 3.4.2 Transmission Electron Microscopy

TEM images were taken and analyzed qualitatively to characterize the state of exfoliation and dispersion of the organoclay in the nanocomposite. TEM images of all concentrations are presented in Figure 4.2, with those on the left processed with the $scCO_2$ aided melt blending method, and those on the right processed with direct blending.

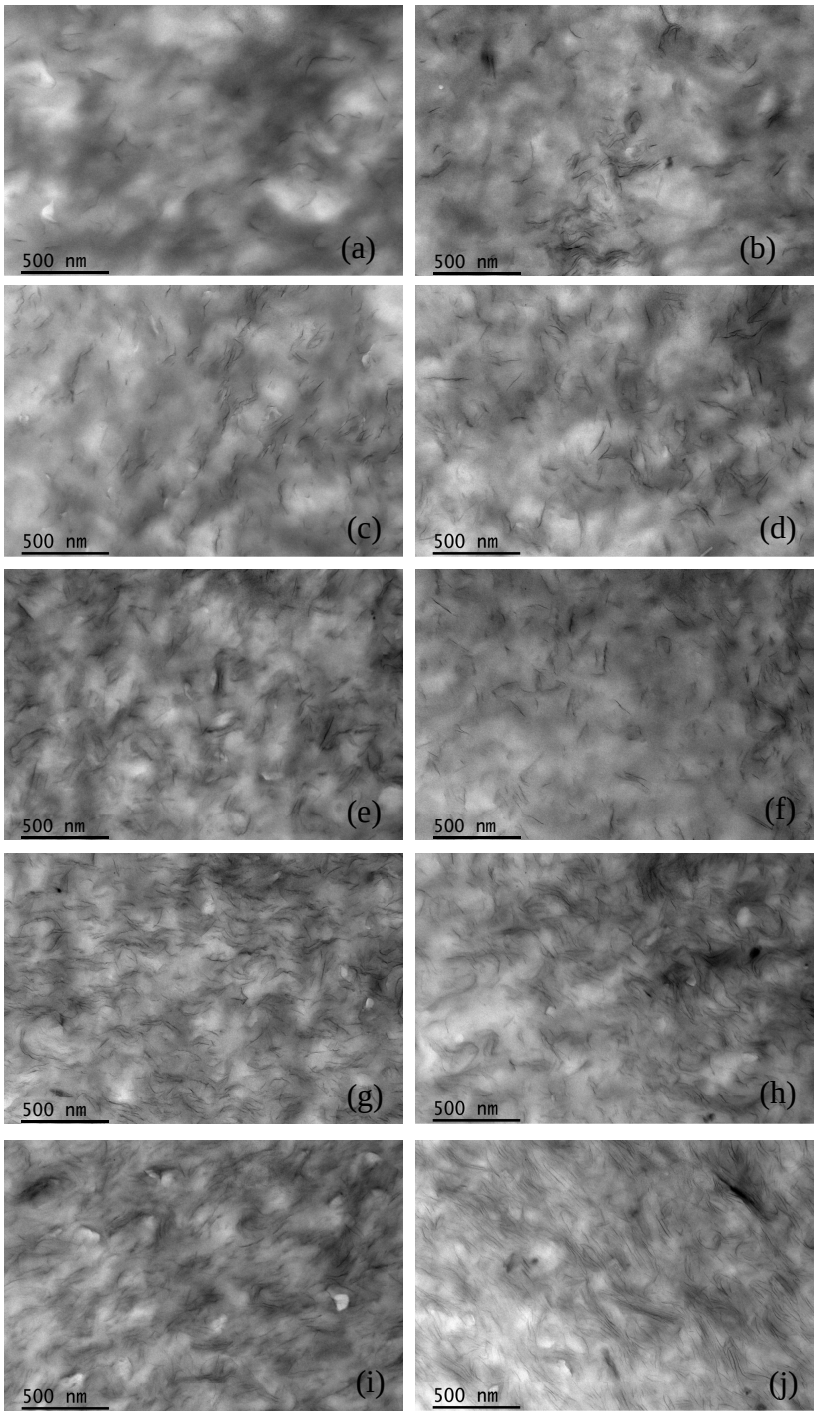


Figure 3.2. TEM of (a) 1 wt % $scCO_2$, (b) 1 wt % DB, (c) 3 wt % $scCO_2$, (d) 3 wt % DB, (e) 5 wt % $scCO_2$, (f) 5 wt % DB , (g) 7 wt % $scCO_2$, (h) 7 wt % DB (i) 10 wt % $scCO_2$ and (j) 10 wt% DB processed composites at a magnification of 34,000 x

The TEM images of 1 wt% organoclay/nylon 6 samples are compared in Figure 2 (a) and (b). The TEM of the 1 wt% DB sample shows multiple regions of large clay aggregation, whereas the image of 1 wt% $scCO_2$ shows none. In addition, the clay tactoids in the sample processed with direct blending are darker than those of the sample processed with $scCO_2$ aided melt blending, indicating higher electron density in these regions. This is likely due to thicker clay tactoids due to incomplete exfoliation indicating better exfoliation from $scCO_2$ aided melt blending. The micrographs of the 3 wt% samples (Figure 2 (c) and (d)) show similar trends as the 1 wt % samples, with more exfoliated clay tactoids in the sample processed with $scCO_2$ aided melt blending than that of the sample processed with direct blending. Both concentrations possess exfoliated morphologies with individual platelets arising from favorable polar interactions between polymer and clay. However, there are less regions of clay aggregation and fewer platelets per clay tactoid suggesting better dispersion from $scCO_2$ processing.

The TEM images of the 5 and 7 wt% samples also show improved morphology due to $scCO_2$ aided melt blending. The 5 wt% samples are compared in Figure 2 (e) and (f). Comparing the two processing methods, the clay tactoids appear to possess the same number of clay platelets and express the same degree of exfoliation. However, the homogeneity of distribution concerning the clay tactoids in the images is different. This deals with the microscopic dispersion of the organoclay, which is also affected by the $scCO_2$ treatment. The image indicates more regions void of clay in the 5 wt% sample prepared with direct blending than the composite prepared with $scCO_2$ aided melt blending. The TEM images presented here qualitatively compare to those investigated with twin screw compounding at similar concentrations [12]. Figure 2 (g) and (h), show the 7 wt% DB and 7 wt% $scCO_2$ samples, respectively. Similar to the 5 wt% samples, the 7 wt% $scCO_2$ sample contains less regions of clay aggregation compared to the 7

wt% DB sample, and fewer regions which are void of nanofiller. The improved homogeneity in nanoclay dispersion in the 5 wt% and 7 wt% $scCO_2$ samples indicates higher degrees of micro scale dispersion for samples processed with the $scCO_2$ aided melt blending method. This emerges from improved organoclay/ matrix interactions with the aid of the $scCO_2$ treatment to the nanomaterial. The nature of the interaction between the nylon 6 and organoclay has been studied in the literature [19, 39] , and was found to arise from ionic interactions between the matrix and clay surface. The $scCO_2$ processing increases the gallery spacing immediately before melt processing, allowing for easier diffusion of the polymer between the platelets and onto the clay surface during the melt blending step. A portion of these favorable interactions may remain intact throughout melt compounding, and prevent re-aggregation of clay platelets.

The TEM images of 10 wt% nanoclay/nylon 6 samples are displayed in Figure 2 (i) and (j). Both of these samples show more intercalated morphologies, with multiple clays per tactoid. There is no noticeable difference in morphology due to the processing method. This morphology is counter to what we would expect given the WAXD pattern discussed in Section 3.3.3. Paul et al. [13] suggest that the absence of a peak in the WAXD pattern may be due to lack of sensitivity in the scan rather than an exfoliated morphology, which may be the case here. It is interesting to note that the degree of dispersion of these relatively high concentration clay samples is still improved compared to other systems [2]. This is due to the very favorable organoclay/polymer interactions that have been well documented in the literature [3, 4].

Transmission electron microscopy helps provide visual evidence of clay dispersion, although it is not a bulk characterization technique. The TEM images were taken of isolated regions and may not be representative of the bulk properties, which are analyzed with rheology and mechanical analyses in following sections.

### 3.4.3 Dynamic Mechanical Properties

The dynamic mechanical properties were investigated for the organoclay/nylon 6 composites in order to determine if there is a correlation of the dynamic response of the materials with WAXD and TEM. The complex viscosities ($\eta^*$) and storage moduli (G') of the materials as functions of angular frequency ($\omega$) (ranging from 0.1 rad/s to 100 rad/s) were obtained at a temperature of 240$^{o}$C for all concentrations processed. The results are compared in Figure 3.3 and Figure 4.4 respectively on log-log plots. In Figure 3.3 the scale of the ordinate axis does not increase by orders of ten as is conventional, rather the scale was truncated in order to better demonstrate the relevant data. In this section, the general trends in $\eta^*$ and G' due to changes in concentration will be discussed, followed by specific comments on variations observed due to processing methods.

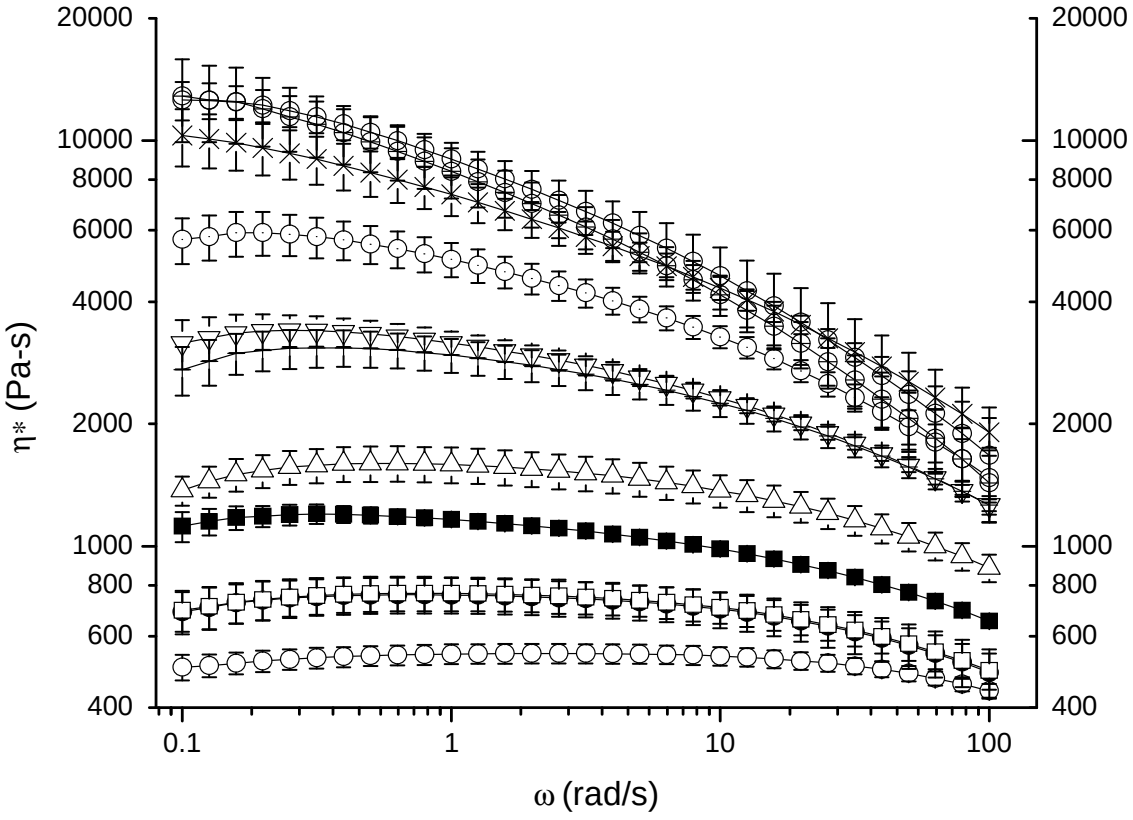


Figure 3.3. Complex viscosity, η*, vs. frequency, ω, of the organoclay/ nylon 6 composites with different processing conditions and at different concentrations. Nylon 6 (-○-), 1 wt% DB (-●-), 1 wt% scCO2 (-□-), 3 wt% DB (-■-), 3 wt% scCO2 (-△-) , 5 wt% DB (-▽-), 5 wt% scCO2 (-+-) , 7 wt% DB (-⊙-), 7wt% scCO2(-×-), 10 wt% DB (-Θ-), and 10 wt% scCO2 (-Φ-)

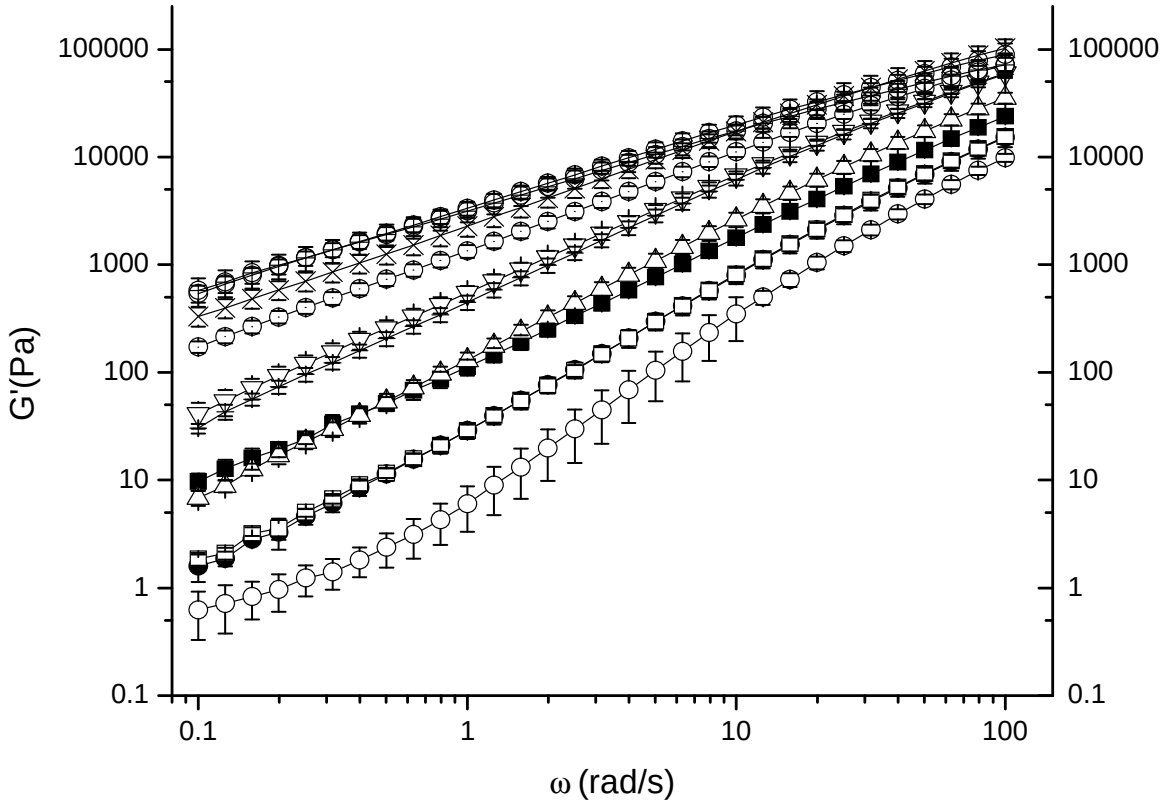


Figure 3.4. Storage modulus, G', vs. frequency, ω, of the organoclay/ nylon 6 composites with different processing conditions and at different concentrations. Nylon 6 (-○-), 1 wt% DB (-●-), 1 wt% scCO2 (-□-), 3 wt% DB (-■-), 3 wt% scCO2 (-△-) , 5 wt% DB (-▽-), 5 wt% scCO2 (-+-) , 7 wt% DB (-⊙-), 7wt% scCO2(-×-), 10 wt% DB (-Θ-), and 10 wt% scCO2 (-Φ-)

In general, it was found that dynamic mechanical properties were a function of organoclay content more than processing method for this system. Poslinski [40] studied rheological properties of filled polymer systems and observed that at a higher volume fraction of filler, the viscosity curve will translate to higher values. They also found that the onset of shear thinning will shift to lower frequencies with increasing filler content, which is also attributed to increased volume fraction of filler. In this study, both the η* and G' curve shift to higher values as filler concentration increases to 10 wt%. In Figure 3.3, the onset of shear thinning behavior in the η* curves shifts to lower frequencies as concentration increases as well, which follows expected trends. In addition to these interpretations, many authors suggest that a tail in the low frequency behavior of G' indicates the existence of a percolated network formed from an exfoliated nanocomposite [17, 41]. Recent work in our laboratory has shown this observation can also be due to agglomerate network formation and so is not necessarily an indicator of an exfoliated nanocomposite [24, 26]. In this study, no tail was observed in G' over the concentrations processed.

Differences in the dynamic mechanical response of the composites due to processing methods were observed for select concentrations. The η*, and G' values showed no variation due to scCO2 aided melt blending at 1 wt% within experimental error. This conflicts with the results found in the TEM images, where greater exfoliation and dispersion were found due to scCO2 processing. It could be that the concentration of nanofiller was too low to affect the dynamic response of the sample significantly, or that the differences in nanoscale dispersion evident in TEM did not translate to the bulk morphology. There was variation observed for η* values due to processing method for the composites processed at 3 wt%. The sample processed with $scCO_2$ aided melt blending showed an increase in η* values compared to the sample processed with

direct blending, as well as a shift in the onset of shear thinning to lower frequencies. If the weight fraction of filler is the same, then more exfoliated organoclay filler will occupy a larger volume fraction than an agglomerated or intercalated tactoid. For this reason, it might be proposed that the variations in the η* curves of the 3 wt% samples result from improved exfoliation or dispersion due to $scCO_2$ aided melt blending. This supports the evidence from TEM results where a more exfoliated nanocomposite was observed. Although there appears to be a difference in the shape of the G' curve of the 3 wt% samples with different processing methods, the values are within experimental error of one another. The dynamic response of 5 wt% samples were found to be within experimental error for both η* and G' for the different processing methods. The dynamic responses of the 7 wt% samples depended greatly on the preparation techniques. For the $scCO_2$ sample, the value of η* as ω approaches zero as  is nearly twice that of the DB processed sample and close to that of the 10 wt% samples. The onset of shear thinning for the $scCO_2$ sample also occurs at significantly lower frequencies than that of the DB sample. These results are similar to those of the 3 wt% samples, suggesting that the nanofiller in the sample prepared at 7 wt% with $scCO_2$ aided melt blending occupies a larger volume fraction than that of the sample prepared with direct blending. Supporting evidence from TEM suggests this is due to improved dispersion rather than an improved degree of exfoliation. The G' values are also at least two decades higher for the $scCO_2$ processed sample, which backs this claim. The η*, and G' values of the 10 wt% samples were within experimental error of each other suggesting no difference in morphology due to processing method. Although rheological measurements are helpful in understanding the bulk morphology in the melt, the mechanical properties may provide the most relevant data for distinguishing the sample preparation methods.

### 3.4.4 Mechanical Properties

The effect of the $scCO_2$ aided melt blending method on the mechanical properties of the organoclay/nylon 6 composites is investigated in this section. First, the combined data is presented in a table for the reader's convenience. This is followed by a discussion of the modulus of composites with different concentrations and processing methods, and a comparison to twin screw compounding results reported in the literature. The morphological contributions to increased modulus values observed in this work are also commented on. The high concentration barrier to improved modulus is then addressed with explanations and suggestions. Next, the tensile strength values are evaluated from the table. Finally, the elongation at break values are compared and discussed.

Relevant data from the organoclay composite mechanical data was collected and tabulated. The actual weight percent organoclay, modulus, strength and normalized elongation at break along are compared in Table 3.1.

Table 3.1. Actual organoclay loading and mechanical properties of organoclay/ nylon 6 nanocomposites

| Sample | Actual Organoclay Loading (wt%) | Young's Modulus (Gpa) | % Increase | Tensile Strength (Mpa) | % Increase | Normalized Elongation at Break | % Increase |
|---|---|---|---|---|---|---|---|
| Nylon 6 | - | 3.147 ± 0.113 | - | 73.19 ± 1.08 | - | 1.00 ± 0.29 | - |
| 1%DB | 1 | 3.467 ± 0.109 | 10.2 | 74.09 ± 1.06 | 1.2 | 2.30 ± 0.48 | 129.9 |
| 1%scCO2 | 0.9 | 3.576 ± 0.128 | 13.6 | 74.73 ± 1.11 | 2.1 | 2.33 ± 0.49 | 133.1 |
| 3%DB | 2.9 | 3.968 ± 0.132 | 26.1 | 84.02 ± 1.83 | 14.8 | 0.73 ± 0.22 | -27.1 |
| 3%scCO2 | 3.2 | 3.897 ± 0.137 | 23.8 | 76.08 ± 0.69 | 3.9 | 1.48 ± 0.64 | 48.1 |
| 5%DB | 4.5 | 4.029 ± 0.079 | 28.0 | 78.78 ± 3.16 | 7.6 | 0.33 ± 0.07 | -66.8 |
| 5%scCO2 | 4.9 | 4.61 ± 0.141 | 46.5 | 85.90 ± 2.41 | 17.4 | 0.40 ± 0.14 | -60.1 |
| 7%DB | 7.4 | 4.433 ± 0.048 | 40.9 | 78.81 ± 4.00 | 7.7 | 0.32 ± 0.07 | -68.4 |
| 7%scCO2 | 7.6 | 4.845 ± 0.194 | 54.0 | 82.69 ± 0.99 | 13.0 | 0.28 ± 0.09 | -72.4 |
| 10%DB | 9.9 | 5.050 ± 0.107 | 60.5 | 73.02 ± 5.67 | -0.2 | 0.26 ± 0.07 | -73.7 |
| 10%scCO2 | 9.2 | 4.807 ± 0.143 | 52.7 | 74.94 ± 4.79 | 2.4 | 0.28 ± 0.06 | -72.3 |

The actual organoclay loading was determined by a off technique and is provided for the reader's interest. The young's moduli, tensile strength, and normalized elongation at break values are provided. The standard deviation or error is provided with each value, and percent increases compared to the processed matrix are included for comparison purposes.

The Young's Moduli of the nanocomposites prepared by different processing methods are compared in Figure 3.5.

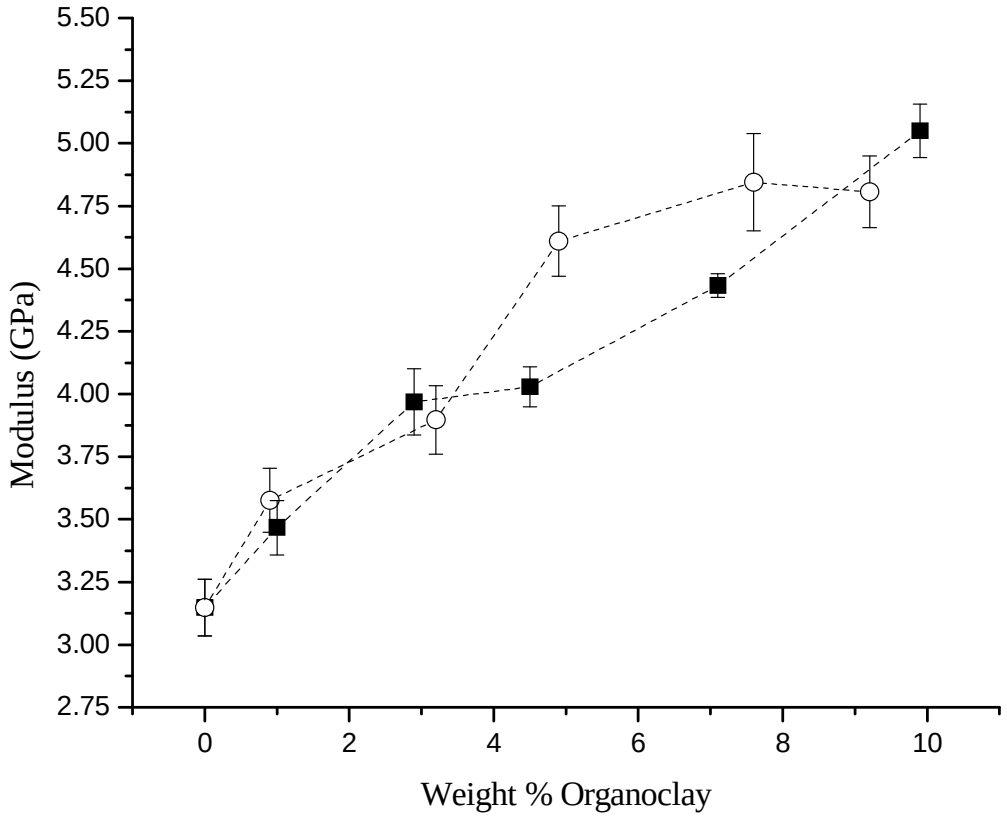


Figure 3.5. Young's moduli of organoclay/ nylon 6 nanocomposites processed by different methods ( DB (-■-) and $scCO_2$ (-○-)) and at different concentrations

The pure nylon 6 used in this study possesses a Young's modulus of 3.147 ± 0.113 GPa. By adding roughly 1 wt % organoclay, the moduli of both the DB and $scCO_2$ samples increased by about 0.3 GPa. These values are within experimental error of one another and confirm the assertion in the previous section; the improved exfoliation evident in TEM and rheology does not translate to bulk properties. The 3 wt% samples processed by different methods are also within experimental error of one another and increase from the virgin matrix by about 0.8 GPa. It is surprising that the moduli of these materials are not larger for the $scCO_2$ blended samples considering improved dispersion and exfoliation which was shown by TEM and inferred with rheology. This may have to do with the complicated crystallization effects that low concentration nanocomposites present, which is documented in the literature. Depending on the degree of crystallinity or the effect of disrupting physical cross-links in the polymer, the properties of the composite can be greatly affected [18, 42]. Adding approximately 5 wt% of organoclay using the conventional melt blending method, the nanocomposite is found to have a Young's modulus of 4.029 ± 0.079 GPa, an increase of about 28% compared to the pure matrix. By implementing the $scCO_2$ aided melt blending method at a comparable concentration, the modulus increases to 4.610 ± 0.l41 GPa, a 1.46 GPa, or a 47% increase. The improved degree of dispersion due to $scCO_2$ treatment, which was demonstrated in the TEM images, translated into improved composite reinforcement. Increasing the nanoclay loading to 7.1 wt% with direct blending resulted in a modulus of 4.845 ± 0.048, a 41% increase in modulus compared to nylon 6. Processing with $scCO_2$ at 7.6 wt% yielded a Young's modulus of 4.433 ± 0.194 GPa, a 54% increase in modulus.

The improvements in modulus at 5 and 7 wt% with $scCO_2$ treatment and single screw melt compounding match or exceed some of the best values found in literature based on mixing

in a twin screw extruder using nylon 6 and Cloisite 30B [19, 20]. At 5 and 7 wt %, the modulus obtained in this study compares to about 10 wt% and 14 wt% glass fiber composite with a similar molecular weight matrix obtained by twin screw melt blending, respectively [21]. Fornes et al. saw a 1.44 GPa increase for 5 wt% of organoclay using twin screw compounding, where we saw an increase of 1.46 GPa with the $scCO_2$ aided melt blending and single screw compounding [19]. They also saw a 1.87 GPa increase at 7 wt % organoclay compared to our observed increase of 1.70 GPa with the $scCO_2$ aided melt blending method. Although this improvement is not as significant as at 5 wt%, it is still within error of the twin screw results. It is also important to note that in Fornes' paper, the polymer matrix used has a $M_N$ = 29,300, whereas the Matrix used in this study has a $M_N$ = 16,130. It has been shown that with all other factors the same, a higher molecular weight polymer promotes the dispersion and exfoliation of nanoclay in the composites. This is due to higher viscosities inducing greater shear forces to separate the clay tactoids, resulting in better mechanical reinforcement from the filler material. In another work by Fornes et al. [43], they look at a similar organoclay filler and analyze the effect of matrix molecular weight. They investigate a resin with $M_N$ similar to the one in this paper, and find a 1 GPa increase in modulus for 5 wt% and a 1.56 GPa increase for 7 wt%. Considering this, the 1.46 GPa and 1.70 GPa increases in modulii at 5 and 7 wt % processed with $scCO_2$ aided melt blending which are reported here become particularly notable. These comparisons are made with a composite which incorportates a different organoclay, so are still not a direct evaluation of the organoclay/nylon 6 system from this study. In order to make a more accurate assessment, the nanofiller, melt temperature, and matrix molecular weight would need to be consistent. Regardless, the modulus of composites prepared with $scCO_2$ treatment that are presented in this

section for 5 and 7 wt% are an encouraging comparison to those processed with twin screw compounding.

The improvement in properties here might be due to an increase in dispersion rather than exfoliation, as is evidenced by TEM and the increased η* and G' values in the case of the 7 wt% sample. From the TEM images and WAXD results, it seems that the method of processing has no effect on the degree of exfoliation at intermediate concentrations. The TEM results suggest that the homogeneity of organoclay in the polymer was improved for the 5 and 7 wt% samples prepared by the $scCO_2$ aided melt blending. In addition, it was proposed that the increased η* and G' values for the 7 wt% sample prepared with $scCO_2$ aided melt blending arise from improved dispersion. For this reason, we propose that the microscopic dispersion has a greater effect on the mechanical properties than the degree of exfoliation in this study. This can be attributed to the strong polymer/organoclay interactions, which are improved as the $scCO_2$ treatment exposes the clay surface to the polar amide functionalities.

Above 7.6 wt%, the composite properties for both direct blended samples and samples processed with $scCO_2$ aided melt blending lie on the curve of the conventional melt blended organoclay/nylon 6 composites within experimental error. Processing the nanocomposite with the $scCO_2$ aided melt blending method has no effect at this concentration but is not detrimental to the composite properties compared to direct blending. These findings match the results from rheology and TEM, where no difference in dynamic response or dispersion was observed for different processing methods. In previous work in our laboratory, this has been attributed to collapse of the clays in the melt compounding step after $scCO_2$ expansion at higher concentrations [15]. The increased volume fraction of fillers means that they are more likely to "bump" into one another during melt processing, resulting in reaggregation at high

concentrations. Because the $scCO_2$ aided melt blending method acts to increase the effective volume fraction of filler, as described in section 3.4.3, we would expect more significant reaggregation to occur for samples processed in this manner. This can be avoided for nonpolar polypropylene by sequential mixing, as explained in Chen et al. [15]. In high concentration nonpolar composites processed with the $scCO_2$ aided melt blending method, extrusion followed by injection molding results in collapse of the clays and a decrease in the composite properties. By reducing the processing steps experienced by a portion of the nanomaterial, sequential mixing allows for increasing properties of composites processed with the $scCO_2$ aided melt blending method. Reducing the number of melt compounding steps in composites with favorable interactions, however, results in poorer dispersion [38]. Whereas properties of nonpolar composites such as PP tend to drop off around 10 wt% nanoclay, it has been shown that with a concentration as high as 20 wt% the Young's Modulus of the organoclay/nylon 6 system continue to improve [12]. Therefore, this lack of increasing properties in samples processed with the $scCO_2$ aided melt blending method must be investigated in further work. By including a twin screw extruder in combination with the $scCO_2$ treatment, these concentration barriers might be overcome.

The tensile strength values were also investigated for the two processing methods, and are compared in Table 3.1. The strength values vary from concentration to concentration, with large error bars in the direct blend sample data. The largest increases in tensile strength are observed for the 3 wt% DB and 5 wt% $scCO_2$ samples. Because it is not clear to the authors why this occurs, the only conclusion that can be made is that the significant increases in Young's Modulus are not accompanied by a decrease in tensile strength for any of the materials tested here. This is a desirable property for thermoplastic nanocomposites.

Percent elongation at break values were measured for each sample and normalized to the virgin matrix. The values are compared in Figure 3.6.

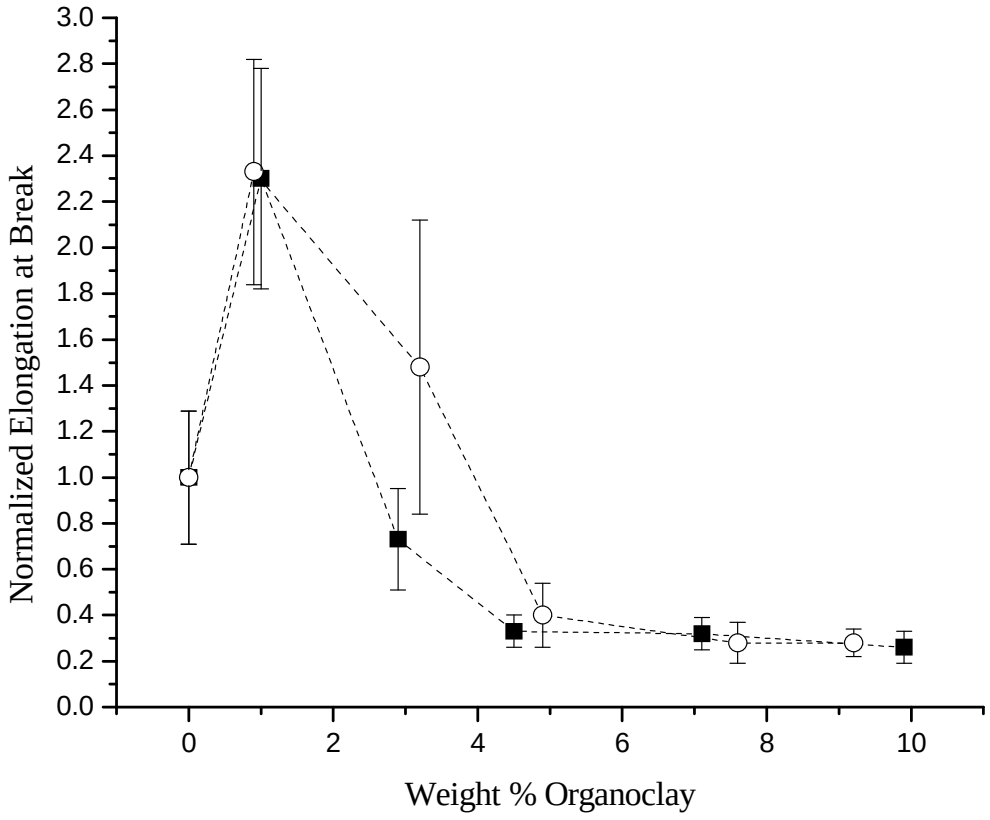


Figure 3.6. Normalized elongation at break of organoclay/ nylon 6 nanocomposites processed by different methods ( DB (-■-) and scCO2 (-○-)) and at different concentrations. Samples were normalized to virgin nylon 6 Note: 1 wt% organoclay/nylon 6 samples did not break within experimental limitations of apparatus

The 1% organoclay composites processed by both methods show higher elongation at break values than those of the pure matrix. They were stretched to the experimental limitation of the apparatus. Similar behavior has been observed in literature, where Ibanes et al. [42] showed increased ductility of drawn nanoclay nylon 6 nanocomposites at 1 wt%. Ibanes et al. claim that at these concentrations, the nanoclays act to disrupt the intercrystalline tie chains which would otherwise induce a physically cross-linked network, essentially increasing the amorphous content. It is interesting that we see a similar behavior for the 3 wt % $scCO_2$ sample where the average elongation at break value exceeds that of the virgin matrix. The mean value of elongation at break of the 3 wt % samples suggests that the material processed with the $scCO_2$ aided melt blending method leads to increased ductility at this concentration. Although extensive crystallization effects were not addressed in this work, other studies in the literature have been conducted to understand the effects of nanoclay on composite crystalline morphology. Kim et al. [44] studied PP-*g*-Ma with organically modified and unmodified clay and found that exfoliated clay morphology retarded crystallization kinetics. A similar morphological phenomenon might be occurring here, resulting in increased elongation at break for the sample processed at 3 wt% with $scCO_2$ aided melt blending. This could be due to better dispersion and exfoliation from $scCO_2$ processing. If that is the case, then this hypothesis is supported by rheology and from TEM analysis as well. Further characterization must be done to investigate the processing effects on the overall morphology of the nanocomposite, similar to work by Fornes et al. [18]. Above the addition of 3 wt % clay, all samples' elongation at break decreases as is expected.

## 3.5 Conclusions and future work

Organoclay/nylon 6 samples were processed in a single screw extruder using the direct blending method and $scCO_2$ aided melt blending to analyze the effect of favorable clay/polymer interactions on supercritical carbon dioxide nanocomposite processing. Whereas previous efforts in our group have focused on using the $scCO_2$ aided melt blending method to enhance nanocomposites with low interaction potential, this study found that the $scCO_2$ aided melt blending method can be effective at improving the dispersion and exfoliation in nanocomposite systems with polar bonding potential. This is likely due to the $scCO_2$ treatment allowing for the matrix to interact with the clay surface more readily. The $scCO_2$ aided melt blending method increases the gallery spacing of the clay tactoids and exposes the clay surface to the polymer, enhancing the interactions between the polymer matrix and organoclay. This is because the polar functionalities of the polymer chain are freer to diffuse near the polar clay surface during melt processing, creating a favorable interaction which facilitates shear separation and prevents reaggregation in the extruder. WAXD characterization was carried out, although no characteristic peaks were observed at the highest concentrations tested. TEM images revealed an improved morphology for all composites processed with $scCO_2$ aided melt blending up to 10 wt%. Compared with those prepared by direct blending, samples prepared with the $scCO_2$ aided melt blending method showed improved exfoliation up to 3 wt% and improved micro-scale dispersion up to 10 wt%. Consequently, it was observed in this study that the degree of dispersion of nanofiller had a greater effect on the Young's modulus than the degree of exfoliation. Dynamic mechanical results obtained through melt state rheology suggested improved exfoliation for samples prepared by $scCO_2$ aided melt blending at 3 wt% as evidenced by an increase in $\eta^*$ and a decrease in the onset of shear thinning. Similar behavior was observed

for the 7 wt% $scCO_2$ processed materials indicating increased volume fraction of organoclay which might stem from improved dispersion. Mechanical testing was carried out, and an increase in tensile modulus from 3.18 GPa to 4.61 is observed for samples prepared via the $scCO_2$ aided method with 4.9% organoclay. In addition, an enhancement in modulus of the samples processed with $scCO_2$ aided melt blending is seen up to 7.6 wt% organoclay compared to direct blending. At 7.6 wt% the modulus is observed to reach approximately 4.75 GPa which is one of the highest increases (~1.7 GPa) reported for these materials at intermediate concentrations. The largest improvements in modulus reported in this work compete with results based on twin screw compounding in the literature and composites filled with nearly twice that weight in glass fiber, but depend greatly on the matrix molecular weight, type of organoclay chosen, and the processing parameters. Continuing improvement of the $scCO_2$ method compared to the direct blending method beyond 7.6 wt% was not realized. Perhaps with the help of twin screw compounding in combination with the $scCO_2$ aided method, the properties could continue to increase beyond 10 wt% addition of organoclay. The tensile strength values were maintained compared to the virgin matrix, indicating that improved stiffness was not accompanied by decreased strength. The elongation at break values suggests interesting morphological considerations at low concentrations that need to be investigated with differential scanning calorimetry and XRD. The lack of continual increasing dispersion and properties with the $scCO_2$ processed samples at higher concentrations must also be investigated in future work.

## 3.6 Acknowledgements

The authors would like to thank Honeywell and Southern Clay Products for donating the nylon 6 and Cloisite 30B, respectively. In addition, the authors acknowledge use of the facilities

and the assistance of Steve McCartney at the Nanocscale Characterization and Fabrication Laboratory at Virginia Polytechnic Institute for the TEM images.

## References


[1] A. Usuki, Y. Kojima, M. Kawasumi, A. Okada, Y. Fukushima, T. Kurauchi, and O. Kamigaito, "SYNTHESIS OF NYLON 6-CLAY HYBRID," *Journal of Materials Research,* vol. 8, 1993.

[2] Y. Kojima, A. Usuki, M. Kawasumi, A. Okada, Y. Fukushima, T. Kurauchi, and O. Kamigaito, "MECHANICAL-PROPERTIES OF NYLON 6-CLAY HYBRID," *Journal of Materials Research,* vol. 8, 1993.

[3] S.D. Burnside and E.P. Giannelis, "Synthesis and Properties of New Poly(Dimethylsiloxane) Nanocomposites," *Chemistry of Materials,* vol. 7, 1995.

[4] J.W. Gilman, "Flammability and thermal stability studies of polymer layered-silicate (clay) nanocomposites," *Applied Clay Science,* vol. 15, 1999.

[5] T. Lan, P.D. Kaviratna, and T.J. Pinnavaia, "On the Nature of Polyimide Clay Hybrid Composites," *Chemistry of Materials,* vol. 6, 1994.

[6] R.A. Vaia, G. Price, P.N. Ruth, H.T. Nguyen, and J. Lichtenhan, "Polymer/layered silicate nanocomposites as high performance ablative materials," *Applied Clay Science,* vol. 15, 1999.

[7] M. Alexandre and P. Dubois, "Polymer-layered silicate nanocomposites: preparation, properties and uses of a new class of materials," *Materials Science & Engineering R-Reports,* vol. 28, 2000.

[8] R.A. Vaia, K.D. Jandt, E.J. Kramer, and E.P. Giannelis, "Microstructural evolution of melt intercalated polymer-organically modified layered silicates nanocomposites," *Chemistry of Materials,* vol. 8, 1996.

[9] E.P. Giannelis, "Polymer layered silicate nanocomposites," *Advanced Materials,* vol. 8, 1996.

[10] S.S. Ray and M. Okamoto, "Polymer/layered silicate nanocomposites: a review from preparation to processing," *Progress in Polymer Science,* vol. 28, 2003.

[11] C. Oriakhi, "Nano sandwiches," *Chemistry in Britain,* vol. 34, 1998.

[12] J.W. Cho and D.R. Paul, "Nylon 6 nanocomposites by melt compounding," *Polymer,* vol. 42, 2001.

[13] D.R. Paul and L.M. Robeson, "Polymer nanotechnology: Nanocomposites," *Polymer,* vol. 49, 2008.

[14] L.M. Liu, Z.N. Qi, and X.G. Zhu, "Studies on nylon 6 clay nanocomposites by melt-intercalation process," *Journal of Applied Polymer Science,* vol. 71, 1999.

[15] C. Chen, J. Samaniuk, D.G. Baird, G. Devoux, M.Q. Zhang, R.B. Moore, and J.P. Quigley, "The preparation of nano-clay/polypropylene composite materials with improved properties using supercritical carbon dioxide and a sequential mixing technique," *Polymer,* vol. 53, 2012.

[16] A. Blumstein, "Polymerization of adsorbed monolayers. II. Thermal degradation of the inserted polymer," *Journal of Polymer Science Part A: General Papers,* vol. 3, 1965.

[17] R. Krishnamoorti, R.A. Vaia, and E.P. Giannelis, "Structure and dynamics of polymer-layered silicate nanocomposites," *Chemistry of Materials,* vol. 8, 1996.

[18] T.D. Fornes and D.R. Paul, "Crystallization behavior of nylon 6 nanocomposites," *Polymer,* vol. 44, 2003.

[19] T.D. Fornes, P.J. Yoon, D.L. Hunter, H. Keskkula, and D.R. Paul, "Effect of organoclay structure on nylon 6 nanocomposite morphology and properties," *Polymer,* vol. 43, 2002.

[20] T.D. Fornes, P.J. Yoon, H. Keskkula, and D.R. Paul, "Nylon 6 nanocomposites: the effect of matrix molecular weight," *Polymer,* vol. 42, 2001.
[21] Y. Yoo, M.W. Spencer, and D.R. Paul, "Morphology and mechanical properties of glass fiber reinforced Nylon 6 nanocomposites," *Polymer,* vol. 52, 2011.
[22] P.J. Yoon, T.D. Fornes, and D.R. Paul, "Thermal expansion behavior of nylon 6 nanocomposites," *Polymer,* vol. 43, 2002.
[23] F. Chavarria, R.K. Shah, D.L. Hunter, and D.R. Paul, "Effect of melt processing conditions on the morphology and properties of nylon 6 nanocomposites," *Polymer Engineering and Science,* vol. 47, 2007.
[24] Q.T. Nguyen and D.G. Baird, "An improved technique for exfoliating and dispersing nanoclay particles into polymer matrices using supercritical carbon dioxide," *Polymer,* vol. 48, 2007.
[25] C. Chen, J. Samaniuk, D.G. Baird, G. Devoux, M. Zhang, R.B. Moore, and J.P. Quigley, "The preparation of nano-clay/polypropylene composite materials with improved properties using supercritical carbon dioxide and a sequential mixing technique," *Polymer,* vol. 53, 2012.
[26] C. Chen and D.G. Baird, "Dispersion of nano-clay at higher levels into polypropylene with carbon dioxide in the presence of maleated polypropylene," *Polymer,* vol. 53, 2012.
[27] M. Garcia Leiner and A.J. Lesser, "CO2-assisted polymer processing: A new alternative for intractable polymers," *Journal of Applied Polymer Science,* vol. 93, 2004.
[28] L. Urbanczyk, C. Calberg, F. Stassin, M. Alexandre, R. Jerome, C. Jerome, and C. Detrembleur, "Synthesis of PCL/clay masterbatches in supercritical carbon dioxide," *Polymer,* vol. 49, 2008.
[29] J. Samaniuk, D. Litchfield, and D. Baird, "Improving the Exfoliation of Layered Silicate in a Poly(ethylene terephthalate) Matrix Using Supercritical Carbon Dioxide," *Polymer Engineering and Science,* vol. 49, 2009.
[30] M. Garcia-Leiner and A.J. Lesser, "Intercalation in polymer-clay nanocomposites promoted by supercritical carbon dioxide.," *Abstracts of Papers of the American Chemical Society,* vol. 226, 2003.
[31] C.W. Manke, E. Gulari, D.F. Mielewski, and E.C.-C. Lee, "System and method of delaminating a layered silicate material by supercritical fluid treatment," U.S. Patent, 2002.
[32] D.F. Mielewski, E.C.-c. Lee, C.W. Manke, and E. Gulari, "System and method of preparing a reinforced polymer by supercritical fluid treatment," U.S. Patent 6753360, 2004.
[33] E. Gulari, K. Rangaramanujam, and G.K. Serhatkulu, "Method of delaminating aggregated particles with a coating agent in a substantially supercritical fluid," US7387749, 2008.
[34] S. Horsch, G. Serhatkulu, E. Gulari, and R.M. Kannan, "Supercritical CO2 dispersion of nano-clays and clay/polymer nanocomposites," *Polymer,* vol. 47, 2006.
[35] C. Chen, M. Bortner, J.P. Quigley, and D.G. Baird, "Using supercritical carbon dioxide in preparing carbon nanotube nanocomposite: Improved dispersion and mechanical properties," *Polymer Composites,* vol. 33, 2012.
[36] J.P. Quigley, "Advanced Thermoplastic Nanocomposite Processing Using an Improved Supercritical Carbon Dioxide Aided Melt Blending Method,"2014.

[37] X.G. Zhang and L.S. Loo, "Morphology and Mechanical Properties of a Novel Amorphous Polyamide/Nanoclay Nanocomposite," *Journal of Polymer Science Part B-Polymer Physics*, vol. 46, 2008.
[38] A.A. Gawad, A.M.K. Esawi, and A.R. Ramadan, "Structure and properties of nylon 6-clay nanocomposites: effect of temperature and reprocessing," *Journal of Materials Science*, vol. 45, 2010.
[39] A. Usuki, A. Koiwai, Y. Kojima, M. Kawasumi, A. Okada, T. Kurauchi, and O. Kamigaito, "Interaction of Nylon-6 Clay Surface and Mechanical-Properties of Nylon-6 Clay Hybrid," *Journal of Applied Polymer Science*, vol. 55, 1995.
[40] A.J. Poslinski, M.E. Ryan, R.K. Gupta, S.G. Seshadri, and F.J. Frechette, "Rheological Behavior of Filled Polymeric Systems .1. Yield Stress and Shear-Thinning Effects," *Journal of Rheology*, vol. 32, 1988.
[41] L. Xu, S. Reeder, M. Thopasridharan, J.X. Ren, D.A. Shipp, and R. Krishnamoorti, "Structure and melt rheology of polystyrene-based layered silicate nanocomposites," *Nanotechnology*, vol. 16, 2005.
[42] C. Ibanes, L. David, M. De Boissieu, R. Seguela, T. Epicier, and G. Robert, "Structure and mechanical behavior of nylon-6 fibers filled with organic and mineral nanoparticles. I. Microstructure of spun and drawn fibers," *Journal of Polymer Science Part B-Polymer Physics*, vol. 42, 2004.
[43] T.D. Fornes, P.J. Yoon, H. Keskkula, and D.R. Paul, "Nylon 6 nanocomposites: the effect of matrix molecular weight (vol 42, pg 9929, 2001)," *Polymer*, vol. 43, 2002.
[44] B. Kim, S.H. Lee, D. Lee, B. Ha, J. Park, and K. Char, "Crystallization kinetics of maleated polypropylene/clay hybrids," *Industrial & Engineering Chemistry Research*, vol. 43, 2004.

# Chapter 4. Benign Reduction of Carbon Nanotube Agglomerates Using a Supercritical Carbon Dioxide Process

John P. Quigley[1], Kevin Herrington[1], Michael Bortner[1], and Donald G. Baird[1,2]

1. Department of Chemical Engineering, Virginia Tech, Blacksburg, Virginia 24061, USA,
2. Macromolecules and Interfaces Institute, Virginia Tech, Blacksburg, Virginia 24061, USA

## Abstract

A method was developed to deagglomerate commercially available multi-walled carbon nanotube (MWCNT) bundles while maintaining the carbon nanotube aspect ratio. The process utilizes the rapid expansion of a supercritical carbon dioxide/MWCNT mixture to separate large primary carbon nanotube agglomerates. High levels of deagglomeration of Baytubes® C 150 P and Nanocyl™ NC-7000 MWCNT bundles were observed, resulting in 30 fold and 50 fold decreases in bulk density, respectively, with median agglomerate sizes < 8 μm in diameter. These results were obtained while retaining the aspect ratio of the as-received nanomaterial, irrespective of the MWCNT agglomerate morphology. It was found that the supercritical temperature and pressure of 40°C and 7.86 MPa were the optimal temperature and pressure for maximum deagglomeration without damage to the MWCNTs. Hydrodynamic models were applied to describe the effect of processing variables on the efficiency of the deagglomeration. These results suggest that combining this process with a composite processing step, such as melt compounding, will result in nanocomposites with enhanced electrical properties.

## 4.1 Background and Motivation

Multi-walled carbon nanotubes (MWCNT) have been of great interest since Iijima's report in 1991 [1]. Individual MWCNTs possess impressive electrical [2] mechanical [3, 4], and thermal [5] properties which make them ideal candidates in a variety of applications. However, most nanotubes received from industrial suppliers are produced using chemical vapor deposition synthesis resulting in large agglomerates which must be separated in order to take advantage of the useful properties of the individual nanotubes [6].

The MWCNT agglomerates are held together by Van der Waals forces and physical entanglements of carbon nanotubes which result in a characteristic agglomerate strength. The cohesive stress associated with the agglomerates may be estimated by the modified Rumpf equation (Eq. (4.1)) for isotropic fiber systems as described in Alig et al. [6, 7]:

$$\sigma_M = \frac{f * F_N}{2A_o} \tag{4.1}$$

In equation (4.1), the strength of the agglomerate, $\sigma_M$, is related to the packing density of the MWCNT bundle, $f$, the mean force for fiber pull out, $F_N$, and the particle's surface area, $A_o$. Higher packing densities lead to larger cohesive forces in the agglomerates. Longer carbon nanotubes will lead to more entangled agglomerates resulting in larger values of $F_N$. Theoretically, when an applied force matches or exceeds this value, deagglomeration may occur. One of the most significant challenges to realizing widespread application of MWCNTs is the deagglomeration of these large bundles while preserving the aspect ratio of the nanomaterial.

Maintaining the high aspect ratio of MWCNTs is essential to applications where electrical, mechanical, or thermal properties are desired in composites. The concentration of fillers in composites is relevant for electrically or thermally conductive networks and is highly

dependent on the aspect ratio of the filler. Eq. (4.2) describes the critical volume filler concentration to form a percolated network [8, 9]:

$$\varphi_p = \frac{D}{2L} \tag{4.2}$$

In equation (4.2) the length and diameter of the MWCNTs are represented by $L$ and $D$ respectively. The critical volume concentration, $\varphi_p$, is the concentration at which a large increase in thermal or electrical conductivity is observed. As the aspect ratio of the filler increases, the critical concentration decreases linearly. Composites consisting of longer carbon nanotubes are expected to reduce the required concentration of nanofiller for a given application. Any damage to the MWCNTs during processing will reduce the potential improvement in these properties. Similarly, equations which model the stiffness and strength of composites are influenced by the aspect ratio of the MWCNTs [10]. By reducing the aspect ratio of the MWCNTs, the potential for mechanical reinforcement is diminished. Therefore, it is desired to investigate a way to circumvent damage to the MWCNTs while sufficiently debundling the agglomerates.

Current deagglomeration methods can effectively disperse and distribute MWCNTs from initial bundles. However, recent literature has recognized significant shortening of the nanotubes during processing. These methods include, but are not limited to, sonication, ball milling, and high shear melt compounding [11-16]. Sonication has been known to cause damage to MWCNTs, evident in surface observations of the nanotubes and from aspect ratio calculations using scanning electron microscopy (SEM). [11, 12]. In special cases, suitable solvents have been shown to disperse MWCNTs with light sonication and minimal damage to the carbon nanotubes. However, few of these systems have practical application on a large scale, due to environmentally hazardous solvents, costly removal of said solvents, and reaggregation issues during drying [17]. Ball milling was used by Menzer et al. [13] to shorten carbon nanotubes,

reducing the potential entanglements in the agglomerate. In their work, Nanocyl™ NC-7000 MWCNT aggregates were disintegrated by dry ball milling, and the median MWCNT lengths were observed to decrease by 50% of their initial value. Although smaller agglomerates were formed in this process, they were found to be more tightly packed than the initial agglomerates, resulting in higher electrical percolation thresholds compared to as-received Nanocyl™ nanocomposites. In a separate work by Krause et al. [17], Nanocyl™ NC-7000 MWCNTs were melt compounded using a twin screw extruder to mix a polycarbonate matrix with the nanomaterial by master batch dilution. The authors reported that the MWCNTs were shortened to 68% of their initial lengths. In similar work, Socher et al. [11] used a conical co-rotating batch mixer to disperse Baytubes® C150P MWCNTs into a high viscosity polycarbonate, reporting a 55 % reduction in length according to the median values. Although more gentle mixing methods have been shown to cause less damage to the MWCNTs, they are often accompanied by poor dispersion of the agglomerates.

In order to better understand and overcome the issue of damage to MWCNTs during nanotube bundle disintegration, we investigate the key deagglomeration mechanisms. The principal mechanisms which occur during the deagglomeration of MWCNT agglomerates are 1) the wetting of the bundle surface by the dispersing media, 2) infiltration into the agglomerate structure by the media, and 3) dispersion through erosion and rupture of the agglomerate [18]. As the fluid comes in contact with the agglomerate, wetting of the bundle surface occurs. Wetting is further defined as the point at which the contact angle between the fluid and the agglomerate surface reaches zero. This is a function of the surface tension of the fluid, and the difference in the interfacial energy between the media and the MWCNTs [19]. Following wetting of the bundle surface, the dispersing media may infiltrate the agglomerates, which are estimated as porous structures. The viscosity of the fluid, packing density of the agglomerate, and other

variables are of importance to determine the depth of infiltration the fluid attains. If the agglomerate is fully infiltrated, then the strength of the agglomerate is reduced significantly [20]. Following wetting and infiltration, the agglomerates are broken up by rupture and erosion mechanisms. Rupture is defined as a process characterized by the catastrophic splitting of an agglomerate into smaller fragments when the cohesive strength of the agglomerate is overcome by an external stress [21]. This may occur on rapid timescales, which presents benefits for scale up, such as in the mass production of nanocomposites. Erosion is described by the removal of fragments from the outside of the agglomerate, usually consisting of smaller agglomerates. This requires less external stress than rupture, but longer timescales [22].

It has been reported that rupture of the dry agglomerate core results in damage to the MWCNTs. An external stress may exceed the strength of an individual nanotube at an entanglement site, breaking the nanotubes at a surface defect where the properties have diminished [23]. Therefore, the wetting and infiltration of the internal surface of the agglomerate are paramount to retaining the aspect ratio of the MWCNTs. If the agglomerates may be sufficiently infiltrated, benign dispersion mechanisms may dominate where lower input energies are required to deagglomerate the nanomaterial.

Supercritical fluids have the potential to rapidly wet and infiltrate the internal surface of the MWCNT agglomerate. The gas-like diffusivity and viscosity of the supercritical fluid permit rapid penetration into the porous agglomerate core, significantly reducing the agglomerate strength [24]. These aspects make supercritical fluids a desirable choice for deagglomerating MWNCT aggregates without reducing the aspect ratio of the nanomaterial. In particular, supercritical carbon dioxide ($scCO_2$) is a promising candidate for this application due to its benign nature, relatively low supercritical point, abundance, and recoverability [25]. Following

the infiltration and dispersion with $scCO_2$, a process must be chosen to provide adequate stresses to disintegrate the MWCNT agglomerate.

The rapid expansion of supercritical solutions (RESS) is a processing technique which has been utilized to produce small particles from large primary agglomerates for some time, and has recently been adapted for supercritical suspensions [26-28]. In this technique, a supercritical suspension is held at high pressure in a primary vessel for a given soak period. Following the soak period, the suspension is rapidly depressurized through a nozzle to either vacuum or atmospheric pressure, depending on the apparatus. During the rapid expansion, two principal mechanisms contribute to the forces to induce particle break-up. First, high shear stresses occur during the rapid flow of the suspension from the primary vessel through a capillary, followed by flow through a small nozzle. Second, the suspension passes into a secondary vessel during which a freely expanding jet forms. In this freely expanding jet, the suspension is accelerated from the conditions in the soak chamber to a supersonic-subsonic flow transition known as the Mach disc. As the suspension impacts the Mach disc, the sudden pressure change results in high shear stresses leading to deagglomeration [26, 27, 29]. This method of deagglomeration requires no solvent or downstream processing, and scales well with current methods. The RESS process has been described in depth elsewhere by To et al. [27] for the deagglomeration of titania and alumina nanopowders in supercritical suspensions.

The rapid expansion of supercritical carbon dioxide and MWCNT bundles has been cited briefly in the literature as a method to deagglomerate MWCNTS. Gulari et al. [30] obtained a patent in 2008 for the processing of nanotubes with $scCO_2$. However, few details were provided as to the mechanism or methodology to accomplish this deagglomeration. Jung et. al.[31] reported reduced damage to nanotubes by $scCO_2$ treatment before sonication. However, the

supercritical $CO_2$and MWCNT mixture was not released into a secondary vessel in this work, sidestepping the deagglomeration from the shear effects induced by rapid flow. The authors address the issue of damage to the MWCNTs by Raman spectroscopy, suggesting the $scCO_2$ processing resulted in less damage to the MWCNTs during sonication. To et. al.[32] conducted a brief study using the RESS process to deagglomerate MWCNT agglomerates. However, they did not investigate the effect of the $scCO_2$ process on the aspect ratio of the MWCNTs nor the effect of the processing variables on the extent of deagglomeration. Recent work by Chen et. al. [33] applied a previously developed $scCO_2$ process to disrupting MWCNT bundles, similar to the RESS process described earlier. In their work, an initial improvement of the $scCO_2$ process was conducted, resulting in a an approximately 6 fold decrease in the bulk density of Nanocyl$^{TM}$ - NC7000 MWCNT agglomerates suggesting substantial deagglomeration of the nanotube aggregates. Limited analysis was performed on the system to investigate processing conditions on the efficiency of the deagglomeration. In addition, it was suggested that the nanotubes were not damaged by surface analysis of the MWCNTs using SEM, although the aspect ratio of the MWCNTs was not measured to ensure shortening did not occur.

The current work attempts to improve the deagglomeration of MWCNT agglomerates by refining the processing of MWCNTs described in Chen et. al. [33]. It is suspected that due to the complex morphology of MWCNT agglomerates, more intensive $scCO_2$ processing might lead to further disentanglement of the primary bundles. Therefore, the maximum extent of deagglomeration obtainable using the current apparatus is investigated to divulge the tunability of the current method. The $scCO_2$ processing of MWCNT agglomerates has been suggested to be more benign than other deagglomeration methods. To further investigate this, the aspect ratios of the MWCNTs are determined using transmission electron microscopy (TEM) to inspect if the MWCNT are damaged by $scCO_2$ processing. Finally the processing variables of temperature,

pressure, soak time, and ratio of MWCNTs to $scCO_2$ are investigated to determine their effect on the deagglomeration efficiency.

## 4.2 Experimental Materials and Methodology

### 4.2.1 Materials

Multi-walled carbon nanotubes from two suppliers were investigated to determine the effect of the $scCO_2$ processing technique on different MWCNT bundle morphologies. The CNT used were Baytubes® C 150 P MWCNTs from Bayer MaterialScience (Leverkusen, Germany) and NC-7000 MWCNT from Nanocyl™ (Sambreville, Belgium). The CNT are generated through fixed bed chemical vapor deposition (CVD) synthesis and were used as-received from the suppliers.

The two types of MWCNTs used in this study possess significantly different morphologies in their as-received states. Scanning electron micrograph (SEM) images portraying the morphologies of the initial bundles as received from their respective suppliers are shown in Figure 4.1, reproduced from Krause et al. [34] with permission. A number of properties referred to in the discussions of this paper are shown in Table 4.1.

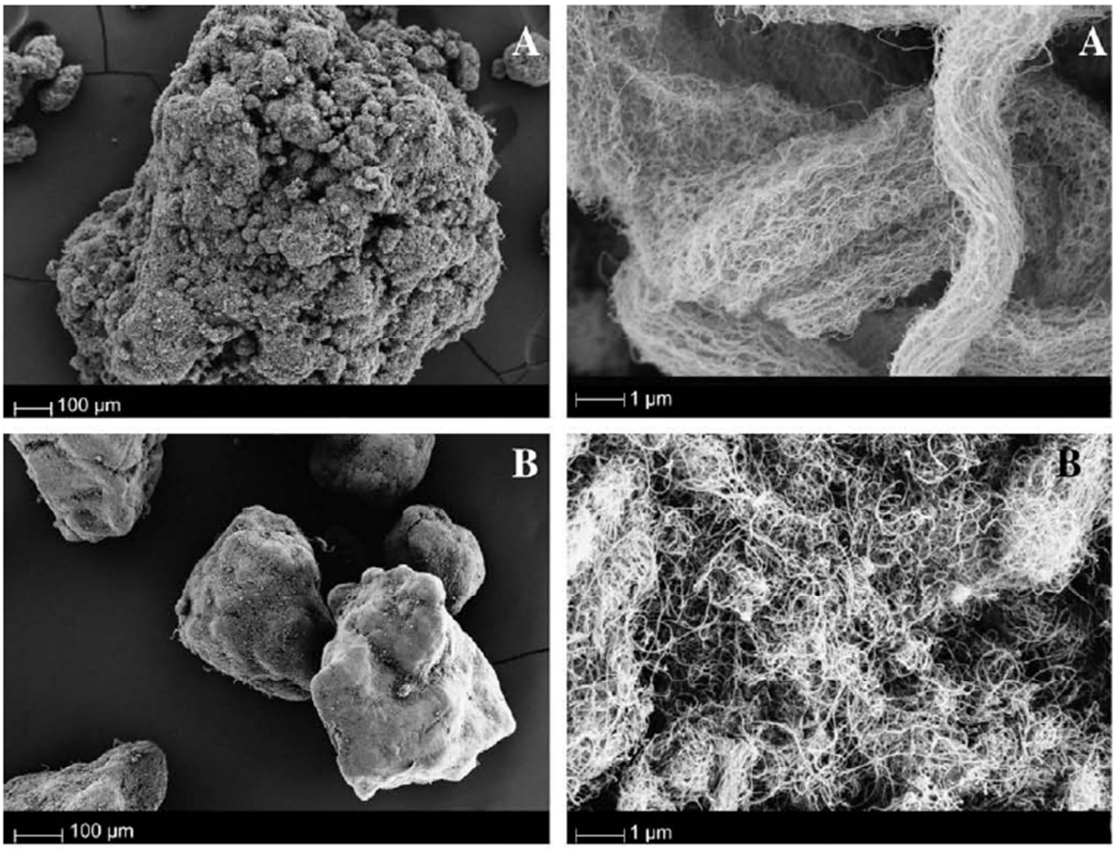


Figure 4.1. Scanning Electron Micrographs (SEM) indicating different morphologies of two types of MWCNT agglomerates. Nanocyl™ NC 7000 (A) and Baytubes® C 150P (B) agglomerates at lower (left) and higher (right) magnifications. Reproduced with permission from Carbon

Table 4.1. Select properties of as-received MWCNT bundles reported from various literature sources

| | **Nanocyl™ NC 7000** | **Baytubes® C 150 P** |
|---|---|---|
| **Diameter** | 9.5 nm [35] | 5-20 nm [36]<br>13-16 nm [37] |
| **Length** | 1.5 µm [35]<br>1.34 µm [17] | 1 – 10 µm [37]<br>0.77 µm [11] |
| **Bulk density (EN DIN 60)** | 66 kg/m$^3$[35] | 120 – 170 kg/m$^3$[36] |
| **Agglomerate size** | >674 µm [34] | 0.1  1 mm [36]<br>314 µm [34] |

The Baytubes® C 150 P aggregates are present as highly entangled bundles, referred to as a "bird's nest" by Alig et al. [6]. This morphology is illustrated in (B) of Figure 4.1. The bulk density of these aggregates is reported to be between 120-170 kg/m$^3$ and suggests these aggregates possess a high packing density, a relationship which has been reported by others [36]. The typical Baytubes® MWCNT agglomerate size, as defined by a circle equivalent diameter, has been reported on the order of 300 microns [34]. The typical Baytubes® MWCNT diameter is around 10 nm. The supplier suggests that individual Baytubes® MWCNTs possess an average length greater than 1 μm [37], but more recent findings suggest they have a median length on the order of 700 nm. The Nanocyl™ NC7000 MWCNTs are bundled in a "combed yarn" like structure, which is more loosely packed than the Baytubes® structure, possessing a bulk density of ~60 kg/ m$^3$ [6, 35]. This morphology is illustrated in (A) of Figure 4.1. A recent study has suggested that the agglomerates are much larger than those of the Baytubes® MWCNTs, with an equivalent diameter >674 μm [34]. The typical Nanocyl™ MWCNTs have reported diameters of about 10 nm, with lengths of around 1.3 μm as reported by Krause et al. [17].

### 4.2.2 Methodology

#### 4.2.2.1 Supercritical $CO_2$ Processing

The MWCNTs were introduced to sc$CO_2$ in a pressurized chamber at varying conditions to understand the effect of processing variables on the supercritical carbon dioxide deagglomeration of MWCNT bundles. The apparatus utilized to accomplish this is illustrated in

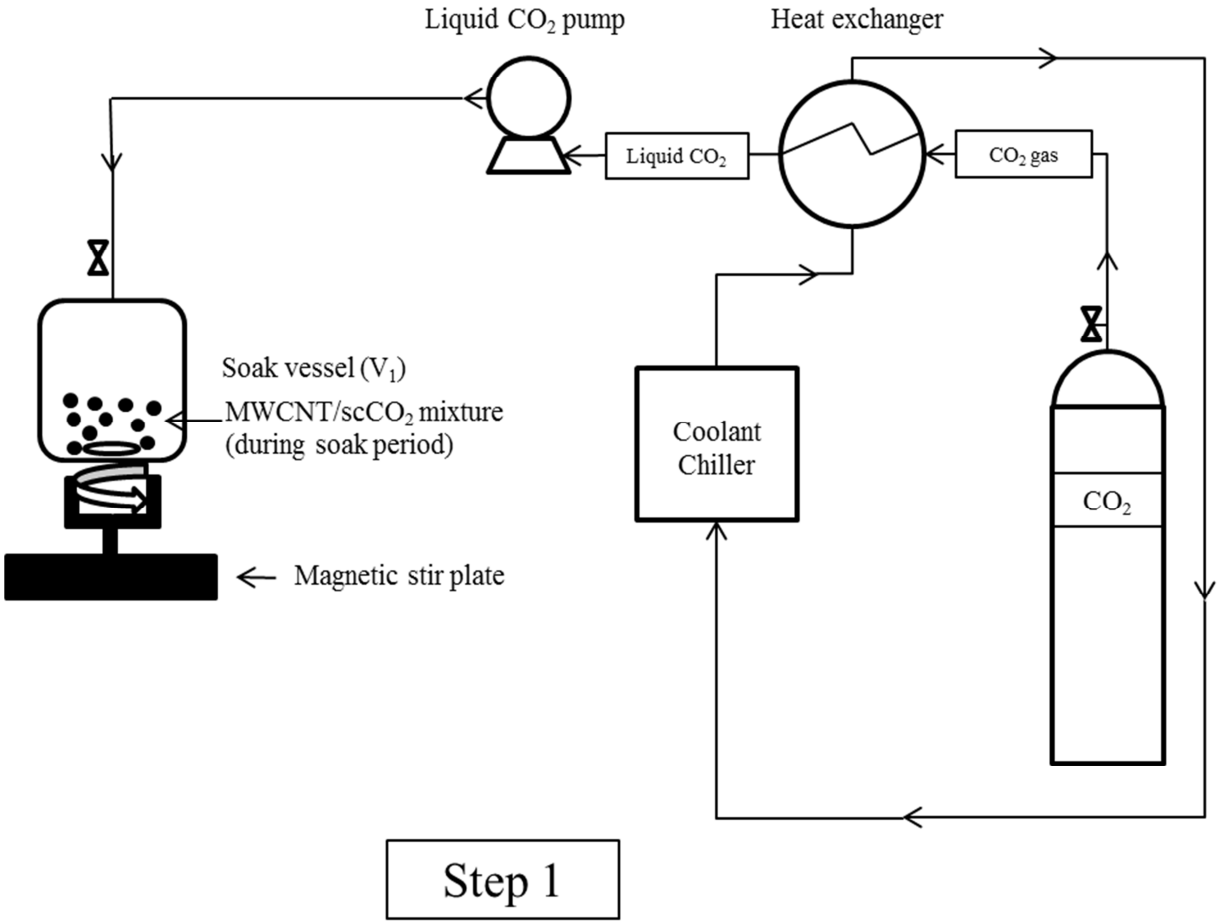
Liquid $CO_2$ pump
Heat exchanger
Liquid $CO_2$
$CO_2$ gas
Soak vessel ($V_1$)
MWCNT/sc$CO_2$ mixture
(during soak period)
Coolant
Chiller
$CO_2$
Magnetic stir plate
Step 1

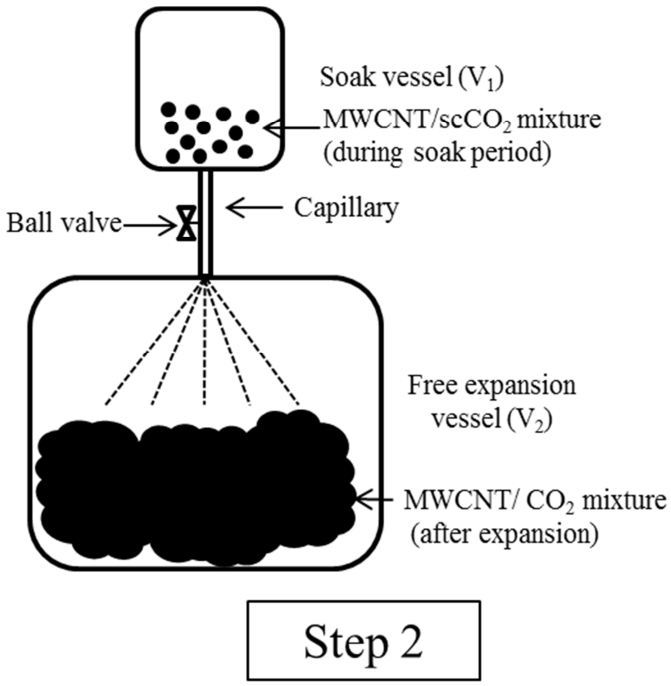


Figure 4.2. Schematic illustration of scCO$_2$ processing apparatus

The primary soak pressure vessel (Parr Instrument Company, Moline, IL) possesses a 300 ml capacity and a maximum operating pressure of 4000 psi. The mixture was held at the processing temperature and pressure for a designated period to ensure maximum infiltration of the initial bundles with supercritical fluid. The mixture was agitated by way of a stir bar driven by a magnetic hot plate. The MWCNT / scCO$_2$ mixture was then released into a 5 gallon (18.9 liter) secondary pressure vessel using rapid depressurization to achieve primary bundle deagglomeration [33]. A capillary (6.35 mm diameter, 200 mm length) was chosen to connect the soak and secondary vessels. Agitation was not utilized in the secondary vessel. Insulating tape was utilized on the connection to reduce the formation of dry ice in the capillary during the expansion. The processed CNTs were then collected from the secondary pressure vessel.

#### 4.2.2.2 Bulk density measurements

A rapid, simple procedure comparing bulk density measurements was utilized to study the degree of deagglomeration for different scCO$_2$ processing variables. The bulk density of

MWCNT agglomerates has been related to the dispersability of MWCNTs in the literature, where agglomerates with lower bulk densities were more dispersible in both polymers and solutions due to a larger contact surface area and greater volume occupied by an agglomerate [13, 38]. Therefore this measurement is considered relevant to relate $scCO_2$ processing to the MWCNT bundle properties. Bulk density measurements were conducted according to EN DIN 60 using a funnel and graduated cylinder before and after CNT processing. To ensure repeatability, at least three iterations of volume and weight measurement were conducted for each experiment. Each processing step was replicated three times, resulting in a total of nine bulk densities per data point. Degree of expansion, which will be referred to throughout the manuscript, refers to the factor by which the original bulk density of MWCNTs is reduced after $scCO_2$ processing. For example, a 15 fold (15X) degree of expansion describes a reduction in bulk density from 150 $kg/m^3$ to 10 $kg/m^3$for the Baytubes® MWCNT after $scCO_2$ processing. Samples are referred to as as-received and $scCO_2$ processed with a modifier (10X, 50X, etc.) for their reported degree of expansion.

#### 4.2.2.3 3D Optical Microscopy

Three dimensional reflective optical microscopy was utilized to determine the MWCNT agglomerate sizes before and after $scCO_2$ processing, and to verify that the degree of expansion convention was a suitable means for describing bundle deagglomeration. 1 mg of dry MWCNT agglomerates was dispersed on a 3 X 3 cm section of clear double sided tape to obtain individual bundles across each image. A Hirox KH-7700 microscope in combination with a multi-focal synthesis was employed to account for the 3D nature of the agglomerates at a magnification of 280X and 140X. Mixed magnifications were sometimes required to capture very large agglomerates. A band pass filter was applied to the resulting images using ImageJ software and the agglomerate diameters were calculated assuming a circle equivalent. At least 300

agglomerates were analyzed per sample to generate a representative distribution. Agglomerates with equivalent diameters less than 2.5 microns were ignored due to the resolution of the instrument. The authors recognize that this imaging technique may ignore small agglomerates at 240x magnification. However, higher magnifications were surveyed and a negligible number of agglomerates were observed.

#### 4.2.2.4 MWCNT Length Measurements

The length distributions of the MWCNTs were measured to investigate the damage to MWCNT lengths from $scCO_2$ processing using a slightly modified method from that described by Krause et al. [24]. Using this approach, 1 mg of CNTs was weighed into a vial and 10 ml of chloroform were added to produce suspensions at 0.1 g/l. The suspension was then sonicated for 5 minutes in a VWR B2500A ultrasonic cleaner with an operating frequency of 42 kHz and an output power of 85W. The short sonication times utilized in this method are believed to minimize the damage to the MWCNTs during deagglomeration [24]. The resulting suspension was dropped onto a carbon coated grid for TEM analysis. TEM measurements were generated utilizing a Philips EM420T microscope with an accelerating voltage of 80 kV. One hundred nanotubes were analyzed for length and diameter to obtain aspect ratio distributions. For length determination, fifteen regions of nanotubes were surveyed, and images were collected at magnifications of 17,000 x, 7,500 x, and 4,500 x to ensure any large nanotubes could be tracked off screen. Gatan Digital Micrograph image analysis software was employed to measure nanotube lengths. A Mann-Whitney-U statistical test with a 95% confidence interval was utilized to determine the validity of any length comparisons between the as-received and $scCO_2$ processed MWCNT.

#### 4.2.2.5 Thermodynamic Considerations

The effect of varying temperatures and pressures during the $scCO_2$ processing of MWCNTs was investigated. A method of carrying out experiments along lines of constant carbon dioxide density (isochors) was conceived. The ancillary processing variables were held constant while temperature and pressure were systematically varied, as illustrated in Figure 4.3.

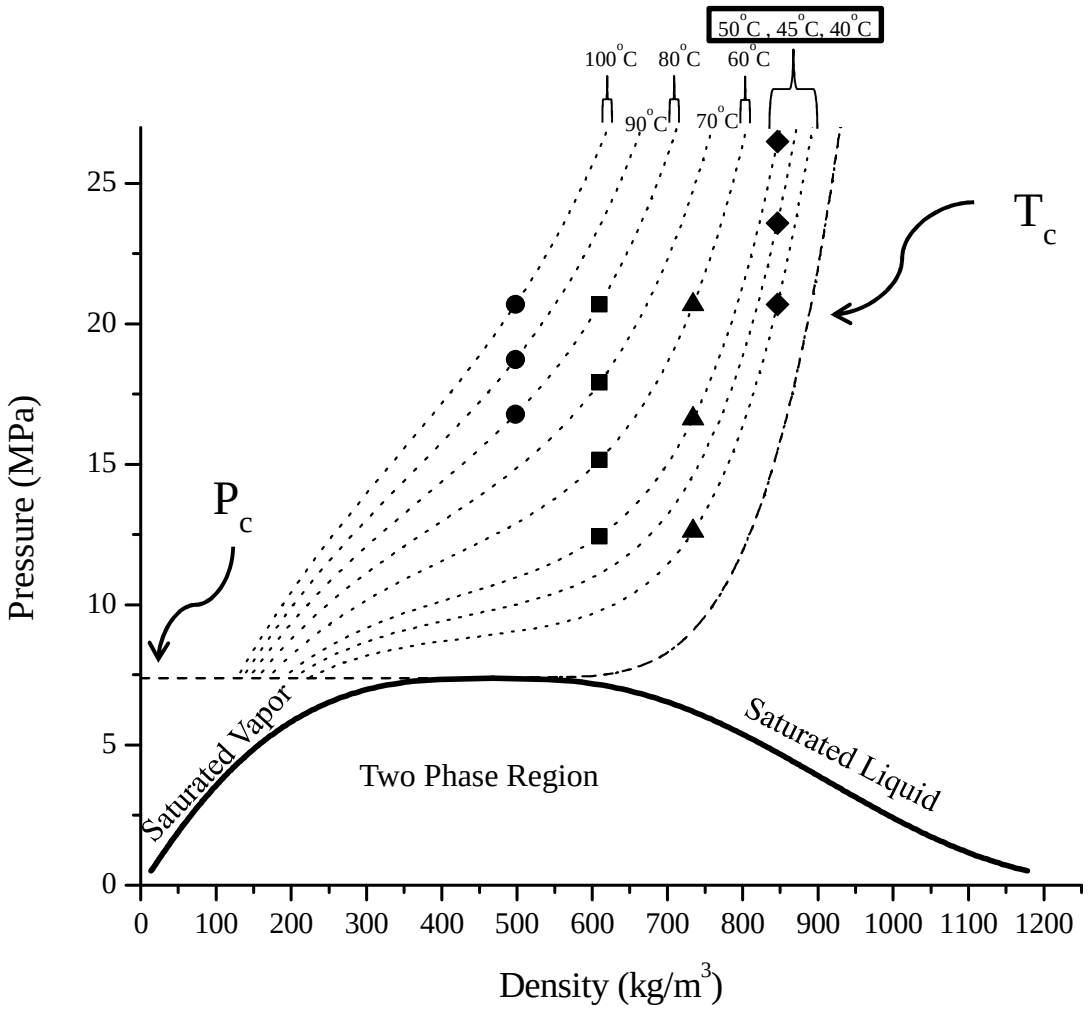


Figure 4.3. Phase diagram of $scCO_2$ using data obtained from NIST webbook [39] presented as pressure (MPa) versus density (kg/m$^3$). Experiments were carried out at constant densities of ~500 kg/m$^3$ (-●-), ~600 kg/m$^3$(-■-), ~730 kg/m$^3$ (-▲-), and ~850 kg/m$^3$(-♦-). Isotherms, phase boundaries, and critical temperature and pressure are labeled to illustrate

Experiments were conducted at intersections of isochors with isotherms of interest. $scCO_2$ processing trials were conducted at isochors of ~500 kg/m$^3$, ~610 kg/m$^3$, ~730 kg/m$^3$, and ~850 kg/m$^3$ using the Baytubes® MWCNTs. The corresponding isotherms are outlined in Figure 4.3. Bulk density measurements were carried out (as described in Section 4.2.2.2) to determine the

effect of the thermodynamic properties of $scCO_2$ on the deagglomeration of primary CNT bundles during processing.

#### 4.2.2.6 Additional processing considerations

Additional processing conditions are considered during the $scCO_2$processing of MWCNTs. The ratio of MWCNTs to $scCO_2$ during processing was studied to determine its effect on the degree of expansion. Different CNT amounts in the primary vessel were investigated to divulge the origin of this effect. Values of 0.1, 0.4, 2.3 and 7.6 MWCNT per 100 g of $scCO_2$ were tested. A scale was utilized to weigh the pressure vessel before and after pressurization to verify these conditions.

The length of the soak period before rapid depressurization was found to affect the degree of deagglomeration. Therefore, the soak time was varied to determine the effect of the soak time on the deagglomeration of MWCNT bundles. Experiments were carried out at intervals of 24 hours, 30 minutes, 15 minutes and 1 minute in order to probe the time dependence of $scCO_2$ infiltration to the primary MWCNT agglomerates.

## 4.3 Results and Discussion

The results and discussion of this manuscript are presented to convey the steps towards understanding and improving the deagglomeration of MWCNT bundles with the aid of $scCO_2$. First, an attempt was made to deagglomerate the MWCNT bundles to the greatest extent using the current apparatus with $scCO_2$ processing for both Baytubes® and Nanocyl™ morphologies. Next, the integrity of individual MWCNTs was investigated using TEM to ensure that the $scCO_2$ treatment did not damage the aspect ratio of the nanomaterial. Finally, processing variables such as temperature, pressure, and other relevant parameters were examined to divulge the mechanism of $scCO_2$ processing on the MWCNT bundles.

### 4.3.1 MWCNT Bundle Deagglomeration

It was desired to obtain the most thorough deagglomeration of primary MWCNT bundles using $scCO_2$ processing for both Baytubes® and Nanocyl™ MWCNTs using the current apparatus. Consecutive $scCO_2$ processing steps (passes) at low weight ratios of MWCNTs (< 1 g MWCNT per 100 g $scCO_2$) were carried out to accomplish this. The low ratio of MWCNTs to $scCO_2$ was employed to ensure maximum infiltration of the bundles by supercritical carbon dioxide. Photographs of the MWCNTs before and after $scCO_2$ processing are presented in Figure 4.4. A previous treatment carried out by Chen et al. [40] is included for comparison.

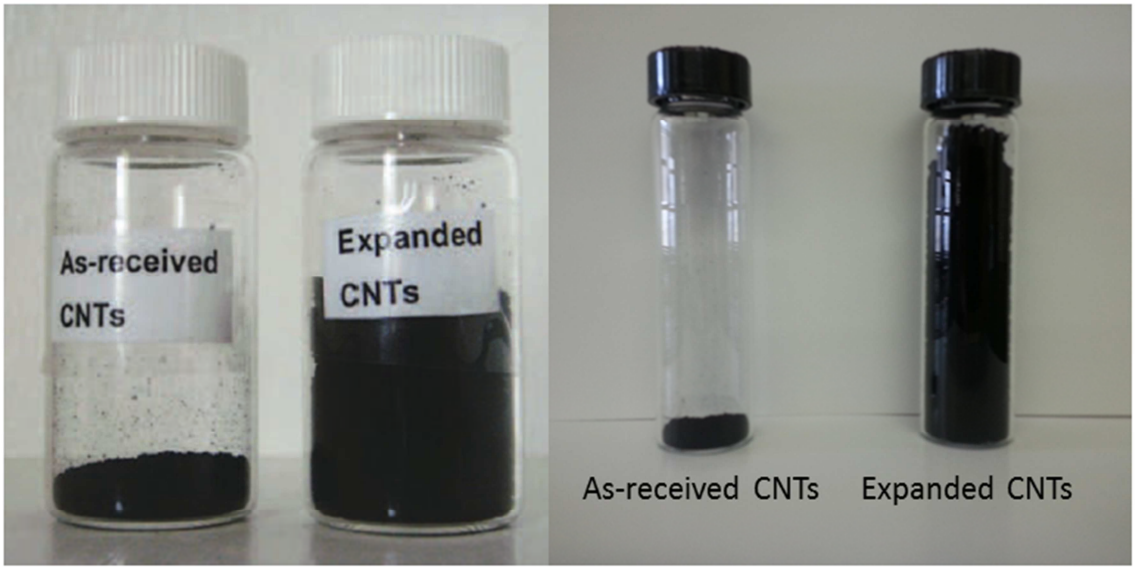



Figure 4.4. 0.1 grams of Nanocyl™ NC 7000 (top) and Baytubes® C 150 P (bottom) MWCNTs at different degrees of deagglomeration. Top left shows Chen's initial optimization of Nanocyl™ MWCNTs [33]. Top right shows the deagglomeration of Nancoyl MWCNTs at an expansion factor of 50X. Bottom (from left to right) displays no scCO2 treatment and a 30X expansion

The bulk density of the as-received Nanocyl™ MWCNT was 50 kg/m$^3$, which is slightly lower than the reported value of 66 kg/m$^3$ from the Nanocyl™ data sheet and reported in Table 4.1 [35]. Multiple passes of the Nanocyl™ MWCNTs using the supercritical carbon dioxide processing led to a final bulk density of 1 kg/m$^3$, a 50X degree of expansion considering the initial bulk density of 50 kg/m$^3$. The initial optimization of this process by Chen et al. [33] suggested a 6X degree of expansion was the "optimal" degree of MWCNT disentanglement obtainable by $scCO_2$ processing. These results suggest that the processing variables utilized in Chen's initial work may be further improved for the deagglomeration of initial MWCNT agglomerates. The as-received Baytubes® MWCNTs were found to possess a bulk density of 150 kg/m$^3$ which is in good agreement with values reported in the supplier's data sheet(Table 4.1) [36]. The Baytubes® MWCNTs were also subjected to multiple processing steps using $scCO_2$ resulting in a maximum degree of expansion of 30X from an intial bulk density of 150 kg/m$^3$ to a final bulk density of 5 kg/m$^3$ after two processing steps. The low bulk densities obtained for the MWCNTs at the maximum degrees of expansion suggest these agglomerates are more dispersible than the as-received samples. Menzer et al. [14] have reported that MWCNT agglomerates possessing lower bulk densities and "fluffier" characteristics led to lower percolation thresholds in melt compounded polymer nanocomposites due to the larger contact area for MWCNTs to interact with the polymer matrix.

Image analysis of the Baytubes® and Nanocyl™ MWCNTs was carried out to quantify the equivalent agglomerate diameters of the as–received and $scCO_2$ processed MWCNTs as described in Section 4.2.2.3. Representative optical images are shown for the samples in Figure 4.5. Cumulative distribution plots were also generated from the equivalent diameters and are shown in Figure 4.6 on a log normal plot. The results are summarized in Table 4.2. Significant

reduction in particle size was observed due to the $scCO_2$ processing for Nanocyl™ and Baytubes® MWCNT agglomerates.

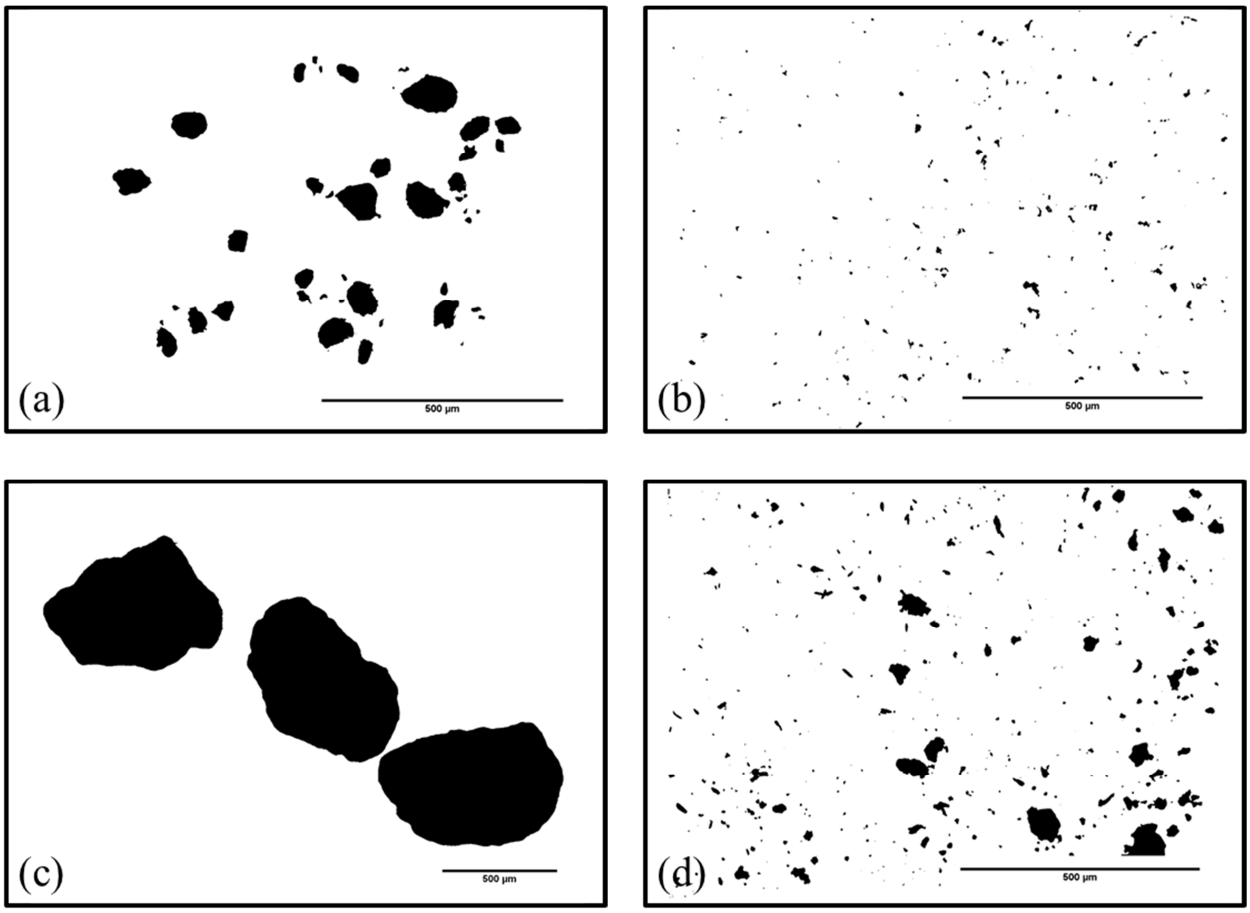


Figure 4.5. 3D optical micrographs of MWCNTs agglomerates before and after $scCO_2$ treatment. Images were taken at 140x magnficaition (c) and 280x magnfication (a),(b),(d). Representative images of as received Nanocyl™ NC 7000 (a), 50X Nanocyl™ NC 7000 (b), as received Baytubes® C150P (c) and 30X Baytubes® C150P (d) are presented

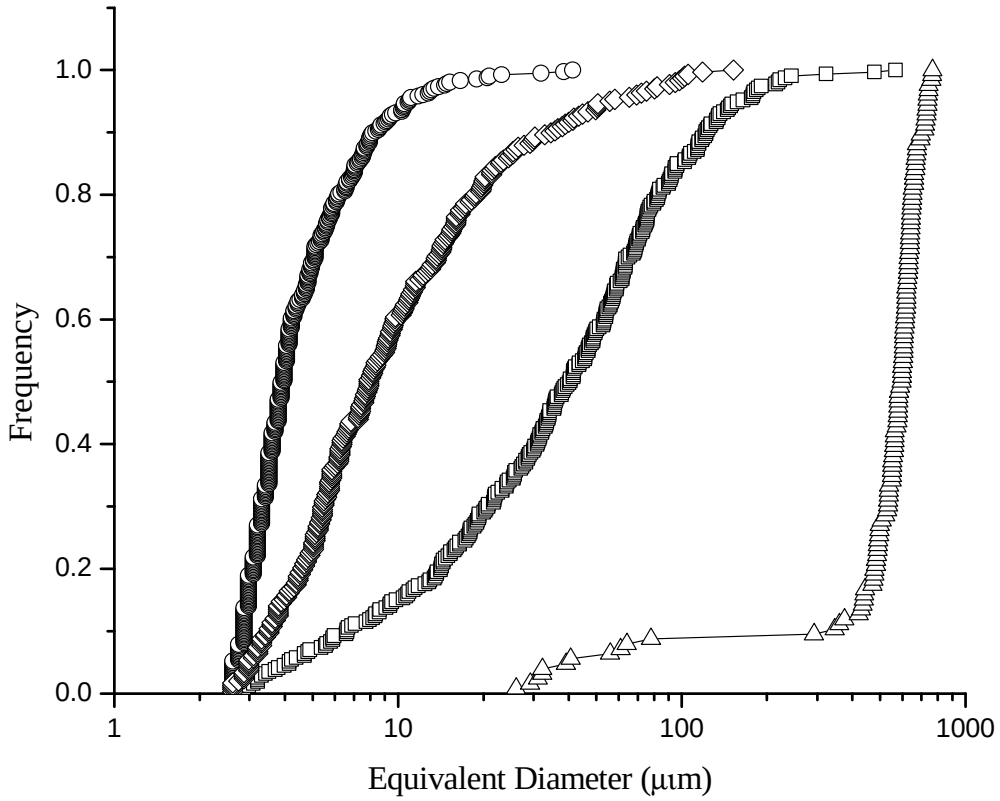


Figure 4.6. Cumulative distribution function of MWCNT agglomerate sizes before and after $scCO_2$ treatment. Equivalent diameter distributions of as received Baytubes® (-Δ-), as received Nanocyl™ (-□-), 30X Baytubes® (-◊-) and 50X Nanocyl™ (-○-) CNT agglomerates are shown

Table 4.2. Median equivalent diameter values for as-received and $scCO_2$ processed Nanocyl™ NC 7000 and Baytubes® C 150 P CNT agglomerates

| Sample | Median Equivaleant Diameter (μm) |
|---|---|
| Nanocyl As-received | 40.5 |
| Nanocyl 50X | 4.0 |
| Baytube As-received | 596.7 |
| Baytube 30X | 7.9 |

Primary Nanocyl™ MWCNT agglomerates possess a median equivalent diameter of 40.5 μm. This value is significantly smaller than values observed by Krause et al. [34], where the median agglomerate size was measured to be >675 μm with laser diffraction. Although our observations are in poor agreement with their study, we suspect that optical microscopy provides more reliable results than laser diffraction. During laser diffraction, agitation is required during sample analysis, which might induce agglomerate break-up, whereas the optical imaging does not. As illustrated in Figure 4.5, all of the Nanocyl™ agglomerates shown are significantly smaller than the 500 μm scale. Furthermore, Figure 4.6 indicates that the largest of the observed Nanocyl™ MWCNT bundles does not exceed 500 μm of over 300 agglomerates sampled. The agglomerate diameters of the as-received Nanocyl™ MWCNTs are reduced significantly with multiple $scCO_2$ processing steps, as suggested by the 50X degree of expansion. The median agglomerate size of the Nanocyl™ MWCNT bundles after three passes through the $scCO_2$ process is 4 μm in diameter, which is shown in Table 4.2, with the largest agglomerate having a diameter less than 30 μm. During the first pass, a fraction of the CNT bundles was deagglomerated, resulting in an expansion of 15X. In order for the most complete deagglomeration to be observed, however, two more passes were required, resulting in an expansion of 50X. (Figure 4.5. (b)). The ISO 18553 standard for the dispersion of fillers in a polymer dictates that agglomerates with diameters smaller than 5 μm are to be neglected and regarded as “dispersed” [41]. Therefore, it is suggested that the over half of the Nanocyl™ MWCNT bundles may be dispersed.

The as-received Baytubes® MWCNT agglomerates were analyzed for their bundle diameter distribution. The Baytubes® MWCNT agglomerates were significantly larger than the Nanocyl™ MWCNT bundles, requiring a lower magnification (140X) to record the agglomerate sizes, observed in the scale of Figure 4.5 (c). The median agglomerate size was determined to be 596.7 μm in diameter, which is reported in Table 4.2. This is larger than previously reported values of 314 microns from the laser diffraction results of Krause et al. [34] and approximately 400 μm reported in Salzano et al. [42], yet is within the range suggested by the supplier (100 μm – 1000 μm) [36]. In contrast to the other samples studied in this analysis, the distribution of aggregate sizes is relatively narrow with no observed particles greater than 800 μm in equivalent diameter, as seen in Figure 4.6. The Baytubes® MWCNT agglomerates were reduced in size significantly upon multiple $scCO_2$ processing steps, as can be seen from Figure 4.5, Figure 4.6, and Table 4.2. The Baytubes® 30X material exhibits diameters on the order of 8 μm, nearly two orders of magnitude smaller than the initial bundles after two passes of the $scCO_2$ process. The particle size distribution is rather broad compared to the other samples surveyed, with the largest aggregates on the order of 100 μm which is illustrated in Figure 4.6. The distribution of sizes may be accounted for by the agglomerates possessing very high cohesive energies that the forces from the rapid expansion are unable to overcome, as indicated by the high packing density [18].

The initial bundle morphologies of the MWCNTs affected the maximum degree of deagglomeration for the aggregates. Following extensive $scCO_2$ processing, the Baytubes® 30X expanded MWCNT agglomerates are approximately two times larger in equivalent diameter than the Nanocyl™ 50X agglomerates. The larger, more tightly packed initial Baytubes® agglomerates result in larger agglomerates after $scCO_2$ processing, and require less processing to reach their maximum deagglomeration. A third processing step was observed to further deagglomerate the Nanocyl™ MWCNT agglomerates, but the Baytubes® bundles are unaffected

with additional $scCO_2$ processing steps. These results corroborate other studies where the ability to disperse Nanocyl™ in both solvents and polymers was compared to the dispersability of Baytubes® MWCNTs, and Nanocyl™ MWCNTs were easier to disperse [34, 43]. These results further support that the initial Baytubes® bundles are comprised of small, densely entangled agglomerates which may not be separable via the methods discussed here. This is apparent upon inspection of Figure 4.5 (b) and (d). Furthermore, it would be of interest to further investigate the morphology of the bundles reduced by $scCO_2$ processing in future work. If the hydrodynamic forces on these bundles may be effectively estimated during the $scCO_2$ processing, the cohesive force of the small agglomerates could be inferred. With this knowledge, appropriate stresses may be induced to minimize breakage of the smaller MWCNT bundles while fully dispersing the nanomaterial.

### 4.3.2 MWCNT Length Measurements

Maintaining the aspect ratio of MWCNTs is important in applications of the nanomaterial [31, 33]. Therefore, diameters and lengths of the carbon nanotubes were measured to investigate the degree of damage experienced by the MWCNTs after $scCO_2$ processing. A procedure previously developed by Krause et al. [17] was utilized, which is described in Section 4.2.2.4. One hundred nanotube lengths and diameters were analyzed to compare the as-received and $scCO_2$processed samples described in Section 4.3.1. The diameters and lengths of the Nanocyl™ MWCNTs are compared to existing literature values and the MWCNT length distributions after $scCO_2$ processing are contrasted to those corresponding to other deagglomeration methods. The same procedure is carried out for Baytubes® MWCNTs. Finally, some closing remarks are made as to the benign nature of the $scCO_2$ processing of MWCNTs.

The diameters of discrete Nanocyl$^{TM}$ MWCNTs were measured and related to previous literature values to divulge any damage to the CNT during processing. The median diameters of the Nanocyl$^{TM}$ CNT were found to be 9.4 ± 2.2 nm for the as-received sample and 9.7 ± 2.0 nm for the 50X sample. These values resemble those given by the supplier for the diameters of the Nanocyl$^{TM}$ MWCNTs of 9.5 nm [35]. Statistical analysis of the data verified no change in the diameters due to $scCO_2$ processing. Castillo et al. [43] report a median diameter of 10.0 nm in a population of several hundred MWCNT diameter measurements, which is within the standard deviations reported in the current work.

The as-received Nanocyl$^{TM}$ MWCNT lengths were measured to determine any degree of length reduction in the MWCNTs following the maximum deagglomeration. The as-received and $scCO_2$ processed distributions of Nanocyl$^{TM}$ MWCNT lengths are presented as a histogram in Figure 4.7 (a). The inset table shows the characteristic values $x_{10}$, $x_{50}$, and $x_{90}$, which designate that 10%, 50%, and 90% of the population are shorter than the corresponding value in the table, respectively.

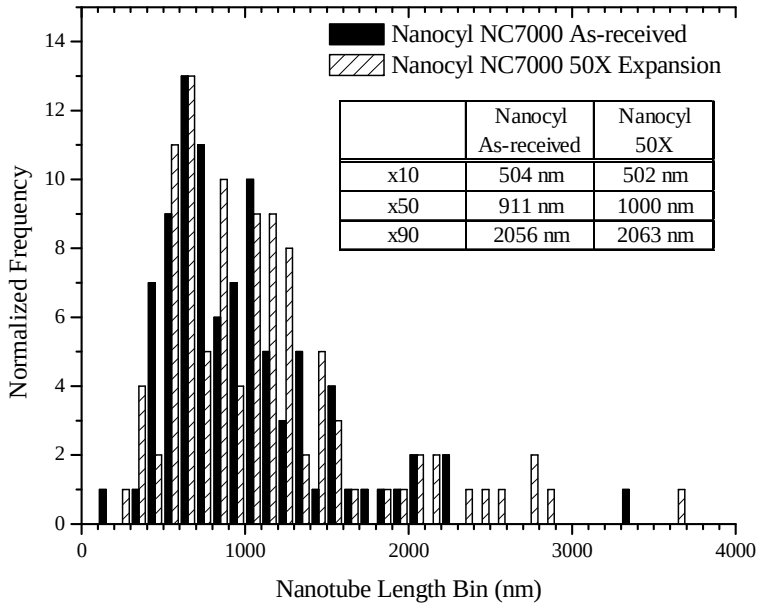


| | Nanocyl As-received | Nanocyl 50X |
|---|---|---|
| x10 | 504 nm | 502 nm |
| x50 | 911 nm | 1000 nm |
| x90 | 2056 nm | 2063 nm |

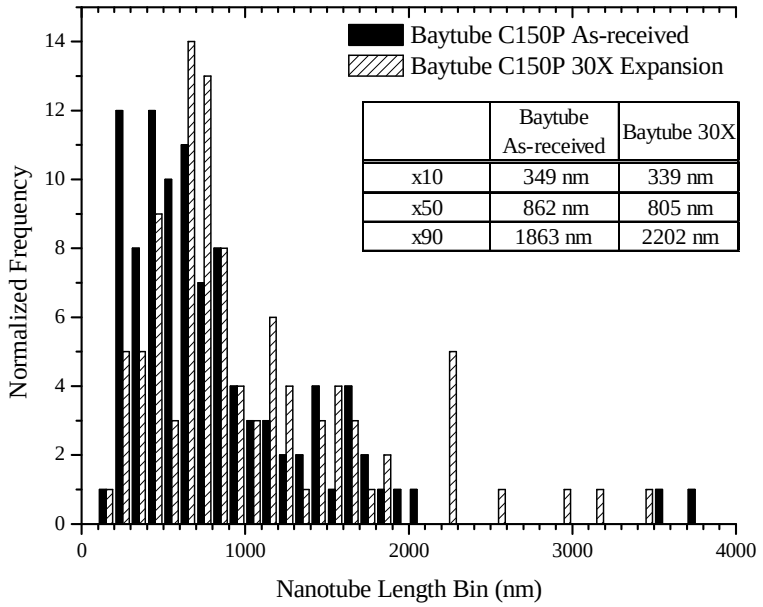


| | Baytube As-received | Baytube 30X |
|---|---|---|
| x10 | 349 nm | 339 nm |
| x50 | 862 nm | 805 nm |
| x90 | 1863 nm | 2202 nm |

Figure 4.7. Length distributions of as-received Nanocyl™ and Nanocyl™ 50X (top) and as-received Baytubes® and Baytubes® 30X (bottom) MWCNTs. Statistical values are included on each graph and were determined using 100 CNT length measurements as described in Krause et al. [17]

The as received Nanocyl$^{TM}$ MWCNT lengths of interest are $x_{10}$ – 512 nm, $x_{50}$ – 1341 nm, and $x_{90}$ – 3314 nm. In similar measurements carried out by Krause et al. [17] Nanocyl$^{TM}$ MWCNT lengths of $x_{10}$ – 504 nm, $x_{50}$ – 911 nm, and $x_{90}$ – 2056 nm were observed. The distribution in the current study suggests smaller MWCNTs than those observed by Krause and coworkers. This could be attributed to two things. First, the sonication time required to fully disperse the nanomaterial in chloroform was 5 minutes during sample preparation rather than the 3 minute sonication treatment utilized in the study by Krause et al. Longer sonication times may lead to further shortening of the MWCNTs. Second, the methodology employed during TEM measurements was slightly different in the current study, discussed in Section 4.2.2.4. In the work by Krause et al., the authors track longer nanotubes by stitching multiple TEM images together. The differences in these methods may lead to variations in the reported values.

The 50X Nanocyl$^{TM}$ MWCNTs were analyzed to determine if there was significant damage to the nanotubes after extensive $scCO_2$ processing, and the observed values were $x_{10}$ – 502 nm $x_{50}$ -1000 nm, and $x_{90}$ –2063 nm. Statistical analysis indicates that the populations were found to be statistically similar, suggesting that the MWCNTs were not damaged after the maximum deagglomeration obtained in this study. Analysis of the $x_{90}$ values indicates that longer nanotubes are not damaged during the processing of Nanocyl$^{TM}$ MWCNTs with $scCO_2$.

Utilizing $scCO_2$ processing, deagglomeration is obtained with negligible damage to the Nanocyl$^{TM}$ MWCNTs in contrast to twin screw melt compounding and ball milling. By comparison, other studies report varying degrees of damage using other deagglomeration methods for Nanocyl$^{TM}$ MWCNT bundles. Menzer et al. [13] applied a ball milling process to Nanocyl$^{TM}$ NC7000 MWCNTs for 5 hours at 50 rpm in an 8 liter container. The resulting nanotubes displayed substantial reductions in length distribution with values $x_{10}$ – 285 nm, $x_{50}$ -

629 nm, and $x_{90}$ –1453 nm. In that study, a 50% decrease in the median CNT lengths was recorded after ball milling, and the longer MWCNT ($x_{90}$) were shortened by 56%. Twin screw melt compounded Nanocyl$^{TM}$ MWCNTs reported in Krause et al. lead to MWCNTs that were shortened to 68% of their initial lengths (calculated from the $x_{50}$ value) with reported values of $x_{10}$ - 222, $x_{50}$ - 418, and $x_{90}$ -764 after high shear melt mixing of a master batch. Significant deagglomeration was observed but the damage to the MWCNTs was severe. Notably, the $x_{90}$ value in this study dropped from 3314 nm to 764 nm after deagglomeration, corresponding to a 77% decrease in length. As evident from the $x_{90}$ value in the current study, the longer nanotube integrity is maintained after deagglomeration.

Baytubes® MWCNT diameters were analyzed from measurements of 100 species. The median diameter of the as-received sample was observed to be 13.6 ± 4.5 nm and 13.9 ± 4.0 nm for the 30X sample. These data are statistical analogues, indicating no change in diameter of the MWCNTs after multiple $scCO_2$ processing steps. The data lie within the range of the as-received MWCNTs provided by the supplier as 13-16 nm in diameter [37].

The length distributions of the as-received Baytubes® MWCNT are presented in the histogram in Figure 4.7 (b). The as-received MWCNTs were observed to possess values of $x_{10}$ – 349 nm $x_{50}$ -862 nm, and $x_{90}$ –1863 nm. The median value of the data set in the current work suggests the MWCNTs are approximately 90 nm longer than suggested by Socher et al. [15] observed 770 nm for the $x_{50}$ value. Values of $x_{10}$ – 290 nm $x_{50}$ -770 nm, and $x_{90}$ –2407 nm were collected for the as-received Bayer MWCNTs in that study. The data reported in the current work slightly contradicts the observations in the work by Socher et al. [15]. However these observations are still within the limits given by the supplier in **Error! Reference source not ound.** and are not drastically different from those of others [10].

The Baytubes® MWCNTs with 30X degree of expansion were studied for their length distribution to determine any damage from extensive $scCO_2$ processing. The experimental values were determined to be $x_{10}$ -339 nm $x_{50}$ - 805 nm, and $x_{90}$ – 2202. As with the Nanocyl™ MWCNTs, the carbon nanotube lengths did not change within a 95% confidence interval. Furthermore, the longer MWCNTs were not damaged by the $scCO_2$ processing.

Other deagglomeration methods show significant damage to Baytubes® MWCNTs. High shear melt processing was used in Socher et al. [15] with a small conical co-rotating batch mixer to disperse the nanomaterial in polymer. The reported values from Socher et al. [15] were used $x_{10}$ – 164 nm $x_{50}$ -350 nm, and $x_{90}$ –570 after melt compounding. Their median MWCNT length showed a decrease in length of 55% compared to the as-received material. The longer nanotubes exhibited higher degrees of damage, with a decrease in length of 76%. Significant damage to individual MWCNTs occurs when deagglomerating the bundles with high shear melt compounding, but the aspect ratios are retained by utilizing the $scCO_2$ processing.

The lack of damage to the MWCNTs during the debundling process is likely due to the physical properties of the $scCO_2$ used in this study. The gas like diffusivity permits rapid infiltration of the $scCO_2$ into the agglomerate core, allowing the $scCO_2$ to wet the internal surface [24]. Rupture of a dry agglomerate core has been suggested as the mechanism of damage to MWCNTs [6]. Hence, with $scCO_2$ processing, rupture of the wetted agglomerate core during rapid depressurization may be accomplished without damaging the individual MWCNTs. As the large MWCNT agglomerates impact the Mach disc during rapid depressurization, they break apart more readily with negligible damage.

The results presented here indicate that longer nanotube aspect ratios are maintained in both types of MWCNTs after $scCO_2$ processing. For application of MWCNTs in

nanocomposites, longer nanotubes contribute more significantly to an electrically percolated network and can provide more substantial mechanical reinforcement [8, 10]. Furthermore, the lack of MWCNT damage suggests that the benign nature of $scCO_2$ processing is not a function of the initial MWCNT bundle morphology.

### 4.3.3 Thermodynamic Considerations

The effect of processing temperature and pressure in the supercritical $CO_2$/MWCNT mixture on the degree of deagglomeration of Baytubes® MWCNT aggregates was also investigated. At least four $scCO_2$ treatments of the MWCNT agglomerates were conducted at a given temperature and pressure combination to ensure repeatability. The methodology is explained in further detail in Section 4.2.2.5 and involves analyzing multiple $scCO_2$ densities. A suitable secondary vessel was chosen to help ensure repeatability. Therefore, the pressure variations in the secondary vessel are neglected. The results from experiments concerned with investigating the temperature and pressure variations during the soak period are summarized in Table 4.3.

Table 4.3. Conditions for iscochoric $scCO_2$ treatment of Baytubes® CNT agglomerates. Treatment was conducted at values of constant density as illustrated in Figure 4.3 at several pressure/temperature combinations. Degrees of expansion are calculated as a ratio of the intial bulk density of the material to the bulk density after $scCO_2$ treatment

| $scCO_2$ soak density ($kg/m^3$) | Soak Pressure (MPa) | Soak Temperature ($^oC$) | Degree of Expansion |
|---|---|---|---|
| 500 | 21 | 100 | 8.2 ± 0.8 |
| | 19 | 90 | 9 ± 0.8 |
| | 17 | 80 | 9.8 ± 0.4 |
| 600 | 21 | 80 | 10.9 ± 0.8 |
| | 18 | 70 | 11.8 ± 0.7 |
| | 15 | 60 | 12.2 ± 0.8 |
| 730 | 21 | 60 | 14.2 ± 0.7 |
| | 17 | 50 | 13.4 ± 0.9 |
| | 13 | 40 | 12.0 ± 0.9 |
| 850 | 26 | 50 | 11.7 ± 0.5 |
| | 24 | 45 | 10.2 ± 0.5 |
| | 21 | 40 | 7.7 ± 0.4 |

The degree of expansion and corresponding deagglomeration was observed to generally increase as a function of supercritical carbon dioxide density during the exposure of the MWCNTs to $scCO_2$ with variations at each termperature/pressure combination (Table 4.3). The highest degree of deagglomeration occurred at a temperature and pressure combination of $60^oC$ and 21 MPa, respectively, resulting in a degree of expansion of 14.2 fold and agglomerates with a median equivaleant diameter of 9.4 microns. The observed degree of expansion improved as the density during the soak period was increased up to a $scCO_2$ density of 730 $kg/m^3$ above which the degree of expansion decreased.

The thermodynamics of the fluid were investgiated in an attempt to describe these phenomena. Assuming an isolated system with constant internal energy throughout $scCO_2$ processing, the thermodynamic pathyway of the fluid can be traced on the phase diagram. The assumption may be valid given the rapid timescales of the experiments, permitting few interactions with the surroundings, which has been confirmed by other studies [26, 27, 44]. Using data from the NIST Chemistry WebBook, the thermodynamic pathways were estimated from the initial conditions in the high pressure vessel. Figure 4.8 illustrates the theoretical thermodynamic pathway of the $scCO_2$ for experiments carried out at 21 MPa and varying temperatures.

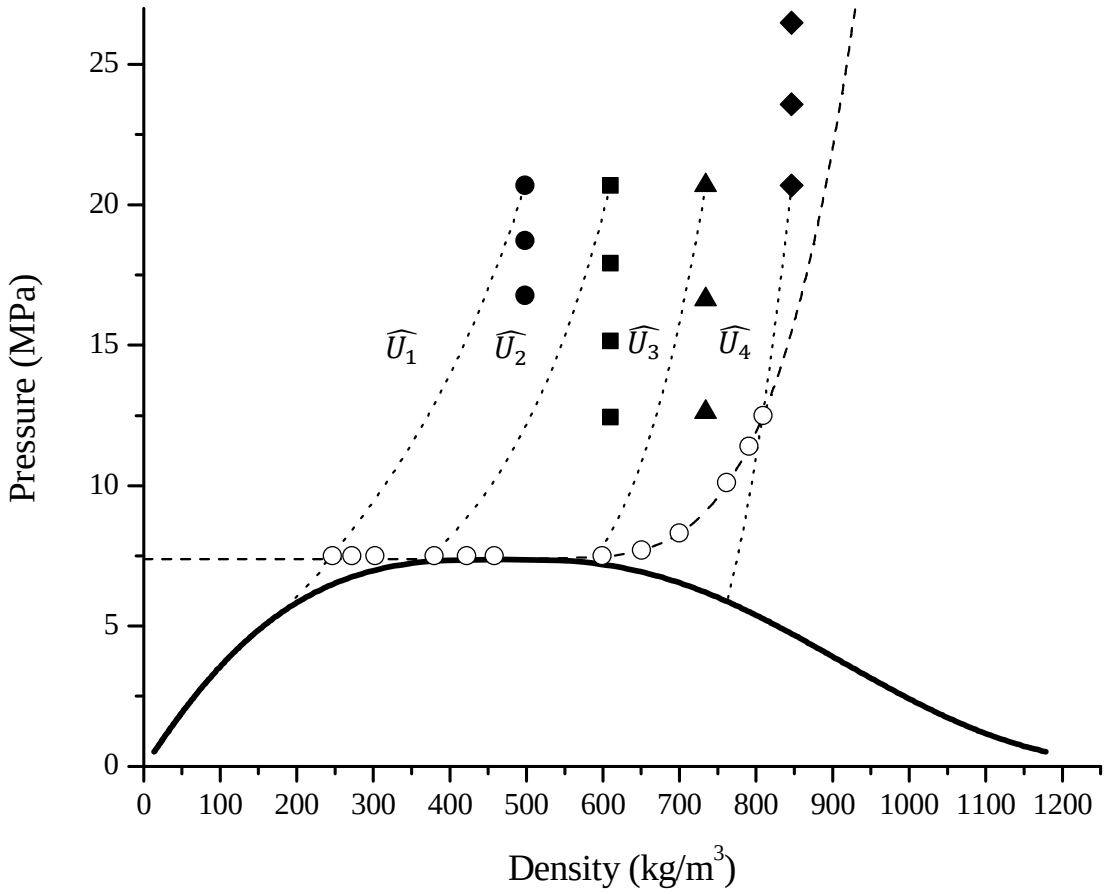


Figure 4.8. Phase diagram of $scCO_2$ using data obtained from NIST webbook. Experiments were carried out at constant densities of ~500 kg/m$^3$ (-●-), ~600 kg/m$^3$(-■-), ~730 kg/m$^3$ (-▲-), and ~850 kg/m$^3$(-♦-). Lines of constant internal energy, represented by dotted lines, are included for select experiments to depict thermodynamic pathway of fluid during $scCO_2$ treatment. From left to right, constant internal energy trends at $\widehat{U}_1$ ~380 kJ/kg, $\widehat{U}_2$ ~340 kJ/kg, $\widehat{U}_3$ ~300 kJ/kg, and $\widehat{U}_4$ ~250 kJ/kg are shown. Phase boundaries are represented by solid lines, and supercritical temperature and pressure are represented by dashed lines. See Figure 4.3 for more details. Points indiciated by ○ are estimated density values used for the domain in Figure 4.9

Several of the trends observed in Table 4.3 may be addressed by making the constant internal energy assumption. The following paragraphs will be devoted to the consideration of these topics.

It was desired to analyze the effect of temperature and pressure during the soak period on the extent of deagglomeration of the MWCNTs. The density of $scCO_2$ near the transition from supercritical is highlighted in Figure 4.8 by open circles for each experiment reported in Table 4.3. Correlating the pathway of constant internal energy to the results in Table 4.3, the highest degrees of expansions are observed at higher $CO_2$ density near the transition from supercritical fluid to subcritical liquid or the two phase region. Figure 4.9 compares this density to the experimentally measured degree of expansion for each pressure/density combination.

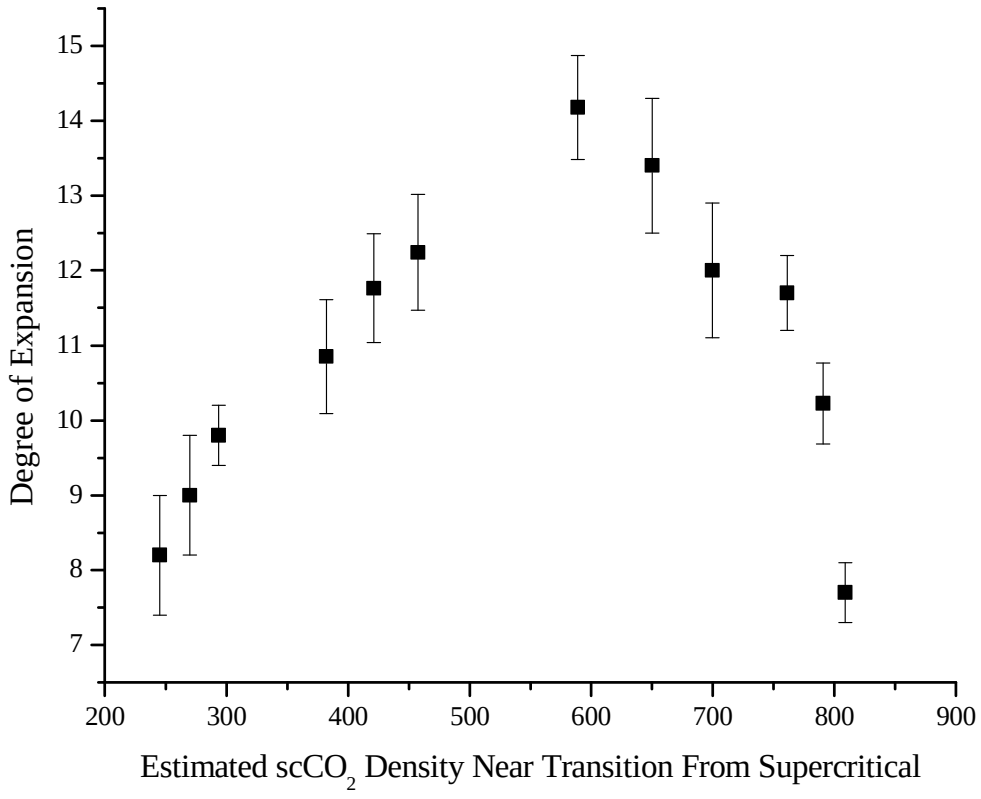


Figure 4.9. Degree of expansion as a function of estimated $scCO_2$ density near the transition from supercritical during $scCO_2$ processing, assuming a thermodynamic path of constant internal energy in a quasi-isolated system. Estimated densities highlighted as ○ in Figure 4.8

Upon inspection of Figure 4.9, an increase in the density of the $scCO_2$ near the transition from supercritical is accompanied by an increase in the degree of expansion up to a density of 600 $kg/m^3$ (corresponding to a soak temperature and pressure of 60°C and 21 MPa) before decreasing at higher values. This result indicates that it is desirable for the fluid to pass through a higher density state near the phase change from supercritical to the two phase region. However, reduced deagglomeration efficiency is observed when the fluid undergoes a transition from supercritical to a subcritical high density liquid. As the density near the transition from supercritical increases further, the degree of expansion continues to drop appreciably. By permitting a transition to the liquid regime during the rapid expansion of the $scCO_2$/MWCNT mixture, the potential exists to create liquid bridging between primary particles, or create capillary effects in the agglomerate. These phenomenon have been previously reported to significantly increase the cohesive strength of agglomerates [45]. Under such conditions, the expansion efficiency will decrease as the overall strength of the agglomerate has increased.

It was desired to further examine the effect of the transition from the supercritical state on the extent of deagglomeration of the MWCNT bundles. Supercritical carbon dioxide treatments of MWCNTs were carried out along the lines of constant internal energy near the supercritical transition of the fluid. It was observed that if the soak temperature and pressure of the $CO_2$ lay on the lines of constant internal energy, a similar degree of expansion was obtained. For example, an expansion was carried out at a soak temperature and pressure of 40°C and 7.86 MPa. The same degree of expansion was observed as the best case (21 MPa and 60°C), resulting in approximately 14 fold decrease in bulk density. These samples possess similar initial internal energies of approximately 340 kJ/g. This finding presents a two-fold implication. First, the previous assumptions of the isolated system are further supported, demonstrating that the density differential resulting from the phase change near the supercritical phase boundary dominates the

extent of deagglomeration. Second, significantly lower pressures and temperatures may be utilized than previously assumed, leading to reduced equipment, processing, and safety costs associated with high pressure processing. This led us to the conclusion that the optimal temperature-pressure combination of those analyzed in the current work is 40$^{o}$C and 7.86 MPa.

The best case $scCO_2$ processing temperature and pressure investigated here are milder conditions than previously reported. Previous work by Chen et al. [33] had suggested a soak pressure of 21 MPa and and 80$^{o}$C, requiring relatively high pressures and temperatures to deagglomerate the MWCNT bundles efficiently. Jung et al. [31] employed 100$^{o}$C and 12.2 MPa as their operating conditions. Other work by To et al. [32] utilized processing conditions of 7.93 MPa and 45$^{o}$C to deagglomerate MWCNT bundles. The soak temperature and pressure of 40$^{o}$C and 7.86 MPa in the current study are the most benign conditions reported to effectively deagglomerate MWCNT bundles with $scCO_2$.

It is recognized that the complication of the two phase region and its effect on the analysis carried out in this section. As can be seen from Figure 4.8, the $scCO_2$ is estimated to enter the two-phase region following the transition from the supercritical state. It is suspected that the presence of a liquid phase would be undesirable due to liquid bridging effects, as was discussed earlier. However, it is estimated that only a small fraction (<5% by weight) consists of liquid $CO_2$ following the transition, by utilizing a weighting factor and the previous assumption of constant internal energy. This suggests that the negative effect the liquid transition would have on the deagglomeration of the CNT is minimal.

### 4.3.4 Investigation of additional processing variables

In addition to thermodynamic variables, a few select processing conditions were analyzed to improve and understand the $scCO_2$ processing of MWCNT agglomerates. Soak time and the CNT to $scCO_2$ ratio were determined to be the most important of these variables in the analysis.

#### 4.3.4.1 MWCNT/$scCO_2$ Ratio

The extent of deagglomeration of Baytubes® MWCNT bundles was found to be a strong function of the weight ratio of MWCNTs to $scCO_2$. Rapid expansions of Baytubes® MWCNT using weight ratios of 0.1, 0.4, 2.3, and 7.6 g CNT per 100 g $scCO_2$ at 21 MPa and 60$^{o}$C were carried out. The corresponding degrees of expansion were 27.7 ± 0.3, 17.8 ± 0.6, 14.2 ± 0.7, and 5.6 ± 0.1, respectively. The large variations in the extent of deagglomeration may be attributed to two things. First, a lower ratio of CNT to $scCO_2$ ensures more complete infiltration of the supercritical fluid into the MWCNT agglomerate, reducing the average strength of the agglomerates and leading to more complete deagglomeration of the primary bundles. Second, several two dimensional simulations suggest that only 50% of the MWCNT mass passes through the Mach disc [27, 44]. Thus, as the mass of CNT processed is reduced, more bundles may be deagglomerated in fixed system geometry. This is a vital processing parameter to consider during scale up or process design in the $scCO_2$ processing of MWCNT agglomerates.

#### 4.3.4.2 Soak Time

The amount of time the supercritical carbon dioxide was permitted to be in contact with the MWCNT was found to affect the degree of deagglomeration of the MWCNT bundles. Furthermore, the soak time was found to be dependent on the weight of carbon nanotubes present in the high pressure vessel. For the processing of 2.3 g MWCNTs/ 100 g $scCO_2$, 30 minutes was the minimum time required promote sufficient infiltration of the bundles with $scCO_2$. In the

processing of 0.1 g MWCNTs/ 100 g $scCO_2$ using the same conditions, less than 5 minutes were required for sufficient infiltration.

#### 4.3.4.3 Agitation

Agitation was briefly investigated to determine its role on the deagglomeration of MWCNT agglomerates during the soak period in the primary pressure vessel. Where agitation was removed, longer time periods were required to reach a similar degree of deagglomeration. This indicates, as mentioned before, that the infiltration of the $scCO_2$ into the MWCNT bundle plays an integral role in reducing the agglomerate strength before the expansion of the $scCO_2$/MWCNT mixture.

## 4.4 Conclusions

The $scCO_2$ processing of MWCNT bundles was proven to successfully separate the agglomerates while maintaining the carbon nanotubes' aspect ratios. A 50X decrease in bulk density was observed with Nanocyl$^{TM}$ NC-7000 MWCNT bundles at the maximum extent of deagglomeration using the current apparatus. A 6X decrease in bulk density of the Nanocyl$^{TM}$ was reported in earlier studies, suggesting that the $scCO_2$ processing is significantly improved in the current work [33]. The median agglomerate diameter was reduced from 40.5 μm to 4.0 μm after a 50X degree of expansion, indicating that over half of the Nanocyl$^{TM}$ MWCNT bundles are deagglomerated. Negligible damage to the aspect ratio of the MWCNTs was observed at the maximum extent of deagglomeration. This is a significant improvement relative to other deagglomeration methods, such as ball milling and high shear melt compounding where the MWCNT lengths have been reduced by 50% [13], and 68% [17], respectively. The Baytubes® C150P MWCNT agglomerates were reduced from 596.7 μm to 7.9 μm, resulting in a 30X decrease in bulk density at the maximum deagglomeration. The 30X Baytubes® samples were compared to the as-received Baytubes® with negligible change in aspect ratio due to $scCO_2$ processing, whereas high shear melt compounding has led to a 55% reduction in length according to other studies [15]. Processing conditions of 40$^{o}$C and 7.86 MPa, along with a low MWCNT:$scCO_2$ ratio with sufficient agitation are recommended for $scCO_2$ treatment of MWCNT agglomerates. Previous reports have indicated that operating conditions of 80$^{o}$C and 20.7 MPa were optimal, suggesting that milder conditions are utilized in the current study [33]. The authors recognize the difference between deagglomeration of MWCNT aggregates by $scCO_2$ processing and melt compounding methods. In work reported elsewhere nanocomposites prepared by melt compounding with $scCO_2$ processed MWCNTs are compared to nanocomposites prepared by high shear melt compounding [46].

## 4.5 Acknowledgements

The authors would like to thank Bayer Material Science and Nanocyl™ for donating the Baytubes® C150P and NC-7000 MWCNT, respectively. In addition, the authors acknowledge use of the facilities at the Nanocscale Characterization and Fabrication Laboratory at Virginia Polytechnic Institute for the TEM and optical images. Finally, the authors would like to thank Dr. Erdogan Kiran for his recommendation of using isochors in conducting the thermodynamic experiments.

## References


[1] S. Iijima, "Helical Microtubules of Graphitic Carbon," *Nature*, vol. 354, 1991.

[2] T.W. Ebbesen, H.J. Lezec, H. Hiura, J.W. Bennett, H.F. Ghaemi, and T. Thio, "Electrical conductivity of individual carbon nanotubes," *Nature*, vol. 382, 1996.

[3] J.P. Salvetat, A.J. Kulik, J.M. Bonard, G.A.D. Briggs, T. Stockli, K. Metenier, S. Bonnamy, F. Beguin, N.A. Burnham, and L. Forro, "Elastic modulus of ordered and disordered multiwalled carbon nanotubes," *Advanced Materials*, vol. 11, 1999.

[4] J.P. Salvetat, G.A.D. Briggs, J.M. Bonard, R.R. Bacsa, A.J. Kulik, T. Stockli, N.A. Burnham, and L. Forro, "Elastic and shear moduli of single-walled carbon nanotube ropes," *Physical Review Letters*, vol. 82, 1999.

[5] Q.W. Li, C.H. Liu, X.S. Wang, and S.S. Fan, "Measuring the thermal conductivity of individual carbon nanotubes by the Raman shift method," *Nanotechnology*, vol. 20, 2009.

[6] I. Alig, P. Potschke, D. Lellinger, T. Skipa, S. Pegel, G.R. Kasaliwal, and T. Villmow, "Establishment, morphology and properties of carbon nanotube networks in polymer melts," *Polymer*, vol. 53, 2012.

[7] D. Stoyan, W.S. Kendall, and J. Mecke, *Stochastic geometry and its applications*. 2nd ed. Wiley series in probability and statistics Applied probability and statistics. 1995, Chichester ; New York: Wiley. xix, 436 p.

[8] A.V. Kyrylyuk and P. van der Schoot, "Continuum percolation of carbon nanotubes in polymeric and colloidal media (vol 105, pg 8221, 2008)," *Proceedings of the National Academy of Sciences of the United States of America*, vol. 105, 2008.

[9] B.P. Grady, *Thermal Conductivity*, in *Carbon Nanotube–Polymer Composites*. 2011, John Wiley & Sons, Inc. p. 283-304.

[10] J.C.H. Affdl and J.L. Kardos, "The Halpin-Tsai equations: A review," *Polymer Engineering & Science*, vol. 16, 1976.

[11] C.J. Kerr, Y.Y. Huang, J.E. Marshall, and E.M. Terentjev, "Effect of filament aspect ratio on the dielectric response of multiwalled carbon nanotube composites," *Journal of Applied Physics*, vol. 109, 2011.

[12] S. Badaire, P. Poulin, M. Maugey, and C. Zakri, "In situ measurements of nanotube dimensions in suspensions by depolarized dynamic light scattering," *Langmuir*, vol. 20, 2004.

[13] K. Menzer, B. Krause, R. Boldt, B. Kretzschmar, R. Weidisch, and P. Potschke, "Percolation behaviour of multiwalled carbon nanotubes of altered length and primary agglomerate morphology in melt mixed isotactic polypropylene-based composites," *Composites Science and Technology*, vol. 71, 2011.

[14] K. Menzer, B. Krause, R. Boldt, B. Kretzschmar, R. Weidisch, and P. Pötschke, "Percolation behaviour of multiwalled carbon nanotubes of altered length and primary agglomerate morphology in melt mixed isotactic polypropylene-based composites," *Composites Science and Technology*, vol. 71, 2011.

[15] R. Socher, B. Krause, M.T. Muller, R. Boldt, and P. Potschke, "The influence of matrix viscosity on MWCNT dispersion and electrical properties in different thermoplastic nanocomposites," *Polymer*, vol. 53, 2012.

[16] J. Guo, Y. Liu, R. Prada-Silvy, Y. Tan, S. Azad, B. Krause, P. Pötschke, and B.P. Grady, "Aspect ratio effects of multi-walled carbon nanotubes on electrical, mechanical, and thermal properties of polycarbonate/MWCNT composites," *Journal of Polymer Science Part B: Polymer Physics*, 2013.

[17] B. Krause, R. Bolcit, and P. Potschke, "A method for determination of length distributions of multiwalled carbon nanotubes before and after melt processing," *Carbon,* vol. 49, 2011.
[18] T. McNally and P. Pötschke, *Polymer-Carbon Nanotube Composites: Preparation, Properties And Applications*. 2011: Elsevier Science.
[19] G. Parfitt, "Fundamental aspects of dispersion," *Dispersion of solids in liquids: with special reference to pigments. Elsevier, Amsterdam, cap,* vol. 3, 1969.
[20] H. Schubert, "Grundlagen des Agglomerierens," *Chemie Ingenieur Technik,* vol. 51, 1979.
[21] I. Manas-Zloczower and D.L. Feke, "Analysis of Agglomerate Rupture in Linear Flow-Fields," *International Polymer Processing,* vol. 4, 1989.
[22] S.P. Rwei, I. Manas-Zloczower, and D.L. Feke, "Observation of Carbon-Black Agglomerate Dispersion in Simple Shear Flows," *Polymer Engineering and Science,* vol. 30, 1990.
[23] G.R. Kasaliwal, S. Pegel, A. Goldel, P. Potschke, and G. Heinrich, "Analysis of agglomerate dispersion mechanisms of multiwalled carbon nanotubes during melt mixing in polycarbonate," *Polymer,* vol. 51, 2010.
[24] D. Sanli, S.E. Bozbag, and C. Erkey, "Synthesis of nanostructured materials using supercritical CO(2): Part I. Physical transformations," *Journal of Materials Science,* vol. 47, 2012.
[25] J.L. Kendall, D.A. Canelas, J.L. Young, and J.M. DeSimone, "Polymerizations in supercritical carbon dioxide," *Chemical Reviews,* vol. 99, 1999.
[26] O. Brandt, A.M. Rajathurai, and P. Roth, "First observations on break-up of particle agglomerates in shock waves," *Experiments in Fluids,* vol. 5, 1987.
[27] D. To, R. Dave, X. Yin, and S. Sundaresan, "Deagglomeration of nanoparticle aggregates via rapid expansion of supercritical or high-pressure suspensions," *Aiche Journal,* vol. 55, 2009.
[28] C.W. Manke, E. Gulari, D.F. Mielewski, and E.C.-C. Lee, "System and method of delaminating a layered silicate material by supercritical fluid treatment," U.S. Patent, 2002.
[29] E. Reverchon and P. Pallado, "Hydrodynamic modeling of the RESS process," *The Journal of Supercritical Fluids,* vol. 9, 1996.
[30] E. Gulari, K. Rangaramanujam, and G.K. Serhatkulu, "Method of delaminating aggregated particles with a coating agent in a substantially supercritical fluid," US7387749, 2008.
[31] W.R. Jung, J.H. Choi, N. Lee, K. Shin, J.H. Moon, and Y.S. Seo, "Reduced damage to carbon nanotubes during ultrasound-assisted dispersion as a result of supercritical-fluid treatment," *Carbon,* vol. 50, 2012.
[32] D. To, S. Sundaresan, and R. Dave, "Nanoparticle mixing through rapid expansion of high pressure and supercritical suspensions," *Journal of Nanoparticle Research,* vol. 13, 2011.
[33] C. Chen, M. Bortner, J.P. Quigley, and D.G. Baird, "Using supercritical carbon dioxide in preparing carbon nanotube nanocomposite: Improved dispersion and mechanical properties," *Polymer Composites,* vol. 33, 2012.
[34] B. Krause, M. Mende, P. Potschke, and G. Petzold, "Dispersability and particle size distribution of CNTs in an aqueous surfactant dispersion as a function of ultrasonic treatment time," *Carbon,* vol. 48, 2010.

[35] Nanocyl S.A., Product. Datasheet Nanocyl NC 7000 series. Edition 2007-02-05. Sambreville, Belgium; 2007.
[36] Bayer MaterialScience AG. Data sheet Baytubes® C150P. Edition 2006-01-18; 2006.
[37] Bayer MaterialScience AG. Data sheet Baytubes® C150P. Edition 2009-02-24. 2009.
[38] B. Krause, M. Ritschel, C. Taschner, S. Oswald, W. Gruner, A. Leonhardt, and P. Potschke, "Comparison of nanotubes produced by fixed bed and aerosol-CVD methods and their electrical percolation behaviour in melt mixed polyamide 6.6 composites," *Composites Science and Technology,* vol. 70, 2010.
[39] E.W.M. Lemmon, M.O. ; Friend, D.G. , "NIST Chemistry WebBook, NIST Standard Reference Database Number 69,"2013.
[40] C. Chen, "The Manufacture of Polymer Nanocomposite Materials Using Supercritical Carbon Dioxide,"2011.
[41] T. Villmow, B. Kretzschmar, and P. Potschke, "Influence of screw configuration, residence time, and specific mechanical energy in twin-screw extrusion of polycaprolactone/multi-walled carbon nanotube composites," *Composites Science and Technology,* vol. 70, 2010.
[42] M. Salzano de Luna, L. Pellegrino, M. Daghetta, C.V. Mazzocchia, D. Acierno, and G. Filippone, "Importance of the morphology and structure of the primary aggregates for the dispersibility of carbon nanotubes in polymer melts," *Composites Science and Technology,* vol. 85, 2013.
[43] F.Y. Castillo, R. Socher, B. Krause, R. Headrick, B.R. Grady, R. Prada-Silvy, and P. Potschke, "Electrical, mechanical, and glass transition behavior of polycarbonate-based nanocomposites with different multi-walled carbon nanotubes," *Polymer,* vol. 52, 2011.
[44] M. Weber and M.C. Thies, "A simplified and generalized model for the rapid expansion of supercritical solutions," *The Journal of Supercritical Fluids,* vol. 40, 2007.
[45] G. Kasaliwal, T. Villmow, S. Pegel, and P. Potschke, "Influence of material and procesing parameters on carbon nanotube dispersion in polymer melts," *Polymer-Carbon Nanotube Composites: Preparation, Properties and Applications,* 2011.
[46] J.P. Quigley, "Advanced Thermoplastic Nanocomposite Processing Using an Improved Supercritical Carbon Dioxide Aided Melt Blending Method,"2014.

# Chapter 5. Enhanced Electrical Properties of Melt Compounded Polycarbonate/ Carbon Nanotube Nanocomposites Prepared with Supercritical Carbon Dioxide

John P. Quigley[1], Kevin Herrington[1], and Donald G. Baird[1,2]

1. Department of Chemical Engineering, Virginia Tech, Blacksburg, Virginia 24061, USA,
2. Macromolecules and Interfaces Institute, Virginia Tech, Blacksburg, Virginia 24061, USA

## Abstract

Polycarbonate/ carbon nanotube (CNT) nanocomposites were generated using a supercritical carbon dioxide ($scCO_2$) aided melt blending method, yielding nanocomposites with enhanced electrical properties and improved dispersion while maintaining the aspect ratio of the as-received CNT. Baytubes® C 150 P CNTs were benignly deagglomerated with $scCO_2$ resulting in 5 fold (5X), 10X, and 15X decreases in bulk density from the as-received CNT. Electrical percolation thresholds were realized at CNT loading levels as low as 0.83 wt% for composites prepared with 15X CNT using the $scCO_2$ aided melt blending method. By comparison, a concentration of 1.5 wt% was required without $scCO_2$ processing. Optical microscopy, transmission electron microscopy, and rheology were used to investigate the dispersion and mechanical network of CNTs in the nanocomposites. The dispersion of CNTs generally improved with $scCO_2$ processing compared to direct melt blending, but was significantly worse than that of twin screw melt compounded nanocomposites reported in the literature. A rheologically percolated network was observed near the electrical percolation of the nanocomposites. The importance of maintaining longer carbon nanotubes during nanocomposite processing rather than focusing on dispersion alone is highlighted in the current efforts.

## 5.1 Background and Motivation

The production of polymer-multi walled carbon nanotube (CNT) nanocomposites has been the focus of studies in the past two decades due to the potential for CNTs to transfer their impressive thermal [1], electrical [2] and mechanical properties [3, 4] to composites. These nanocomposites have become relevant in industry over the past several years, especially in applications of electromagnetic interference shielding [5] and electrostatic dissipation [6].

Commercially available CNTs are typically provided as large agglomerates on the order of several hundred microns in diameter resulting from chemical vapor deposition synthesis [7]. The agglomerates are held together by relatively strong van der Waals forces and physical entanglements of carbon nanotubes, making them difficult to separate.

A method of mixing polymer and CNTs must be chosen so that sufficient energy is applied to destroy the agglomerates and distribute the carbon nanotubes homogenously. Typical methods include *in-situ* polymerization, solution blending, and melt compounding. Melt compounding nanocomposites is of particular interest due to its scalability, flexibility, and lack of processing solvents compared to solution blending and *in-situ* polymerization [8, 9].

Significant effort has been directed at understanding and improving the dispersion of CNT agglomerates in polymer melts to produce nanocomposites with superior electrical properties [10-13]. However, recent studies suggest that dispersing the CNTs from their initial bundles during melt processing leads to significant reduction in the nanofiller aspect ratio [14-16]. The damage to CNTs is suspected to occur when high external stresses are applied to unwetted agglomerates, resulting in rupture of the dry agglomerate core [17]. Reduction in carbon nanotube lengths during processing may result in decreased electrical properties for melt compounded nanocomposites, as the aspect ratio scales inversely with the theoretical percolation

threshold [14]. Therefore, care must be taken in choosing processing conditions that mitigate damage while dispersing the CNT during nanocomposite generation.

A multitude of recent literature has investigated melt processing conditions to determine the effect of input mixing energy on the CNT lengths, agglomeration dispersion and subsequent nanocomposite electrical properties [11, 14-17]. In melt compounding, mixing energy is a quantity used to relate the external stresses on CNT agglomerates to the mixing variables which are dependent on screw speed, residence time, and the applied torque. This allows one to effectively relate dispersion mechanisms, processing conditions, and shortening of the CNTs to the properties of melt compounded polymer nanocomposites [14, 16, 17].

Although the dispersion of CNTs is generally improved with increasing mixing energy, the extent of damage has also been related to increased values of mixing energy. Guo et al. [15] melt compounded polycarbonate nanocomposites in a twin screw micro compounding device using CNTs with very high aspect ratios (474). The authors observed decreased percolation thresholds when mixing times were doubled, from concentrations of 0.07 wt% to 0.2 wt%. The CNTs were shortened by 89% of their initial value to 550 nm after melt compounding at the longer residence times, indicating that gentler mixing led to improved electrical properties. Pötschke et al. [16] investigated the effect of mixing speed on electrical properties of poly (caprolactone) (PCL)/CNT nanocomposites prepared with a twin screw microcompounding device. Increasing mixing energies, controlled by mixing speeds, resulted in better dispersion of the CNTs in the PCL. However, both rheological percolation and electrical percolation decreased at the highest mixing speeds studied where the CNTs were shortened to 70% of their initial length. Socher et al. [11] investigated the effect of matrix viscosity on the dispersion and electrical properties of polycarbonate (PC)/ CNT nanocomposites. Greater dispersion was

observed in the high viscosity nanocomposites due to increased input energies, but the electrical properties were diminished. It was reported that nanocomposites prepared with a higher viscosity matrix reduced the CNT lengths compared to a low viscosity matrix, due to decreased stresses applied to the CNT agglomerates. In summary, these findings suggest that intermediate mixing energies which partially maintain the CNT aspect ratios while providing sufficient dispersion are desired to achieve maximum electrical properties. This issue may be avoided if alternative nanocomposite generation methods are developed which retain the aspect ratio of the CNT during dispersion.

Supercritical carbon dioxide ($scCO_2$) deagglomeration of CNT bundles followed by melt blending has been suggested as a benign way to generate CNT polymer nanocomposites while retaining the aspect ratio of the nanofiller [18, 19]. Gulari et al. [19] obtained a patent in 2008 for the processing of nanotubes with $scCO_2$, followed by melt compounding to generate nanocomposites. However, few specifics were provided for the $scCO_2$ processing of the CNT and the melt compounding step of nanocomposite generation was not described in any detail. A method has been developed by Chen et al. [18] to process CNT aggregates with $scCO_2$ followed by single screw melt compounding, known as the $scCO_2$ aided melt blending method. In applying this method, the authors observed improved mechanical properties in polyphenylsulfone nanocomposites, but limited morphological analysis was conducted and the effect of the process on the aspect ratio of the CNT was not investigated. Furthermore, the work by Chen et al [18] was not concerned with the formation of electrically conductive networks in CNT nanocomposites. More recent work has focused on the deagglomeration of CNT aggregates using $scCO_2$ processing while retaining the aspect ratio of the CNT [20]. It was found that the rapid expansion of the supercritical suspension resulted in varying degrees of deagglomeration for the CNT bundles without damaging the CNT aspect ratio. The varying extents of $scCO_2$

processing yielded CNT with significantly reduced bulk densities with the potential to generate nanocomposites possessing improved dispersion and electrical properties.

The aim of this work is to determine the effect of $scCO_2$ processing of CNT agglomerates on the morphology and surface conductivity of CNT/polycarbonate nanocomposites prepared with the $scCO_2$ aided melt blending method with single screw mixing. Nanocomposites were generated using direct melt blending and varying extents of $scCO_2$ processing, as reported in work elsewhere [20]. Following nanocomposite generation, it is desired to define the extent of damage to individual CNT in the nanocomposites. Furthermore, it is desired to determine whether the deagglomeration of CNT bundles by $scCO_2$ treatment before melt mixing leads to an improvement in the electrical conductivity in polycarbonate/ CNT nanocomposites. Nanocomposite morphologies are investigated by means of optical microscopy, rheological measurements, and transmission electron microscopy to determine the state of CNT dispersion and distribution throughout the polymer. Some comments are offered as to the effect of the $scCO_2$ processing on the mechanical CNT network in the nanocomposites as well.

## 5.2 Experimental

### 5.2.1 Materials

#### 5.2.1.1 Carbon Nanotubes

The multi walled carbon nanotubes (CNT) used in the current study are Baytubes® C 150 P from Bayer MaterialScience (Leverkusen, Germany), which are delivered as large agglomerates in the form of powder with a bulk density of approximately 150 kg/m$^3$. The properties of the CNT and their agglomerates are reported in detail elsewhere [7, 20]. The CNTs are generated through fixed bed chemical vapor deposition (CVD) synthesis and were used as-received from the supplier.

#### 5.2.1.2 Polycarbonate

A medium viscosity polycarbonate (PC), Makrolon 2608 from Bayer MaterialSciences, was chosen as the polymer matrix. The melt flow index is 13 g/10 minute under a load of 1.2 kg at 300$^o$C. Makrolon 2608 possesses a number average molecular weight of ~10,500 g/mol with a polydispersity index of 2.54 as determined by GPC.

### 5.2.2 Methods

#### 5.2.2.1 Composite processing

It was desired to determine the effect of benign $scCO_2$ deagglomeration of CNT bundles on the electrical properties and morphology of nanocomposites prepared by melt compounding. The $scCO_2$ deagglomeration of CNT bundles was thoroughly investigated and is reported elsewhere [20]. The extent of deagglomeration was found to correlate to the bulk density of the $scCO_2$ processed CNT which is measured using the EN DIN 60 standard. Degree of expansion refers to the factor by which the bulk density of the as-received CNT is reduced after $scCO_2$ processing. Increasing degrees of expansion correspond to increasing extents of

deagglomeration. For example, a 15 fold (15X) degree of expansion describes a reduction in bulk density from 150 kg/m$^3$ to 10 kg/m$^3$for the Baytubes® CNT after $scCO_2$ processing, corresponding to agglomerates on the order of 9 μm in diameter. Samples are referred to as direct blended (DB) and $scCO_2$ processed with a modifier (10X, 15X, etc.) for their reported degree of expansion. The DB samples were prepared by mixing polymer pellets with as-received CNT in a Kitchen-aid mixer for 15 minutes, followed by melt compounding. The degrees of expansion covered in this study with their corresponding bulk densities are summarized in Table 5.1.

Table 5.1. Nomenclature for CNT used for nanocomposite generation

| | Sample name | Bulk density (kg/m^3) |
|---|---|---|
| Baytubes® | DB | 150 |
| | 5X | 30 |
| | 10X | 15 |
| | 15X | 10 |

Nanocomposites were generated at concentrations of 0.5, 1, 2, 3, 5 and 7 weight percent (wt%) nanotubes, using CNTs with no $scCO_2$processing (DB), and CNTs processed with $scCO_2$ at 5X, 10X, and 15X degrees of expansion. The higher concentration composites (>3 wt%) were melt compounded using a sequential mixing technique which is described in the work by Chen et al. [21].

Nanocomposites were prepared via the supercritical carbon dioxide aided melt blending method, which is described in detail elsewhere [18, 21]. Polycarbonate pellets and CNTs were dried in a vacuum oven at 120$^o$C overnight before processing. The primary pressure chamber was obtained from Parr Instrument Company (Moline, IL) with a 300 ml capacity and a maximum operating pressure of 4000 psi and 120$^o$C. A soak period permitted the $scCO_2$ to contact and infiltrate the CNT bundles, followed by rapid release of the CNTs and $scCO_2$ suspension into a larger secondary pressure vessel (18.9 liter) containing the polymer pellets.

The polycarbonate/CNT mixture was then collected from the secondary pressure vessel and poured into the feed throat of a single screw extruder. The melt compounding device was a Killion KL-100 single screw extruder with a 25.4 mm (1 in) diameter and an L/D of 30:1. The nanocomposites were extruded at an average barrel temperature of 255$^{o}$C and a screw speed of 25 rpm using a capillary die with a 1.59 mm diameter and 20:1 L/D. The nanocomposite strands were then chopped into pellets and dried at 120°C in a vacuum oven overnight.

It has been reported that samples containing well dispersed CNTs exhibit lower electrical properties than samples possessing CNTs in secondary agglomerates, or clusters [9, 22]. This phenomena has been related to insulating effects from the polymer on well dispersed CNTs in addition to the formation of a conductive superstructure when the CNTs are loosely agglomerated in secondary clusters [9, 22]. Furthermore, injection molded parts may possess an insulating skin layer which may reduce the surface conductivity. Therefore, nanocomposite pellets were compression molded into plaques with sufficient annealing time to allow formation of the conductive superstructure and minimize the surface resistivity of the nanocomposites. The composite pellets were dried for a minimum of six hours in a vacuum oven at 120°C before compression molding. Square plaques (76 mm diameter, 1 mm thickness) were processed at 260°C with an applied force of 1 kN over 5 minutes. A minimum of five samples for each set of conditions was generated.

#### 5.2.2.2 Post- Melt Processing Length Measurements

The lengths of post melt-processed CNTs were studied to determine any damage to the CNTs from the $scCO_2$ aided melt blending method using a technique previously described by Krause et al. [23]. Nanocomposites were mixed in chloroform for 1 hour at 0.1 g CNT/ liter

chloroform under agitation to remove the CNTs from the polymer. The suspension was sonicated for 5 minutes in a VWR B2500A ultrasonic cleaner and dropped onto a carbon coated grid for TEM analysis. TEM measurements were generated with a Philips EM420T with an accelerating voltage of 80 kV. One hundred CNT length measurements were collected for each sample. Gatan Digital Micrograph image analysis software was used to measure the nanotube lengths at 17,000x 7,500 x and 4,500 x magnifications to ensure any large nanotubes were not omitted. A Mann-Whitney-U statistical test with a 95% confidence interval was utilized to determine the validity of any comparisons between the as-received unprocessed CNTs, the melt processed CNTs (DB), and the CNTs processed by the $scCO_2$ aided melt blending method (15X).

#### 5.2.2.3 Surface Conductivity

The compression molded samples were investigated for surface resistivity using A Prostat PRF-911 Concentric Ring Set and Keithley 2000 multi-meter with sensitivity of $1 \times 10^{-10}$ ohms in accordance with ASTM D-257. Corresponding conductivity values were calculated by taking the inverse of the measured resistivity. Reported conductivities are the median of measurements of at least 5 plaques. Percolation thresholds were fitted from the power law model for composite conductivity near the electrical percolation threshold as described in other work [24]:

$$\sigma(p) = B\,(p - p_c)^t \qquad (5.1)$$

In Equation (1), the weight percent percolation threshold, $p_c$, is fit using a power law relationship with a proportionality constant, $B$, and the critical exponent, $t$ , for values of conductivity above the percolation threshold.

#### 5.2.2.4 Optical Microscopy

The microscale dispersion was investigated using reflective optical microscopy of relatively thick sections for select samples (0.5 μm). Compression molded samples were microtomed using a Diatome 3.0 mm 35$^{o}$ diamond knife at -80$^{o}$C. Images were captured at a magnification of 1400x using a Hirox KH-7700 microscope in combination with a multi-focal synthesis to account for any folding or curvature in the sections. A band pass filter was applied to the resulting images using ImageJ software and the agglomerate diameters were calculated assuming a circle equivalent. Agglomerates with circle equivalent diameters < 5μm were ignored according to the ISO-18553 standard. The agglomerate area fraction ($A_A$) is reported as the percent area of aggregates with respect to the area investigated, as described in Pötschke et al. [25]. At least 5 sections were imaged per sample to obtain a more circumspect understanding of the microscale morphology of the nanocomposites.

#### 5.2.2.5 Transmission Electron Microscopy

Transmission electron microscopy (TEM) was used to qualitatively investigate the nanoscale CNT dispersion and network in the composites for select concentrations. Sections were microtomed from compression molded plaques to a thickness of 100 nm using a Diatome 3.0 mm 35$^{o}$ diamond knife at -80$^{o}$C. TEM measurements were generated with a Philips EM420T with an accelerating voltage of 100 kV. Twenty regions were imaged at 17,000x and 9,600 x magnification to generate adequately representative images for each sample.

#### 5.2.2.6 Rheology

Melt rheology was carried out to investigate the mechanically percolated network and the state of CNT dispersion for select nanocomposites. Experiments were performed using a Rheometrics Mechanical Spectrometer model 800 (RMS-800). Discs 25mm in diameter were cut from compression molded plaques and dried overnight at 120$^{o}$C in a vacuum oven. Dynamic

frequency sweep experiments were performed under a continuous nitrogen atmosphere using a 25 mm parallel plate fixture at 260$^{o}$C. The complex viscosities ($\eta^*$) and storage moduli (G') of the nanocomposites as functions of angular frequency ($\omega$) (ranging from 0.1 rad/s to 100 rad/s) were obtained at a temperature of 260$^{o}$C and a strain of 5%. This strain was found to be within the linear viscoelastic region of the pure matrix from strain sweeps at 1.0 rad/s and 260$^{o}$C.

## 5.3 Results and Discussion

### 5.3.1 Post- Melt Processing Length Measurements

CNT lengths were investigated to determine the effect of the $scCO_2$ aided melt blending method on the shortening of carbon nanotubes. In work reported elsewhere, the CNT lengths were reported after $scCO_2$ processing alone with negligible observed damage to the CNT [20]. Therefore, any damage reported here may be attributed to the melt compounding step of the $scCO_2$ aided melt blending method. The length distributions of DB Baytubes® and 15X Baytubes® are compared in Figure 5.1 to the as-received Baytubes® to determine any shortening due to melt compounding, or melt compounding in combination with the $scCO_2$ processing.

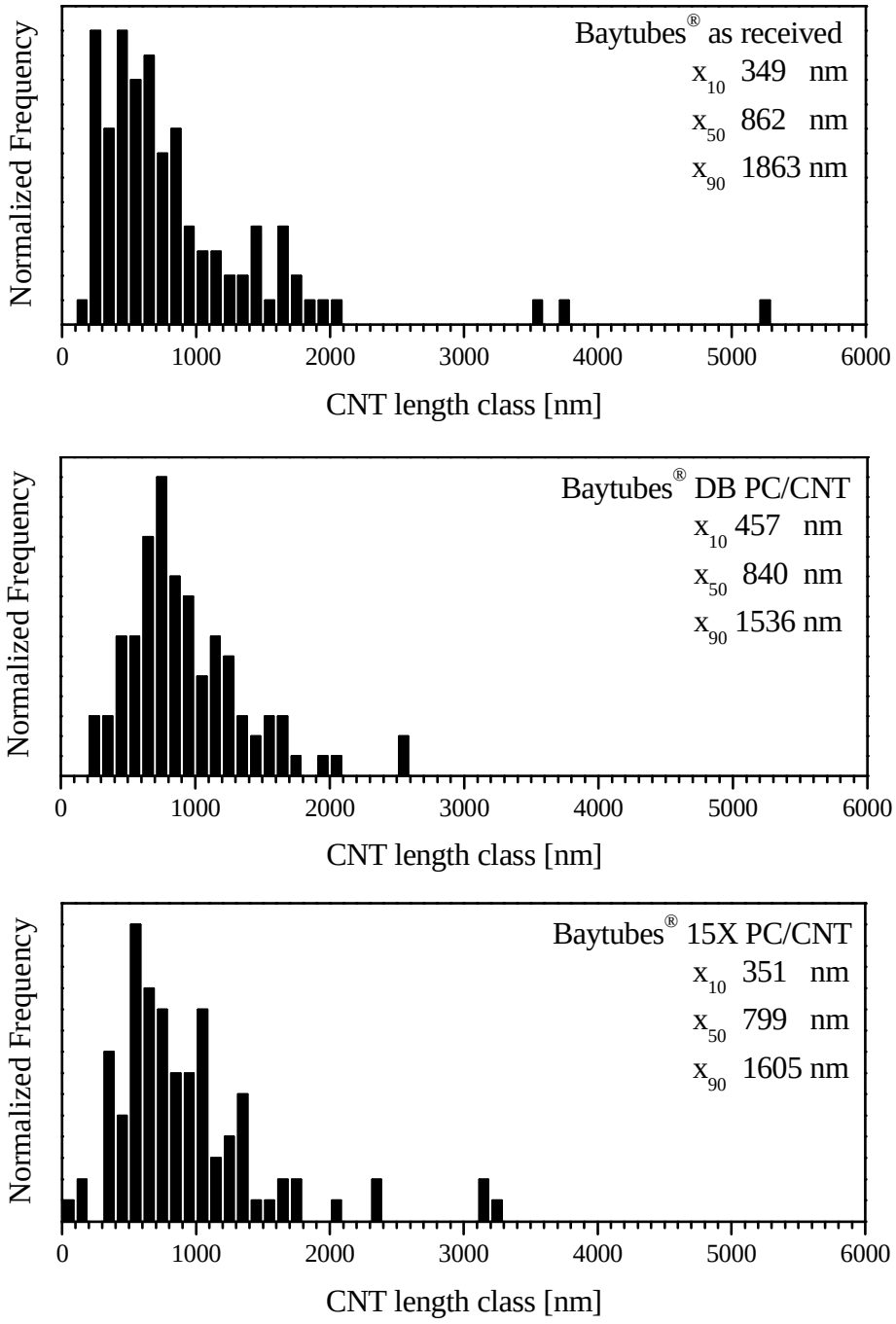


Figure 5.1. Length distributions of as-received Baytubes® (top), CNTs from 3 wt% DB polycarbonate nanocomposite (middle) and CNT from 3 wt% 15X polycarbonate nanocomposite (bottom). Values of interest are included on each graph and were calculated from 100 CNT length measurements as described in Krause et al. [23]

The inset data shows the characteristic values $x_{10}$, $x_{50}$, and $x_{90}$, indicating that 10%, 50%, and 90% of the population are shorter than the corresponding value, respectively.

Negligible shortening was observed for the CNT dissolved from 3 wt% DB and 15X melt compounded PC/CNT samples, as determined from statistical analysis. The results may be compared to the shortening of CNT from nanocomposites prepared with high shear melt compounding methods in the literature. Baytubes®/ polycarbonate nanocomposites were generated by twin-screw microcompounding in Socher et al. [11], where increased damage to the nanomaterial was observed. The medium viscosity matrix in Socher et al. [11] led to CNT shortening by 46%, with the longer nanotubes reduced by 61%. The Makrolon 2608 polycarbonate utilized in the current study possesses an intermediate viscosity, which is comparable to theirs. The lack of significant damage to the CNT in the nanocomposites prepared with and without $scCO_2$ processing indicates that the mixing energies are low enough to preserve the CNT lengths using the current apparatus. Furthermore, the lack of damage to the CNT during melt compounding suggests that any differences in morphology or properties of the nanocomposites may be attributed to variations in the state of dispersion rather than the CNT length.

The $x_{90}$ values for the DB and 15X samples suggest that the longer CNTs are shortened during melt compounding, as illustrated in Figure 5.1. The DB and 15X samples show 18% and 14% reduction in the $x_{90}$ value, respectively. This reduction is attributed to shear forces during extrusion which induce rupture of the dry agglomerate core [9]. The degree of shortening to the longer nanotubes is significantly lower than that of other melt compounding methods due to the low applied shear stress associated with single screw extrusion [11, 15]. However this indicates that the $scCO_2$ aided melt compounding method is not entirely benign. It is desired to maintain

the aspect ratio of longer nanotubes as they contribute substantially to the formation of an electrically conductive network [26].

## 5.4 Surface Conductivity

The effect of the $scCO_2$ aided melt blending method on the electrical properties of the PC/CNT nanocomposites is illustrated in Figure 5.2.

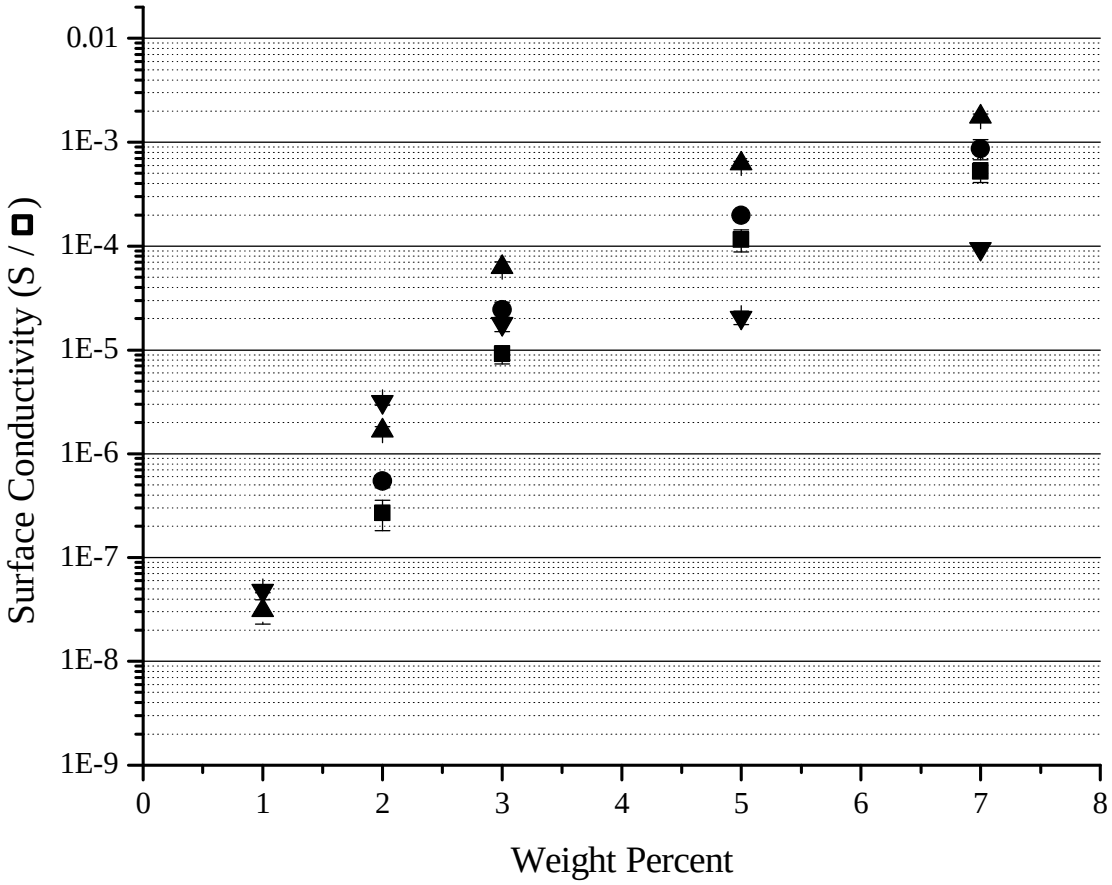


Figure 5.2. Surface conductivity of nanocomposites at varying concentrations and processing conditions using DB (-■-), 5X (-●-), 10X (-▲-), and 15X (-▼-) processing

Values for surface resistivity were not measured for the DB and the 5X nanocomposites at a concentration of 1 wt% CNT within the limits of measuring capability currently available to us. However, the 15X and 10X $scCO_2$ processed nanocomposites resulted in measured surfaces conductivities of $3.1 \times 10^{-8} \pm 8.1 \times 10^{-9}$ S and $4.8 \times 10^{-8} \pm 2.0 \times 10^{-9}$ S , respectively. More extensive deagglomeration of CNT bundles leads to improved surface conductivity in the samples prepared with 15X and 10X $scCO_2$ processing at lower concentrations than the DB and

5X nanocomposites. The surface conductivities measured at the higher degrees of expansion are comparable to work by Socher et al. [11]. In that work, volume conductivity on the order of $10^{-9}$ S/cm was observed at 1 wt% for Baytubes® polycarbonate nanocomposites prepared using a twin screw micro compounding device. The nanocomposites showed a highly disperse morphology, but shortening of the CNT by 55%. Although the CNT agglomerates are less disperse in the results reported here, the nanocomposites prepared by $scCO_2$ aided melt blending possess enhanced electrical properties due to the presence of longer nanotubes which may connect the agglomerates, promoting the formation of a conductive network. In the report by Socher et al. [11], less damage to the CNTs was realized by using a lower viscosity polycarbonate, leading to an improved conductivity of $10^{-5}$S/cm at 1 wt% Baytubes®. These results further illustrate the importance of retaining the CNT lengths during nanocomposite generation [11].It is recognized that the work by Socher et al. [11] reports bulk conductivity rather than surface conductivity, and therefore further analysis will consider the percolation threshold of the CNT nanocomposites to make a more suitable comparison.

A power law model for electrical percolation was utilized to further analyze the surface conductivity data at low concentrations. The proportionality constant, *B*, percolation threshold, $p_c$, and critical exponent, *t*, are summarized in Table 5.2 for each processing method [24].

Table 5.2. Values fitted from power law electrical percolation threshold model for Baytubes® C150P CNT nanocomposites

| *Sample* | ***B* [S]** | $p_c$ | ***t*** |
|---|---|---|---|
| ***Baytubes® DB*** | $2.7 \times 10^{-6}$ | 1.53 | 3.1 |
| ***Baytubes® 5X*** | $3.4 \times 10^{-6}$ | 1.29 | 3.2 |
| ***Baytubes® 10X*** | $2.5 \times 10^{-6}$ | 1.01 | 3.9 |
| ***Baytubes® 15X*** | $1.99 \times 10^{-6}$ | 0.83 | 2.1 |

The proportionality constant and critical exponents do not convey recognizable trends, but lie within the range of reported values from the literature [27]. The percolation threshold was found to decrease as the extent of $scCO_2$ processing increased. Increasing the $scCO_2$ processing reduces the bulk density of CNT agglomerates, which has been related to more dispersible nanotubes in both polymers and solutions [7, 28]. The less dense CNT agglomerates provide more surface area for polymer interaction during melt compounding, and the greater volume occupied by these bundles increases the agglomerate interaction radius to reduce the distance between CNT connections. These factors contribute to a decrease in the percolation threshold in nanocomposites processed using CNT samples with low bulk densities. The fitted percolation value for the direct blend sample is 1.53 wt% CNT. This is reduced to 0.83 wt% by processing with the $scCO_2$ aided melt blending method for the 15X sample. Castillo et al. [14] report a slightly lower value of 0.61 wt% for the onset of percolation in Baytubes®/ polycarbonate nanocomposites which were generated using a twin screw micro compounding device. The slight decrease in percolation threshold observed in Castillo et al. [14] is likely due to a significant increase in dispersion of the nanofiller resulting from high shear melt compounding. The

increase in dispersion is accompanied by shortening of the CNT by 45%, according to the reported $x_{50}$ value. These results suggest that more complete dispersion of the CNT may be accompanied by the benign deagglomeration of CNT bundles using $scCO_2$ processing, resulting in nanocomposites with lower percolation thresholds.

Increasing degrees of expansion from $scCO_2$ processing led to increased surface conductivities for the nanocomposites prepared at 2 wt% CNT. The lowest surface conductivity of $2.7 \times 10^{-7} \pm 8.6 \times 10^{-8}$ S was measured for the DB sample, compared to $3.2 \times 10^{-6} \pm 2.3 \times 10^{-7}$ S for the 15X sample, indicating nearly an order of magnitude increase in surface conductivity. Although the $scCO_2$ aided melt blending method may enhance the conductivity in CNT nanocomposites compared to the DB method, high shear melt compounding leads to even further improved electrical properties at 2 wt%. At this concentration, Socher et al. [11] report volume conductivities on the order of $10^{-5}$S/cm for Baytubes® nanocomposites prepared with a high viscosity polycarbonate and $10^{-2}$S/cm when mixing with a low viscosity polycarbonate. Beyond this concentration, increases in the volume conductivity are not observed for the nanocomposites prepared by Socher et al. [11].

Above 2 wt%, the Baytubes®15X nanocomposites decrease in surface conductivity compared to the DB, 5X, and 10X samples at 5 and 7 wt% filler. This may be attributed to the large density differential between the polymer pellets and the bulk carbon nanotube powder inducing a settling effect, which becomes noticeable at higher concentrations of filler. Specifically, the polymer pellets settle to the bottom of the feed throat preceding extrusion and induce feed fluctuations to the solids flow region. An attempt was made to mitigate this effect by providing a pseudo- starve feed to the extruder. However, it is suspected that this complication re-emerges along the solids flow region resulting in poor distribution of the CNT throughout the

polymer [29]. Therefore, alternative mixing methods which may improve the quality of the premix, such as using powder polymer, are desired for melt compounding polymer with CNT processed with extensive $scCO_2$ treatment.

The measured surface conductivities of nanocomposites produced using $scCO_2$ aided melt blending are substantially lower than those prepared with high shear melt compounding above 2 wt%. The surface conductivity of nanocomposites prepared by the $scCO_2$ aided melt blending method continue to improve over those generated by direct blending up to 7 wt%, with the 10X samples possessing the most enhanced surface conductivities. These observations are not consistent with the conductivities reported in literature for high shear melt compounded nanocomposites. At 7 wt% CNT, the nanocomposites prepared by the $scCO_2$ aided melt blending method begin to approach the plateau conductivity observed by others at significantly lower concentrations [11, 14]. This implies that the benefits of maintaining the CNT aspect ratio are overshadowed by the importance of dispersion at higher nanofiller concentrations.

### 5.4.1 Optical Microscopy

Optical microscopy was employed to relate the micro scale dispersion to the electrical properties of the CNT nanocomposites at select concentrations. The morphology of plaques prepared with 1 wt % and 3 wt% CNT are investigated to analyze the onset of percolation and the decrease in conductivity for the 15X $scCO_2$ processed nanocomposite, respectively. The agglomerate sizes and states of microscale dispersion are evident in representative images at these concentrations, which are compared in Figure 5.3. Image analysis of these samples yields the area fraction of aggregates with respect to the total area analyzed ($A_A$), which is summarized for the different processing conditions in Table 5.3.

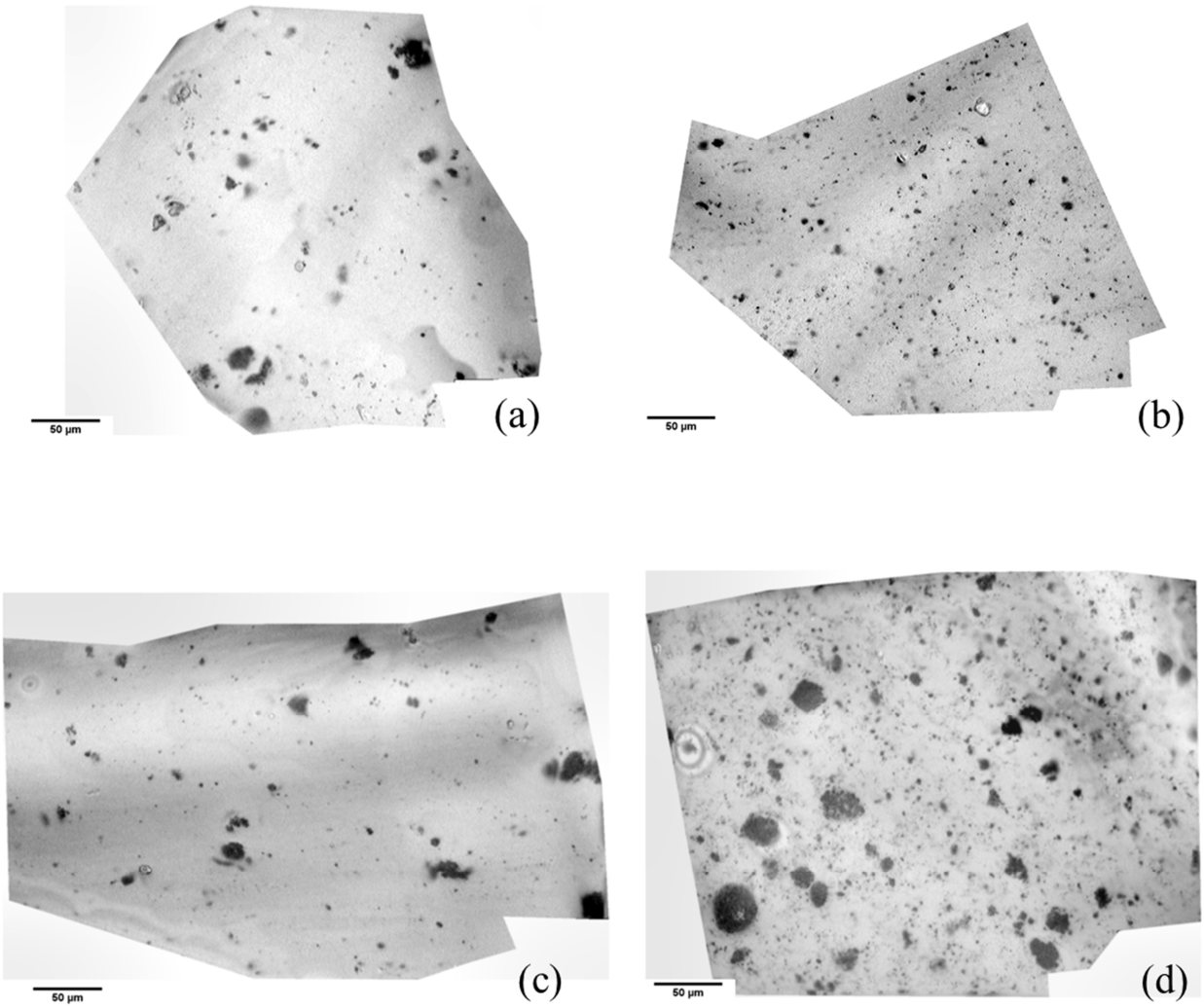


Figure 5.3. Representative 2D Optical micrographs of Polycarbonate / Baytubes® nanocomposites at 1 wt% CNT loading without $scCO_2$treatment (a) and with 15X $scO_2$ treatment (b) and at 3 wt% CNT loading without $scCO_2$treatment (c) and with 10X $scCO_2$ treatment (d)

Table 5.3. Image analysis results of images in Figure 5.3. $A_A$ specifies the fraction of area occupied by agglomerates larger than 5 μm in circle equivaleant diameter with respect to the total area sampled

| | Concentration | DB | 5X | 10X | 15X |
|---|---|---|---|---|---|
| $A_A$ [%] | 1 wt % | 12.5 | 5.6 | 2.9 | 1.9 |
| | 3 wt % | 24.5 | 8.2 | 7.8 | 8.3 |

The $scCO_2$ processing of CNT agglomerates led to better dispersion in nanocomposites prepared by the $scCO_2$ aided melt blending method at a concentration of 1 wt% CNT. Increasing degrees of expansion in $scCO_2$ processing led to improved dispersion, illustrated by decreasing $A_A$ in Table 5.3. These results correlates well with other work where CNT possessing low bulk densities rae more dispersible than more dense agglomerates, as suggested before [7, 28]. The DB sample consists of 12.5% aggregates, compared to 1.9% for the 15X sample. This is further demonstrated in Figure 5.3 (a) and (b) where the DB sample shows large regions void of CNT and larger agglomerates than the 15X nanocomposite. The results correlate with the measured electrical properties, where surface conductivity was observed for samples prepared with 10X and 15X degrees of expansion using the $scCO_2$ aided melt blending method, but not for the DB and 5X samples.

The efficiency of dispersing CNT agglomerates in polycarbonate by high shear melt compounding has been reported in the literature through optical microscopy [11, 22]. Socher et al. [11] reported results from optical microscopy of 1 wt% Baytubes® PC/CNT nanocomposites prepared with twin screw microcompounding. The authors report the $A_A$ to be 0.3% or lower, compared to 1.9% $A_A$ observed for the 15X sample in the current analysis. This indicates significantly better dispersion due to high shear melt compounding than that of the $scCO_2$ aided melt blending method. It is important to mention that the sections analyzed in the work by

Socher et al. [11] were 5 μm thick, which are 10 times thicker than samples analyzed in the current study. This suggests that the disparity in the extent of dispersion is underestimated by a direct comparison of $A_A$. Considering the large difference in dispersion, it is remarkable that the electrical conductivity of the 15X $scCO_2$ processed sample is comparable to the findings of Socher et al. [11] at 1 wt% (Section 5.4). This is due to the processing of the CNT using the $scCO_2$ aided melt blending method, in which negligible damage to carbon nanotube lengths are observed, compared to the destructive processing evident from high shear mixing. The longer nanotubes observed in composites processed with the $scCO_2$ aided melt blending method contribute to improve the electrical conductivity of these nanocomposites. These results demonstrate the importance of maintaining longer carbon nanotubes during nanocomposite processing.

The area fraction of aggregates at 3 wt% decreases as a function of increasing $scCO_2$ processing to a minimum of 7.8% for the 10X nanocomposite in Table 5.3. The highest degree of expansion, 15X, shows a slight increase in the agglomeration of CNT to 8.3% by area, indicating inferior dispersion of CNT compared to the 10X and 5X samples. These results support the findings in Section 5.4 where a decrease in surface conductivity was observed for this sample. The drop in surface conductivity was attributed to the low bulk density 15X sample which led to melt processing issues during compounding, resulting in worse distribution of CNTs throughout the polymer. The 3 wt% DB sample in Figure 5.3 (c) is notably void of CNT agglomerates considering the large $A_A$ value reported in Table 5.3 (24.5%). Several of the sections analyzed for the 3 wt% DB sample contain very large agglomerates (500 μm or larger) which would encompass the entire image if included in Figure 5.3. Therefore, we chose to present representative images illustrating the apparent lack of CNTs dispersion in this sample compared

to the 10X nanocomposite, indicating that most of the CNTs are entrained in very large agglomerates.

### 5.4.2 Transmission Electron Microscopy

The qualitative dispersion of nanotubes in the compression molded plaques was investigated for samples prepared at 1 and 3 wt% CNT loading using TEM. The images discussed in this section are characteristic of many samples micrographs which were analyzed to ensure adequate representation. Drastically different states of dispersion were observed due to the processing method, as illustrated in representative micrographs in Figure 5.4.

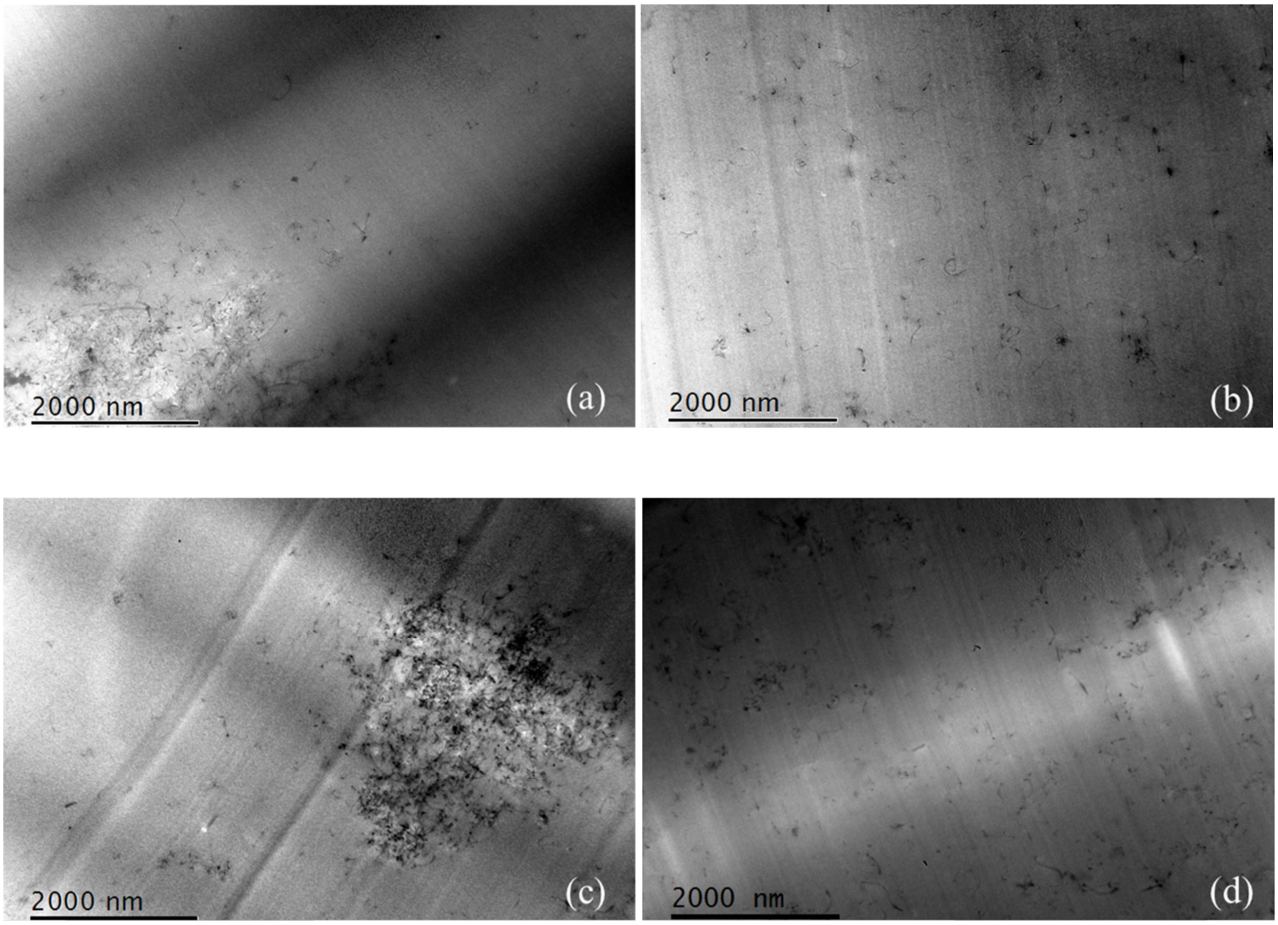


Figure 5.4. Representative TEM images of 1 wt% PC / Baytubes® nanocomposites with (a) no $scCO_2$ treatment (DB), (b)15X $scCO_2$ treatment, and 3 wt% with (c) no $scCO_2$ treatment (DB), and (d) 10X $scCO_2$ treatment at 9,600x magnificaiton

Images generated from the 1 wt% nanocomposites prepared by direct melt blending contained several large aggregates, (Figure 5.4 (a)), and fewer CNTs in the polymer rich region. As the degree of $scCO_2$processing increased, smaller aggregates were observed and more CNTs were detected in the polymer rich region. The most disperse morphology was observed for the 1 wt% $scCO_2$ aided melt blended sample with 15X $scCO_2$ processing, illustrated in Figure 5.4 (b). Fewer aggregates were observed in these images, with large fractions of CNTs in the polymer rich region which may be able to partake in the surface conductivity. These observations support the optical microscopy and surface conductivity results, indicating that more extensive deagglomeration of CNT bundles with $scCO_2$ processing yields greater CNT dispersion and nanocomposites with improved surface conductivity.

Analysis of TEM micrographs for nanocomposites prepared with 3 wt% CNT indicates that increasing degrees of expansion for the $scCO_2$ aided melt blending method lead to improved nanoscale dispersion from DB to 10X $scCO_2$ processing. Images obtained from the direct melt blended sample contain very large CNT aggregates on the order of several microns in diameter, with fewer CNT dispersed in the polymer matrix. This is illustrated in the representative image in Figure 5.4 (c). Several smaller aggregates were observed in the images obtained from plaques generated using 10X $scCO_2$ processing, with more carbon nanotubes distributed throughout the polymer matrix (Figure 5.4 (d)). TEM images of nanocomposites prepared with 15X $scCO_2$processing displayed large aggregates and generally poor distribution of the CNT throughout the polymer, further supporting the results from surface conductivity and optical microscopy analyses.

### 5.4.3 Rheology

Rheological measurements were carried out to develop a correlation between bulk morphology and the rheological response of the materials. Characteristic trends in the complex viscosity and storage moduli were investigated to determine the presence of mechanically percolated networks in the nanocomposites. An increase in the low frequency complex viscosity was observed as a function of increasing degree of $scCO_2$ processing for nanocomposites with 1 wt% CNT, which is illustrated in Figure 5.5 (a).

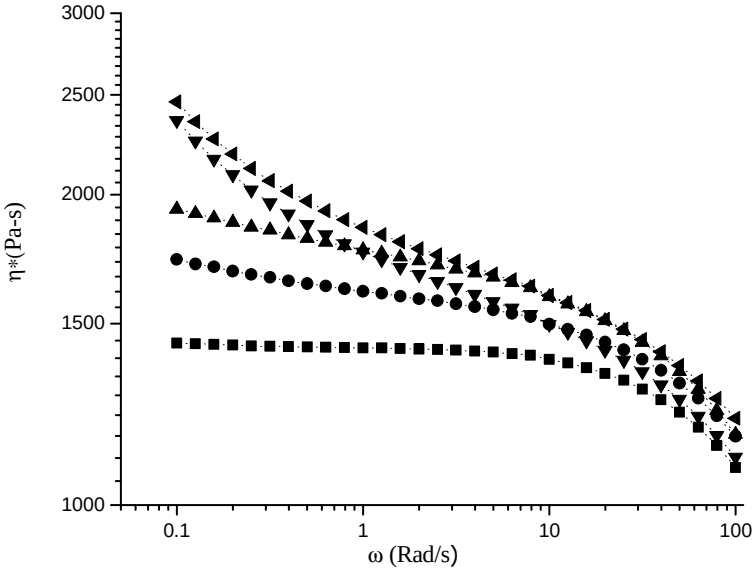


(a)

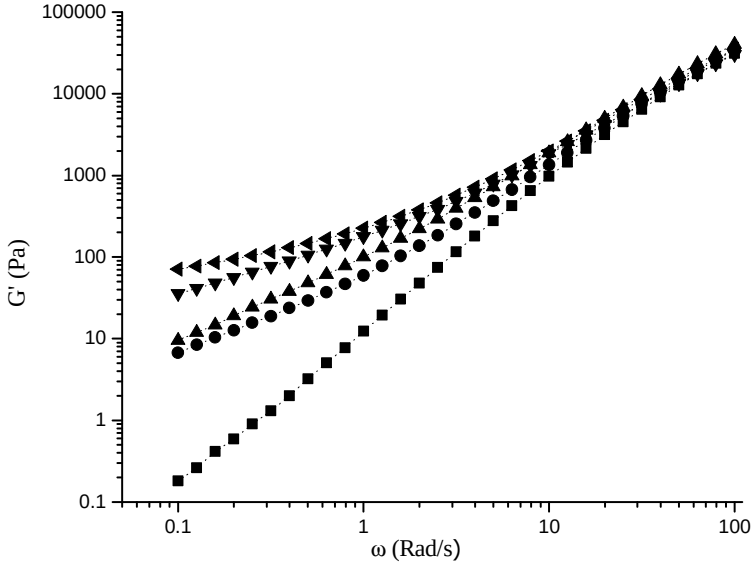


(b)

Figure 5.5. Rheological properties of PC / Baytubes® nanocomposites at 1 wt% with varying degrees of $scCO_2$ treatment at 260°C. Complex viscosity (a) and storage modulus (b) are shown of Pure Bayer PC (-■-), 3% DB (-●-), 3% 5X $scCO_2$ (-▲-), 3% 10X $scCO_2$ (-▼-), and 15X $scCO_2$ (-◀-). Reported measurements are the average of three experiments with error less than 3% of the indicated values.

Previous reports suggest that an increase in the low frequency complex viscosity indicates an increase in the volume fraction of disperse filler [16, 18, 21, 30]. Therefore, improved CNT

dispersion is observed with increasing degrees of $scCO_2$ processing from DB to 15X. Furthermore, an increase in the shear thinning behavior below 1 rad/s is observed in the transition between the 5X and 10X samples, indicating the onset of a rheologically percolated network [31]. The storage moduli increase as a function of increasing degrees of expansion in the low frequency region, demonstrating a greater fraction of dispersed nanofiller in the nanocomposites processed with $scCO_2$ [30]. The onset of mechanical percolation may be observed in the storage modulus as well as the complex viscosity [32]. The frequency dependence of G' below 1 rad/s (Figure 5.5 (b)) decreases for nanocomposites processed with increasing degrees of $scCO_2$ processing. This is particularly evident in the transition from the 5X and 10X nanocomposites, illustrated by the onset of a more pronounced "plateau" in the storage modulus at low frequencies. This observation has been attributed to the formation of a mechanically percolated network, which correlates well with the analysis of the complex viscosity [32]. The onset of rheological percolation may not be directly connected to the electrical percolation threshold, as has been reported by others [16, 33]. However, the transition from liquid-like to solid-like behavior evident in the complex viscosity and storage moduli data correlates well with the onset of electrical percolation in the current study.

The complex viscosities and storage moduli of the 3 wt% samples were analyzed to determine the bulk morphology of these nanocomposites, as illustrated in Figure 5.6 (a) and (b) respectively.

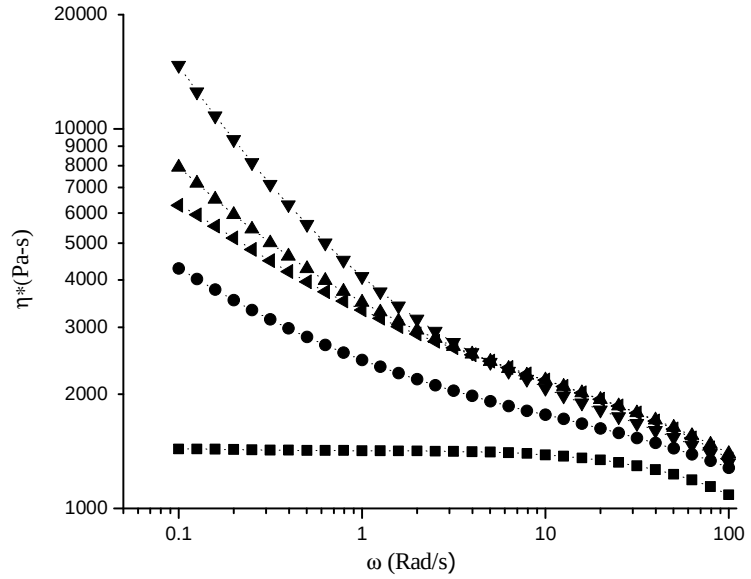


(a)

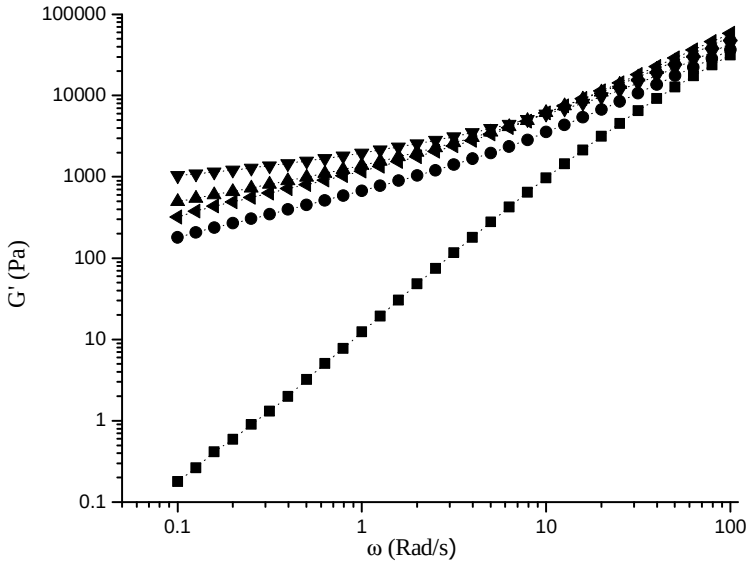


(b)

Figure 5.6. Rheological properties of PC / Baytubes® nanocomposites at 3 wt% with varying degrees of $scCO_2$ treatment at 260°C. Complex viscosity (a) and storage modulus (b) are shown of Pure Bayer PC (-■-), 3% DB (-●-), 3% 5X $scCO_2$ (-▲-), 3% 10X $scCO_2$ (-▼-), and 15X $scCO_2$ (-◀-).Reported measurements are the average of three experiments with error less than 3% of the indicated values.

Similar trends were observed in the complex viscosities and storage moduli of the 3wt % samples as compared to the 1 wt% nanocomposites. The complex viscosity (Figure 5.6(a)) shows a general increase in the absolute value and shear thinning behavior for increasing degrees of expansion below 1 rad/s, indicating improved dispersion of the CNT agglomerates up to 10X $scCO_2$ processing [16, 30]. The complex viscosity and storage modulus of the 15X sample decrease below that of the 5X sample at 3 wt% suggesting a reduction in CNT dispersion. It is suspected that this results from a decrease in the dispersion of CNT according to the increased area fraction of aggregates from optical microscopy.

## 5.5 Conclusions

The method previously developed in our lab for the benign deagglomeration of CNT bundles was applied to the $scCO_2$ aided melt blending method to produce polycarbonate nanocomposites with improved surface conductivity while retaining the CNT aspect ratio [20]. A surface conductivity of $4.8 \times 10^{-8} \pm 2.0 \times 10^{-9}$ S was observed for samples prepared with the $scCO_2$ aided melt blending at 15X $scCO_2$ processing, corresponding to a percolation threshold of 0.83 wt%. A rheological network was observed at 1 wt% CNT in the nanocomposites prepared with 10X and 15X $scCO_2$ processing, evidenced by the complex viscosity and storage modulus versus frequency data. Enhanced dispersion was observed for the $scCO_2$ processed samples at 1 wt% using optical microscopy, yielding $A_A$ values of 12.5% with DB processing and 1.9% with 15X $scCO_2$ processing. The percolation threshold of the nanocomposite prepared with 15X $scCO_2$ processing approaches values reported in literature for similar systems processed by high shear melt compounding [11, 14]. However, the dispersion observed in the nanocomposite prepared by 15X $scCO_2$ processing followed by melt blending in a single screw extruder is drastically worse than that of high shear melt compounded nanocomposites, where $<0.3\%$ $A_A$ has been reported [11]. In that work, a 45% reduction in CNT lengths was reported. Given the comparative onset of percolation for these samples, the disparity in the measured dispersion highlights the importance of maintaining longer carbon nanotubes during nanocomposite processing, rather than focusing on dispersion alone. By combining the benign $scCO_2$ deagglomeration of CNT aggregates with higher shear melt compounding methods, the benefits of these two techniques could yield nanocomposites with ultra-low electrical percolation thresholds.

## 5.6 Acknowledgements

The authors would like to acknowledge Bayer Material Science for donating the Baytubes® C150P and Makrolon 2608, respectively, as well as providing funding for this study in its early stages. In addition, the authors acknowledge use of the facilities at the Nanocscale Characterization and Fabrication Laboratory at Virginia Polytechnic Institute for the TEM and optical images.

## References


[1] Q.W. Li, C.H. Liu, X.S. Wang, and S.S. Fan, "Measuring the thermal conductivity of individual carbon nanotubes by the Raman shift method," *Nanotechnology*, vol. 20, 2009.

[2] T.W. Ebbesen, H.J. Lezec, H. Hiura, J.W. Bennett, H.F. Ghaemi, and T. Thio, "Electrical conductivity of individual carbon nanotubes," *Nature*, vol. 382, 1996.

[3] J.P. Salvetat, A.J. Kulik, J.M. Bonard, G.A.D. Briggs, T. Stockli, K. Metenier, S. Bonnamy, F. Beguin, N.A. Burnham, and L. Forro, "Elastic modulus of ordered and disordered multiwalled carbon nanotubes," *Advanced Materials*, vol. 11, 1999.

[4] J.P. Salvetat, G.A.D. Briggs, J.M. Bonard, R.R. Bacsa, A.J. Kulik, T. Stockli, N.A. Burnham, and L. Forro, "Elastic and shear moduli of single-walled carbon nanotube ropes," *Physical Review Letters*, vol. 82, 1999.

[5] J.-M. Thomassin, I. Huynen, R. Jerome, and C. Detrembleur, "Functionalized polypropylenes as efficient dispersing agents for carbon nanotubes in a polypropylene matrix; application to electromagnetic interference (EMI) absorber materials," *Polymer*, vol. 51, 2010.

[6] J.G. Smith Jr, D.M. Delozier, J.W. Connell, and K.A. Watson, "Carbon nanotube-conductive additive-space durable polymer nanocomposite films for electrostatic charge dissipation," *Polymer*, vol. 45, 2004.

[7] B. Krause, M. Mende, P. Potschke, and G. Petzold, "Dispersability and particle size distribution of CNTs in an aqueous surfactant dispersion as a function of ultrasonic treatment time," *Carbon*, vol. 48, 2010.

[8] D.R. Paul and L.M. Robeson, "Polymer nanotechnology: Nanocomposites," *Polymer*, vol. 49, 2008.

[9] I. Alig, P. Potschke, D. Lellinger, T. Skipa, S. Pegel, G.R. Kasaliwal, and T. Villmow, "Establishment, morphology and properties of carbon nanotube networks in polymer melts," *Polymer*, vol. 53, 2012.

[10] K. Menzer, B. Krause, R. Boldt, B. Kretzschmar, R. Weidisch, and P. Pötschke, "Percolation behaviour of multiwalled carbon nanotubes of altered length and primary agglomerate morphology in melt mixed isotactic polypropylene-based composites," *Composites Science and Technology*, vol. 71, 2011.

[11] R. Socher, B. Krause, M.T. Muller, R. Boldt, and P. Potschke, "The influence of matrix viscosity on MWCNT dispersion and electrical properties in different thermoplastic nanocomposites," *Polymer*, vol. 53, 2012.

[12] C. McClory, P. Potschke, and T. McNally, "Influence of Screw Speed on Electrical and Rheological Percolation of Melt-Mixed High-Impact Polystyrene/MWCNT Nanocomposites," *Macromolecular Materials and Engineering*, vol. 296, 2011.

[13] T. Villmow, B. Kretzschmar, and P. Potschke, "Influence of screw configuration, residence time, and specific mechanical energy in twin-screw extrusion of polycaprolactone/multi-walled carbon nanotube composites," *Composites Science and Technology*, vol. 70, 2010.

[14] F.Y. Castillo, R. Socher, B. Krause, R. Headrick, B.R. Grady, R. Prada-Silvy, and P. Potschke, "Electrical, mechanical, and glass transition behavior of polycarbonate-based nanocomposites with different multi-walled carbon nanotubes," *Polymer*, vol. 52, 2011.

[15] J. Guo, Y. Liu, R. Prada-Silvy, Y. Tan, S. Azad, B. Krause, P. Pötschke, and B.P. Grady, "Aspect ratio effects of multi-walled carbon nanotubes on electrical, mechanical, and thermal properties of polycarbonate/MWCNT composites," *Journal of Polymer Science Part B: Polymer Physics*, 2013.

[16] P. Pötschke, T. Villmow, and B. Krause, "Melt mixed PCL/MWCNT composites prepared at different rotation speeds: Characterization of rheological, thermal, and electrical properties, molecular weight, MWCNT macrodispersion, and MWCNT length distribution," *Polymer*, vol. 54, 2013.

[17] G.R. Kasaliwal, S. Pegel, A. Goldel, P. Potschke, and G. Heinrich, "Analysis of agglomerate dispersion mechanisms of multiwalled carbon nanotubes during melt mixing in polycarbonate," *Polymer*, vol. 51, 2010.

[18] C. Chen, M. Bortner, J.P. Quigley, and D.G. Baird, "Using supercritical carbon dioxide in preparing carbon nanotube nanocomposite: Improved dispersion and mechanical properties," *Polymer Composites*, vol. 33, 2012.

[19] E. Gulari, K. Rangaramanujam, and G.K. Serhatkulu, "Method of delaminating aggregated particles with a coating agent in a substantially supercritical fluid," US7387749, 2008.

[20] J.P. Quigley, "Advanced Thermoplastic Nanocomposite Processing Using an Improved Supercritical Carbon Dioxide Aided Melt Blending Method,"2014.

[21] C. Chen, J. Samaniuk, D.G. Baird, G. Devoux, M.Q. Zhang, R.B. Moore, and J.P. Quigley, "The preparation of nano-clay/polypropylene composite materials with improved properties using supercritical carbon dioxide and a sequential mixing technique," *Polymer*, vol. 53, 2012.

[22] T. McNally and P. Pötschke, *Polymer-Carbon Nanotube Composites: Preparation, Properties And Applications*. 2011: Elsevier Science.

[23] B. Krause, R. Bolcit, and P. Potschke, "A method for determination of length distributions of multiwalled carbon nanotubes before and after melt processing," *Carbon*, vol. 49, 2011.

[24] D. Stauffer and A. Aharony, *Introduction To Percolation Theory*. 1994: Taylor & Francis.

[25] P. Pötschke, B. Krause, S.T. Buschhorn, U. Köpke, M.T. Müller, T. Villmow, and K. Schulte, "Improvement of carbon nanotube dispersion in thermoplastic composites using a three roll mill at elevated temperatures," *Composites Science and Technology*, vol. 74, 2013.

[26] A.V. Kyrylyuk and P. van der Schoot, "Continuum percolation of carbon nanotubes in polymeric and colloidal media (vol 105, pg 8221, 2008)," *Proceedings of the National Academy of Sciences of the United States of America*, vol. 105, 2008.

[27] W. Bauhofer and J.Z. Kovacs, "A review and analysis of electrical percolation in carbon nanotube polymer composites," *Composites Science and Technology*, vol. 69, 2009.

[28] K. Menzer, B. Krause, R. Boldt, B. Kretzschmar, R. Weidisch, and P. Potschke, "Percolation behaviour of multiwalled carbon nanotubes of altered length and primary agglomerate morphology in melt mixed isotactic polypropylene-based composites," *Composites Science and Technology*, vol. 71, 2011.

[29] R. Rothon, *Particulate-filled Polymer Composites*. 2003: Rapra Technology.

[30] A.J. Poslinski, M.E. Ryan, R.K. Gupta, S.G. Seshadri, and F.J. Frechette, "Rheological Behavior of Filled Polymeric Systems .1. Yield Stress and Shear-Thinning Effects," *Journal of Rheology*, vol. 32, 1988.

[31] P. Potschke, M. Abdel-Goad, I. Alig, S. Dudkin, and D. Lellinger, "Rheological and dielectrical characterization of melt mixed polycarbonate-multiwalled carbon nanotube composites," *Polymer*, vol. 45, 2004.

[32] F.M. Du, R.C. Scogna, W. Zhou, S. Brand, J.E. Fischer, and K.I. Winey, "Nanotube networks in polymer nanocomposites: Rheology and electrical conductivity," *Macromolecules*, vol. 37, 2004.

[33] M. Abdel-Goad and P. Potschke, "Rheological characterization of melt processed polycarbonate-multiwalled carbon nanotube composites," *Journal of Non-Newtonian Fluid Mechanics*, vol. 128, 2005.

## 5.7 Conclusions from this research

1. The supercritical carbon dioxide aided melt blending method was successfully applied to nanocomposites of Nylon 6 and organically modified montmorillonite with the potential for the polymer to interact favorably with the clay surface. Increases in the Young's modulus were obtained for composites processed with $scCO_2$ at 4.9 wt% and 7.6 wt% compared to direct blended samples, with 47% and 54% increases compared to the virgin matrix, respectively. The reported mechanical properties were competitive with values reported in the literature for twin screw melt compounded nanocomposites [1]. The improvements in dispersion and mechanical properties indicate the importance of processing nanocomposites with polymers that can interact with the clay surface.

2. The separation of MWCNT agglomerates via $scCO_2$ processing was enhanced while maintaining the carbon nanotubes' aspect ratios. Greater extents of deagglomeration of the CNT were observed compared to previous reports, generating agglomerates <8 μm in diameter for both Nanocyl™ NC-7000 and Baytubes® C 150 P MWCNT. The most complete deagglomeration of CNTs using the current apparatus was accomplished with negligible damage to the CNTs, whereas other deagglomeration methods significantly shorten the CNTs (up to 70% [2]). The effect of processing conditions on the extent of deagglomeration from $scCO_2$ was analyzed using thermodynamic principles. Significantly lower processing temperatures, pressures, and soak times were obtained in the current study, leading to a 40°C

reduction in temperature, 12 MPa reduction in pressure, and 23 hour reduction in processing time compared to recent work [3].

3. The $scCO_2$ aided melt blending method was used to produce polycarbonate nanocomposites with improved electrical conductivity while retaining the CNT aspect ratio. A surface conductivity of $4.8 \times 10^{-8}$ S was observed for samples prepared at 1 wt% Baytubes® C 150 P CNTs with the $scCO_2$ aided melt blending at 15X $scCO_2$ processing, corresponding to a percolation threshold of 0.83 wt%. The percolation threshold of the nanocomposite prepared with 15X $scCO_2$ processing approaches values reported in literature for similar systems processed by high shear melt compounding. However, a low degree of dispersion was observed compared to nanocomposites prepared by high shear melt compounding [4]. These results illustrate the importance of maintaining longer carbon nanotubes during nanocomposite processing.

## 5.8 Recommendations for future work

1. Increased ductility was observed in select Nylon 6/OMMT nanocomposites, evident from the elongation at break values in Chapter 3. In particular, nanocomposites prepared at 3 wt% OMMT using $scCO_2$ processing showed increased elongation at break compared to the direct melt blended samples. Future work should investigate the effect of $scCO_2$ processing on crystalline morphology of low concentration nylon 6/OMMT nanocomposites. Furthermore, this effect suggests the potential for producing drawn nanocomposites with improved mechanical properties at higher concentrations than previously expected. Therefore, it is suggested that future work investigate the effect of drawing Nylon 6/organoclay nanocomposites at low concentrations (< 5 wt% OMMT) generated by the $scCO_2$ aided melt blending method. It is suspected that drawing the nanocomposites will yield more preferential orientation of the nanoclay, which may yield further enhancement of the mechanical properties in Nylon/OMMT nanocomposites.

2. In Chapter 3, the mechanical properties of Nylon 6/OMMT nanocomposites processed with the $scCO_2$ aided melt blending method failed to improve beyond 7.6 wt% nanofiller compared to samples prepared with direct melt blending. The morphological results suggest that the clays collapse after $scCO_2$ processing in the melt compounding step at higher concentrations. It is desired to understand where and how this collapse occurs. Therefore, it would be of interest to stop the extruder mid-process and analyze the morphology of the nanocomposite along flights of the compounding screw. If it can be determined where and how this collapse occurs, it

might be possible to feed the $scCO_2$ processed nanoclay to the extruder at another location and improve the mechanical properties beyond 7.6 wt% with the $scCO_2$ aided melt blending method.

3. It is desired to overcome the high concentration barrier to nanocomposite mechanical property improvement with the $scCO_2$ aided melt blending method in Nylon 6/organoclay nanocomposites in Chapter 3. By directly injecting the nanoclay/$scCO_2$ mixture into the melt of the extruder, the collapse to the clays might be avoided. Alternatively, combining the $scCO_2$ processing of nanoclay with twin screw or other high shear melt compounding process may yield nanocomposites with improved mechanical properties beyond the concentrations analyzed in the current work.

4. The current apparatus utilized in Chapter 4 consists of a large capillary (6.35 mm diameter, 200 mm length) between the pressure vessels to aid in the deagglomeration of primary MWCNT bundles. It is suspected that more extensive deagglomeration might be obtained by including a narrow capillary followed by a narrow expansion nozzle to increase the shear effects experienced by CNT bundles during rapid expansion.

5. The apparatus described in Chapter 4 involves a high pressure primary vessel and a secondary low pressure vessel to which the supercritical suspension of $scCO_2$ and CNTs is released into. It would be desirable to operate this second vessel under

vacuum rather than ambient pressure to increase the change in pressure experienced by the suspension to improve the deagglomeration of the primary MWCNT bundles.

6. A more thorough treatment of the analysis in Chapter 4 may be obtained by measuring or modeling the pressure drop experienced by the supercritical $CO_2$ and MWCNT mixture from the primary vessel to the capillary and the capillary to the secondary vessel. This effort may help predict the effect of temperature, pressure, capillary length, nozzle geometry, and other variables on the deagglomeration of CNT bundles.

7. The findings of Chapter 4 indicate that the $scCO_2$ processing of CNT agglomerates prevents damage to the aspect ratio of carbon nanotubes while dispersing the nanomaterial effectively. Therefore, applying a cost analysis to the scale up of this process would be of interest. The operational costs and equipment costs may be evaluated against the CNT suppliers' desire (an opportunity cost) to maintain the aspect ratio of the nanomaterial.

8. The CNT powder generated by the $scCO_2$ process in Chapter 4 possessed very low bulk densities. During the nanocomposite generation in Chapter 5, issues arose from the solids feed section of the extruder resulting in inefficient dispersion of the CNTs in polycarbonate. This resulted in decreased electrical properties when using CNT powder with a bulk density below 10 $kg/m^3$. It is suggested that future work should investigate the use of polymer powder to improve the quality of the PC/CNT

premix. This may permit the use of the very low bulk density CNT powder, such as the <3 kg/$m^3$samples reported from Chapter 4.

9. The $scCO_2$ aided melt blending method maintains the aspect ratio of CNT as reported in Chapter 5. However, greater dispersion of CNT agglomerates is desired in nanocomposites generated using this technique. High shear melt compounding has proven to drastically reduce the aspect ratio of the CNTs during deagglomeration of the bundles, but results in a thoroughly disperse CNT morphology in nanocomposites. Therefore, it is suggested that future work incorporate the $scCO_2$ treatment of CNT in combination with either twin screw extruders or other higher shear mixing devices to yield nanocomposites with high levels of dispersion without damaging the CNT. By deagglomerating the CNTs with $scCO_2$ processing followed by higher shear melt compounding with polymer, it is suspected that further rupture of dry agglomerates will be either reduced or avoided completely, yielding nanocomposites with superior electrical properties.

## References


[1] T.D. Fornes, P.J. Yoon, H. Keskkula, and D.R. Paul, "Nylon 6 nanocomposites: the effect of matrix molecular weight," *Polymer*, vol. 42, 2001.

[2] B. Krause, R. Bolcit, and P. Potschke, "A method for determination of length distributions of multiwalled carbon nanotubes before and after melt processing," *Carbon*, vol. 49, 2011.

[3] M.B. Chen Chen, John P. Quigley, Donald G. Baird, "Using Supercritical Carbon Dioxide in Preparing Carbon Nanotube Nanocompsite: Improved Dispersion and Mechanical Properties," *Polymer Composites*, 2012.

[4] F.Y. Castillo, R. Socher, B. Krause, R. Headrick, B.R. Grady, R. Prada-Silvy, and P. Potschke, "Electrical, mechanical, and glass transition behavior of polycarbonate-based nanocomposites with different multi-walled carbon nanotubes," *Polymer*, vol. 52, 2011.

## Appendix A: X-ray Diffraction Data

Table A.1 WAXD data from Nylon 6/ Cloisite 30B injection molded nanocomposites

| | Intensity (abritrary units) | | | | | | | | | | | |
|---|---|---|---|---|---|---|---|---|---|---|---|---|
| 2 θ | Cloisite 30B | Nylon 6 | 1% DB | 1% scCO2 | 3% DB | 3% sc CO2 | 5% DB | 5% sc CO2 | 7% DB | 7% scCo2 | 10% DB | 10% scCO2 |
| 2.179 | 796 | 656 | 727 | 706 | 647 | 674 | 719 | 751 | 917 | 801 | 717 | 884 |
| 2.246 | 700 | 582 | 719 | 724 | 578 | 596 | 607 | 639 | 675 | 677 | 750 | 789 |
| 2.313 | 692 | 739 | 866 | 722 | 647 | 674 | 785 | 810 | 967 | 801 | 717 | 892 |
| 2.38 | 654 | 759 | 849 | 748 | 703 | 720 | 767 | 830 | 1047 | 940 | 884 | 1016 |
| 2.447 | 726 | 832 | 1003 | 993 | 824 | 756 | 919 | 933 | 1168 | 1048 | 975 | 1182 |
| 2.514 | 529 | 870 | 917 | 928 | 788 | 815 | 998 | 909 | 1186 | 1055 | 975 | 1160 |
| 2.581 | 669 | 842 | 930 | 964 | 735 | 809 | 963 | 910 | 1240 | 1135 | 987 | 1212 |
| 2.648 | 697 | 919 | 870 | 1017 | 830 | 803 | 899 | 1055 | 1185 | 1022 | 933 | 1269 |
| 2.715 | 706 | 933 | 929 | 945 | 799 | 776 | 970 | 951 | 1236 | 1053 | 998 | 1208 |
| 2.782 | 699 | 914 | 928 | 1003 | 721 | 860 | 953 | 891 | 1161 | 1132 | 874 | 1251 |
| 2.849 | 732 | 891 | 919 | 920 | 797 | 920 | 958 | 980 | 1259 | 940 | 1039 | 1369 |
| 2.916 | 699 | 888 | 975 | 956 | 805 | 906 | 999 | 982 | 1267 | 1120 | 1007 | 1304 |
| 2.983 | 659 | 887 | 980 | 914 | 759 | 919 | 974 | 961 | 1342 | 1032 | 973 | 1236 |
| 3.05 | 713 | 823 | 932 | 993 | 881 | 956 | 1079 | 960 | 1203 | 1163 | 824 | 1171 |
| 3.117 | 785 | 938 | 1021 | 929 | 845 | 937 | 951 | 946 | 1322 | 1031 | 1027 | 1293 |
| 3.184 | 781 | 860 | 982 | 979 | 845 | 914 | 993 | 982 | 1198 | 1064 | 860 | 1210 |
| 3.251 | 789 | 905 | 885 | 985 | 829 | 971 | 1031 | 975 | 1125 | 963 | 917 | 1171 |
| 3.318 | 769 | 771 | 1029 | 893 | 793 | 940 | 972 | 944 | 1198 | 1024 | 933 | 1210 |
| 3.385 | 824 | 795 | 881 | 926 | 864 | 841 | 901 | 927 | 1209 | 1066 | 955 | 1155 |
| 3.452 | 921 | 805 | 931 | 899 | 778 | 891 | 869 | 982 | 1206 | 961 | 857 | 1083 |
| 3.519 | 1036 | 868 | 973 | 873 | 856 | 836 | 955 | 896 | 1049 | 977 | 949 | 1065 |
| 3.586 | 1019 | 878 | 849 | 918 | 812 | 892 | 951 | 931 | 1130 | 984 | 913 | 1099 |
| 3.653 | 1151 | 877 | 935 | 982 | 858 | 820 | 940 | 948 | 1159 | 1109 | 983 | 1187 |
| 3.72 | 1366 | 859 | 968 | 966 | 817 | 846 | 926 | 1032 | 1123 | 1007 | 955 | 1207 |

| | | | | | | | | | | | | |
|---|---|---|---|---|---|---|---|---|---|---|---|---|
| 3.787 | 1404 | 957 | 985 | 991 | 909 | 824 | 945 | 1030 | 1190 | 1020 | 892 | 1203 |
| 3.854 | 1587 | 882 | 927 | 953 | 839 | 910 | 1049 | 977 | 1217 | 1053 | 965 | 1167 |
| 3.921 | 1830 | 906 | 1020 | 994 | 873 | 965 | 1030 | 981 | 1107 | 1111 | 972 | 1159 |
| 3.988 | 2047 | 865 | 996 | 957 | 892 | 925 | 978 | 958 | 1151 | 1013 | 1072 | 1142 |
| 4.055 | 2305 | 934 | 984 | 948 | 918 | 1015 | 1001 | 1001 | 1221 | 1047 | 987 | 1210 |
| 4.122 | 2608 | 980 | 959 | 954 | 955 | 926 | 1078 | 1031 | 1248 | 1100 | 952 | 1206 |
| 4.189 | 2986 | 926 | 1018 | 928 | 868 | 889 | 981 | 1016 | 1213 | 1126 | 936 | 1167 |
| 4.256 | 3283 | 919 | 909 | 953 | 917 | 999 | 1022 | 978 | 1197 | 1070 | 971 | 1237 |
| 4.323 | 3735 | 853 | 901 | 1004 | 943 | 883 | 959 | 1009 | 1200 | 1027 | 1051 | 1184 |
| 4.39 | 4251 | 846 | 961 | 934 | 851 | 931 | 885 | 930 | 1169 | 1020 | 989 | 1228 |
| 4.457 | 4847 | 833 | 928 | 859 | 901 | 839 | 872 | 946 | 1105 | 1023 | 895 | 1157 |
| 4.524 | 5262 | 797 | 903 | 857 | 868 | 851 | 894 | 871 | 1132 | 1045 | 946 | 1002 |
| 4.591 | 5876 | 753 | 835 | 791 | 726 | 816 | 938 | 906 | 1100 | 938 | 880 | 1012 |
| 4.658 | 6305 | 729 | 852 | 750 | 790 | 747 | 837 | 902 | 1037 | 965 | 851 | 1032 |
| 4.725 | 6750 | 690 | 812 | 786 | 737 | 759 | 848 | 825 | 1055 | 873 | 869 | 908 |
| 4.792 | 6894 | 762 | 808 | 777 | 786 | 732 | 823 | 857 | 1006 | 921 | 885 | 999 |
| 4.859 | 6890 | 759 | 811 | 780 | 677 | 748 | 755 | 868 | 1034 | 822 | 860 | 983 |
| 4.926 | 6345 | 740 | 827 | 783 | 739 | 758 | 823 | 829 | 1004 | 827 | 843 | 968 |
| 4.993 | 5694 | 674 | 813 | 702 | 685 | 748 | 761 | 819 | 1029 | 880 | 767 | 967 |
| 5.06 | 5112 | 726 | 775 | 780 | 655 | 720 | 735 | 783 | 994 | 832 | 819 | 916 |
| 5.127 | 4408 | 650 | 815 | 682 | 576 | 724 | 713 | 794 | 893 | 843 | 736 | 924 |
| 5.194 | 3795 | 641 | 719 | 691 | 702 | 694 | 768 | 785 | 947 | 817 | 788 | 931 |
| 5.261 | 3243 | 658 | 680 | 707 | 668 | 722 | 745 | 838 | 923 | 808 | 749 | 884 |
| 5.328 | 2770 | 661 | 758 | 739 | 654 | 670 | 719 | 755 | 925 | 840 | 693 | 911 |
| 5.395 | 2356 | 680 | 756 | 702 | 669 | 685 | 742 | 766 | 916 | 826 | 728 | 948 |
| 5.462 | 2058 | 708 | 737 | 725 | 633 | 648 | 721 | 730 | 978 | 787 | 701 | 897 |

| | | | | | | | | | | | | |
|---|---|---|---|---|---|---|---|---|---|---|---|---|
| 5.529 | 1799 | 684 | 817 | 751 | 677 | 692 | 725 | 736 | 962 | 870 | 743 | 925 |
| 5.596 | 1553 | 655 | 727 | 743 | 649 | 654 | 694 | 802 | 906 | 880 | 728 | 923 |
| 5.663 | 1410 | 646 | 748 | 731 | 687 | 725 | 731 | 735 | 917 | 849 | 713 | 918 |
| 5.73 | 1311 | 642 | 738 | 708 | 640 | 721 | 763 | 794 | 935 | 868 | 771 | 906 |
| 5.797 | 1184 | 664 | 729 | 666 | 648 | 747 | 695 | 801 | 950 | 812 | 736 | 890 |
| 5.864 | 1096 | 692 | 710 | 725 | 640 | 671 | 752 | 777 | 971 | 837 | 758 | 889 |
| 5.931 | 989 | 663 | 737 | 731 | 659 | 699 | 719 | 783 | 932 | 800 | 726 | 869 |
| 5.998 | 958 | 637 | 723 | 706 | 633 | 689 | 734 | 787 | 938 | 809 | 769 | 856 |
| 6.065 | 964 | 676 | 743 | 693 | 668 | 703 | 733 | 729 | 975 | 786 | 713 | 964 |
| 6.132 | 899 | 656 | 728 | 687 | 632 | 697 | 679 | 732 | 909 | 805 | 734 | 865 |
| 6.199 | 825 | 703 | 699 | 727 | 687 | 693 | 730 | 748 | 905 | 815 | 699 | 870 |
| 6.266 | 732 | 635 | 724 | 716 | 674 | 643 | 734 | 770 | 882 | 794 | 716 | 878 |
| 6.333 | 710 | 635 | 755 | 692 | 625 | 661 | 728 | 769 | 961 | 801 | 724 | 904 |
| 6.4 | 726 | 682 | 759 | 676 | 629 | 681 | 713 | 756 | 950 | 793 | 715 | 859 |
| 6.467 | 658 | 668 | 717 | 750 | 671 | 717 | 695 | 737 | 893 | 788 | 717 | 937 |
| 6.534 | 732 | 646 | 731 | 698 | 652 | 689 | 719 | 754 | 936 | 829 | 726 | 935 |
| 6.601 | 687 | 634 | 717 | 673 | 635 | 700 | 764 | 746 | 922 | 791 | 692 | 887 |
| 6.668 | 688 | 669 | 728 | 730 | 619 | 672 | 732 | 749 | 913 | 822 | 736 | 846 |
| 6.735 | 716 | 654 | 772 | 717 | 678 | 686 | 733 | 767 | 906 | 802 | 725 | 882 |
| 6.802 | 715 | 663 | 732 | 687 | 649 | 682 | 750 | 759 | 915 | 790 | 721 | 931 |
| 6.869 | 693 | 658 | 717 | 708 | 643 | 677 | 757 | 739 | 921 | 845 | 699 | 872 |
| 6.936 | 652 | 639 | 716 | 704 | 651 | 656 | 681 | 756 | 934 | 811 | 742 | 854 |
| 7.003 | 728 | 678 | 713 | 722 | 663 | 669 | 712 | 768 | 907 | 826 | 691 | 879 |
| 7.07 | 731 | 635 | 743 | 736 | 655 | 724 | 732 | 741 | 912 | 791 | 734 | 925 |
| 7.137 | 742 | 673 | 784 | 678 | 669 | 729 | 733 | 741 | 945 | 774 | 705 | 884 |
| 7.204 | 692 | 676 | 711 | 707 | 681 | 763 | 788 | 749 | 961 | 817 | 794 | 908 |

| | | | | | | | | | | | | |
|---|---|---|---|---|---|---|---|---|---|---|---|---|
| 7.338 | 701 | 686 | 745 | 731 | 665 | 738 | 749 | 778 | 893 | 798 | 737 | 949 |
| 7.405 | 667 | 692 | 759 | 742 | 674 | 715 | 710 | 794 | 920 | 808 | 746 | 920 |
| 7.472 | 740 | 675 | 742 | 747 | 636 | 718 | 709 | 759 | 942 | 815 | 721 | 888 |
| 7.539 | 711 | 615 | 750 | 701 | 642 | 686 | 753 | 787 | 941 | 815 | 699 | 861 |
| 7.606 | 691 | 677 | 706 | 700 | 652 | 739 | 767 | 762 | 921 | 795 | 709 | 872 |
| 7.673 | 674 | 668 | 729 | 734 | 629 | 692 | 720 | 735 | 934 | 792 | 741 | 910 |
| 7.74 | 692 | 648 | 724 | 703 | 697 | 698 | 742 | 737 | 993 | 800 | 728 | 888 |
| 7.807 | 739 | 672 | 752 | 697 | 633 | 685 | 736 | 759 | 915 | 817 | 696 | 914 |
| 7.874 | 697 | 685 | 738 | 718 | 655 | 663 | 724 | 780 | 914 | 790 | 715 | 907 |
| 7.941 | 703 | 652 | 736 | 684 | 638 | 682 | 700 | 724 | 924 | 809 | 735 | 887 |
| 8.008 | 679 | 684 | 782 | 727 | 663 | 671 | 714 | 756 | 920 | 837 | 778 | 898 |
| 8.075 | 697 | 680 | 736 | 743 | 637 | 687 | 756 | 755 | 896 | 789 | 747 | 889 |
| 8.142 | 737 | 672 | 728 | 733 | 636 | 723 | 724 | 767 | 921 | 798 | 686 | 937 |
| 8.209 | 709 | 666 | 739 | 727 | 665 | 736 | 683 | 765 | 958 | 796 | 703 | 938 |
| 8.276 | 707 | 694 | 738 | 700 | 675 | 711 | 726 | 749 | 921 | 822 | 743 | 911 |
| 8.343 | 699 | 644 | 746 | 737 | 632 | 679 | 743 | 749 | 959 | 810 | 720 | 895 |
| 8.41 | 701 | 703 | 723 | 706 | 652 | 669 | 751 | 759 | 897 | 846 | 742 | 899 |
| 8.477 | 701 | 679 | 707 | 723 | 637 | 677 | 738 | 776 | 936 | 827 | 743 | 873 |
| 8.544 | 709 | 650 | 742 | 719 | 660 | 682 | 743 | 755 | 903 | 814 | 689 | 875 |
| 8.611 | 738 | 667 | 741 | 691 | 644 | 676 | 694 | 751 | 903 | 831 | 729 | 894 |
| 8.678 | 711 | 626 | 727 | 716 | 673 | 655 | 749 | 762 | 936 | 785 | 709 | 891 |
| 8.745 | 670 | 673 | 751 | 692 | 653 | 700 | 756 | 789 | 943 | 809 | 733 | 885 |
| 8.812 | 718 | 663 | 725 | 747 | 643 | 715 | 789 | 765 | 886 | 803 | 710 | 904 |
| 8.879 | 694 | 670 | 792 | 733 | 647 | 705 | 718 | 769 | 925 | 801 | 723 | 930 |
| 8.946 | 703 | 669 | 749 | 725 | 659 | 702 | 733 | 796 | 934 | 791 | 722 | 872 |
| 9.013 | 743 | 660 | 666 | 776 | 675 | 731 | 713 | 803 | 922 | 819 | 716 | 879 |

| | | | | | | | | | | | | |
|---|---|---|---|---|---|---|---|---|---|---|---|---|
| 9.08 | 768 | 659 | 734 | 749 | 623 | 680 | 707 | 768 | 910 | 827 | 721 | 903 |
| 9.147 | 720 | 685 | 745 | 734 | 631 | 683 | 734 | 750 | 891 | 824 | 721 | 887 |
| 9.214 | 768 | 692 | 751 | 731 | 667 | 723 | 709 | 782 | 963 | 861 | 716 | 884 |
| 9.281 | 781 | 675 | 733 | 709 | 648 | 703 | 745 | 805 | 977 | 814 | 715 | 882 |
| 9.348 | 762 | 690 | 727 | 703 | 634 | 687 | 723 | 773 | 939 | 773 | 718 | 884 |
| 9.415 | 727 | 721 | 739 | 676 | 647 | 713 | 737 | 712 | 913 | 798 | 714 | 916 |
| 9.482 | 762 | 690 | 728 | 714 | 665 | 695 | 746 | 735 | 944 | 812 | 752 | 883 |
| 9.549 | 797 | 692 | 727 | 731 | 647 | 674 | 719 | 751 | 917 | 803 | 717 | 892 |
| 9.616 | 731 | 724 | 799 | 743 | 625 | 663 | 730 | 784 | 925 | 801 | 723 | 919 |
| 9.683 | 706 | 679 | 766 | 706 | 647 | 678 | 738 | 754 | 933 | 805 | 718 | 906 |
| 9.75 | 707 | 680 | 788 | 693 | 661 | 694 | 733 | 748 | 918 | 801 | 777 | 936 |
| 9.817 | 707 | 688 | 757 | 726 | 605 | 637 | 749 | 778 | 946 | 848 | 728 | 930 |
| 9.884 | | 663 | 744 | 726 | 667 | 684 | 733 | 760 | 932 | 809 | 721 | 886 |

## Appendix B: Dynamic Oscillatory Rheological Data

Table B.1. Complex viscosity data for pure Nylon6 and 1 wt% Nylon 6/ Cloisite 30B samples

| | η* (Pa-s) | | | | | |
|---|---|---|---|---|---|---|
| ω (rad/s) | Nylon 6 | St Dev | 1%DB | St Dev | 1%scCO2 | St Dev |
| 0.10 | 503.03 | 36.40 | 688.63 | 81.62 | 694.84 | 80.36 |
| 0.13 | 507.52 | 32.52 | 706.00 | 83.82 | 709.69 | 84.63 |
| 0.16 | 514.59 | 32.06 | 724.41 | 80.82 | 727.11 | 81.99 |
| 0.20 | 520.95 | 31.23 | 735.69 | 81.14 | 738.10 | 82.06 |
| 0.25 | 526.08 | 30.75 | 744.13 | 78.68 | 748.54 | 79.20 |
| 0.32 | 530.58 | 30.82 | 750.25 | 78.09 | 755.93 | 77.89 |
| 0.40 | 533.88 | 30.73 | 755.22 | 78.45 | 761.10 | 76.48 |
| 0.50 | 536.47 | 30.68 | 757.32 | 77.41 | 763.40 | 75.61 |
| 0.63 | 538.90 | 30.47 | 758.87 | 77.38 | 765.72 | 74.56 |
| 0.79 | 540.42 | 30.54 | 758.29 | 76.67 | 765.88 | 74.31 |
| 1.00 | 542.00 | 30.46 | 757.67 | 75.85 | 764.94 | 73.46 |
| 1.26 | 543.12 | 30.43 | 756.12 | 75.17 | 763.63 | 72.40 |
| 1.58 | 543.71 | 30.40 | 753.48 | 75.06 | 761.10 | 71.74 |
| 2.00 | 544.06 | 30.27 | 749.97 | 74.16 | 757.65 | 70.72 |
| 2.51 | 544.10 | 29.99 | 744.82 | 74.56 | 753.96 | 73.00 |
| 3.16 | 543.62 | 30.01 | 741.49 | 74.29 | 747.97 | 68.25 |
| 3.98 | 543.00 | 29.70 | 735.59 | 72.83 | 742.86 | 68.70 |
| 5.01 | 542.10 | 29.36 | 727.47 | 72.16 | 735.56 | 65.74 |
| 6.31 | 540.67 | 29.15 | 719.87 | 71.57 | 726.35 | 65.89 |
| 7.94 | 538.72 | 28.88 | 710.18 | 71.28 | 717.16 | 65.33 |
| 10.00 | 535.83 | 28.36 | 698.49 | 70.48 | 705.75 | 62.94 |
| 12.59 | 532.16 | 27.81 | 685.97 | 71.86 | 692.44 | 60.76 |
| 15.85 | 527.54 | 26.87 | 671.22 | 71.32 | 677.20 | 58.91 |
| 19.95 | 521.59 | 25.85 | 653.59 | 72.52 | 659.31 | 57.41 |
| 25.11 | 514.94 | 24.76 | 635.01 | 72.93 | 640.66 | 56.35 |
| 31.61 | 506.51 | 23.51 | 614.85 | 73.05 | 620.19 | 55.26 |
| 39.80 | 496.69 | 22.21 | 593.09 | 72.86 | 598.04 | 54.33 |
| 50.10 | 485.44 | 20.89 | 569.70 | 72.00 | 574.33 | 53.32 |
| 63.08 | 472.30 | 19.52 | 544.59 | 70.92 | 549.06 | 52.62 |
| 79.41 | 457.25 | 17.95 | 518.15 | 69.31 | 522.60 | 51.59 |
| 100.00 | 440.19 | 16.50 | 488.26 | 68.03 | 493.29 | 50.73 |

Table B.2. Complex viscosity data for Nylon/ Cloisite 30B samples at 3 and 5 wt%

| | η* (Pa-s) | | | | | | | |
|---|---|---|---|---|---|---|---|---|
| ω (rad/s) | 3%DB | St Dev | 3%scCO2 | St Dev | 5%DB | St Dev | 5%scCO2 | St Dev |
| 0.10 | 1118.12 | 95.70 | 1372.92 | 113.38 | 3169.05 | 440.70 | 2723.25 | 371.69 |
| 0.13 | 1149.36 | 86.42 | 1443.90 | 127.22 | 3263.24 | 401.79 | 2856.62 | 367.61 |
| 0.16 | 1175.50 | 78.52 | 1501.20 | 138.98 | 3354.63 | 362.43 | 2988.11 | 345.93 |
| 0.20 | 1185.48 | 70.67 | 1535.38 | 143.66 | 3386.26 | 337.26 | 3036.29 | 341.84 |
| 0.25 | 1194.20 | 69.88 | 1566.39 | 150.84 | 3403.98 | 309.75 | 3072.84 | 336.09 |
| 0.32 | 1201.28 | 66.22 | 1582.89 | 154.44 | 3394.18 | 288.89 | 3085.32 | 330.46 |
| 0.40 | 1197.54 | 59.17 | 1595.92 | 157.34 | 3373.02 | 274.49 | 3085.08 | 318.25 |
| 0.50 | 1191.09 | 55.00 | 1599.82 | 159.73 | 3336.93 | 259.51 | 3066.16 | 312.25 |
| 0.63 | 1182.92 | 48.31 | 1600.84 | 160.55 | 3289.41 | 241.08 | 3039.80 | 300.44 |
| 0.79 | 1173.54 | 46.97 | 1595.98 | 160.29 | 3233.15 | 224.65 | 3000.21 | 292.63 |
| 1.00 | 1163.32 | 44.69 | 1589.59 | 159.71 | 3170.44 | 213.07 | 2956.04 | 285.76 |
| 1.26 | 1150.53 | 40.96 | 1579.52 | 158.72 | 3104.15 | 198.22 | 2906.57 | 274.79 |
| 1.58 | 1136.40 | 38.47 | 1565.86 | 156.61 | 3029.59 | 185.73 | 2849.98 | 264.38 |
| 2.00 | 1121.66 | 36.31 | 1550.49 | 154.66 | 2953.40 | 172.97 | 2789.93 | 253.54 |
| 2.51 | 1106.60 | 34.10 | 1531.93 | 150.01 | 2872.52 | 164.16 | 2724.12 | 242.73 |
| 3.16 | 1089.17 | 31.14 | 1513.35 | 148.81 | 2788.11 | 150.14 | 2657.15 | 231.16 |
| 3.98 | 1069.82 | 29.29 | 1490.63 | 144.53 | 2701.03 | 138.52 | 2582.73 | 219.71 |
| 5.01 | 1051.58 | 27.72 | 1463.16 | 140.91 | 2609.34 | 127.59 | 2504.70 | 205.75 |
| 6.31 | 1030.07 | 25.90 | 1435.01 | 135.97 | 2516.39 | 116.57 | 2424.50 | 194.18 |
| 7.94 | 1008.07 | 23.29 | 1404.78 | 131.28 | 2419.93 | 108.71 | 2339.71 | 183.51 |
| 10.00 | 983.04 | 22.58 | 1370.12 | 126.14 | 2318.78 | 99.40 | 2251.43 | 171.36 |
| 12.59 | 957.18 | 21.48 | 1333.92 | 121.05 | 2217.70 | 91.57 | 2160.04 | 159.47 |
| 15.85 | 930.06 | 20.74 | 1294.04 | 115.58 | 2113.40 | 84.65 | 2065.38 | 146.94 |
| 19.95 | 900.31 | 19.82 | 1250.99 | 109.06 | 2006.59 | 77.98 | 1967.45 | 135.57 |
| 25.11 | 869.86 | 19.16 | 1206.05 | 103.39 | 1899.77 | 71.86 | 1868.47 | 124.08 |
| 31.61 | 837.45 | 18.55 | 1157.82 | 97.16 | 1792.30 | 66.33 | 1768.34 | 113.72 |
| 39.80 | 803.54 | 17.98 | 1107.10 | 91.25 | 1684.55 | 61.20 | 1666.73 | 103.61 |
| 50.10 | 768.44 | 17.30 | 1055.03 | 85.02 | 1578.38 | 56.59 | 1565.91 | 93.92 |
| 63.08 | 732.03 | 16.81 | 1000.43 | 79.19 | 1472.57 | 52.11 | 1465.20 | 84.93 |
| 79.41 | 694.13 | 16.05 | 943.93 | 73.44 | 1368.30 | 47.96 | 1364.66 | 76.16 |
| 100.00 | 653.94 | 15.48 | 884.45 | 68.25 | 1262.55 | 43.51 | 1262.40 | 67.67 |

Table B.3. Complex viscosity data for Nylon/ Cloisite 30B samples at 7 and 10 wt%

| | η* (Pa-s) | | | | | | | |
|---|---|---|---|---|---|---|---|---|
| ω (rad/s) | 7%DB | St Dev | 7%scCO2 | St Dev | 10%DB | St Dev | 10%scCO2 | St Dev |
| 0.10 | 5695.62 | 735.34 | 10289.47 | 1658.22 | 12874.61 | 2977.82 | 12568.83 | 1357.08 |
| 0.13 | 5792.90 | 732.17 | 10069.04 | 1535.46 | 12588.12 | 2698.66 | 12559.24 | 1260.60 |
| 0.16 | 5923.17 | 744.93 | 9873.07 | 1441.63 | 12456.68 | 2639.64 | 12435.30 | 1188.17 |
| 0.20 | 5929.19 | 733.77 | 9594.49 | 1381.52 | 11972.48 | 2318.69 | 12203.50 | 1107.46 |
| 0.25 | 5868.75 | 687.44 | 9293.44 | 1290.55 | 11446.32 | 2059.87 | 11832.17 | 1043.06 |
| 0.32 | 5795.10 | 667.27 | 8994.70 | 1221.04 | 10962.25 | 1873.02 | 11445.81 | 1019.44 |
| 0.40 | 5686.19 | 620.76 | 8666.07 | 1136.24 | 10446.51 | 1723.70 | 10978.18 | 976.88 |
| 0.50 | 5554.68 | 595.58 | 8336.38 | 1067.64 | 9915.36 | 1555.78 | 10485.39 | 930.44 |
| 0.63 | 5409.31 | 560.54 | 8011.37 | 984.31 | 9393.72 | 1421.37 | 9988.28 | 914.33 |
| 0.79 | 5254.84 | 525.09 | 7681.56 | 917.49 | 8885.95 | 1295.25 | 9490.09 | 894.26 |
| 1.00 | 5087.59 | 493.31 | 7353.70 | 845.30 | 8388.28 | 1183.68 | 8995.88 | 879.65 |
| 1.26 | 4922.34 | 463.19 | 7033.16 | 776.91 | 7910.91 | 1078.25 | 8515.00 | 866.59 |
| 1.58 | 4747.11 | 430.84 | 6711.18 | 711.78 | 7442.83 | 982.80 | 8039.37 | 854.86 |
| 2.00 | 4570.12 | 399.36 | 6397.13 | 647.38 | 6990.02 | 890.90 | 7576.84 | 843.54 |
| 2.51 | 4388.21 | 366.28 | 6083.44 | 585.02 | 6544.02 | 806.73 | 7120.03 | 843.16 |
| 3.16 | 4209.75 | 337.00 | 5780.86 | 527.42 | 6121.52 | 731.83 | 6681.36 | 835.29 |
| 3.98 | 4026.03 | 307.02 | 5481.43 | 472.34 | 5711.90 | 662.78 | 6257.06 | 828.38 |
| 5.01 | 3839.44 | 277.09 | 5185.85 | 419.49 | 5305.12 | 599.53 | 5833.79 | 824.98 |
| 6.31 | 3653.14 | 249.48 | 4895.62 | 369.06 | 4910.83 | 545.97 | 5425.12 | 824.71 |
| 7.94 | 3468.68 | 225.59 | 4612.95 | 324.35 | 4540.59 | 504.13 | 5033.71 | 818.03 |
| 10.00 | 3277.35 | 203.35 | 4328.44 | 282.10 | 4167.26 | 471.16 | 4638.25 | 810.13 |
| 12.59 | 3087.98 | 185.56 | 4052.63 | 245.83 | 3813.15 | 447.61 | 4261.99 | 800.38 |
| 15.85 | 2899.09 | 174.21 | 3783.63 | 214.11 | 3485.41 | 428.68 | 3909.80 | 782.04 |
| 19.95 | 2704.87 | 169.18 | 3515.65 | 189.69 | 3157.00 | 415.11 | 3559.31 | 765.51 |
| 25.11 | 2513.15 | 172.81 | 3257.38 | 172.48 | 2848.88 | 402.82 | 3227.73 | 742.74 |
| 31.61 | 2325.88 | 179.27 | 3009.13 | 160.75 | 2565.93 | 387.39 | 2917.94 | 708.90 |
| 39.80 | 2144.99 | 185.76 | 2770.85 | 154.22 | 2304.84 | 372.31 | 2630.04 | 672.97 |
| 50.10 | 1970.46 | 191.13 | 2541.77 | 152.53 | 2065.21 | 355.13 | 2364.30 | 635.74 |
| 63.08 | 1802.47 | 194.00 | 2323.02 | 153.79 | 1842.79 | 334.88 | 2120.63 | 598.49 |
| 79.41 | 1641.36 | 193.22 | 2116.22 | 153.96 | 1639.85 | 313.25 | 1897.51 | 560.31 |
| 100.00 | 1475.42 | 194.59 | 1909.44 | 160.80 | 1432.21 | 289.66 | 1673.25 | 524.60 |

Table B.4. Storage modulus data for pure Nylon6 and 1 wt% Nylon 6/ Cloisite 30B samples

| | G' (Pa) | | | | | |
|---|---|---|---|---|---|---|
| ω (rad/s) | Nylon 6 | St Dev | 1%DB | St Dev | 1%scCO2 | St Dev |
| 0.10 | 0.63 | 0.30 | 1.59 | 0.46 | 1.86 | 0.25 |
| 0.13 | 0.72 | 0.34 | 1.86 | 0.29 | 2.09 | 0.27 |
| 0.16 | 0.83 | 0.32 | 2.81 | 0.24 | 3.17 | 0.46 |
| 0.20 | 0.97 | 0.37 | 3.28 | 1.02 | 3.59 | 0.79 |
| 0.25 | 1.23 | 0.40 | 4.63 | 0.76 | 5.02 | 0.43 |
| 0.32 | 1.40 | 0.44 | 6.11 | 1.07 | 6.74 | 0.69 |
| 0.40 | 1.81 | 0.56 | 8.53 | 1.38 | 9.03 | 1.13 |
| 0.50 | 2.37 | 0.83 | 11.40 | 1.60 | 11.61 | 1.17 |
| 0.63 | 3.11 | 1.23 | 15.56 | 1.96 | 15.69 | 1.99 |
| 0.79 | 4.28 | 1.78 | 20.98 | 3.38 | 21.09 | 2.78 |
| 1.00 | 6.01 | 2.70 | 28.91 | 4.90 | 28.91 | 3.68 |
| 1.26 | 8.97 | 4.25 | 39.52 | 6.82 | 39.64 | 5.61 |
| 1.58 | 13.14 | 6.42 | 54.87 | 9.46 | 54.84 | 8.12 |
| 2.00 | 19.75 | 9.87 | 76.48 | 13.00 | 76.30 | 11.61 |
| 2.51 | 29.76 | 15.31 | 105.57 | 17.52 | 104.22 | 13.35 |
| 3.16 | 44.84 | 23.13 | 149.01 | 24.51 | 149.14 | 23.53 |
| 3.98 | 68.69 | 34.72 | 208.21 | 38.62 | 207.93 | 37.68 |
| 5.01 | 104.51 | 50.41 | 296.27 | 47.07 | 298.11 | 54.79 |
| 6.31 | 156.61 | 73.68 | 413.41 | 74.99 | 418.27 | 69.56 |
| 7.94 | 234.27 | 106.84 | 572.76 | 99.82 | 581.16 | 92.77 |
| 10.00 | 348.31 | 152.17 | 798.67 | 136.22 | 817.04 | 136.25 |
| 12.59 | 499.07 | 74.66 | 1112.11 | 186.96 | 1129.71 | 174.56 |
| 15.85 | 726.25 | 103.32 | 1534.35 | 256.02 | 1560.34 | 235.87 |
| 19.95 | 1046.72 | 139.43 | 2098.29 | 357.42 | 2140.44 | 316.98 |
| 25.11 | 1495.13 | 187.86 | 2857.66 | 489.81 | 2909.11 | 423.52 |
| 31.61 | 2113.80 | 245.57 | 3855.26 | 654.91 | 3937.28 | 553.17 |
| 39.80 | 2952.59 | 325.98 | 5162.13 | 897.09 | 5251.04 | 729.04 |
| 50.10 | 4071.16 | 418.49 | 6862.53 | 1204.78 | 6977.14 | 945.26 |
| 63.08 | 5550.84 | 530.15 | 9037.28 | 1600.78 | 9185.86 | 1251.77 |
| 79.41 | 7457.27 | 661.65 | 11803.42 | 2112.71 | 11981.32 | 1643.99 |
| 100.00 | 9868.86 | 819.67 | 15218.64 | 2816.69 | 15452.89 | 2183.07 |

Table B.5. Storage modulus data for Nylon/ Cloisite 30B samples at 3 and 5 wt%

| | G' (Pa) | | | | | | | |
|---|---|---|---|---|---|---|---|---|
| ω (rad/s) | 3%DB | St Dev | 3%scCO2 | St Dev | 5%DB | St Dev | 5%scCO2 | St Dev |
| 0.10 | 9.70 | 1.75 | 6.85 | 1.08 | 41.06 | 11.12 | 30.19 | 3.15 |
| 0.13 | 12.68 | 2.78 | 8.84 | 1.15 | 53.91 | 14.82 | 43.07 | 6.93 |
| 0.16 | 16.06 | 3.57 | 12.57 | 1.60 | 71.46 | 15.68 | 56.26 | 7.05 |
| 0.20 | 19.37 | 3.03 | 16.96 | 2.86 | 92.86 | 20.19 | 73.19 | 10.17 |
| 0.25 | 24.10 | 2.56 | 22.77 | 3.45 | 120.21 | 23.84 | 95.85 | 13.77 |
| 0.32 | 32.94 | 7.21 | 29.76 | 4.66 | 153.63 | 31.48 | 122.71 | 16.88 |
| 0.40 | 41.00 | 7.02 | 40.00 | 6.54 | 200.14 | 37.91 | 158.84 | 22.34 |
| 0.50 | 51.30 | 7.53 | 53.72 | 9.09 | 257.12 | 48.32 | 205.27 | 30.62 |
| 0.63 | 67.84 | 12.49 | 72.37 | 12.33 | 331.32 | 58.33 | 267.06 | 38.65 |
| 0.79 | 86.56 | 15.15 | 97.14 | 15.93 | 424.65 | 73.47 | 343.41 | 51.56 |
| 1.00 | 112.13 | 18.52 | 130.33 | 21.86 | 546.85 | 89.39 | 446.81 | 67.95 |
| 1.26 | 145.67 | 22.00 | 176.08 | 30.16 | 703.81 | 112.05 | 582.59 | 87.43 |
| 1.58 | 190.53 | 29.47 | 238.05 | 40.28 | 906.70 | 136.48 | 756.90 | 114.26 |
| 2.00 | 249.79 | 35.26 | 322.66 | 54.23 | 1169.95 | 166.96 | 988.76 | 147.47 |
| 2.51 | 334.17 | 45.40 | 438.10 | 67.48 | 1507.94 | 205.02 | 1288.80 | 186.03 |
| 3.16 | 435.88 | 57.71 | 595.00 | 97.48 | 1949.73 | 250.85 | 1683.82 | 240.90 |
| 3.98 | 577.12 | 65.29 | 804.50 | 129.12 | 2502.45 | 299.54 | 2201.19 | 312.13 |
| 5.01 | 764.18 | 88.87 | 1087.58 | 175.07 | 3215.65 | 364.45 | 2856.81 | 384.87 |
| 6.31 | 1016.18 | 106.37 | 1461.93 | 232.65 | 4128.31 | 429.33 | 3705.79 | 488.04 |
| 7.94 | 1343.29 | 126.26 | 1968.06 | 304.98 | 5280.50 | 509.59 | 4795.42 | 614.13 |
| 10.00 | 1779.82 | 149.60 | 2635.75 | 400.57 | 6736.04 | 598.76 | 6179.93 | 761.60 |
| 12.59 | 2352.45 | 178.20 | 3517.11 | 528.15 | 8565.79 | 705.80 | 7924.78 | 931.26 |
| 15.85 | 3103.75 | 219.46 | 4662.93 | 678.19 | 10837.01 | 825.56 | 10108.07 | 1134.84 |
| 19.95 | 4064.56 | 250.01 | 6143.28 | 866.21 | 13639.43 | 957.46 | 12835.60 | 1376.64 |
| 25.11 | 5318.51 | 287.41 | 8056.35 | 1110.50 | 17103.93 | 1102.71 | 16218.10 | 1654.61 |
| 31.61 | 6923.69 | 342.11 | 10488.26 | 1385.19 | 21347.01 | 1270.69 | 20382.18 | 1992.86 |
| 39.80 | 8959.93 | 404.75 | 13566.77 | 1736.85 | 26520.17 | 1463.06 | 25467.69 | 2355.69 |
| 50.10 | 11545.66 | 470.29 | 17432.03 | 2165.11 | 32789.35 | 1697.67 | 31678.61 | 2777.90 |
| 63.08 | 14794.59 | 560.59 | 22229.13 | 2655.75 | 40335.29 | 1963.84 | 39171.10 | 3278.81 |
| 79.41 | 18840.14 | 650.11 | 28143.18 | 3252.45 | 49336.50 | 2258.77 | 48152.47 | 3801.10 |
| 100.00 | 23824.63 | 781.70 | 35392.20 | 3982.83 | 59874.58 | 2592.26 | 58736.89 | 4380.70 |

Table B.6. Storage modulus data for data for Nylon/ Cloisite 30B samples at 7 and 10 wt%

| | G' (Pa-s) | | | | | | | |
|---|---|---|---|---|---|---|---|---|
| ω (rad/s) | 7%DB | St Dev | 7%scCO2 | St Dev | 10%DB | St Dev | 10%scCO2 | St Dev |
| 0.10 | 172.47 | 20.96 | 331.84 | 66.96 | 574.90 | 167.92 | 540.13 | 97.13 |
| 0.13 | 215.30 | 28.86 | 398.30 | 80.68 | 690.21 | 190.07 | 658.85 | 115.14 |
| 0.16 | 265.97 | 35.75 | 484.00 | 95.72 | 838.52 | 236.84 | 800.48 | 132.87 |
| 0.20 | 327.41 | 42.00 | 583.97 | 115.09 | 985.86 | 254.36 | 963.65 | 154.00 |
| 0.25 | 401.56 | 51.06 | 703.47 | 140.58 | 1163.91 | 292.22 | 1155.21 | 179.43 |
| 0.32 | 490.24 | 66.36 | 853.83 | 170.46 | 1371.58 | 330.54 | 1380.80 | 210.66 |
| 0.40 | 596.25 | 76.38 | 1034.51 | 209.17 | 1613.32 | 377.13 | 1644.50 | 245.95 |
| 0.50 | 730.07 | 96.44 | 1254.83 | 252.25 | 1905.61 | 441.59 | 1957.50 | 282.20 |
| 0.63 | 891.26 | 121.82 | 1524.95 | 307.19 | 2247.04 | 508.77 | 2332.79 | 330.52 |
| 0.79 | 1089.83 | 146.59 | 1860.70 | 372.58 | 2654.94 | 586.50 | 2780.94 | 390.64 |
| 1.00 | 1338.93 | 179.04 | 2271.33 | 452.31 | 3146.10 | 681.15 | 3322.05 | 463.32 |
| 1.26 | 1650.35 | 223.25 | 2780.18 | 545.39 | 3733.48 | 790.63 | 3976.02 | 553.27 |
| 1.58 | 2033.48 | 273.34 | 3401.11 | 659.55 | 4430.76 | 915.02 | 4757.11 | 662.53 |
| 2.00 | 2510.13 | 335.43 | 4173.22 | 791.89 | 5269.74 | 1057.43 | 5705.95 | 804.22 |
| 2.51 | 3106.56 | 410.65 | 5118.45 | 945.50 | 6263.81 | 1210.68 | 6835.77 | 989.70 |
| 3.16 | 3855.07 | 490.78 | 6284.11 | 1124.39 | 7465.88 | 1404.68 | 8198.61 | 1229.79 |
| 3.98 | 4775.42 | 596.45 | 7705.59 | 1321.24 | 8869.68 | 1605.19 | 9834.76 | 1548.79 |
| 5.01 | 5907.74 | 710.34 | 9442.71 | 1549.72 | 10531.29 | 1842.13 | 11754.91 | 1951.95 |
| 6.31 | 7316.32 | 843.58 | 11558.12 | 1797.32 | 12470.95 | 2108.49 | 14042.47 | 2495.17 |
| 7.94 | 9058.57 | 993.62 | 14150.63 | 2082.45 | 14780.18 | 2426.82 | 16748.56 | 3167.93 |
| 10.00 | 11171.86 | 1164.86 | 17225.49 | 2367.34 | 17368.35 | 2796.59 | 19846.28 | 4044.03 |
| 12.59 | 13743.67 | 1354.97 | 20949.71 | 2682.61 | 20364.05 | 3261.55 | 23460.34 | 5171.98 |
| 15.85 | 16846.58 | 1599.95 | 25389.51 | 3019.76 | 23884.25 | 3865.19 | 27699.69 | 6512.82 |
| 19.95 | 20516.71 | 1890.64 | 30619.16 | 3375.24 | 27730.35 | 4657.67 | 32448.49 | 8243.17 |
| 25.11 | 24882.73 | 2385.91 | 36806.32 | 3761.32 | 32097.06 | 5656.81 | 37858.99 | 10338.88 |
| 31.61 | 30060.11 | 3055.83 | 44121.96 | 4251.91 | 37050.44 | 6820.66 | 44033.51 | 12734.82 |
| 39.80 | 36168.27 | 3973.03 | 52724.28 | 4836.91 | 42708.15 | 8285.45 | 51094.98 | 15609.45 |
| 50.10 | 43363.38 | 5191.69 | 62716.71 | 5681.00 | 49087.69 | 10060.47 | 59120.26 | 19052.59 |
| 63.08 | 51750.08 | 6766.37 | 74320.64 | 6820.98 | 56191.26 | 12091.40 | 68284.28 | 23143.24 |
| 79.41 | 61427.91 | 8722.71 | 87727.50 | 8325.64 | 64051.94 | 14424.27 | 78658.41 | 27996.33 |
| 100.00 | 71801.12 | 11374.01 | 102492.71 | 10698.31 | 71336.81 | 17011.64 | 89172.83 | 33895.96 |

Table B.7. Complex viscosity data for 1 wt% Baytube PC/CNT nanocomposites

| | η* (Pa-s) | | | | | | | | | |
|---|---|---|---|---|---|---|---|---|---|---|
| ω (rad/s) | Pure PC | St Dev | DB | St Dev | 5X scCO2 | St Dev | 10X scCO2 | St Dev | 15X scCO2 | St Dev |
| 0.10 | 1435.76 | 28.39 | 1730.95 | 64.00 | 1937.30 | 48.41 | 2361.41 | 65.11 | 2461.41 | 65.11 |
| 0.13 | 1434.61 | 29.36 | 1713.65 | 69.03 | 1918.01 | 40.67 | 2255.14 | 62.02 | 2355.14 | 62.02 |
| 0.16 | 1431.65 | 28.65 | 1703.14 | 68.07 | 1898.76 | 44.83 | 2166.16 | 60.97 | 2266.16 | 60.97 |
| 0.20 | 1429.72 | 28.34 | 1686.23 | 65.09 | 1881.04 | 41.61 | 2091.24 | 57.48 | 2191.24 | 57.48 |
| 0.25 | 1426.87 | 26.66 | 1673.79 | 66.64 | 1860.65 | 44.20 | 2020.81 | 60.92 | 2120.81 | 60.92 |
| 0.32 | 1425.73 | 26.58 | 1663.27 | 65.62 | 1849.30 | 44.64 | 1964.45 | 59.30 | 2064.45 | 59.30 |
| 0.40 | 1424.09 | 26.66 | 1650.80 | 66.80 | 1829.08 | 43.72 | 1915.54 | 57.59 | 2015.54 | 57.59 |
| 0.50 | 1423.24 | 27.62 | 1640.51 | 66.64 | 1814.48 | 45.92 | 1871.08 | 58.22 | 1971.08 | 58.22 |
| 0.63 | 1422.57 | 27.82 | 1631.38 | 66.36 | 1799.89 | 44.73 | 1829.45 | 56.34 | 1929.45 | 56.34 |
| 0.79 | 1421.52 | 28.15 | 1621.65 | 67.70 | 1784.23 | 44.24 | 1792.31 | 56.65 | 1892.31 | 56.65 |
| 1.00 | 1420.86 | 28.25 | 1612.56 | 67.29 | 1768.88 | 44.58 | 1759.56 | 55.54 | 1859.56 | 55.54 |
| 1.26 | 1420.59 | 28.14 | 1604.62 | 67.37 | 1755.50 | 44.83 | 1729.80 | 55.45 | 1829.80 | 55.45 |
| 1.58 | 1418.62 | 28.51 | 1595.09 | 67.54 | 1740.56 | 44.10 | 1700.97 | 55.32 | 1800.97 | 55.32 |
| 2.00 | 1417.17 | 28.11 | 1586.17 | 66.98 | 1726.14 | 44.02 | 1673.61 | 54.20 | 1773.61 | 54.20 |
| 2.51 | 1415.54 | 28.37 | 1578.32 | 63.58 | 1710.50 | 42.26 | 1648.59 | 54.92 | 1748.59 | 54.92 |
| 3.16 | 1413.89 | 28.01 | 1567.28 | 65.79 | 1694.29 | 43.37 | 1625.11 | 53.54 | 1725.11 | 53.54 |
| 3.98 | 1411.29 | 28.15 | 1557.37 | 65.98 | 1680.51 | 42.48 | 1600.94 | 50.75 | 1700.94 | 50.75 |
| 5.01 | 1407.28 | 28.04 | 1546.87 | 64.11 | 1663.69 | 41.47 | 1576.12 | 51.81 | 1676.12 | 51.81 |
| 6.31 | 1402.86 | 28.04 | 1534.13 | 62.43 | 1644.53 | 39.46 | 1553.27 | 50.22 | 1653.27 | 50.22 |
| 7.94 | 1397.38 | 28.14 | 1523.67 | 63.14 | 1625.73 | 39.81 | 1530.28 | 48.70 | 1630.28 | 48.70 |
| 10.00 | 1384.48 | 27.36 | 1497.53 | 60.79 | 1593.12 | 33.02 | 1497.30 | 46.33 | 1597.30 | 46.33 |
| 12.59 | 1373.28 | 27.09 | 1480.76 | 59.66 | 1567.91 | 32.65 | 1471.23 | 44.84 | 1571.23 | 44.84 |
| 15.85 | 1359.35 | 27.11 | 1461.76 | 57.74 | 1541.29 | 32.04 | 1443.79 | 43.32 | 1543.79 | 43.32 |
| 19.95 | 1341.85 | 26.87 | 1439.02 | 55.99 | 1510.30 | 30.61 | 1413.45 | 41.69 | 1513.45 | 41.69 |
| 25.12 | 1321.32 | 26.19 | 1414.07 | 54.26 | 1476.92 | 29.37 | 1381.74 | 40.35 | 1481.74 | 40.35 |
| 31.62 | 1296.14 | 25.79 | 1385.20 | 51.69 | 1438.97 | 28.07 | 1346.72 | 38.83 | 1446.72 | 38.83 |
| 39.81 | 1265.98 | 25.36 | 1351.07 | 49.15 | 1395.83 | 26.70 | 1307.94 | 36.49 | 1407.94 | 36.49 |
| 50.12 | 1231.05 | 25.02 | 1313.13 | 46.28 | 1348.02 | 25.09 | 1266.16 | 34.22 | 1366.16 | 34.22 |
| 63.09 | 1190.02 | 24.50 | 1269.86 | 43.30 | 1294.74 | 23.25 | 1219.62 | 32.00 | 1319.62 | 32.00 |
| 79.43 | 1142.89 | 23.98 | 1220.39 | 40.08 | 1235.78 | 21.16 | 1168.54 | 29.60 | 1268.54 | 29.60 |
| 100.00 | 1087.36 | 24.93 | 1166.28 | 36.68 | 1171.67 | 19.18 | 1113.60 | 27.20 | 1213.60 | 27.20 |

Table B.8. Storage modulus data for 1 wt% Baytube PC/CNT nanocomposites

| | G' (Pa) | | | | | | | | | |
|---|---|---|---|---|---|---|---|---|---|---|
| ω (rad/s) | Pure PC | St Dev | DB | St Dev | 5X scCO2 | St Dev | 10X scCO2 | St Dev | 15X scCO2 | St Dev |
| 0.10 | 0.18 | 0.02 | 6.70 | 1.99 | 9.53 | 0.71 | 35.73 | 4.47 | 71.20 | 3.40 |
| 0.13 | 0.26 | 0.02 | 8.41 | 2.42 | 11.94 | 0.54 | 41.19 | 3.61 | 77.63 | 2.49 |
| 0.16 | 0.41 | 0.05 | 10.37 | 1.51 | 14.75 | 1.23 | 48.33 | 3.63 | 85.22 | 1.93 |
| 0.20 | 0.59 | 0.03 | 12.67 | 1.22 | 19.16 | 1.06 | 56.09 | 3.11 | 94.12 | 2.08 |
| 0.25 | 0.90 | 0.02 | 15.63 | 2.12 | 24.30 | 0.63 | 65.47 | 2.91 | 103.69 | 1.76 |
| 0.32 | 1.31 | 0.02 | 18.87 | 2.23 | 30.70 | 0.74 | 76.61 | 2.57 | 115.11 | 2.02 |
| 0.40 | 1.99 | 0.05 | 23.80 | 2.33 | 38.15 | 1.14 | 89.75 | 2.38 | 129.92 | 1.94 |
| 0.50 | 3.21 | 0.14 | 29.30 | 2.41 | 48.39 | 1.00 | 105.49 | 2.72 | 146.64 | 1.64 |
| 0.63 | 5.04 | 0.17 | 37.09 | 1.66 | 61.25 | 0.81 | 124.68 | 1.31 | 167.79 | 1.99 |
| 0.79 | 7.75 | 0.10 | 46.69 | 1.27 | 77.91 | 0.83 | 148.18 | 1.66 | 193.01 | 1.15 |
| 1.00 | 12.37 | 0.24 | 59.45 | 1.26 | 101.05 | 0.87 | 177.08 | 2.39 | 224.99 | 1.31 |
| 1.26 | 19.43 | 0.37 | 77.93 | 0.23 | 128.78 | 0.71 | 212.84 | 4.55 | 264.94 | 1.70 |
| 1.58 | 30.51 | 1.00 | 103.17 | 0.62 | 169.16 | 1.82 | 256.83 | 8.41 | 316.34 | 3.18 |
| 2.00 | 48.00 | 0.94 | 137.20 | 3.85 | 221.61 | 3.91 | 315.16 | 12.03 | 379.58 | 4.52 |
| 2.51 | 74.57 | 1.36 | 185.15 | 10.45 | 292.48 | 5.75 | 382.43 | 22.46 | 459.65 | 11.60 |
| 3.16 | 116.82 | 2.49 | 255.30 | 11.82 | 396.74 | 9.44 | 484.12 | 22.16 | 573.43 | 16.04 |
| 3.98 | 180.58 | 3.42 | 349.43 | 19.39 | 533.15 | 14.62 | 608.60 | 38.78 | 716.50 | 20.54 |
| 5.01 | 278.42 | 8.96 | 490.33 | 35.68 | 724.01 | 23.17 | 782.22 | 59.11 | 909.67 | 27.88 |
| 6.31 | 425.69 | 11.01 | 671.49 | 43.13 | 990.11 | 24.55 | 1014.00 | 82.33 | 1172.46 | 36.90 |
| 7.94 | 648.30 | 19.89 | 957.84 | 64.30 | 1364.54 | 49.40 | 1323.35 | 115.69 | 1520.35 | 54.29 |
| 10.00 | 974.39 | 26.66 | 1351.01 | 105.63 | 1882.73 | 61.23 | 1847.40 | 222.82 | 1992.58 | 83.63 |
| 12.59 | 1452.15 | 46.39 | 1911.30 | 132.08 | 2604.14 | 86.59 | 2400.01 | 264.28 | 2645.07 | 108.10 |
| 15.85 | 2149.61 | 67.24 | 2706.50 | 190.43 | 3616.65 | 118.32 | 3153.78 | 320.94 | 3526.75 | 157.33 |
| 19.95 | 3139.80 | 98.28 | 3816.77 | 276.93 | 5004.73 | 161.56 | 4182.53 | 407.39 | 4732.14 | 200.14 |
| 25.12 | 4544.21 | 141.34 | 5375.08 | 380.39 | 6906.78 | 224.33 | 5570.93 | 519.59 | 6366.26 | 277.07 |
| 31.62 | 6487.94 | 204.93 | 7511.14 | 527.40 | 9473.15 | 292.45 | 7453.53 | 672.02 | 8564.03 | 378.52 |
| 39.81 | 9152.43 | 283.78 | 10396.64 | 699.50 | 12905.72 | 414.49 | 9976.30 | 878.85 | 11489.87 | 508.14 |
| 50.12 | 12755.97 | 400.13 | 14269.94 | 919.26 | 17441.55 | 548.21 | 13325.47 | 1155.06 | 15360.91 | 668.95 |
| 63.09 | 17496.32 | 569.20 | 19378.90 | 1213.41 | 23330.05 | 694.78 | 17671.80 | 1472.83 | 20384.18 | 858.55 |
| 79.43 | 23643.28 | 765.53 | 25995.12 | 1562.61 | 30885.92 | 913.59 | 23293.34 | 1881.67 | 26835.44 | 1107.44 |
| 100.00 | 31415.86 | 1062.25 | 34444.30 | 1975.55 | 40367.17 | 1153.21 | 30519.22 | 2346.43 | 35004.21 | 1359.05 |

Table B.9. Complex viscosity data for 3 wt% Baytube PC/CNT nanocomposites

| | η* (Pa-s) | | | | | | | | | |
|---|---|---|---|---|---|---|---|---|---|---|
| ω (rad/s) | Pure PC | St Dev | DB | St Dev | 5X scCO2 | St Dev | 10X scCO2 | St Dev | 15X scCO2 | St Dev |
| 0.10 | 1435.76 | 28.39 | 4285.76 | 63.60 | 7938.26 | 114.20 | 14682.31 | 569.33 | 6293.15 | 360.11 |
| 0.13 | 1434.61 | 29.36 | 4017.89 | 97.26 | 7194.98 | 55.82 | 12531.10 | 392.35 | 5942.48 | 432.47 |
| 0.16 | 1431.65 | 28.65 | 3766.54 | 105.37 | 6529.42 | 25.99 | 10812.79 | 309.38 | 5544.94 | 418.88 |
| 0.20 | 1429.72 | 28.34 | 3536.74 | 109.06 | 5951.54 | 12.96 | 9366.86 | 242.02 | 5157.06 | 382.24 |
| 0.25 | 1426.87 | 26.66 | 3327.68 | 111.93 | 5442.28 | 26.54 | 8157.87 | 172.26 | 4811.27 | 328.55 |
| 0.32 | 1425.73 | 26.58 | 3146.94 | 115.71 | 5006.33 | 40.36 | 7151.07 | 125.28 | 4490.53 | 285.96 |
| 0.40 | 1424.09 | 26.66 | 2980.86 | 116.84 | 4620.50 | 52.06 | 6309.89 | 82.39 | 4212.88 | 231.90 |
| 0.50 | 1423.24 | 27.62 | 2831.52 | 113.97 | 4283.74 | 56.99 | 5606.21 | 52.17 | 3949.81 | 201.13 |
| 0.63 | 1422.57 | 27.82 | 2696.40 | 112.29 | 3988.36 | 61.50 | 5007.47 | 37.07 | 3725.44 | 164.70 |
| 0.79 | 1421.52 | 28.15 | 2574.48 | 110.85 | 3727.61 | 64.51 | 4504.53 | 30.68 | 3517.84 | 137.69 |
| 1.00 | 1420.86 | 28.25 | 2463.37 | 108.28 | 3497.38 | 65.81 | 4079.46 | 33.15 | 3333.60 | 106.65 |
| 1.26 | 1420.59 | 28.14 | 2363.91 | 106.10 | 3295.59 | 67.45 | 3721.71 | 40.49 | 3165.65 | 85.09 |
| 1.58 | 1418.62 | 28.51 | 2272.35 | 103.03 | 3112.74 | 69.72 | 3415.49 | 45.78 | 3017.11 | 62.36 |
| 2.00 | 1417.17 | 28.11 | 2189.20 | 100.59 | 2950.31 | 69.50 | 3155.15 | 55.05 | 2880.43 | 44.44 |
| 2.51 | 1415.54 | 28.37 | 2112.98 | 94.63 | 2806.76 | 69.19 | 2930.47 | 55.09 | 2756.46 | 27.71 |
| 3.16 | 1413.89 | 28.01 | 2040.69 | 95.30 | 2672.63 | 68.94 | 2739.90 | 61.21 | 2647.49 | 13.17 |
| 3.98 | 1411.29 | 28.15 | 1979.20 | 93.14 | 2552.31 | 67.11 | 2571.84 | 64.42 | 2538.16 | 7.89 |
| 5.01 | 1407.28 | 28.04 | 1917.85 | 90.61 | 2441.66 | 66.52 | 2426.74 | 64.94 | 2443.22 | 17.05 |
| 6.31 | 1402.86 | 28.04 | 1862.10 | 87.11 | 2341.09 | 65.39 | 2299.69 | 65.17 | 2349.61 | 32.53 |
| 7.94 | 1397.38 | 28.14 | 1810.28 | 85.25 | 2246.96 | 63.57 | 2187.82 | 64.64 | 2261.39 | 36.42 |
| 10.00 | 1384.48 | 27.36 | 1766.11 | 71.02 | 2181.36 | 63.96 | 2071.99 | 58.92 | 2176.40 | 33.09 |
| 12.59 | 1373.28 | 27.09 | 1721.63 | 64.00 | 2096.96 | 62.98 | 1980.29 | 55.12 | 2096.73 | 40.32 |
| 15.85 | 1359.35 | 27.11 | 1672.19 | 63.02 | 2016.13 | 59.33 | 1896.97 | 52.58 | 2018.16 | 43.84 |
| 19.95 | 1341.85 | 26.87 | 1625.29 | 60.48 | 1936.51 | 56.88 | 1818.50 | 51.19 | 1939.23 | 48.73 |
| 25.12 | 1321.32 | 26.19 | 1581.47 | 55.52 | 1861.58 | 56.67 | 1745.40 | 48.35 | 1861.49 | 52.33 |
| 31.62 | 1296.14 | 25.79 | 1534.56 | 54.05 | 1785.95 | 53.95 | 1674.99 | 46.35 | 1783.44 | 54.05 |
| 39.81 | 1265.98 | 25.36 | 1486.94 | 51.38 | 1710.42 | 51.09 | 1606.03 | 43.89 | 1702.33 | 55.55 |
| 50.12 | 1231.05 | 25.02 | 1439.43 | 47.63 | 1634.84 | 49.54 | 1537.96 | 41.62 | 1619.64 | 55.38 |
| 63.09 | 1190.02 | 24.50 | 1388.87 | 44.61 | 1556.92 | 46.59 | 1468.79 | 39.25 | 1534.18 | 54.92 |
| 79.43 | 1142.89 | 23.98 | 1336.18 | 41.18 | 1477.82 | 42.94 | 1396.19 | 35.71 | 1444.13 | 52.70 |
| 100.00 | 1087.36 | 24.93 | 1280.94 | 37.58 | 1395.96 | 40.46 | 1319.40 | 32.44 | 1350.26 | 49.99 |

Table B.10. Storage modulus data for 3 wt% Baytube PC/CNT nanocomposites

| | G' (Pa) | | | | | | | | | |
|---|---|---|---|---|---|---|---|---|---|---|
| ω (rad/s) | Pure PC | St Dev | DB | St Dev | 5X scCO2 | St Dev | 10X scCO2 | St Dev | 15X scCO2 | St Dev |
| 0.10 | 0.18 | 0.02 | 180.21 | 15.48 | 497.10 | 28.86 | 1035.84 | 76.85 | 320.08 | 27.42 |
| 0.13 | 0.26 | 0.02 | 208.18 | 10.40 | 547.51 | 26.51 | 1084.01 | 72.59 | 379.04 | 36.60 |
| 0.16 | 0.41 | 0.05 | 237.05 | 9.12 | 602.08 | 25.44 | 1145.50 | 72.17 | 437.27 | 46.61 |
| 0.20 | 0.59 | 0.03 | 269.23 | 7.71 | 663.25 | 24.26 | 1210.92 | 76.76 | 493.69 | 55.88 |
| 0.25 | 0.90 | 0.02 | 305.61 | 6.48 | 731.02 | 23.45 | 1286.59 | 75.89 | 560.09 | 60.97 |
| 0.32 | 1.31 | 0.02 | 347.43 | 4.44 | 807.12 | 22.41 | 1367.66 | 80.04 | 631.17 | 66.88 |
| 0.40 | 1.99 | 0.05 | 395.30 | 3.96 | 893.18 | 20.41 | 1462.81 | 75.41 | 715.38 | 72.03 |
| 0.50 | 3.21 | 0.14 | 449.73 | 2.00 | 991.46 | 20.53 | 1564.07 | 79.93 | 803.44 | 81.83 |
| 0.63 | 5.04 | 0.17 | 513.76 | 0.07 | 1105.31 | 20.27 | 1681.23 | 89.33 | 910.02 | 91.23 |
| 0.79 | 7.75 | 0.10 | 588.52 | 2.29 | 1234.71 | 18.97 | 1814.63 | 93.51 | 1032.68 | 99.30 |
| 1.00 | 12.37 | 0.24 | 674.14 | 5.53 | 1384.03 | 18.53 | 1963.93 | 94.59 | 1175.56 | 104.50 |
| 1.26 | 19.43 | 0.37 | 774.69 | 7.40 | 1559.82 | 15.59 | 2136.28 | 101.64 | 1344.75 | 111.52 |
| 1.58 | 30.51 | 1.00 | 895.55 | 11.96 | 1764.30 | 12.12 | 2332.41 | 102.23 | 1543.39 | 122.20 |
| 2.00 | 48.00 | 0.94 | 1037.25 | 17.40 | 2003.99 | 10.33 | 2558.69 | 103.04 | 1774.17 | 138.56 |
| 2.51 | 74.57 | 1.36 | 1203.23 | 17.09 | 2286.78 | 6.25 | 2819.47 | 98.01 | 2057.38 | 135.08 |
| 3.16 | 116.82 | 2.49 | 1413.12 | 35.54 | 2634.24 | 11.25 | 3126.05 | 102.33 | 2404.95 | 141.65 |
| 3.98 | 180.58 | 3.42 | 1670.45 | 50.90 | 3051.14 | 18.02 | 3488.43 | 99.91 | 2801.28 | 180.09 |
| 5.01 | 278.42 | 8.96 | 1967.26 | 58.35 | 3543.85 | 25.99 | 3921.04 | 77.16 | 3353.87 | 197.92 |
| 6.31 | 425.69 | 11.01 | 2353.63 | 84.01 | 4158.42 | 47.69 | 4431.87 | 83.97 | 4023.69 | 153.98 |
| 7.94 | 648.30 | 19.89 | 2836.98 | 116.66 | 4919.84 | 67.43 | 5074.99 | 73.83 | 4820.83 | 173.90 |
| 10.00 | 974.39 | 26.66 | 3582.58 | 54.08 | 6188.16 | 316.34 | 5899.16 | 35.38 | 6089.26 | 508.03 |
| 12.59 | 1452.15 | 46.39 | 4373.95 | 105.48 | 7473.48 | 383.37 | 6857.33 | 36.02 | 7428.03 | 501.75 |
| 15.85 | 2149.61 | 67.24 | 5398.76 | 155.44 | 9047.92 | 458.30 | 8094.23 | 55.04 | 9189.01 | 541.56 |
| 19.95 | 3139.80 | 98.28 | 6733.24 | 223.28 | 11047.91 | 570.57 | 9645.25 | 101.70 | 11412.37 | 520.65 |
| 25.12 | 4544.21 | 141.34 | 8478.53 | 297.06 | 13648.14 | 738.37 | 11659.41 | 184.72 | 14347.17 | 492.06 |
| 31.62 | 6487.94 | 204.93 | 10702.61 | 407.96 | 16949.56 | 915.57 | 14235.00 | 266.34 | 18092.73 | 473.00 |
| 39.81 | 9152.43 | 283.78 | 13637.39 | 547.39 | 21136.69 | 1110.17 | 17586.09 | 409.26 | 22849.01 | 432.08 |
| 50.12 | 12755.97 | 400.13 | 17450.89 | 707.18 | 26500.03 | 1402.43 | 21886.58 | 579.01 | 28915.67 | 350.90 |
| 63.09 | 17496.32 | 569.20 | 22319.98 | 983.24 | 33255.13 | 1701.87 | 27401.21 | 788.35 | 36578.01 | 264.63 |
| 79.43 | 23643.28 | 765.53 | 28584.50 | 1274.50 | 41764.82 | 2054.66 | 34390.55 | 1073.09 | 46090.32 | 297.52 |
| 100.00 | 31415.86 | 1062.25 | 36522.65 | 1650.53 | 52353.07 | 2471.83 | 43154.14 | 1384.66 | 57891.21 | 412.81 |

## Appendix C: Carbon Nanotube Aspect Ratio Measurements

Table C.1. Summary of carbon nanotube lengths for aspect ratio measurements

| Count # | Baytube as-received | Baytube 30X | Baytube DB post melt processing | Baytube 15X post melt compounding | Nanocyl as-received | Nanocyl 50X |
|---|---|---|---|---|---|---|
| 1 | 109.86 | 198.24 | 241.23 | 85.66 | 188.84 | 216.03 |
| 2 | 169.95 | 221.2 | 247.7 | 130.52 | 393.93 | 218.58 |
| 3 | 280.89 | 225.48 | 278.27 | 198.88 | 407.95 | 227 |
| 4 | 292.87 | 251.3 | 310.98 | 330.1 | 423.01 | 272.67 |
| 5 | 298.69 | 262.76 | 338.86 | 347.69 | 424.45 | 286.364 |
| 6 | 318.63 | 270.27 | 374 | 351.41 | 455.47 | 305.15 |
| 7 | 321.66 | 316.56 | 404.98 | 355.39 | 463.18 | 332.05 |
| 8 | 322.82 | 318.76 | 405.46 | 360.52 | 485.56 | 350.63 |
| 9 | 348.03 | 321.95 | 425.58 | 385.8 | 496.74 | 354.52 |
| 10 | 348.67 | 338.98 | 457.09 | 389.38 | 503.47 | 356.28 |
| 11 | 385.11 | 367.78 | 473.89 | 391.39 | 512.26 | 356.96 |
| 12 | 386.76 | 403.2 | 494.17 | 422.01 | 541.09 | 364.33 |
| 13 | 389.59 | 405.64 | 496.38 | 444.22 | 541.09 | 373.5 |
| 14 | 396.65 | 429.48 | 531.14 | 450.02 | 568.34 | 420.83 |
| 15 | 397.45 | 429.74 | 532.53 | 488.7 | 574.78 | 465.22 |
| 16 | 398.66 | 452.3 | 539.65 | 488.93 | 574.78 | 466.36 |
| 17 | 417.12 | 455.8 | 542.23 | 503.95 | 582.65 | 490.46 |
| 18 | 417.3 | 464.92 | 549.29 | 504.34 | 598.46 | 496.4 |
| 19 | 442.2 | 474.61 | 570.05 | 512.19 | 600.68 | 503.33 |
| 20 | 447.39 | 485.79 | 579.1 | 534.96 | 601.58 | 529.46 |
| 21 | 473.6 | 516.07 | 601.18 | 538.4 | 602.28 | 545.33 |
| 22 | 517 | 530.5 | 644.23 | 538.54 | 610.83 | 547.21 |
| 23 | 517.24 | 563.92 | 657.63 | 542.01 | 620.28 | 553.61 |
| 24 | 519.33 | 606.33 | 659.69 | 545.3 | 622.86 | 567.22 |
| 25 | 529.88 | 607.15 | 662.8 | 560.87 | 631.69 | 584.84 |
| 26 | 537.31 | 608.93 | 668.02 | 564.94 | 634.87 | 585.22 |
| 27 | 537.74 | 610.38 | 668.96 | 571.38 | 648.25 | 627.03 |
| 28 | 540.18 | 632.67 | 682.63 | 589.85 | 658.23 | 669.42 |
| 29 | 542.58 | 634.51 | 687 | 593.34 | 678.12 | 678.72 |
| 30 | 551.96 | 647.56 | 689.61 | 599.22 | 678.17 | 684.49 |

| | | | | | | |
|---|---|---|---|---|---|---|
| 31 | 557.86 | 649.27 | 691.06 | 606.3 | 686.6 | 695.96 |
| 32 | 594.12 | 661.16 | 700.36 | 617.62 | 718.7 | 718.77 |
| 33 | 594.18 | 662.16 | 700.36 | 617.62 | 725.22 | 721.86 |
| 34 | 620.6 | 670.58 | 701.75 | 618.59 | 726.95 | 723.68 |
| 35 | 624.01 | 681.73 | 705.51 | 627.22 | 728.33 | 725.02 |
| 36 | 626.42 | 691.96 | 711.87 | 642.81 | 746.79 | 761.41 |
| 37 | 629.82 | 698.28 | 727.97 | 685.67 | 753.6 | 766.36 |
| 38 | 634.5 | 713.78 | 729.54 | 685.98 | 760.56 | 766.8 |
| 39 | 635.5 | 722.4 | 734.79 | 687.1 | 761.98 | 798.21 |
| 40 | 636.07 | 726.12 | 745.47 | 692.43 | 767.74 | 823.74 |
| 41 | 640.62 | 734.72 | 764.18 | 698.81 | 780.65 | 827.85 |
| 42 | 653.91 | 734.81 | 768.66 | 728.7 | 791.46 | 870.12 |
| 43 | 664.96 | 736.82 | 769.32 | 731.25 | 818.72 | 893.4 |
| 44 | 744.94 | 751.02 | 774.23 | 761.46 | 827.98 | 895.71 |
| 45 | 783.46 | 751.09 | 776.04 | 763.29 | 827.98 | 967.73 |
| 46 | 791.57 | 764.26 | 780.03 | 764.9 | 883.51 | 984.25 |
| 47 | 818.12 | 769.02 | 793.94 | 776.29 | 891.34 | 987.43 |
| 48 | 831.14 | 779.61 | 814.94 | 787.53 | 899.45 | 1006.27 |
| 49 | 837.28 | 785.91 | 815.26 | 791.11 | 910.25 | 1028.32 |
| 50 | 859.42 | 793.55 | 836.86 | 792.52 | 910.62 | 1101.73 |
| 51 | 865.02 | 816.66 | 840.04 | 799.1 | 938.58 | 1109.77 |
| 52 | 914.22 | 837.71 | 846.9 | 813.07 | 951.27 | 1111.29 |
| 53 | 950.03 | 841.22 | 849.51 | 814.78 | 951.44 | 1118.54 |
| 54 | 950.16 | 855.47 | 849.62 | 828.59 | 991.14 | 1201.08 |
| 55 | 990.12 | 855.52 | 858.15 | 834.19 | 991.47 | 1208.07 |
| 56 | 996.71 | 864.53 | 884.69 | 838.03 | 993.89 | 1215.2 |
| 57 | 1006.24 | 881.12 | 888.83 | 854.84 | 1009.24 | 1227.53 |
| 58 | 1008.26 | 895.84 | 922.3 | 899.94 | 1014.51 | 1228.44 |
| 59 | 1010.45 | 924.13 | 923.75 | 904.38 | 1020.9 | 1235.45 |
| 60 | 1015.88 | 964.58 | 944.9 | 907.97 | 1027.47 | 1253.09 |
| 61 | 1017.27 | 974.89 | 945.95 | 908.68 | 1027.72 | 1268.77 |

| | | | | | | |
|---|---|---|---|---|---|---|
| 62 | 1071.12 | 999.16 | 948.21 | 922.47 | 1033.82 | 1320.9 |
| 63 | 1096.54 | 1011.84 | 958.12 | 984.64 | 1049.41 | 1346.02 |
| 64 | 1098.47 | 1018.65 | 967.96 | 986.24 | 1049.99 | 1349.81 |
| 65 | 1126.68 | 1039.51 | 976.56 | 987.65 | 1067.86 | 1374.49 |
| 66 | 1130.48 | 1112.78 | 981.92 | 1007.3 | 1099.94 | 1432.73 |
| 67 | 1158.59 | 1134.24 | 1006.91 | 1029.03 | 1112.47 | 1458.43 |
| 68 | 1163.5 | 1148.4 | 1036.92 | 1030.88 | 1116.92 | 1464.96 |
| 69 | 1174.8 | 1148.96 | 1048.05 | 1046.28 | 1118.14 | 1472.63 |
| 70 | 1208.76 | 1153.93 | 1093.36 | 1048.51 | 1163.1 | 1497.05 |
| 71 | 1274.21 | 1148.96 | 1097.93 | 1055.27 | 1163.96 | 1519.63 |
| 72 | 1307.59 | 1212.17 | 1101.2 | 1063.5 | 1229.14 | 1529.01 |
| 73 | 1323.16 | 1218.31 | 1114.85 | 1066.68 | 1236.44 | 1541.74 |
| 74 | 1330.45 | 1219.65 | 1142.13 | 1071.34 | 1240.06 | 1562.7 |
| 75 | 1336.21 | 1235.72 | 1159.99 | 1078.3 | 1333.55 | 1594.38 |
| 76 | 1372.11 | 1329.11 | 1170.66 | 1120.99 | 1365.81 | 1633.54 |
| 77 | 1373.84 | 1429.44 | 1172.84 | 1147.44 | 1382.28 | 1664.39 |
| 78 | 1374.59 | 1458.56 | 1183.67 | 1173.15 | 1386.61 | 1667.34 |
| 79 | 1475.88 | 1496.31 | 1200.94 | 1205.72 | 1389.43 | 1780.25 |
| 80 | 1518.47 | 1503.68 | 1204.33 | 1208.13 | 1440.22 | 1890.64 |
| 81 | 1529.91 | 1514.79 | 1204.33 | 1210.08 | 1509.4 | 2051.36 |
| 82 | 1549.51 | 1561.05 | 1210.67 | 1296.51 | 1539.29 | 2060.4 |
| 83 | 1579.27 | 1586.76 | 1214.14 | 1312.73 | 1553.23 | 2147.28 |
| 84 | 1580.98 | 1638.38 | 1236.93 | 1320.05 | 1559.41 | 2154.32 |
| 85 | 1595.68 | 1647.3 | 1366.76 | 1334.53 | 1633.01 | 2220.7 |
| 86 | 1643.3 | 1667.49 | 1391.2 | 1334.67 | 1712.14 | 2349.25 |
| 87 | 1769.79 | 1769.09 | 1392.34 | 1334.84 | 1892.71 | 2413.79 |
| 88 | 1795.24 | 1829.2 | 1409.75 | 1393.25 | 1910.9 | 2463.36 |
| 89 | 1829.84 | 1879.03 | 1475.73 | 1443.15 | 2051.46 | 2634.93 |
| 90 | 1862.54 | 2201.9 | 1501.73 | 1585.94 | 2056.15 | 3061.58 |
| 91 | 1902.83 | 2205.38 | 1536.07 | 1604.86 | 2252.43 | 3108.42 |
| 92 | 1960.13 | 2224.69 | 1598.81 | 1636.68 | 2269.86 | 3155.45 |
| 93 | 1963.182 | 2249.84 | 1662.3 | 1752.42 | 3312.5 | 3156.32 |
| 94 | 1976.39 | 2257.75 | 1686.2 | 1771.98 | 4010.45 | 3186.72 |
| 95 | 2059.41 | 2587.66 | 1691.52 | 2057.15 | 4147.82 | 3254.38 |
| 96 | 2224.95 | 2961.49 | 1701.97 | 2311.53 | 4194 | 3294.53 |
| 97 | 2373.15 | 3131.54 | 1903.75 | 2332.54 | 4467.08 | 3849.6 |
| 98 | 2567.67 | 3417.83 | 2087.88 | 3106.61 | 6009.8 | 3858.85 |
| 99 | 2589.77 | 4882.8 | 2509.27 | 3156.36 | 6850.69 | 3945.59 |
| 100 | 3087.6 | 5512.89 | 2541.4 | 3241.53 | 9034.33 | 4518 |

Table C.2. Summary of carbon nanotube diameters for aspect ratio measurements

| Count # | Baytube as-received | Baytube 30X | Nanocyl as-received | Nanocyl 50X |
|---|---|---|---|---|
| 1 | 6.28 | 7.09 | 4.83 | 4.32 |
| 2 | 6.58 | 7.28 | 4.91 | 4.89 |
| 3 | 6.73 | 7.59 | 6.6 | 5.06 |
| 4 | 7.78 | 7.67 | 6.73 | 5.45 |
| 5 | 7.94 | 7.77 | 6.85 | 5.62 |
| 6 | 8.18 | 8.05 | 7.09 | 5.83 |
| 7 | 8.44 | 8.13 | 7.09 | 6 |
| 8 | 8.51 | 8.76 | 7.21 | 6.11 |
| 9 | 8.63 | 9.21 | 7.28 | 6.16 |
| 10 | 9.23 | 9.51 | 7.4 | 6.23 |
| 11 | 9.26 | 9.56 | 7.47 | 6.55 |
| 12 | 9.27 | 10.37 | 7.71 | 6.55 |
| 13 | 9.3 | 10.46 | 7.72 | 6.56 |
| 14 | 9.39 | 10.46 | 7.89 | 6.63 |
| 15 | 9.6 | 10.48 | 7.9 | 6.94 |
| 16 | 9.6 | 10.79 | 8.13 | 7.02 |
| 17 | 9.63 | 10.92 | 8.15 | 7.04 |
| 18 | 9.67 | 11.05 | 8.23 | 7.05 |
| 19 | 9.75 | 11.11 | 8.27 | 7.14 |
| 20 | 9.9 | 11.27 | 8.29 | 7.16 |
| 21 | 10.02 | 11.34 | 8.45 | 7.21 |
| 22 | 10.03 | 11.34 | 8.46 | 7.38 |
| 23 | 10.11 | 11.43 | 8.51 | 7.38 |
| 24 | 10.37 | 11.58 | 8.58 | 7.54 |
| 25 | 10.95 | 11.82 | 8.61 | 7.59 |
| 26 | 11.05 | 11.85 | 8.66 | 7.7 |
| 27 | 11.16 | 11.97 | 8.66 | 7.72 |
| 28 | 11.16 | 12.12 | 8.79 | 7.74 |
| 29 | 11.19 | 12.14 | 8.79 | 7.75 |
| 30 | 11.65 | 12.15 | 8.81 | 7.76 |

| | | | | |
|---|---|---|---|---|
| 31 | 11.88 | 12.17 | 8.84 | 7.78 |
| 32 | 11.9 | 12.22 | 8.85 | 7.97 |
| 33 | 11.91 | 12.42 | 8.91 | 8.01 |
| 34 | 11.97 | 12.58 | 8.91 | 8.14 |
| 35 | 12.15 | 12.59 | 8.96 | 8.19 |
| 36 | 12.17 | 12.81 | 8.98 | 8.25 |
| 37 | 12.18 | 12.84 | 9.01 | 8.34 |
| 38 | 12.22 | 12.86 | 9.1 | 8.52 |
| 39 | 12.24 | 12.9 | 9.13 | 8.58 |
| 40 | 12.31 | 12.93 | 9.14 | 8.85 |
| 41 | 12.77 | 12.98 | 9.19 | 8.96 |
| 42 | 12.86 | 13.08 | 9.24 | 8.97 |
| 43 | 12.87 | 13.23 | 9.29 | 8.98 |
| 44 | 12.9 | 13.42 | 9.43 | 9.05 |
| 45 | 12.95 | 13.58 | 9.46 | 9.17 |
| 46 | 13.03 | 13.71 | 9.48 | 9.29 |
| 47 | 13.05 | 13.73 | 9.56 | 9.3 |
| 48 | 13.24 | 13.81 | 9.61 | 9.34 |
| 49 | 13.38 | 13.81 | 9.62 | 9.36 |
| 50 | 13.46 | 13.83 | 9.68 | 9.36 |
| 51 | 13.79 | 13.88 | 9.69 | 9.43 |
| 52 | 13.81 | 13.96 | 9.71 | 9.43 |
| 53 | 13.93 | 14.03 | 9.75 | 9.46 |
| 54 | 13.95 | 14.09 | 9.77 | 9.51 |
| 55 | 13.97 | 14.16 | 9.77 | 9.54 |
| 56 | 14.09 | 14.22 | 9.85 | 9.59 |
| 57 | 14.15 | 14.24 | 9.85 | 9.65 |
| 58 | 14.16 | 14.26 | 9.85 | 9.76 |
| 59 | 14.19 | 14.3 | 9.87 | 9.76 |
| 60 | 14.78 | 14.46 | 9.92 | 9.77 |

| | | | | |
|---|---|---|---|---|
| 61 | 15.37 | 15.04 | 9.94 | 9.86 |
| 62 | 15.39 | 15.05 | 9.96 | 10.08 |
| 63 | 15.64 | 15.16 | 9.96 | 10.08 |
| 64 | 15.94 | 15.24 | 9.99 | 10.11 |
| 65 | 16.11 | 15.6 | 10.07 | 10.12 |
| 66 | 16.11 | 15.73 | 10.16 | 10.13 |
| 67 | 16.13 | 16.25 | 10.18 | 10.21 |
| 68 | 16.27 | 16.28 | 10.19 | 10.21 |
| 69 | 16.34 | 16.36 | 10.2 | 10.33 |
| 70 | 16.35 | 16.46 | 10.41 | 10.53 |
| 71 | 16.55 | 16.55 | 10.46 | 10.53 |
| 72 | 16.68 | 16.91 | 10.58 | 10.56 |
| 73 | 16.71 | 17.08 | 11 | 10.59 |
| 74 | 16.79 | 17.14 | 11.1 | 10.73 |
| 75 | 16.88 | 17.22 | 11.12 | 10.74 |
| 76 | 17.12 | 17.32 | 11.16 | 10.79 |
| 77 | 17.36 | 17.33 | 11.22 | 10.85 |
| 78 | 17.75 | 17.43 | 11.27 | 10.93 |
| 79 | 18.29 | 17.46 | 11.28 | 10.93 |
| 80 | 18.36 | 17.66 | 11.31 | 11.13 |
| 81 | 18.37 | 17.77 | 11.43 | 11.23 |
| 82 | 18.49 | 17.77 | 11.5 | 11.36 |
| 83 | 18.64 | 17.9 | 11.5 | 11.38 |
| 84 | 19 | 17.95 | 11.52 | 11.42 |
| 85 | 19.02 | 18.03 | 11.85 | 11.56 |
| 86 | 19.33 | 18.17 | 12.04 | 11.61 |
| 87 | 19.59 | 18.51 | 12.08 | 11.68 |
| 88 | 19.88 | 18.6 | 12.42 | 11.78 |
| 89 | 20.23 | 19.27 | 12.57 | 12.08 |
| 90 | 20.31 | 19.56 | 12.88 | 12.22 |
| 91 | 20.33 | 20.13 | 12.9 | 12.34 |
| 92 | 20.36 | 20.3 | 13.05 | 12.39 |
| 93 | 20.43 | 20.79 | 13.08 | 12.43 |
| 94 | 20.62 | 20.94 | 13.8 | 12.5 |
| 95 | 21.3 | 20.95 | 13.85 | 12.63 |
| 96 | 22.97 | 21 | 13.86 | 12.64 |
| 97 | 23.33 | 21.31 | 13.96 | 13 |
| 98 | 24.12 | 22.27 | 14.29 | 13.1 |
| 99 | 24.38 | 22.35 | 14.64 | 13.33 |
| 100 | 30.54 | 31.04 | 15.39 | 15.2 |